

N° d'ordre :3866



THÈSE

PRÉSENTÉE A

L'UNIVERSITÉ BORDEAUX 1

ÉCOLE DOCTORALE DES SCIENCES CHIMIQUES

Par Cheng-Che, CHU

POUR OBTENIR LE GRADE DE

DOCTEUR

SPÉCIALITÉ : CHIMIE ORGANIQUE

Hydrogen-bonded supramolecular materials for organic photovoltaic applications

Soutenue le : 10 Novembre 2009

Après avis de :

M. JANSSEN, René A. J., *Professeur, Eindhoven University of Technology*
Mme CHANE-CHING, Kathleen, *Directeur de Recherche, LCC CNRS*

Rapporteur
Rapporteur

Devant la commission d'examen formée de :

M. TOUPANCE, Thierry, *Professeur, Université Bordeaux I*
M. JANSSEN, René A. J., *Professeur, Eindhoven University of Technology*
Mme CHANE-CHING, Kathleen, *Directeur de Recherche, LCC CNRS*
M. TRAVERS, Jean-Pierre, *Directeur de Recherche, CEA CNRS U. J. Fourier*
M. BASSANI, Dario M., *Directeur de Recherche, ISM CNRS*
M. HIRSCH, Lionel, *Chargé de Recherche, IMS CNRS*

Président
Rapporteur
Rapporteur
Examineur
Examineur
Examineur

Acknowledgements

First of all I would like to show my deepest and foremost gratitude to my advisor: Dr. Dario M. Bassani, Directeur de Recherche in the Institut des Sciences Moléculaires (ISM) in University of Bordeaux. With his acceptance to me to join his group, the past three and half years become a precious period in my life. This thesis will not be complete without his scientific instructions and cares in daily life. His positive and motivated attitudes toward problems make a good model to me to face coming challenges.

I would also like to express my great appreciation to the co-advisor: Dr. Lionel Hirsch, Chargé de Recherche in the Laboratoire de l'Intégration du Matériau au Système (IMS) in University of Bordeaux. His patient guidance in device experiments allows me to learn more (physics) beyond what I have been trained for (chemistry) and further polishes this study. His humorous style helps me to integrate myself into the life in France which is one of the most memorable parts in my life.

This thesis will not be finished without the help from many people. I am grateful to Dr. Brice Kauffmann in the European Institute of Chemistry and Biology for the efforts to obtain the crystallography data from Soleil Synchrotron. I want to also thank Dr. Gediminas Jonusauskas in the Centre de Physique Moleculaire Optique et Hertzienne (CPMOH) for the experiments in time-resolved spectroscopy and the discussion. I would like to thank Prof. Alexander Kuhn in ISM for the electrochemistry experiments and discussion. Many thanks to Dr. Christelle Absalon and Dr. Christiane Vitry in the Centre d'Etude Structurale et d'Analyse des Molecules Organiques (CESAMO) for the MALDI-ms experiments and Madame Odile Babot in ISM for the TGA measurements.

I am grateful to the juries for accepting the invitation and offering their valuable

advices and discussion in the final stage of thesis: Prof. Thierry Toupance in University of Bordeaux 1, Prof. René A. J. Janssen from Eindhoven University of Technology, Dr. Jean-Pierre Travers, Directeur de Recherche in the group Structure et Propriétés d'Architectures Moleculaires, CNRS, Dr. Kathleen Chane-Ching, Directeur de Recherche in Laboratoire de Chimie de Coordination, CNRS.

This thesis involves both chemistry and physics which gave me the opportunity to work with two different groups. In physics part, in the material group of IMS, I would like to thank researchers: Guillaume (Wantz), Pascal, Laurence and other members Minh Trung, Habiba, Guillaume (Gonçalves), Adrien, Loïc, Mélanie for the help in laboratory work and kind assistance in daily life. In the chemistry part, in group (NEO) in IMS, I would like to show my deep appreciation to the researchers: Jean-Pierre, Jean-Luc, Jean-Marc, Nathan, Brigitte, Martine, Sylvain, Christian, Carlo, Debdas and other team members: Pascale, Marie-Hélène, Aurélie, Guillaume (Sevez), Guillaume (Raffy), Arthur, Laura, Damien, Aurélien, Ren-Wei, Chih-Kai, Ming-Tzu for the great atmosphere in the laboratory we have and every moment we share.

I also would like to show my gratitude to fore members in NEO, Henry for his share of laboratory and life experience; Alex and Cécile for their warm care and help which make me feel less away from home.

Besides working side, I would like to thank friends for supporting and care in 3.5 years life: Fabien, Alya and Vincent.

It is not easy to detail every daily instant where I worked and lived with friends in France, I would like to thank all my friends appearing during this period, with their existence, my French life is more joyful.

Finally, I want to thank my parents, sisters and my girl, Comet. Without their unconditioned love and supporting, I can not go through these 3.5 tough years. The pride of accomplishing this work is attributed to my family.

Outline

1	GENERAL INTRODUCTION	1
1.1	THE DEVELOPMENT OF PHOTOVOLTAIC CELLS	3
1.2	OUTLINE OF THE THESIS.....	8
1.3	REFERENCES	9
2	SUPRAMOLECULAR CHEMISTRY	11
2.1	SUPRAMOLECULAR CHEMISTRY.....	13
2.1.1	Supramolecular Interactions	13
2.1.1.1	Strong Interactions	15
2.1.1.2	Moderate Interactions	15
2.1.1.3	Weak Interactions.....	19
2.1.1.4	Mechanical Bond.....	19
2.1.1.5	Hydrogen Bonds.....	20
2.1.2	H-Bonding Guided Supramolecular Assembly.....	21
2.1.3	Charge Transport in Supramolecular Assemblies	22
2.2	SYNTHESES OF ELECTRON DONOR AND ACCEPTOR MOLECULES	27
2.2.1	Syntheses of Donors	27
2.2.1.1	Pentathiophene-based Donor.....	27
2.2.1.2	Oligothiophene via Controlled Polymerization	30
2.2.2	Syntheses of Acceptor.....	37
2.3	SUPRAMOLECULAR EFFECTS ON THE EXCITED STATE BEHAVIOR OF PHT AND BAF.....	47
2.3.1	Quenching of PPHT Emission in Solution	47
2.3.2	Time-Resolved Emission Spectroscopy.....	49
2.3.3	Time-Resolved Absorption Spectroscopy.....	50
2.3.4	Supramolecular Photo-polymerization of Fullerene	53
2.3.5	BAF Crystal and Devices	56
2.4	CONCLUSION.....	60
2.5	REFERENCE	61
3	SUPRAMOLECULAR INTERACTION ASSISTED ORGANIC PHOTOVOLTAIC SOLAR CELLS	69
3.1	INTRODUCTION.....	71
3.1.1	Working Principle	73
3.1.2	Characterization of PV Cells	76
3.1.3	Bulk Heterojunction Solar cell	78
3.1.4	Strategies to Improve B-H PV Cell Efficiency	80
3.2	SUPRAMOLECULAR SOLID STATE SOLAR CELL	84
3.2.1	Different Electron D and A Pairs	85
3.2.1.1	Blend of PPHT and 2.2.....	85

3.2.1.2	Blend of PPHT and BAF.....	89
3.2.2	Ratio and annealing	91
3.2.2.1	Variation of D/A Ratio.....	91
3.2.2.2	Annealing Treatment.....	95
3.2.2.3	Addition of DMSO.....	100
3.2.3	Cell Analysis.....	101
3.2.3.1	Incident Photon to Current Efficiency (IPCE)	101
3.2.3.2	Recombination Mechanism.....	102
3.2.3.3	Charge Transport Characteristics of Materials.....	106
3.2.3.3.1	Hole Mobility	107
3.2.3.3.2	Electron Mobility.....	108
3.3	CONCLUSION.....	111
3.4	REFERENCE.....	112
4	SUMMARY AND CONCLUSION	117
	REFERENCES.....	121
5	EXPERIMENTAL SECTION.....	123
5.1	GENERAL	125
5.2	MATERIALS	126
5.3	X-RAY DIFFRACTION CRYSTALLOGRAPHY	126
5.4	ELECTROCHEMISTRY MEASUREMENTS	126
5.5	PICOSECOND TIME-RESOLVED SPECTROSCOPY	127
5.5.1	Transient Absorption Set-up	127
5.5.2	Time resolved Fluorescence Set-ups	127
5.6	GENERAL PROCEDURE TO PREPARE SOLID STATE CELLS	128
5.7	GENERAL PROCEDURE TO PREPARE FIELD EFFECT TRANSISTORS	129
5.7.1	O3HT Transistors.....	129
5.7.2	C ₆₀ and BAF Transistors.....	130
5.8	JSC VS. IRRADIATION MEASUREMENTS.....	130
5.9	IPCE MEASUREMENTS.....	130
5.10	SYNTHESIS	132
5.11	REFERENCE.....	162
	APPENDIX.....	165
	ABBREVIATION.....	184
	COMPOUND LIST.....	186

1 General Introduction

General Introduction

1.1 The Development of Photovoltaic Cells

Following the industrial revolution, the development of human civilization has mainly depended on fossil fuels. With growing scientific activities and technological innovations, the demand for energy increased rapidly and continuously. Over the past decade, global attention was drawn to the latent crisis stemmed from not only the limited amount of fossil fuels, but also the consequence of burning this energy source. The energy consumption in the next decades is predicted to be over twice what it is in the late 20th century (Figure 1.1.a).¹ Such an enormous demand of energy based on fossil fuel pressures global economics and raises instability worldwide. Additionally, gaseous emission from the combustion of carbon-based fossil fuels increases greenhouse gas emission, which is related to the acceleration of global warming (Figure 1.1.b).¹ This consequence jeopardizes long-term human existence. Therefore, to increase the portion of renewable sources among the total energy used is a crucial task at present.

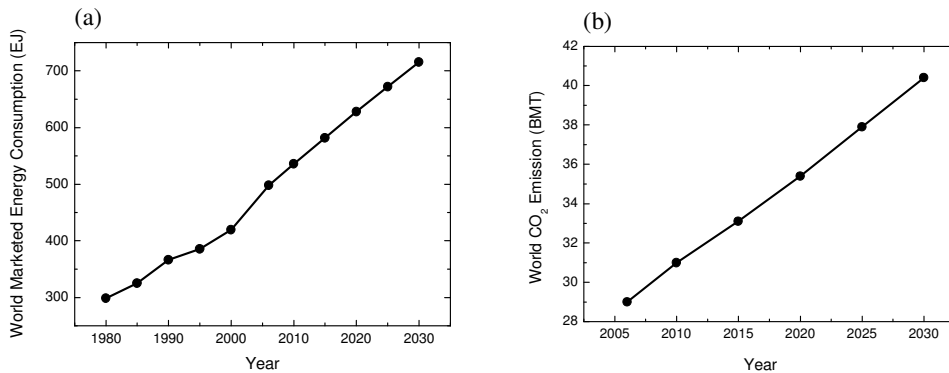


Fig. 1.1 (a) World market energy consumption in exajoule ($\text{EJ} = 10^{18} \text{ J}$). (b) World carbon dioxide emission in billion metric ton (BMT).¹

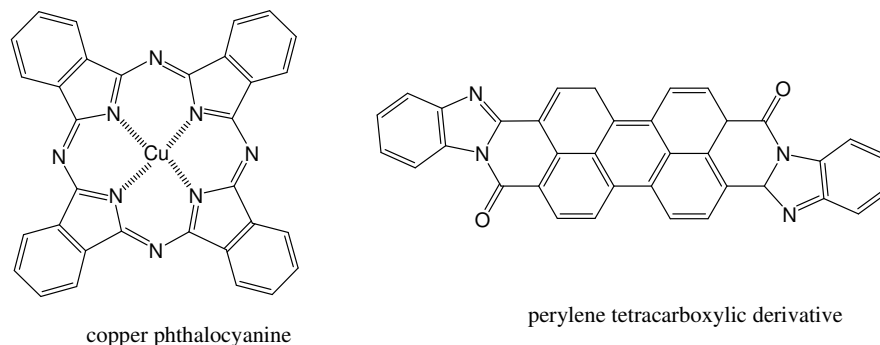
Extensive efforts have been put in exploiting various renewable energy sources to respond to the growing demand in energy consumption. For hydropower, expansion is limited because most sites are already utilized. In the case of wind power, the ideal location to deploy wind turbines depends critically on geographic and climate conditions since the generated power is proportional to the cube of the wind speed. Most of these places are far from population and industry. However, the earth receives approximately 430 EJ per hour from the sun.² Compared to other energy sources and global consumption, solar energy is the most attractive and abundant (Table 1.1).

Table 1.1 Comparison of global renewable energy and consumption.^{1,2}

	EJ/year
Solar energy	430/h
Hydropower	1.9
Wind power	0.4
Geothermal	0.04
Global consumption	480

Since Becquerel first reported the observation of photocurrent generated when light illuminated a platinum plate covered with silver bromide or silver chloride in 1839,³ the road to transforming solar irradiation into electricity was begun. Smith and Adams' work on the photoconductivity of selenium in 1873⁴ and 1876,⁵ respectively, led to further understanding of PV effect. The first inorganic silicon – based solar cell with an efficiency of 6% was realized by Pearson, Fuller and Chapin at Bell Laboratories in 1954.⁶ During the 1960s and 1970s, the terrestrial installation of PV cells opened the initial market of daily utilization.⁷ Over the years, the efficiency of crystalline silicon cell has recently attained 25 % thanks to devices developed by M. A. Green's group.⁸

Meanwhile, the research on the photo-electronic properties of organic molecules and devices gained momentum after photoconductivity was observed in anthracene by Pochettino in 1906⁹ and Volmer in 1913.¹⁰ During the 1950-60s, the development of organic materials as photoreceptors expanded the possibility of organic molecules as electronics materials.¹¹ The first organic heterojunction solar cell based on a copper phthalocyanine and a perylene tetracarboxylic acid derivative was published by Tang in 1986 (Scheme 1.1).¹²



Scheme 1.1

Since the discovery of conductivity on π -conjugated polymer chains by Heeger, MacDiarmid and Shirakawa in 1976,^{13, 14} polymer science provides a new path to exercise organic materials for electronics application. The ultrafast charge transfer between poly[2-methoxy-5-(2'-ethyl-hexyloxy)-1,4-phenylene vinylene] (MEH-PPV) and buckminsterfullerene (C_{60}) was reported by Sariciftci et al. in 1992.¹⁵ Following this major observation, a rapid increase of research followed. In the past years, novel device configurations and polymer design are tested to achieve nowadays efficiencies surpassing $\eta = 6.1\%$ (Table 1.2).¹⁶

Table 1.2 Development timeline of organic PV cells.

Year	Author	Contribution	Ref
1986	C. W. Tang	First organic heterojunction PV cell.	12
1991	Hiramoto et al.	First dye/dye bulk heterojunction PV cell.	17
1993	Sariciftci et al.	First polymer/C ₆₀ heterojunction PV cell.	18
1994	Yu et al.	First bulk polymer/C ₆₀ heterojunction PV cell.	19
1995	Yu et al./Halls et al.	First bulk polymer/polymer heterojunction PV cell.	20, 21
2000	Peeters et al.	Oligomer-C ₆₀ dyads/triads PV cells.	22
2001	Schmidt-Mende et al.	Self-organized liquid crystalline PV cell.	23
2001	Ramos et al.	Double cable polymer PV cells.	24
2002	Brabec et al.	First low-band gap polymer/PCBM PV cell with $\eta = 1\%$	25
2003	Wienk et al.	First bulk heterojunction polymer/PC ₇₀ BM PV cell	26
2009	Sung et al.	World recorded efficiency $\eta = 6.1\%$	16

Silicon-based photovoltaic cells (PV) play a major part in solar energy production. Although the market of solar energy has grown gradually in last decade, the reduction rate of solar energy cost has slowed and the cost nowadays is estimated close to limit practical price (Figure 1.2).²⁷ With growing demand on feedstock of silicon PV cells, the material source from rejected Si in semiconductor industry is gradually insufficient. Thin layer silicon PV cell could partially help alleviate the shortage, but the inheriting poor light absorption properties of these devices leave the solution less optimistic. For a general energy source to release the economical and ecological stress brought about by consuming fossil fuels, the solar energy cost needs to be lowered down by 3 times to *ca.* 1 dollar per Watt (Figure 1.2).²⁸

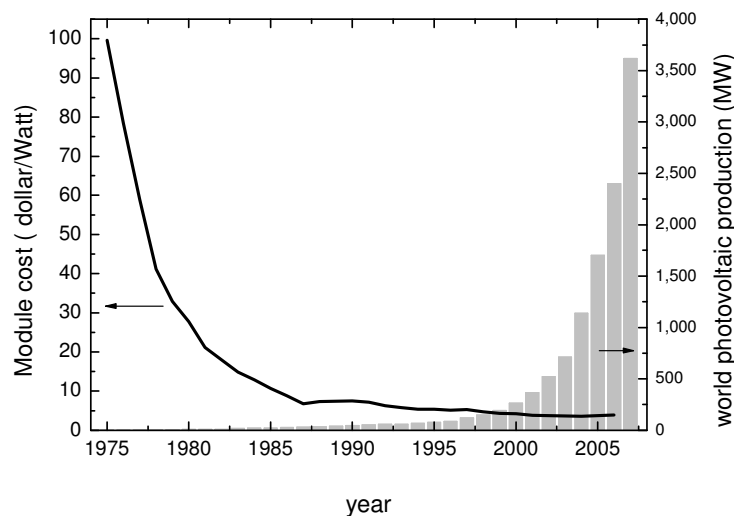


Fig. 1.2. World annual photovoltaic production in megawatts (MW) and module cost in dollar per Watt.²⁹

Semiconducting organic polymer offers a cheaper alternative to silicon technology. The soluble properties of polymers enable their deposition from solution which is impossible for silicon-based materials. With well-developed technologies from organic semiconductors and plastic industries, rapid mass production of PV modules, such as roll-to-roll drum printing, inkjet³⁰ and screen printing³¹ is promising. The flexible nature of polymer PV cells provides convenient method to installation, hence the deployment of PV cell may expand to curved surface. Polymer PV cells facilitates personal use such as cell phone chargers owing to the portability and low cost which are reflected in light module weight.

1.2 Outline of the Thesis

Among numerous parameters, such as solvent, spin rate and post treatment etc., that affect the micro-structure of the active layer in a organic PV cell, a supramolecular interaction guided approach was adopted in order to induce the designed arrangement of electron donors (D) and acceptors (A). The chemistry aspect of the thesis is presented in chapter 2. In section 2.2.1 and 2.2.2, the details of the syntheses and basic physical properties of different electron D and A molecules are described. The physical characterization, such as fluorescence quenching and transient spectroscopy, and supramolecular interactions between electron D-A pairs, and the observation of interactions between electron A molecules, such as dimerization and crystallography, are detailed in section 2.2.3.

In chapter 3, the physics part of the thesis is discussed. The fabrication and characterization of PV cells with different materials are reported in section 3.2.1. The result of changing fabrication parameters, D-A ratio, annealing temperature and addition of dimethylsulfoxide (DMSO), are described in section 3.2.2. The physical analyses of the PV cells, such as incident light to current efficiency (IPCE), recombination mechanism, and material field effect transistor mobilities, are discussed in section 3.2.3.

1.3 References

- 1 *International Energy Outlook 2009*, Energy Information Administration, **2009**,
<http://www.eia.doe.gov/oiaf/ieo/>
- 2 Renée M. Nault, *Basic energy sciences workshop on solar energy utilization*, Argonne National Laboratory, **2005**.
- 3 A.E. Becquerel, *Compt. Rend. Acad. Sci.* **1839**, 9, 145.
- 4 W. Smith, *Nature* **1873**, 7, 303.
- 5 W.G. Adams, R.E. Day, *Proc. R. Soc. Lond.* **1876**, 25, 113.
- 6 D.M. Chapin, C.S. Fuller, G.L. Pearson, *J. Appl. Phys.* **1954**, 25, 676.
- 7 J. Perlin, *From space to earth: The story of solar electricity*. Harvard University Press, Cambridge, MA, **2002**.
- 8 J. Zhao, A. Wang, M. A. Green, *Prog. Photovoltaics* **1999**, 7, 471. The value is recalculated to 25 % with a revision of international standard in 2008.
- 9 A. Pochettino, *Acad. Lincei Rend.* **1906**, 15, 355.
- 10 M. Volmer, *Ann. Physik* **1913**, 40, 775.
- 11 P.M. Borsenberger, D.S. Weiss, *Organic photoreceptors for imaging systems*, Marcel Dekker, New York, **1993**.
- 12 C. W. Tang, *Appl. Phys. Lett.* **1986**, 48, 183.
- 13 H. Shirakawa, E. J. Louis, A. G. MacDiarmid, C. K. Chiang, A. J. Heeger, *Chem. Commun.* **1977**, 578.
- 14 C. K. Chiang, C. R. Fincher Jr., Y. W. Park, A. J. Heeger, H. Shirakawa, E. J. Louis, *Phys. Rev. Lett.* **1977**, 39, 1098.
- 15 N. S. Sariciftci, L. Smilowitz, A. J. Heeger, F. Wudl, *Science* **1992**, 258, 1474.
- 16 S. H. Park, A. Roy, S. Beaupré, S. Cho, N. Coates, J. S. Moon, D. Moses, M.

-
- Leclerc, K. Lee, A. J. Heeger *Nature Photonics* **2009** 3, 297.
- 17 M. Hiramoto, H. Fujiwara, M. Yokoyama, *Appl. Phys. Lett.* **1991**, 58, 1062.
- 18 N. S. Sariciftci, D. Braun, C. Zhang, V. I. Srdanov, A. J. Heeger, G. Stucky, F. Wudl, *Appl. Phys. Lett.* **1993**, 62, 585.
- 19 G. Yu, K. Pakbaz, A. J. Heeger, *Appl. Phys. Lett.* **1994**, 64, 3422.
- 20 G. Yu, J. Gao, J. C. Hummelen, F. Wudl, A. J. Heeger, *Science* **1995**, 270, 1789.
- 21 J. J. M. Halls, C. A. Walsh, N. C. Greenham *Nature* **1995**, 376, 498.
- 22 E. Peeters, P.A. Van Hal, J. Knol, C. J. Brabec, N. S. Serdar Sariciftci, J. C. Hummelen, R. A. J. Janssen, *J. Phys. Chem. B* **2000**, 104, 10174.
- 23 L. Schmidt-Mende, A. Fechtenkötter, K. Müllen, E. Moons, R. H. Friend, J. D. MacKenzie, *Science* **2001**, 293, 1119.
- 24 A. M. Ramos, M. T. Rispens, J. C. Hummelen, R. A. J. Janssen, *Syn. Metals* **2001**, 119, 171.
- 25 C. J. Brabec, C. Winder, N. S. Sariciftci, *Adv. Funct. Mater.* **2002**, 12, 709.
- 26 M. M. Wienk, J. M. Kroon, W. J. H. Verhees, *Angew. Chem. Int. Ed.* **2003**, 42, 3371.
- 27 T. Surek, in: Third World Conference on Photovoltaic Energy Conversion, Osaka, May 11–18, 2003 (paper 8PLE301)
- 28 K. Zweibel, NREL Report No. TP-520-38350, 2005
- 29 Worldwatch, Prometheus Institute, REN21
- 30 V. Marin, E. Holder, M. M. Wienk, E. Tekin, D. Kozodaev, U. Schubert, *Macromol. Rapid Commun.* **2005**, 26, 319.
- 31 S. E. Shaheen, R. Radspinner, N. Peyhambarian, G. E. Jabbour, *Appl. Phys. Lett.* **2001**, 79, 18.

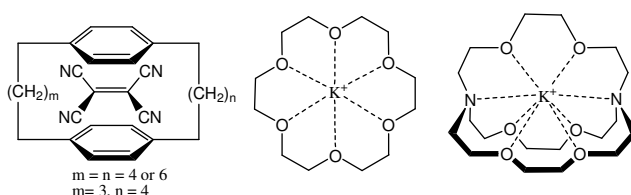
2 Supramolecular Chemistry

Supramolecular Chemistry

2.1 Supramolecular Chemistry

2.1.1 Supramolecular Interactions

Fundamental work in supramolecular chemistry was pioneered by 1987 Nobel Prize laureates Lehn, Cram and Pedersen in the 1960s and 1970s. Early definitions of “supramolecular” chemistry were mainly focused on the non-covalent interactions between “host” and “guest” molecules, *e.g.* a tetracyanoethylene inside cyclophanes,¹ metal cations inside crown ethers² or cryptands (Scheme 2.1).³



Scheme 2.1

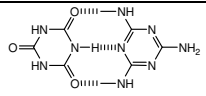
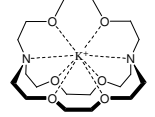
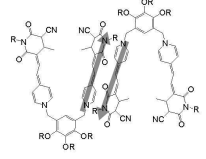
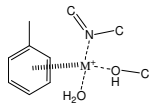
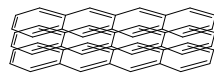
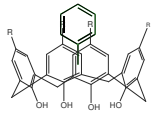
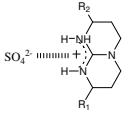
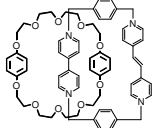
Over the past decades, the rapid expansion of supramolecular chemistry gave birth to a large diversity of non-covalent chemical systems.⁴ In addition to host-guest complexes, today supramolecular chemistry encompasses numerous designs of 2-D and 3-D architectures capable of various functionalities, such as sensors,⁵ catalysts,⁶ switches,⁷ and signal amplification devices.⁸ Meanwhile, the concept of supramolecular chemistry provides a helpful “bottom-up” approach to meet the technological demand of the nanotechnology era.

Much of the recent developments in supramolecular chemistry emphasize using self-assembly properties to synthesize large molecular arrays. In Nature, self-assembly is an essential process that enables sophisticated biological structures to be built up from isolated subunits. This strategy allows Nature to generate organizations with multiple specific functionalities in a highly precise and efficient

manner. Examples playing vital role in regulating biological functionalities present in living organism include photosystem I⁹ and II,¹⁰ ATPase¹¹ (ATP: adenosine triphosphate) and cytochrome b₆/f complex¹² etc.

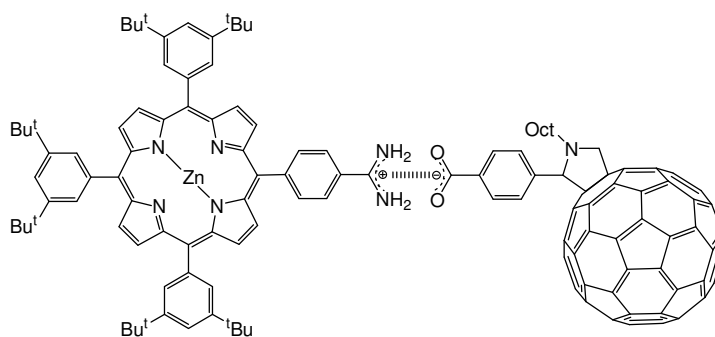
In self-assembly, different units are driven to unique positions and orientations by various non-covalent interactions which draw molecules together or repel them.¹³ These non-covalent interactions span a wide range of forces which are affected by the nature of the molecular fragments and their environment (Table 2.1).

Table 2.1 Summary of various non-covalent interactions.

Type	Intensity (KJ/mol) ¹⁴	Example	Ref.
Hydrogen bonding	4-120		15
Metal-ligand coordination	50-200		2
Dipole-dipole interactions	5-50		31
Cation- π interactions	5-80		16
Aromatic interactions	0-50		17
Van der Waals Forces	<5		18
Coulombic interactions	100-350		19
Mechanical Bonds	-		20

2.1.1.1 Strong Interactions

Coulombic interactions have comparable strengths to covalent bonds and are sensitive to the environment. For instance, the interaction between Na^+ and Cl^- in salt crystals is broken in water because solvation effects overwhelm the mutual electrostatic attraction.²¹ In the case of organic species, the amidinium-carboxylate pair was used to associate a fullerene and porphyrin compound in an electron transfer dyad in solution (Scheme 2.2).²² In this system, hydrogen bonds between the amidinium and the carboxylate also contribute to the strong association constant ($K_a = 10^7 \text{ M}^{-1}$). An analogous supramolecular synthon, the ammonium-carboxylate pair,²³ is widely used in crystal engineering to control the supramolecular structures in the solid state and to guide further reaction, such as, for example, single-crystal-to-single-crystal topochemical polymerization of diacetylenes.²⁴

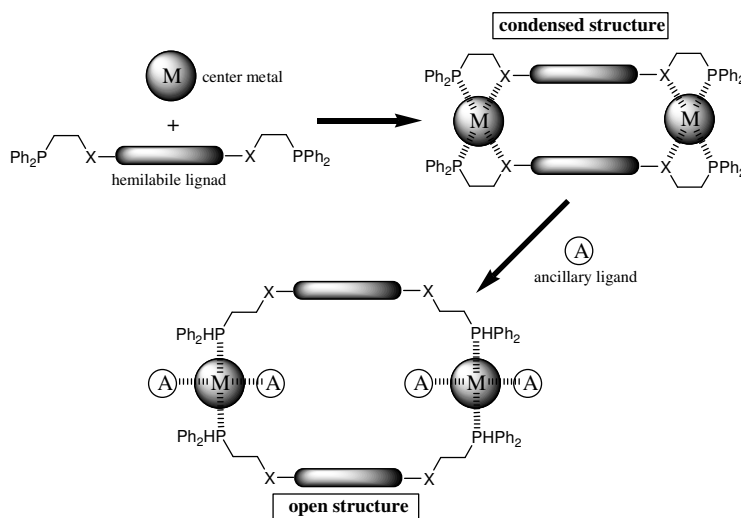


Scheme 2.2

2.1.1.2 Moderate Interactions

Metal-ligand interactions have been extensively employed in the construction of supramolecular assemblies.²⁵ Moderate to strong binding and specific coordination geometries allow coordination metals in metal-ligand interaction-based supramolecules to direct the formation of specific architectures. Furthermore, vacant coordinative sites may be available for further reaction without requiring disassembly

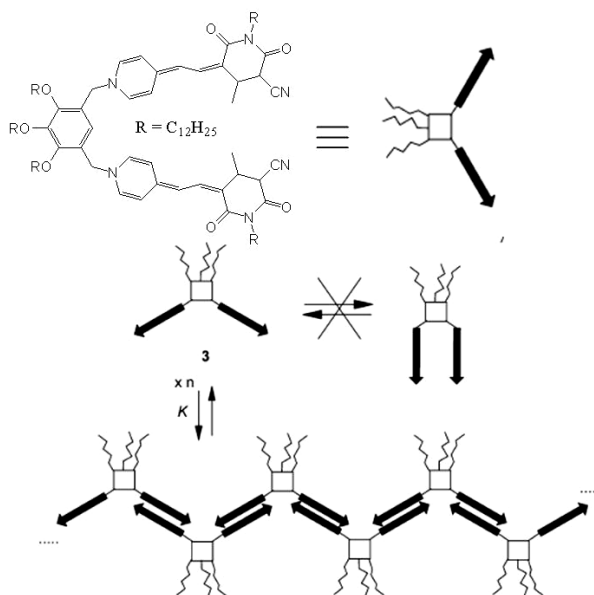
of the supramolecular structure. Three basic elements can be considered to build a metal-ligand complex: the metal center, a hemilabile ligand, and ancillary ligands (Scheme 2.3). These elements are under thermodynamic and kinetic control, and provide access to a variety of 2-D and 3-D supramolecular structures with tunable properties. In some case, weaker metal-heteroatom interactions can be selectively broken by introduction of small molecules or ions which have a higher binding affinity to the metal center or to the ligand to liberate specific sub-components.²⁶



Scheme 2.3 Example of a metal-ligand interaction based structure (M=Rh^I).²⁶

Dipole-dipole interactions in low molecular weight intramolecular charge-transfer (ICT) complexes comprising organic sub-units have been used by supramolecular chemists to synthesize assemblies that possess fascinating applications in materials for nonlinear optical applications,²⁷ chemiluminescent materials,²⁸ fluorescence probes,²⁹ and dye-sensitized solar cells.³⁰ Recent reports show that donor-acceptor dipole-dipole interaction in ICT assemblies offer a facile access to form 1-D or semi 1-D micro- or nanomaterials. For example, the formation of fibers constructed by supramolecular dye polymers from merocyanine derivatives

(Scheme 2.4) was reported by Würthner's group.³¹ Meanwhile, it has also been reported that dithiole-tetranitrofluorene³² derivatives form distinct micro-scale structures which have aggregation-induced emission properties.³³



Scheme 2.4 Dipole-dipole interactions used to induce the formation of a supramolecular merocyanine polymer.³¹

Cation- π interactions play a significant role in living organisms.³⁴ A protein database research revealed that for every 77 amino acid residues, the cation- π interaction between a positively charged amino acid and aromatic amino acid is involved in the structuring of a protein.³⁵ Cation- π interactions are, therefore, considered to be an essential force in generating the tertiary and quaternary structures of proteins. These interactions are also important in biological processes such as protein-ligand³⁶ and protein-DNA³⁷ complex formation.

Aromatic interactions (also called π - π stacking interactions) exist between two aromatic systems separated by *ca.* 3.4 ~ 3.8 Å. There are two types of π - π stacking conformations: face-to-face stacking and edge-to-face.³⁸ An electrostatic interaction

model was proposed to rationalize these two conformations.³⁸ In this model, an aromatic ring can be viewed as a σ -framework sandwiched between two layers of negatively charged π -electron clouds (Figure 2.1.a). Whether the interaction is attractive or repulsive depends on the relative distant offset and angle (Figure 2.1.b).

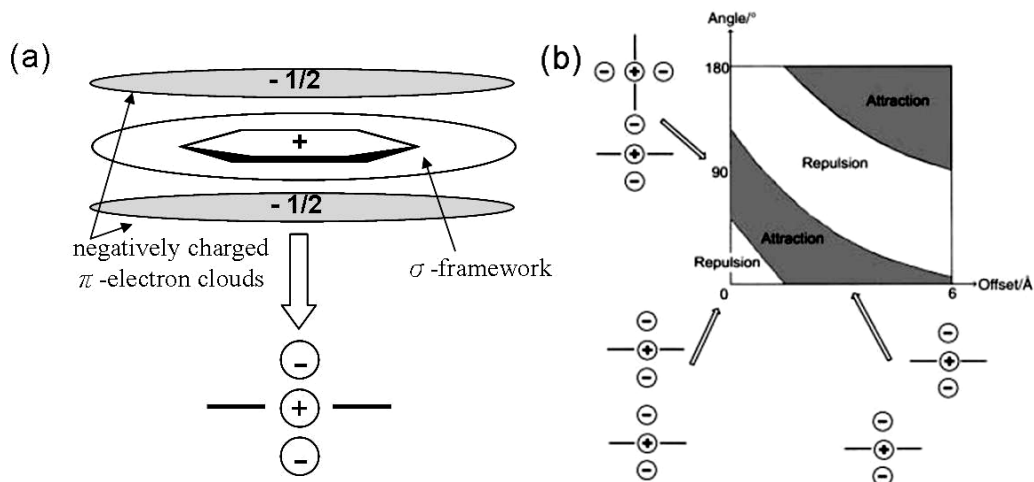


Fig. 2.1. (a) Graphic representation of an aromatic ring from the electrostatic model. (b) Electrostatic interactions between π -charged distributions as a function of orientation and distance.³⁸

The packing mode of π -conjugated polymer chains in aggregates is in part induced by π - π stacking interactions and profoundly affects the charge transfer efficiency. From theoretical calculations,^{17, 39} it has been concluded that in cofacial tetracene, the INDO-calculated charge transfer integral increases when the spacing approaches the π - π stacking interaction regime.³³ High charge mobilities in organic field effect transistors (o-FET)⁴⁰ and in PV cells⁴¹ have been experimentally verified when the π -conjugated systems are well organized. The high charge mobilities were attributed to the close packing of poly-3-hexylthiophene (P3HT) induced by strong π - π stacking interactions.⁴²

2.1.1.3 Weak Interactions

Van der Waals interactions originate from the polarization of the electron cloud by close neighboring nuclei, resulting in a weak electrostatic force. Because Van der Waals interactions are relatively weak with respect to other interactions and are non-directional, they are more difficult to use in the design of specific hosts for selective recognition. In supramolecular chemistry, Van der Waals interactions are most important for the behavior of inclusion assemblies, for example, the inclusion of a toluene molecule in the “pocket” of a *p-tert*-butylcalix[4]arene (Table 2.1).¹⁸ They are especially important in physiological process of living organism where, for example, the hydrophobic interaction between membrane surface and amphipathic amyloid- β peptide affects the folding behavior involving in Alzheimer's disease.⁴³

2.1.1.4 Mechanical Bond

Mechanical bonds are obtained when two or more molecular units are “interlocked” without the existence of direct covalent or non-covalent interactions and prevent the supramolecular assembly from dissociating by mechanical interlacing.⁴⁴ By using mechanical bonds, chemists have synthesized supramolecules with topological complexity, such as catenanes,⁴⁵ rotaxanes,⁴⁶ knots,⁴⁷ and Borromean rings (Figure 2.2).⁴⁸

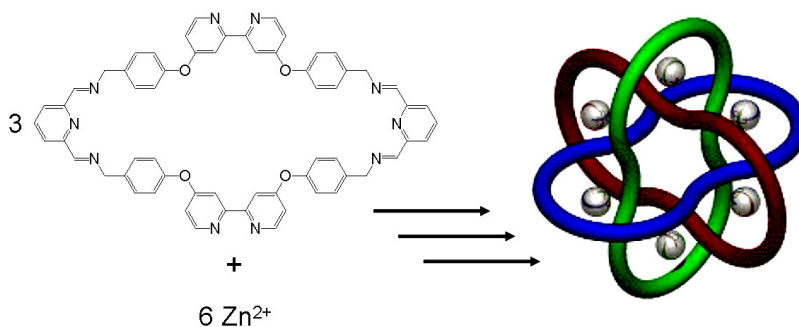


Fig. 2.2. A molecular Borromean ring contains three macro cycles and zinc ions used as template in its synthesis.⁴⁸

2.1.1.5 Hydrogen Bonds

Hydrogen-bonds (H-Bonds) can be viewed as a type of dipole-dipole interaction in which a hydrogen atom linked to an electronegative atom (or to an electron withdrawing group) is attracted to the dipole of an adjacent molecule or functional group. The intensity of the H-bond varies according to the nature of the atom to which the hydrogen atom is attached and of the neighboring dipole. Although H-bonds are only moderate in strength amongst non-covalent interactions, they are the, in the words of J.-M. Lehn, “the master key interaction in supramolecular chemistry”⁴ owing to their directionality and versatility.⁴⁹

In general, the more electronegative the atom of a H-bond donor (D) group where hydrogen connects, or in the H-bond acceptor (A), the stronger the H-bond. In a multiple H-bonding system, the number and arrangement of H-bonds also affects the overall strength. The association constant of an assembly consisting of AAA-DDD is over 3 orders of magnitude greater than that of DAD-ADA system (Figure 2.3).⁵⁰ This difference in strength is attributed to the secondary interactions between vicinal D-A pairs.⁵¹ The attractive diagonal interactions in an AAA-DDD pair contribute to the high association constant. However, in a DAD-ADA pair, the repulsion between adjacent D-A dipoles decreases the stability.

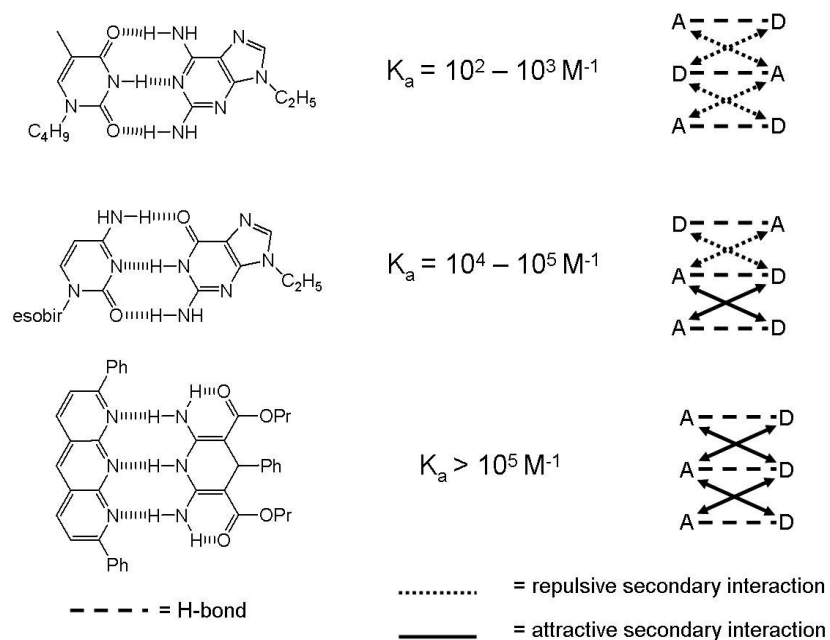
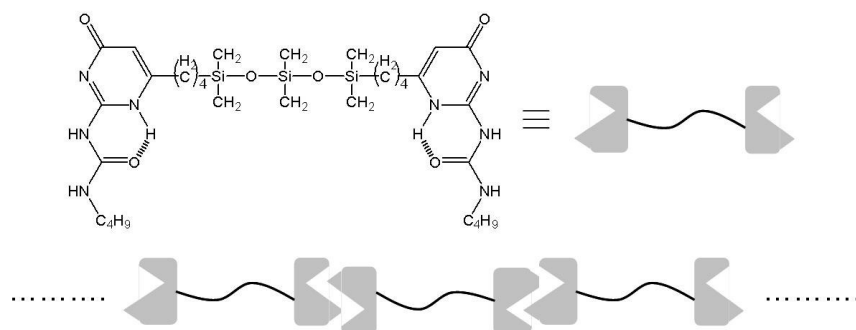


Fig. 2.3. The stability of multiple H-bonding interaction depends on the number and arrangement of the H-bonding.

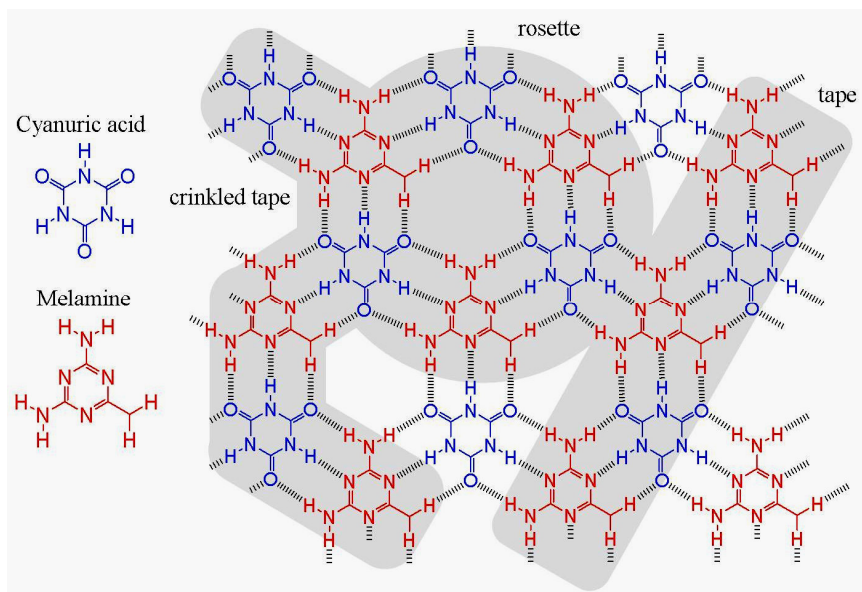
2.1.2 H-Bonding Guided Supramolecular Assembly

H-bonding has provided chemists with a precise and efficient tool to build designed supramolecular architectures.⁵² Molecules with multiple H-bonding sites provide access to precise finite or continuous assemblies such as the supramolecular polymers containing tetra-H-bonding functionalized monomers reported by Meijer and co-workers (Scheme 2.5).⁵³



Scheme 2.5. A supramolecular polymer induced by the quadruple complementary H-bonds on ureidopyrimidone units.⁵⁴

The cyanuric acid-melamine motif is one of the most studied H-bonding D-A systems.⁵⁵ Its complementary ADA-DAD structure offers three complementary H-bonding sites between the two components. Because of their symmetrical structure, cyanuric acid-melamine pairs can form infinite architectures such as tapes and crinkled tapes, as well as finite structures, such as rosettes (Scheme 2.6).⁵⁶ Barbituric acid is ditopic alternative to cyanuric acid that limits the formation of infinite 2-D sheets. Further buildup into 3-D assemblies was achieved by the groups of Kitamura;⁵⁷ Whitesides⁵⁸ and Reinhoudt.⁵⁹

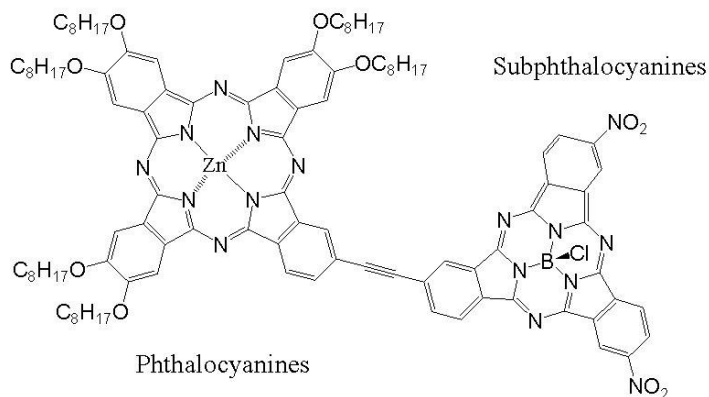


Scheme 2.6. Infinite sheet structure containing rosette, tape and crinkled tape sub-structure formed by cyanuric acid and melamine.

2.1.3 Charge Transport in Supramolecular Assemblies

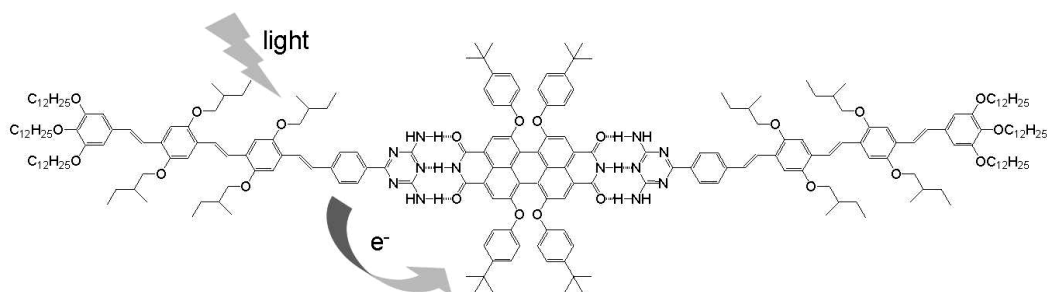
In addition to charge transport between π -conjugated systems, charge transfer has also been observed in covalently linked D-A dyads.⁶⁰ Due to the small spacing between the donor segments, charge transfer rates were enhanced with respect to which in a non-bound charge D and A systems. For example, it has been reported that

an efficient photoinduced charge transfer from phthalocyanines to subphthalocyanines took place when the subphthalocyanines was functionalized with nitro groups (Scheme 2.7).⁶¹



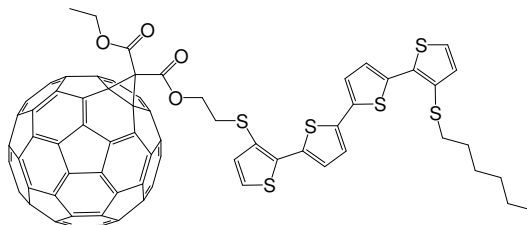
Scheme 2.7.

Enhanced charge transfer has also been observed between non-covalently linked D-A dyads. For example, fast photoinduced charge transfer from oligophenylene-vinylene (OPV) to a bisindie associated through three H-bonds was observed by Meijer's group (Scheme 2.8).⁶² In this system, electrons are transferred from the peripheral OPVs to the center perylene moieties, and the supramolecular hierarchical structure induced by aromatic interaction can serve as nanoscale building block in solid state devices.



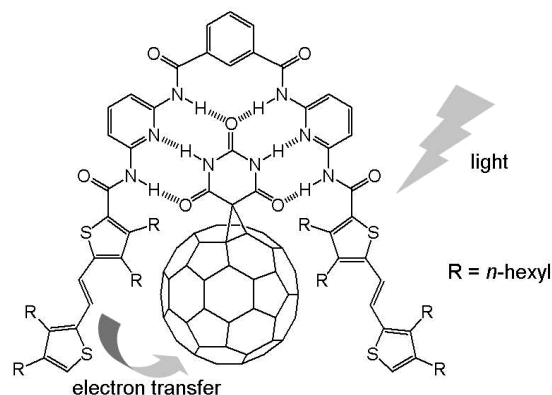
Scheme 2.8. Charge transfer dyad associated by multiple H-Bonding prepared by Meijer's group.⁶²

Similarly, efficient charge transfer was also found in a dyad when a fullerene serves as an electron accepter.⁶³ A dyad composed of a tetrathiophene electron donor covalently functionalized to a C₆₀ acceptor exhibited fast intra-molecular electron transfer ($k_{ET} > 3.3 \times 10^{12} \text{ s}^{-1}$) in toluene, as reported by Roncali's group (Scheme 2.9).⁶⁴



Scheme 2.9. Covalently linked oligothiophene-fullerene charge transfer dyad prepared by Roncali's group.⁶⁴

Ultrafast electron transfer was also reported in a non-covalent D-A dyad based on H-bonding interaction to induce its association.⁶⁵ In solution, very fast photoinduced charge transfer rate ($k_{ET} = 5.5 \times 10^{12} \text{ s}^{-1}$) is observed from a oligothiophenevinylene segment functionalized with a Hamilton receptor to a barbituric acid fullerene derivative (Scheme 2.10).⁶⁶ This fast electron transfer was ascribed to the close proximity between the D-A pair induced by multiple complementary H-bonds.



Scheme 2.10.

Theoretical calculations suggest that charge transport along the perpendicular axis of a π -conjugated system dimer is strongly affected by the relative orientation and distance of the sub-units.^{17, 67} Indeed, experimental observations show that the hole mobility in a sexithiophene single crystal is four orders of magnitude higher than in amorphous films.⁶⁸ The high charge carrier mobilities in P3HT FETs under different experimental conditions such as molecular weight,⁶⁹ regioregularity,⁷⁰ processing solvents,⁷¹ post annealing⁷² are well documented. These results also suggest that increased FET mobilities are the consequence P3HT chains aligned in a parallel fashion which facilitates charge hopping between polymer chains. Therefore, well-ordered packing of π -conjugated systems is a key issue to organic materials-based electronics application.

Along these lines, the incorporation of complementary H-bonding D-A pairs with electron D-A units might allow the development of more efficient charge separation and collection systems (Figure 2.4). Derivatives of cyanuric acid and melamine (barbituric acid and 2,4,5,6-tetraaminopyrimidine) offer a promising platform as they can be chemically functionalized with electron acceptor fullerene and electron donor oligothiophene, respectively, and direct the formation of linear assemblies. The close intermolecular spacing induced by H-bonding is conducive to charge transfer from oligothiophene backbone to fullerene. Meanwhile, the interchain distance between oligothiophene chains is conceived to be shortened by π - π interactions, which could further facilitate inter-chain charge transfer.

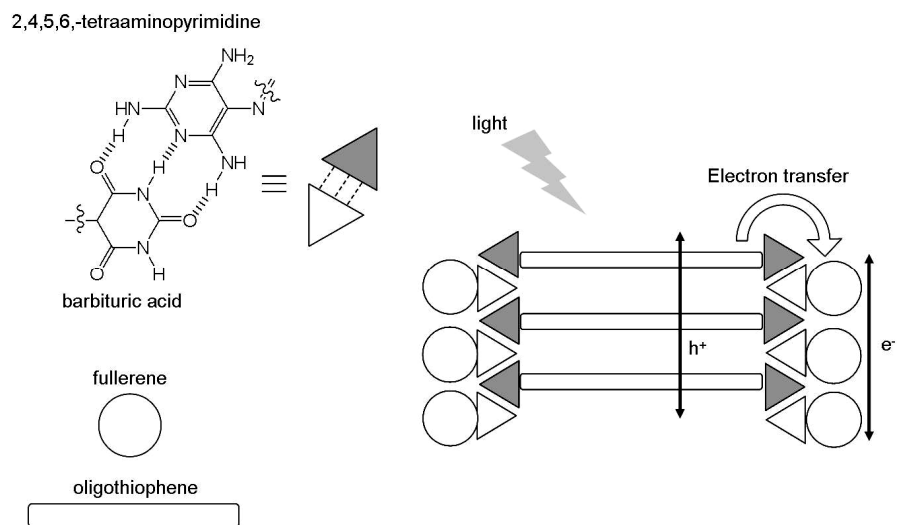
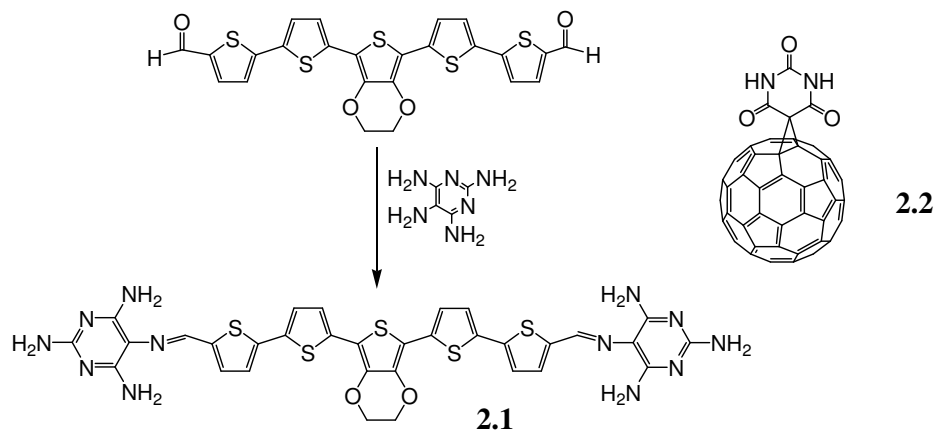


Fig. 2.4. H-bond guided supramolecular assembly of π -conjugated system is envisaged to facilitate charge transport efficiency.

2.2 Syntheses of Electron Donor and Acceptor Molecules

Previous work on electron D-A assemblies using melamine-terminated pentathiophene **2.1** and a barbituric acid-functionalized fullerene **2.2** established a concise synthetic route through a condensation reaction (Scheme 2.11).⁷³ Previous results from solution-phase photoelectrochemical devices suggest that this approach may hold interest in the design of solid-state solar cells. However, because solubility is a key factor in processing organic materials in solid state devices such as PV cells and o-FETs, solution-processable molecules with good solubility are necessary.



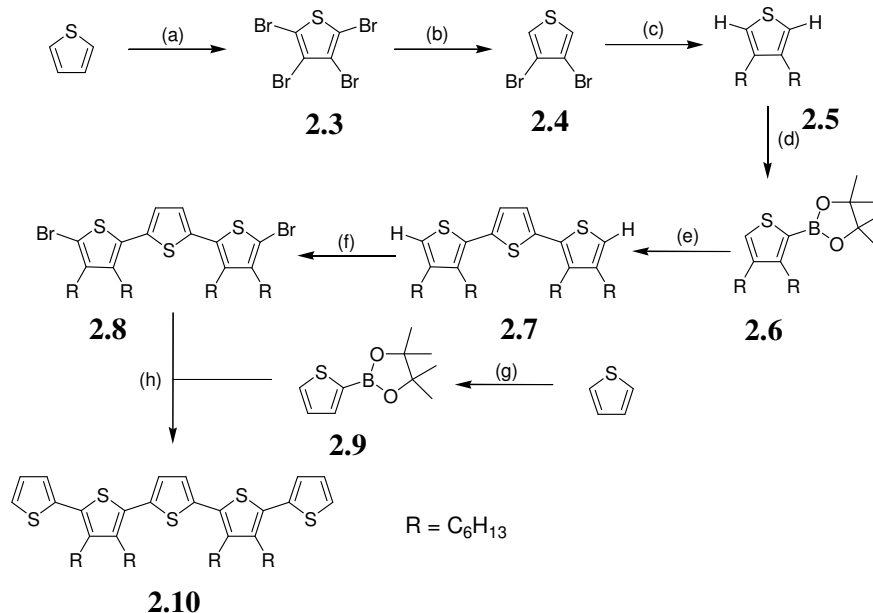
Scheme 2.11. Electron donating and accepting molecules used in previous photoelectrochemical devices. The electron donor is synthesized through a simple condensation reaction.

2.2.1 Syntheses of Donors

2.2.1.1 Pentathiophene-based Donor

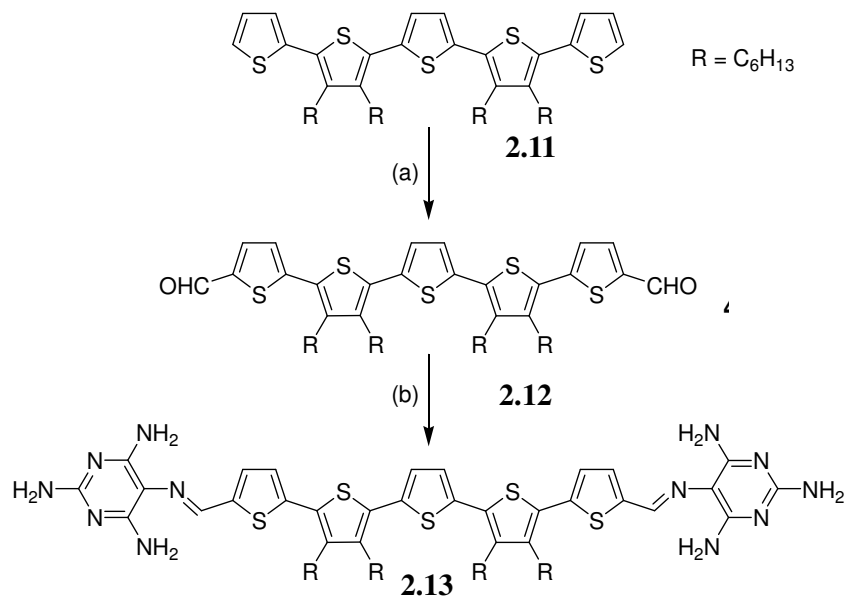
To improve the solubility of **2.1** while minimizing distortions in the pentathiophene structure, the central EDOT moiety was replaced by four alkyl chains located on non-adjacent thiophenes. The target molecule, compound **2.13**, thus possesses an alternating thiophene-3,4-dialkylthiophene structure in which four *n*-hexyl chains are incorporated in the pentathiophene backbone through Kumada coupling in order to promote solubility.⁷⁴ The core oligothiophene **2.10** is composed

of an alternating dihexyl-substituted or unsubstituted thiophene monomers, and is prepared *via* sequential bromination and Suzuki coupling reactions (Scheme 2.12).⁷⁵



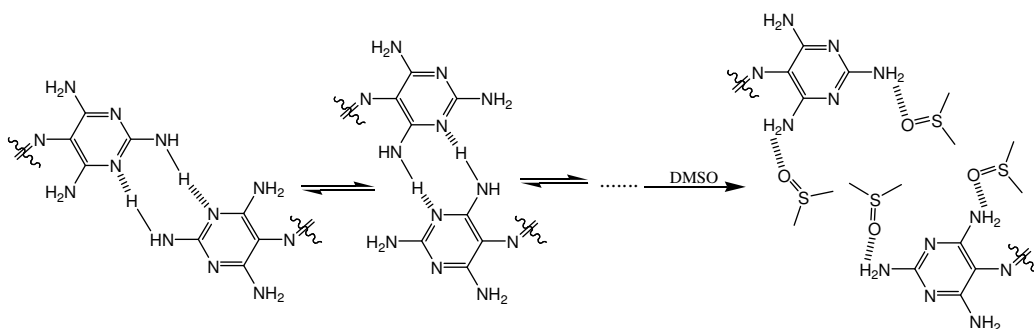
Scheme 2.12. Reagents and conditions: (a) Br₂, CHCl₃, rt, 24h, reflux, 2h, 96%; (b) Zn, AcOH/H₂O, rt, 1h, reflux, 3.5h, 60%; (c) *n*-hexylmagnesiumbromide, [1,3-bis-(diphenyl-phosphino)-propane]-nickel(II)-chloride, toluene, reflux 16h, 87%; (d) *n*-BuLi, THE, -80°C, then 2'-isopropoxy-4',4',5',5'-tetramethyl-1,3,2-dioxaborolane, 89%; (e) 2,5-dibromothiophene, Pd(PPh₃)₄, K₂CO₃, THF/toluene/H₂O, reflux overnight, 50%; (f) *N*-bromosuccinimide, DMF, rt, 6h, 50%; (g) *n*-BuLi, THE, -80°C, then 2'-isopropoxy-4',4',5',5'-tetramethyl-1,3,2-dioxaborolane, 90%; (h) Pd(PPh₃)₄, K₂CO₃, THF/toluene/H₂O, reflux overnight, 58%.

The parent oligothiophene **2.10** is subsequently modified by a double Vilsmeier-Haack formylation to give dialdehyde-functionalized oligothiophene **2.12**.^{73, 76} Two terminal melamine groups for H-bonding were introduced by Schiff base formation (Scheme 2.13).⁷³ The equilibrium for the formation of the Schiff base can be driven toward the products by using an excess of 2,4,5,6-tetraaminopyrimidine sulfate and long reaction times, to afford final product **2.13** in 75% isolated yield.



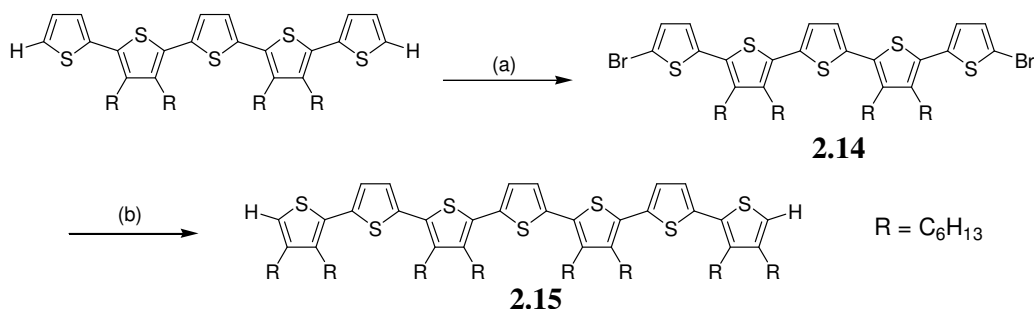
Scheme 2.13. Reagents and conditions: (a) POCl₃, DMF, CH₂Cl₂, reflux, overnight, 58% (b) 2,4,5,6-tetraaminopyrimidine sulfate, K₂CO₃, EtOH/DMSO, reflux, 5d, 75%.

Despite the assistance of four alkyl chains, compound **2.13** possesses low solubility in common organic solvents (CHCl₃: 1.6 mg/mL = 1.5 mM, chlorobenzene: 0.4 mg/mL = 3.6 mM). Due to the H-bonds between melamine groups, molecule **2.13** may form large aggregates which lower the solubility. The later can be restored by adding DMSO, which breaks the H-bonds between the melamine units (Scheme 2.14).



Scheme 2.14. The H-bonding between melamines were blocked by DMSO molecules.

To further enhance the solubility, a system based on a longer heptathiophene donor possessing eight alkyl chains was undertaken (Scheme 2.15). However, the low overall yield of the synthesis (0.54%) made this impractical for further studies. Therefore, a more direct route to oligoalkylthiophenes through controlled polymerization was envisaged.



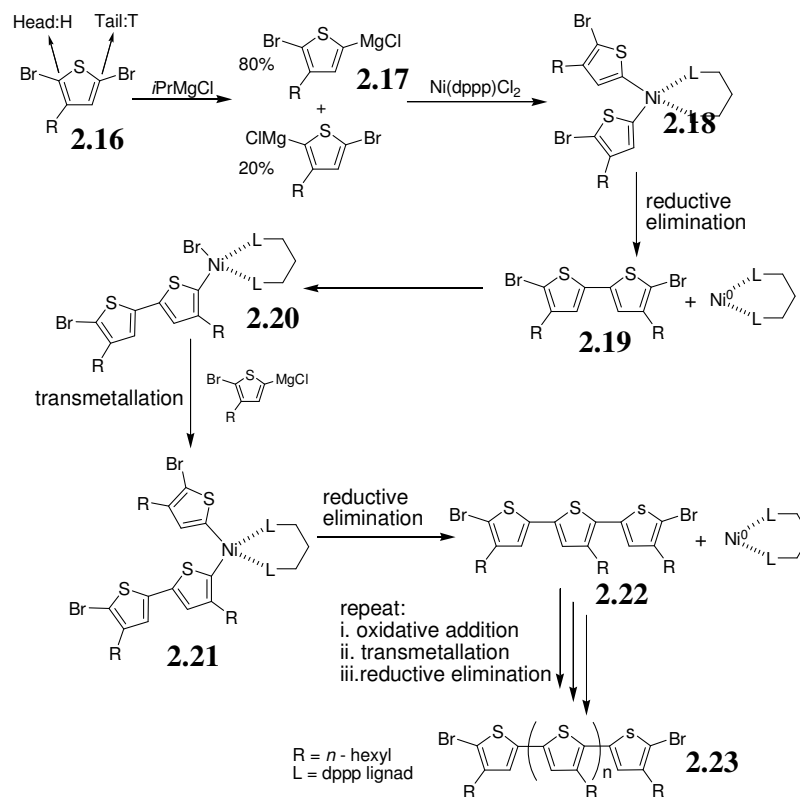
Scheme 2.15. Reagents and conditions: (a) *N*-bromosuccinimide, DMF, rt, 9h, 89%; (b) Pd(PPh₃)₄, K₂CO₃, THF/toluene/H₂O, reflux 3h, 40%

2.2.1.2 Oligothiophene *via* Controlled Polymerization

Rapid synthesis of short oligothiophene backbones can be achieved by employing metal-catalyzed cross-coupling polymerization.⁷⁷ The chemical synthesis of regioregular head-to-tail (HT) poly-3-alkylthiophene (P3AT) was reported by McCullough and Lowe using Ni-catalyzed dehalogenative polymerization,⁷⁸ and the physical properties of regioregular HT-P3AT are superior to those of the regiorandom one. This method was recently modified by introducing 2-bromo-5-chloromagnesium-3-hexylthiophene to reduce polydispersity (PD),⁷⁹ which is a common problem in the conventional method. The first step in the mechanism involves the formation of 2-bromo-5-chloromagnesium-3-hexylthiophene monomer **2.17**, which is generated *in situ* from 2,5-dibromo-3-hexylthiophene **2.16**. It reacts with Ni(propene-1,3-diylbis(diphenyl-phosphane))Cl₂ (Ni(dppp)Cl₂), yielding organonickel intermediate **2.18** (Scheme 2.16).⁸⁰ The dimer **2.19** obtained from reductive elimination then undergoes

fast oxidative addition to the nickel center to yield intermediate **2.20**. Subsequently, growth of the polymer chain occurs by insertion of one monomer at a time as shown in the reaction cycle.

By adopting the polymerization route, good overall yields of the final product, which were not achieved in the case of small molecule synthesis, can be obtained. Additionally, a greater proportion of alkyl chains are incorporated onto the polymer backbone, which improves solubility. However, due to the very nature of polymerization reactions, some PD is necessarily introduced, resulting in a statistic molecular weight distribution. The dispersed molecular weight distribution complicates the determination of the exact chemical structure of the product and will affect the supramolecular self assembly process. Therefore, a short oligothiophene (O3HT) of *ca.* 10 monomer units was envisaged to be a good compromise between the electronic properties of the molecule and small PD.



Scheme 2.16. The mechanism of Ni-catalyzed polymerization.

Short O3HT chains **2.23** were prepared by Grignard metathesis (GRIM) polymerization as mentioned above. Residual bromide end groups were then reduced by LiAlH_4 to afford “uncapped” O3HT chains, which were further derivatized by Vilsmeier-Haack formylation⁸¹ to give α,ω -diformyl O3HT chains. Different formylation reagents and conditions were tested in order to prevent formylation on the O3HT backbones (Table 2.2). The condition in Table 2.2-entry 6 was adopted to synthesize α,ω -diformyl O3HT, which gave a backbone:terminal (formyl proton) ratio = 14:1 as judged from the NMR spectrum, and ~100% conversion. The proton positions are indicated in Figure 2.5.

Table 2.2. Formylation condition tested to synthesize α,ω -diformyl O3HT. Equivalents were based on $M \sim 1700 \text{ gmol}^{-1}$ for the O3HT chain.

	POCl_3 (eq.)	DMF (eq.)	TFMSA ^a (eq.)	<i>N</i> -methylanilide (eq.)	Condition	Formylation ^c	Conversion (%)
1	40	40	-	-	DCE Reflux	-	-
2 ^b	30	30	-	-	DCE Reflux	13.5:1	75
3	700	700	-	-	DCE Reflux	no backbone formylation	31
4 ⁸²	-	-	700	700	DCM 28°C	4.4:1	90
5 ⁸²	-	-	700	700	DCM 0°C	11:1	75
6 ⁸¹	700	-	-	700	Toluene 75°C	14:1	~100

a: Trifluoromethanesulfonic anhydride, b: POCl_3 was distilled, c: the ratio is backbone formyl proton:terminal formyl proton. DCE: dichloroethane, DCM: dichloromethane.

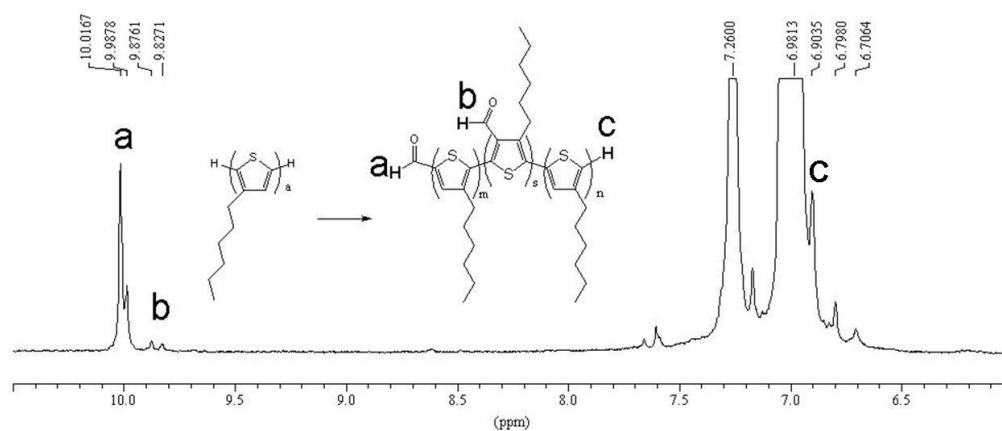
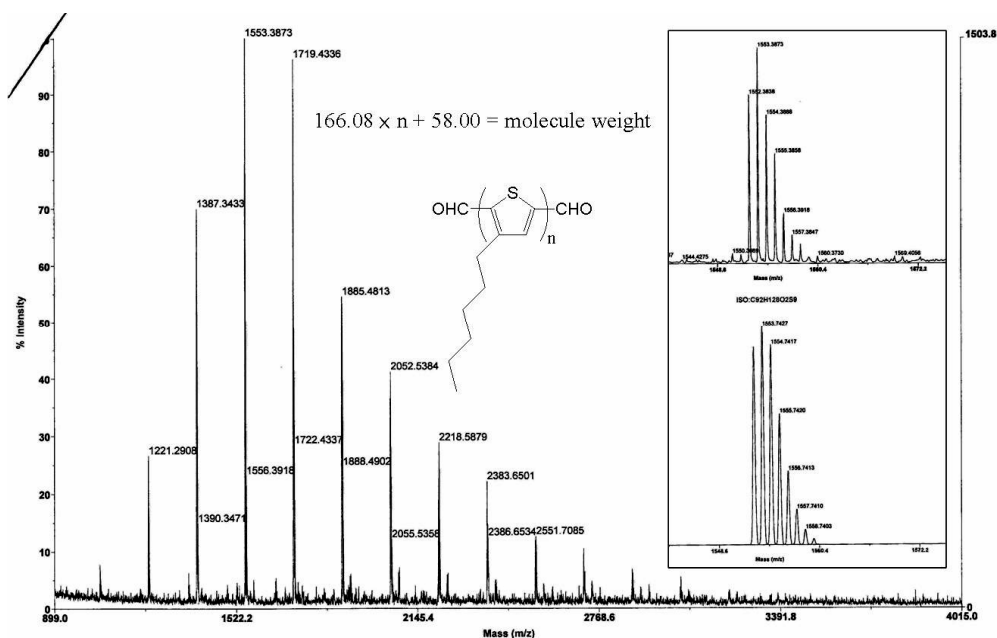
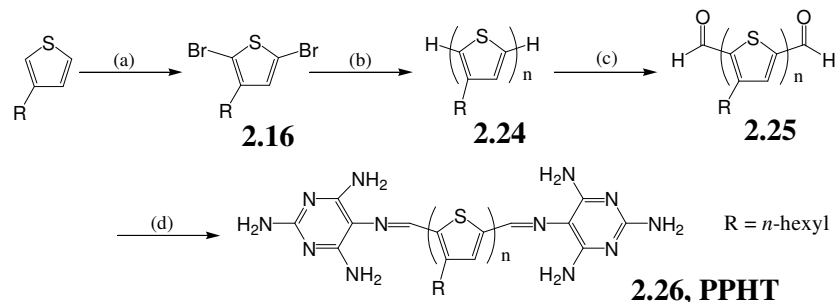


Fig. 2.5. Chemical shifts of protons on: (a) terminal formyl, (b) backbone formyl groups and (c) unreacted terminal positions.

The degree of polymerization (DP) was controlled by adjusting the dose of nickel catalyst.⁸³ One part of Ni(dppp)Cl₂ to 10 parts of monomer was used to obtain O3HT of DP ~ 10. The resulting O3HT was determined by matrix-assisted laser desorption/ionization mass (MALDI-ms) spectroscopy which gave the number-averaged molecular weight (M_n) of O3HT to be 1670 gmol⁻¹ (estimated DP ~ 10) and PDI = 1.12. α,ω -diformyl O3HT has M_n = 1595 gmol⁻¹ and a lower PDI (1.07, Figure 2.6).



proton source for the condensation. A few drops of DMSO are added to partially dissolve 2,4,5,6-tetraaminopyrimidine sulfate.



Scheme 2.17. Reagents and conditions: (a) NBS, $\text{CHCl}_3/\text{AcOH}$, reflux, 2h, 85%; (b) *i*-PrMgCl, 30°C, 3h; *ii*: Ni(dppp)Cl₂, THF, 2h; *iii*: LiAlH₄, overnight, 40%; (c) POCl₃, *N*-methylformanilide, toluene, 75°C, 24h, 62%; (d) 2,4,5,6-tetraaminopyrimidine sulfate, K₂CO₃, DMSO/ODCB /EtOH, 3d, 75%.

Table 2.3. The reaction conditions tested in the Schiff base formation.

	Solvent (v/v)	Melamine (eq.)	base (eq.)	dehydrant	DMSO (mL)	conversion (reflux for days)
1	EtOH/THF (2/1)	20	K ₂ CO ₃ (30)	K ₂ CO ₃	0.5	19.4% (6)
2	IPA	40	K ₂ CO ₃ (60)	K ₂ CO ₃	0.5	14.7% (8)
3	EtOH/DCM (1/1)	40	K ₂ CO ₃ (60)	K ₂ CO ₃	0.5	20% (3)
4	EtOH/THF (2/1)	50	Et ₃ N (100)	MgSO ₄	0.5	no reaction (3)
5	EtOH/DCM (6/1)	40	K ₂ CO ₃ (60)	MgSO ₄	0.5	10.2% (5)
6	EtOH/DCM (10/1)	200	K ₂ CO ₃ (300)	K ₂ CO ₃	1.0	6.7% (4)
7	EtOH/DCM (6/1)	40	Na ^t BuO (60)	K ₂ CO ₃	0.5	30% (5)
8	EtOH/toluene (1/1)	40	K ₂ CO ₃ (60)	K ₂ CO ₃	0.5	26% (2)
9	KOH(aq) 5%	40	KOH	-	-	no reaction (2)
10	HCl(aq)	40	-	-	-	no reaction (2)
11	EtOH/DCM (1/1)	40	NH(<i>i</i> -pr) ₂ (5mL)	K ₂ CO ₃	5.0	no reaction (3)
12	EtOH/DCE (1/1)	40	K ₂ CO ₃ (60)	K ₂ CO ₃	0.5	84% (7)
13	EtOH/chlorobenzene (1/1)	40	K ₂ CO ₃ (60)	K ₂ CO ₃	0.5	95% (5)

THF: tetrahydrofurane

In the NMR spectra of PPHT, two peaks at 4.51 and 4.75 ppm replace the peaks at 9.89 and 10.01 corresponding to the formyl protons (Figure 2.7).

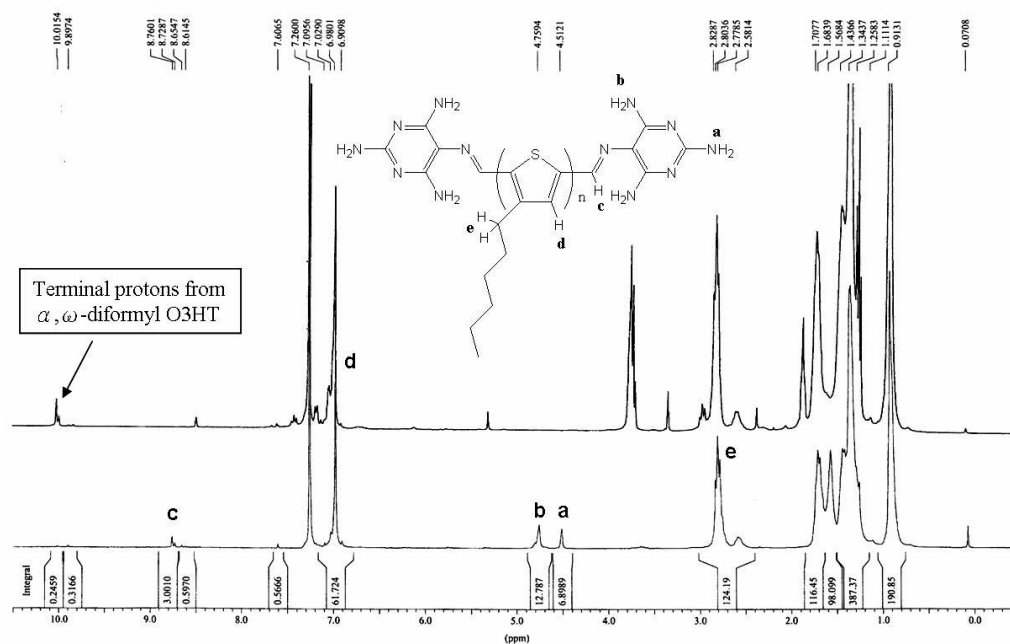


Fig. 2.7. NMR spectra of PPHT overlapped with the α,ω -diformyl O3HT spectra.

After condensation of the melamine end groups, a brittle solid was obtained after drying, which differs from the soft and adhesive parent dihydro or diformyl O3HT solid. The difference in the physical appearance is attributed to the existence of H-bonding between the terminal melamine groups which provide additional interactions between O3HT chains.

Thermal gravimetric analysis (TGA) showed that PPHT possesses high thermal stability, up to 400°C under nitrogen atmosphere (Figure 2.8).

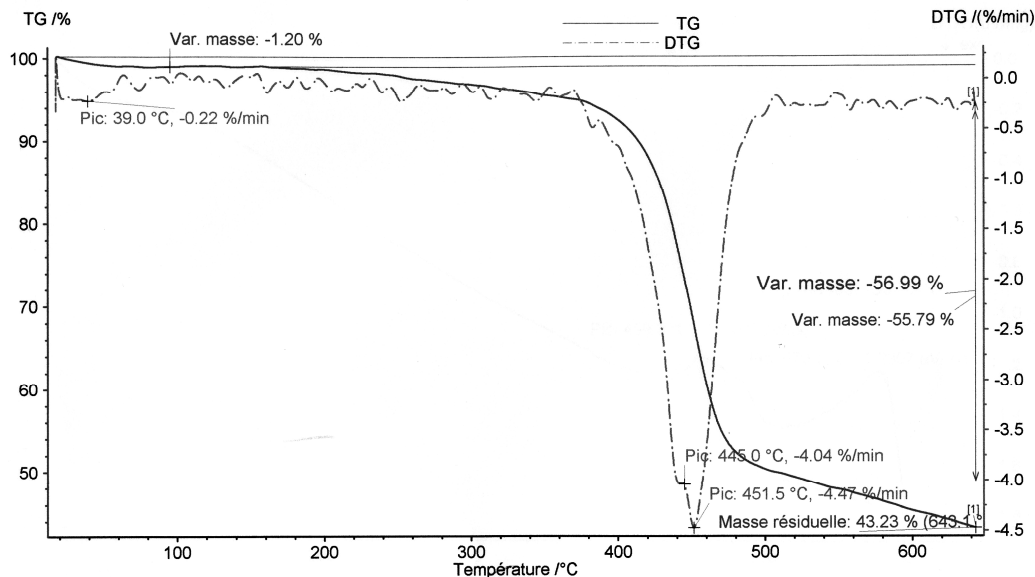


Fig. 2.8. Thermal gravimetric analysis (TGA) of PPHT under nitrogen atmosphere. Solid line: thermal gravimetric analysis, dot-dash line: differential thermal gravimetric analysis.

Electrochemical studies show that PPHT possesses an oxidation onset at 0.22 V (vs. Fc/Fc^+ , 0.1 M Bu_4NPF_6 in AcCN, Figure 2.9.a) in the cyclic voltammogram (CV), which is 0.20 V higher than commercial P3HT (0.02 V).⁸⁴ The optical band gap was calculated from the absorption onset (2.22 eV) in an electronic absorption spectrum (Figure 2.9.b). The energy levels of PPHT thus estimated from CV and optical absorption are shown in Figure 2.10.

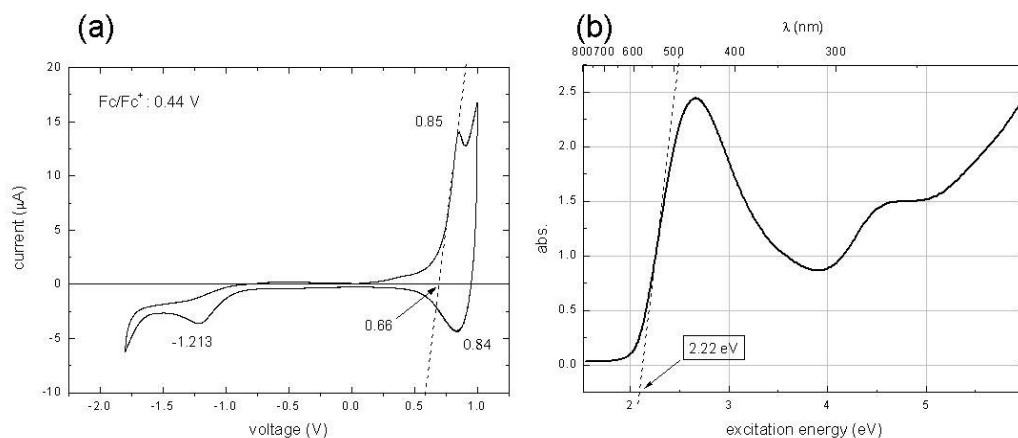


Fig. 2.9. (a) Cyclic voltammogram of PPHT on a platinum plate electrode in 0.1 M Bu_4NPF_6 , AcCN solution. The extrapolated oxidation onset (0.66 V) is used to estimate the energy of highest occupied molecular orbital (HOMO) level. (b) Optical absorption spectra of PPHT, the extrapolated absorption onset is 2.22 eV.

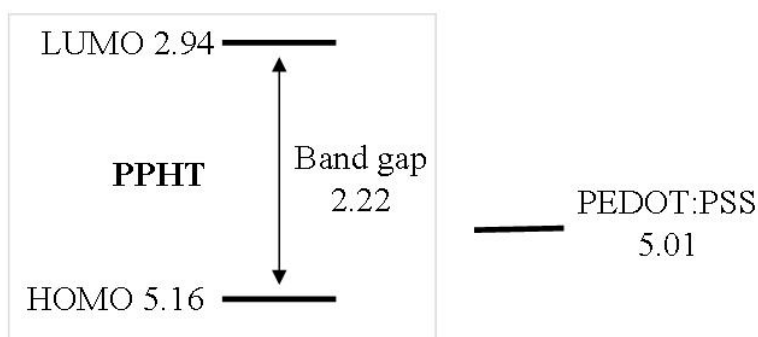
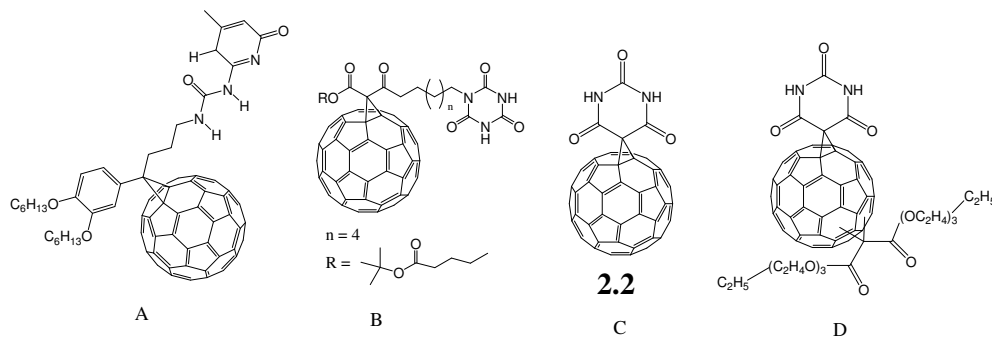


Fig. 2.10. The energy levels in eV of PPHT and PEDOT:PSS.

2.2.2 Syntheses of Acceptor

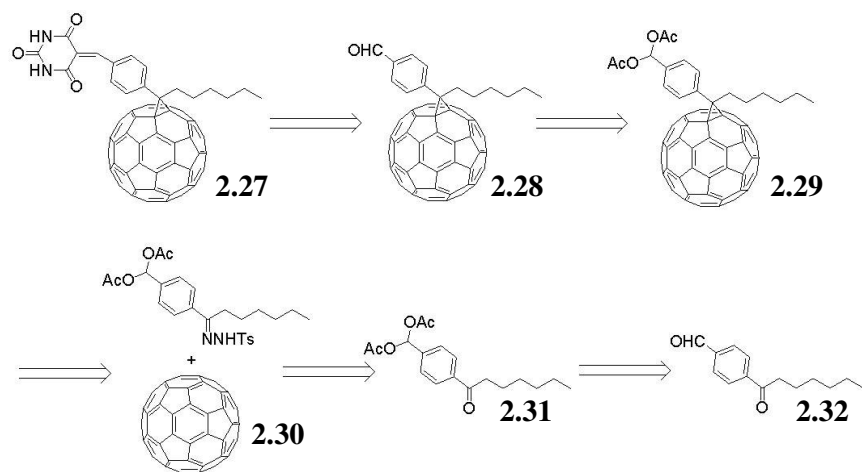
The discovery of fullerene *ca.* 25 years ago⁸⁵ has greatly impacted the area of donor-acceptor chemistry.⁸⁶ The superior electron affinity of C_{60} , which can accept up to 6 electrons, combined with its low reorganization energy makes this carbon allotrope an ideal electron acceptor.⁸⁷ The occurrence of fast photoinduced charge transfer between conjugated organic polymers and C_{60} has led to a vast body of research in photochemistry and photovoltaics.⁸⁸ Enhancement of the solubility of C_{60} in common organic solvents by chemical modification⁸⁹ has expanded its processability and allowed wider application. More recently, derivatives of C_{60}

bearing H-bonding recognition groups have been reported by several groups as possible bricks for supramolecular self-assembly (Scheme 2.18).



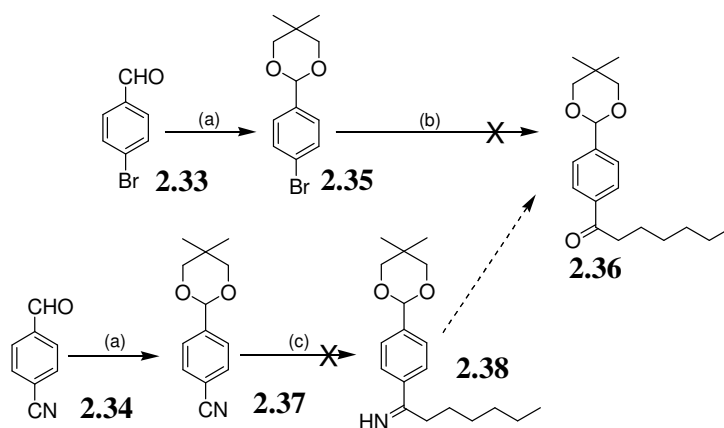
Scheme 2.18. Various C_{60} structures bearing H-Bonding groups synthesized by (A): Meijer's^{65(a), 90}, (B): Hirsch's⁹¹ and (C) Bassani's⁹² (D) Zhu's⁹³ group.

Compound **2.2** was used to investigate the effect of supramolecular interaction on the electronic properties of supramolecular architectures. It is conveniently prepared in one step (Scheme 2.11) and offers a rigid scaffold that controls the geometry during supramolecular synthesis. However, it possesses low solubility which makes the fabrication of solid state devices difficult. Additionally, the close proximity of carbonyl groups of the barbituric acid and the C_{60} cage induces bond strain in the bridging cyclopropane ring, thus decreasing the stability of **2.2** with respect to conventional Bingel adducts. A better linker between the C_{60} and the barbituric acid should have (1) sufficient rigidity to decisively determine the overall geometry, and (2) sufficient solubility provided by *e.g.* long alkyl chains or aromatic residues. An analogue **2.27** to PCBM bearing a barbituric acid group was therefore envisaged (Scheme 2.19).



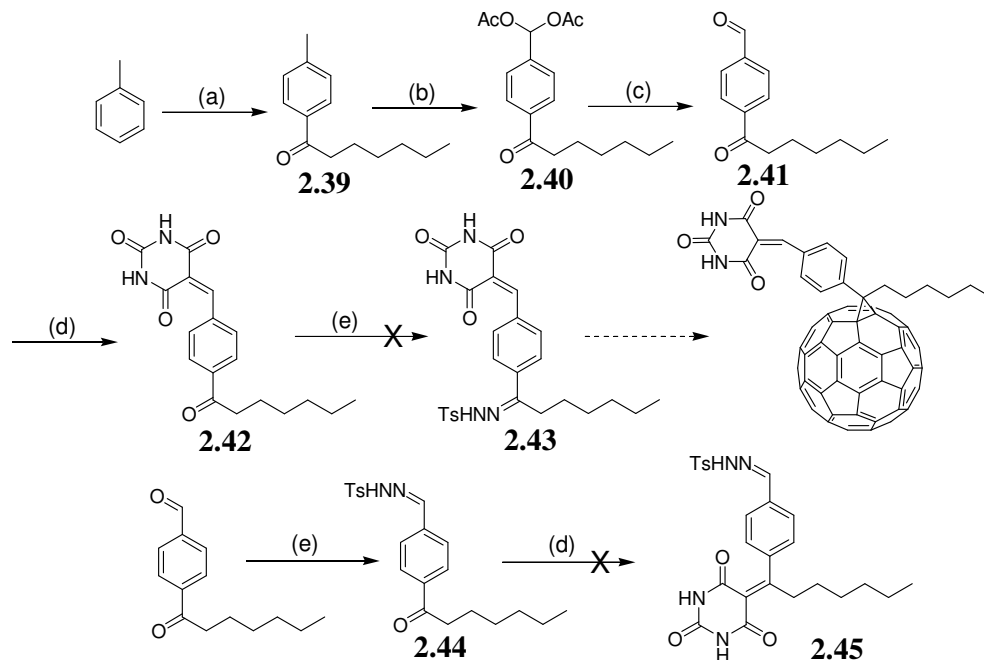
Scheme 2.19.

Compound **2.32** might be obtained from starting material **2.33** or **2.34**. In either route, the aldehyde group is first protected with 2,2-dimethyl-1,3-propanediol. Starting from **2.33**, the subsequent reaction of the Grignard reagent generated *in situ* with the corresponding electrophile gave only trace amounts of the desired benzophenone **2.36** (conversion: 7%), perhaps due to incomplete formation of the Grignard reagent. In the case of starting material **2.34**, the desired imine **2.38** could not be obtained from the nucleophilic addition of *n*-hexyl magnesium bromide to the imine group (Scheme 2.20).



Scheme 2.20. Reagents and conditions: (a) 2,2-dimethyl-1,3-propanediol, trifluoroacetic acid, toluene, 90°C, overnight, 96%; (b) *i*: Mg, ether, reflux, 2.5h; *ii*: heptanoyl chloride, ether, 95°C, overnight, (c) C₆H₁₃MgBr, THF, rt, overnight.

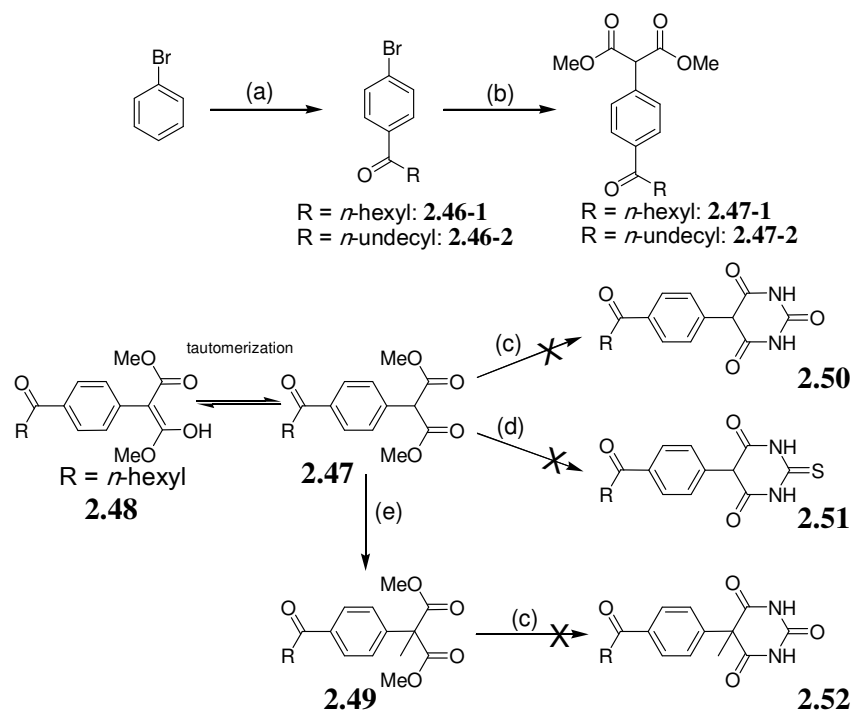
To overcome the difficulties encountered above, a different route for the transformation of two carbonyl groups was adopted (Scheme 2.21). Benzophenone **2.39** was obtained from toluene through Friedel-Craft acylation and oxidized at the benzylic position to afford protected benzaldehyde **2.40**. Functionalization of dicarbonyl **2.41** with barbituric acid yielded barbiturate **2.42** in 50% yield. In the next step, however, the carbene precursor **2.43** was not observed by NMR spectroscopy. Instead, the barbituric acid group was replaced, giving hydrazone **2.44**. The condensation of hydrazone **2.44** with barbituric acid was attempted, but without success.



Scheme 2.21. Reagents and conditions: (a) heptanoyl chloride, AlCl₃, neat, 100°C, 1h, 55%; (b) CrO₃, H₂SO₄, AcOH/AcOAc, 0-5°C, 3h, 20%; (c) TFA, H₂O/EtOH, reflux, overnight, 80%; (d) barbituric acid, H₂O/EtOH, rt, overnight, 59%; (e) *p*-toluenesulfonyl hydrazide, MeOH, reflux, overnight.

Substituted barbituric acids can be prepared by the condensation of the corresponding malonic acid derivatives with urea (Scheme 2.22). Malonate **2.47** was thus prepared from bromobenzene through Friedel-Craft acylation and Pt-catalyzed α -arylation.⁹⁴ During the following step involving the condensation of **2.47** with

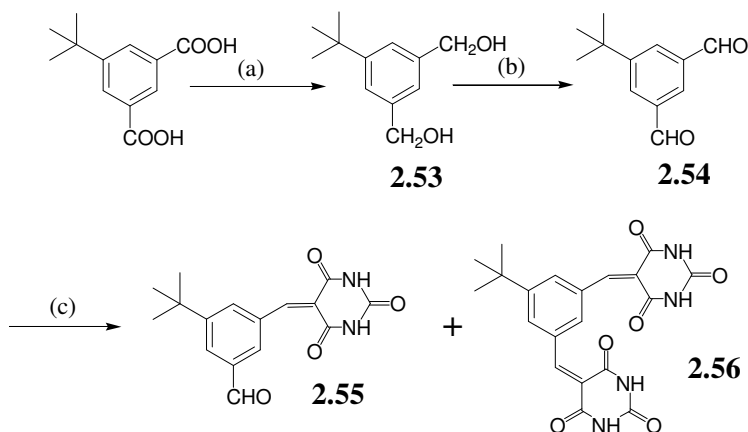
either urea or thiourea, no reaction took place. The lack of reactivity was initially attributed to tautomerization between **2.47** and **2.48**, where the enol tautomer is less reactive. Methylation of **2.47** was employed to replace α proton and block the tautomerization. Although the possibility of tautomerization was discarded, the condensation did not take place with the use of **2.49**.



Scheme 2.22. Reagents and conditions: (a) heptanoyl chloride or dodecanoyl chloride, CS_2 , AlCl_3 , reflux, 1h, 55%; (b) dimethyl malonate, K_3PO_4 , tri-*tert*-butylphosphine, $\text{Pd}(\text{dba})_2$, toluene, 70°C , overnight, 80%; (c) urea, base, EtOH, reflux, overnight; (d) thiourea, $t\text{-BuONa}$, DMSO, reflux, overnight; (e) NaH, iodomethane, THF, rt, reflux, overnight.

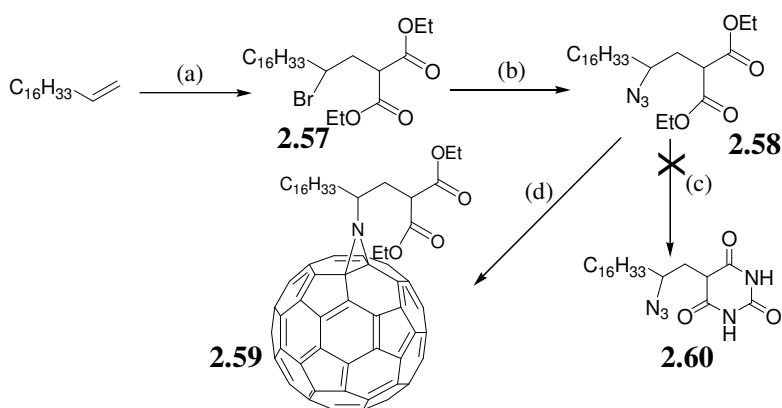
The use of bifunctional starting materials might simplify the complexity encountered in introducing functional groups stepwise. With this in mind, an *iso*-phthalaldehyde derivative was prepared and used to react with different equivalents of barbituric acid. The NMR showed both mono-substituted **2.55** and di-substituted **2.56** which could not be separated (Scheme 2.23). Furthermore, the mixture exhibited poor solubility which indicated that the solubility promoted by a

single *tert*-butyl group is probably not sufficient.



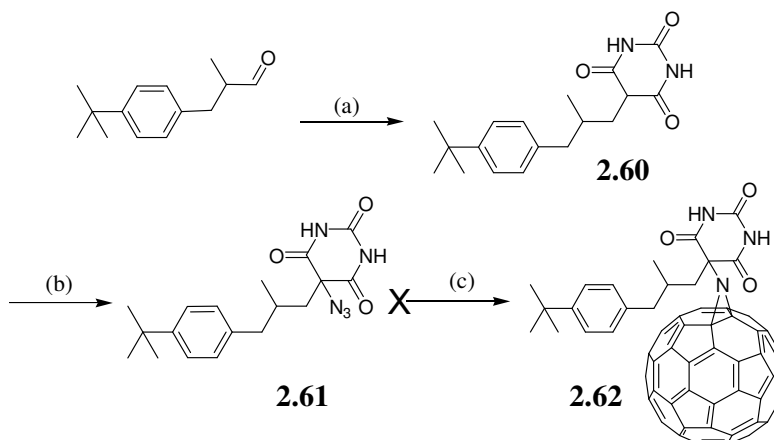
Scheme 2.23. Reagents and conditions: (a) $\text{BH}_3\text{-SMe}_2$, THF, 70°C , 2h, 80%, (b) pyridinium chlorochromate, celite, CH_2Cl_2 , rt, 36h, 90%, (c) barbituric acid, EtOH/ H_2O , piperidine, rt, overnight.

A difunctionalized long hydrocarbon chain **2.58** was prepared from *n*-octadecene by atom-transfer radical addition⁹⁵ followed by an $\text{S}_{\text{N}}2$ reaction with NaN_3 .⁹⁶ The solubility difference between the hydrophilic urea and the hydrophobic alkylated malonate **2.58** imposed difficulties in the ensuing condensation reaction (Scheme 2.24). Although trace amounts of the fullerene derivative **2.59** were observed by MALDI-ms spectroscopy, the low solubility still prevented large scale synthesis.



Scheme 2.24. Reagents and conditions: (a) α -bromoethylmalonate, H_2O , Et_3B , air, rt, 2.5h, 70%, (b) NaN_3 , H_2O , Aliquat[®] 336, 100°C , overnight, 93%, (c) barbituric acid, EtOH/ H_2O , piperidine, rt, overnight, (d) C_{60} , PhCl, reflux, 24h, trace.

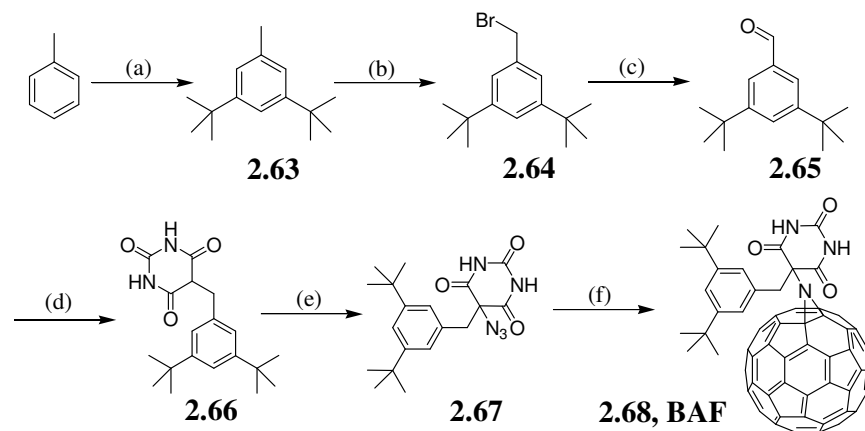
The solubility problems encountered in the various approaches described above suggested that the presence of both alkyl chains and aromatic groups will be necessary to efficiently promote the solubility of a fullerene barbituric acid derivative. Commercially-available lilyal was a good candidate to test the viability of this approach. The carbonyl group on lilyal was alkylated reductively with barbituric acid using Pt-C catalyst, followed by bromination and substitution to afford azido barbiturate **2.61** in 54% yield (Scheme 2.25). Although a *tert*-butylphenyl and a three carbon alkyl segment present in the barbiturate, this product **2.61** also exhibits low solubility in common organic solvents, which inhibited [3+2] cyclization reaction with C₆₀.



Scheme 2.25. Reagents and conditions: (a) barbituric acid, AcOH, Pt-C/H₂, rt, 3 d, 51%, (b) *i*: NBS, DMF, rt, overnight, *ii*: NaN₃, DMF, 50°C, 2h, 54%, (c) C₆₀, PhCl, reflux, 24h.

An aromatic ring with two *tert*-butyl groups was therefore prepared in order to enhance product solubility. It was obtained by Friedel-Craft alkylation of toluene to introduce two *meso tert*-butyl groups, followed by bromination to afford **2.64**. Previously-described methodology was then used in coupling with barbituric acid and subsequently formation of the azide precursor **2.67**. The resulting compound **2.67** possesses extraordinary solubility in most common organic solvents, and is even

soluble in pentane. The [3+2] cyclization onto fullerene, followed by nitrogen elimination proceeded smoothly and afforded a barbituric acid fullerene derivative **2.68** (BAF) with good solubility (Scheme 2.26). The structure of BAF was confirmed by MALDI-ms (Figure 2.11) and X-ray crystallography.



Scheme 2.26. Reagents and conditions: (a) 2-chloro-2-methylpropane, benzene, AlCl₃, rt, 8h, 40%, (b) NBS, benzene, benzoyl peroxide, reflux, 5h, 60%, (c) hexamethylenetetramine, MeOH/H₂O, reflux, 4h, 90%, (d) barbituric acid, toluene/AcOH, Pt-C/H₂, rt, 5 d, 85%, (e) *i*: NBS, DMF, rt, 4h, *ii*: NaN₃, DMF, 60°C, overnight, 92%, (f) C₆₀, PhCl, reflux, 2d.

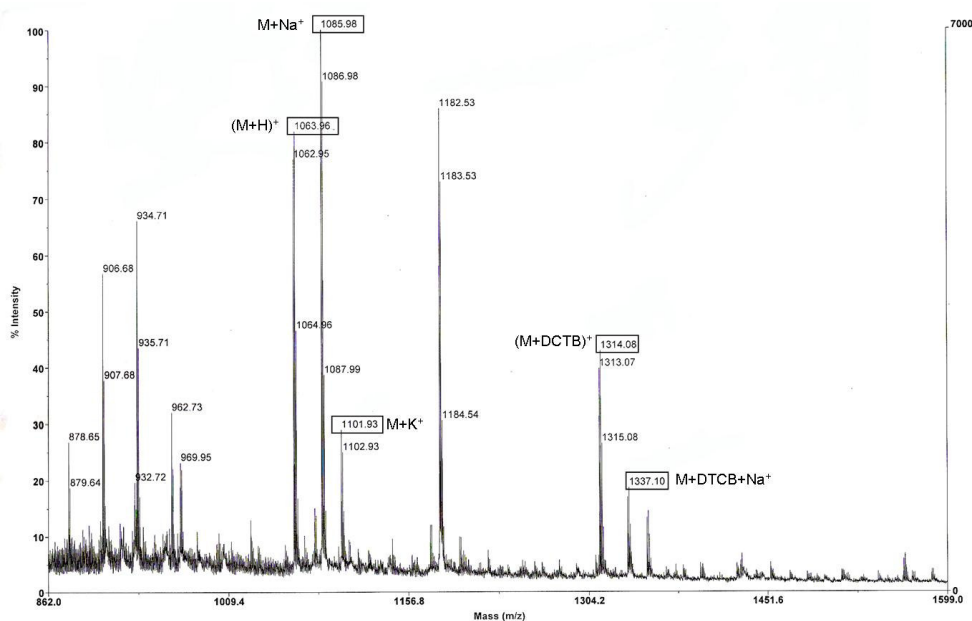


Fig. 2.11. The MALDI-ms measurement of BAF. M and DTCB represent BAF and the matrix (2-[(2E)-3(4-tert-butylphenyl)-2-methylprop-2-enylidene]malononitrile), respectively.

It has been reported that the formation of aziridine can take place on [5,6] or [6,6] junction of C_{60} after loss of diatomic nitrogen after thermolysis of the triazoline.⁹⁷ In the preparation of BAF, both isomers were observed in the NMR spectrum where two sets of protons on benzylic position and acetylacetamide nitrogen are present in a 1:1 ratio. These isomers were subjected to photoisomerization experiments and the isomer ratio was changed, but some decomposed product appeared which can not be purified. Thermal-gravimetric analysis showed that BAF is stable up to 90°C under nitrogen atmosphere (Figure 2.12). BAF exhibited two well defined reduction peaks at -1.21 V and -1.67 V (vs. Fc/Fc^+ , 0.1 M Bu_4NPF_6 in ODCB:AcCN = 2:1, Figure 2.13.a) and an optical band gap 2.89 eV (Figure 2.13.b). The energy levels of BAF estimated from CV and electronic absorption are shown in Figure 2.14.

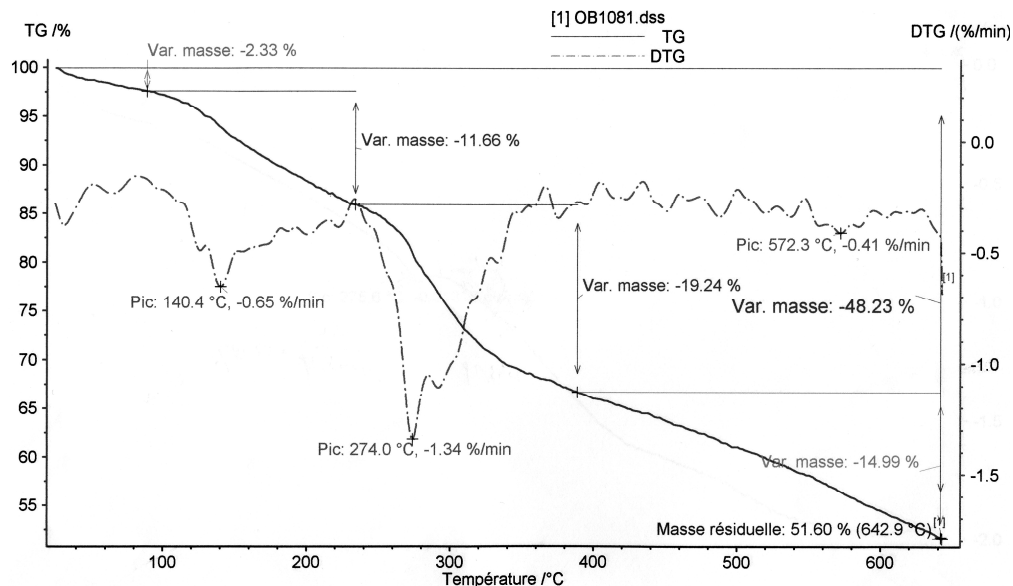


Fig. 2.12. Thermal gravimetric analysis (TGA) of BAF under nitrogen atmosphere. Solid line: thermal gravimetric analysis, dot-dash line: differential thermal gravimetric analysis.

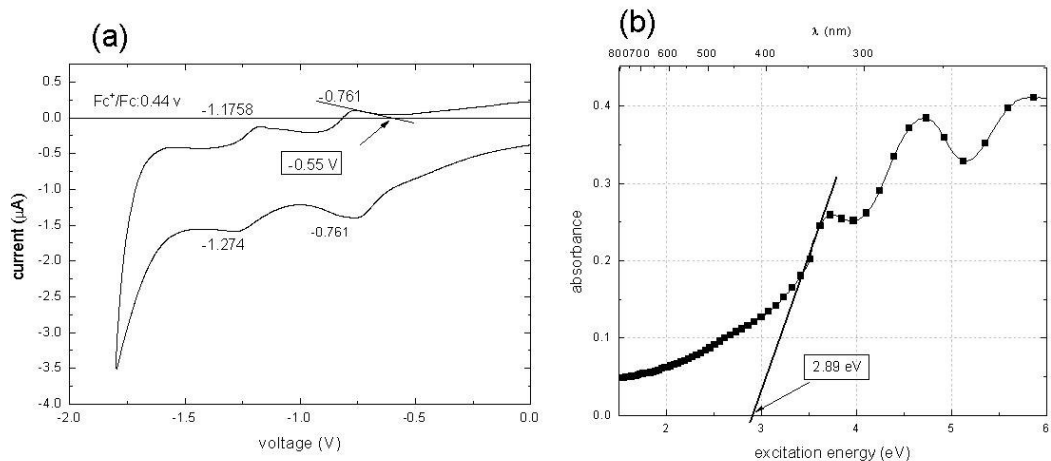


Fig. 2.13. (a) Cyclic voltammogram of BAF in 0.1 M Bu_4NPF_6 , AcCN/ODCB (1/2) mixture. The extrapolated reduction onset (-0.55 V) is used to estimate lowest unoccupied molecular orbital (LUMO) level. (b) Electronic absorption spectra of BAF, the extrapolated absorption onset is 2.89 eV .

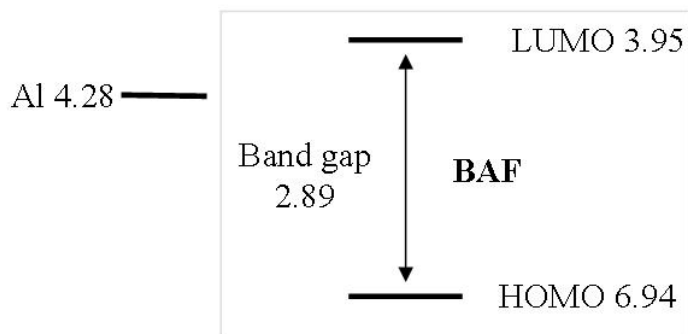
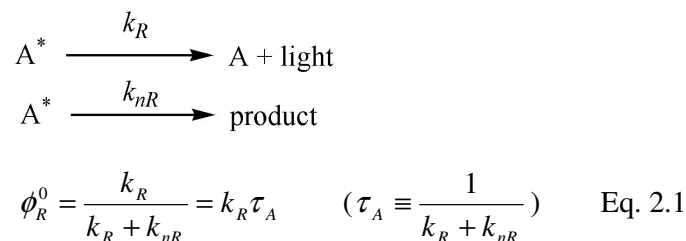


Fig. 2.14. The energy levels in eV of BAF and Aluminum electrode.

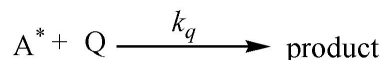
2.3 Supramolecular Effects on the Excited State Behavior of PHT and BAF

2.3.1 Quenching of PPHT Emission in Solution

An excited molecule (A^*) can be deactivated by emission of light or chemical reaction, or other photophysical process (*e.g.* internal conversion or intersystem crossing). The reaction efficiency of emissive relaxation (Φ_R) can be expressed in the following manner:



where k_R and k_{nR} represent the rate constant of the radiative and non-radiative pathways, respectively. In the presence of an added quencher, an additional deactivation pathway is introduced. The bimolecular rate constant, k_q describes the quenching process by quencher Q according to



In the presence of Q,

$$\phi_R = \frac{k_R}{k_R + k_{nR} + k_q [Q]} \quad \text{Eq. 2.2}$$

By recording the relative fluorescence intensity in the absence and present of added quencher, a straight line described by Equation 2.3 can be obtained, where the slope K_{sv} indicates the quenching efficiency.

$$\frac{\phi_R^0}{\phi_R} = \left(\frac{k_R}{k_R + k_{nR}} \right) \left(\frac{k_R + k_{nR} + k_q [Q]}{k_R} \right) = 1 + k_q \tau_A [Q] = 1 + K_{sv} [Q] \quad \text{Eq. 2.3}$$

The Stern-Volmer⁹⁸ constant (K_{sv}) of BAF or C_{60} as quenchers of excited PPHT was measured (Figure 2.15). To a PPHT solution in ODCB excited at λ_{ex} (475 nm) was added either BAF or C_{60} in ODCB and the maximum fluorescence intensity at 650 nm recorded. A 6-fold increased slope ($K_{sv} = 6.7 M^{-1}$ vs. $1.1 M^{-1}$) was found for BAF vs. C_{60} , respectively. The increased quenching efficiency can be attributed either to static quenching induced by H-bonds between PPHT and BAF molecules, or to the difference in the driving force for electron transfer quenching.

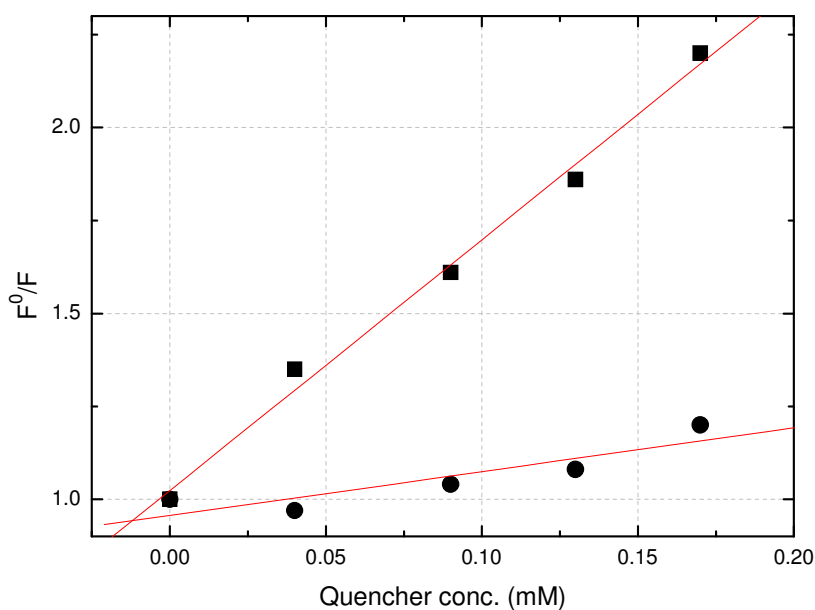


Fig. 2.15. Quenching of PPHT emission ($\lambda_{ex} = 475$ nm, $\lambda_{em} = 650$ nm) by BAF (■) and C_{60} (●).

In cases when the quenching process is static, the Stern-Volmer constant is equal to the binding constant for the species in solution. In non-polar solvents, the melamine-barbituric acid binding constant is *ca.* $10^2 M^{-1}$, that is much greater than the observed $K_{sv}(\text{BAF})$. According to the Rehm-Weller equation, the driving force for photoinduced electron transfer is given by:

$$\ln k_{ET} = -\frac{\Delta G_{ET}}{RT} \quad \text{Eq. 2.4}$$

$$\Delta G_{ET} = E(D^{*+} / D) - E(A / A^{*-}) - \frac{e^2}{\epsilon d'} - E^* \quad \text{Eq. 2.5}$$

where ΔG_{ET} is the free energy for electron transfer, and $E(D^{*+}/D)$ and $E(A/A^{*-})$ are the oxidation and reduction potential of the electron donor and acceptor, respectively, ϵ is the dielectric constant of the solvent, d' is the distance separating the donor and acceptor, and E^* is the energy of the excited donor or acceptor (in eV). Since $K_{sv} = k_q\tau_A$ (Equation 2.3), k_q of $1.29 \times 10^{10} \text{ M}^{-1}\text{s}^{-1}$ was calculated from observed K_{sv} (6.7 M^{-1}) and τ_A (0.52 ns, from single photon counting experiment in section 2.3.2), and this value is close to the range of diffusion limit. With Equation 2.3, the ratio of K_{sv} between BAF and C_{60} can be estimated as

$$\frac{K_{sv}(BAF)}{K_{sv}(C_{60})} = \frac{k_q(BAF)}{k_q(C_{60})} = 6.7 \quad \text{Eq. 2.6}$$

therefore,

$$RT \ln \left(\frac{k_q(BAF)}{k_q(C_{60})} \right) = \Delta G_{ET}(C_{60}) - \Delta G_{ET}(BAF) \quad \text{Eq. 2.7}$$

From Equation 2.7, the difference in free energy for electron transfer quenching between BAF and C_{60} is estimated to be 1 kcal/mol (0.04 eV per molecule), which is in agreement with the nearly identical reduction potential of C_{60} and BAF determined from cyclic voltammetry (-1.16 and -1.21 V vs. Fc/Fc^+ for C_{60} and BAF, respectively).⁹⁹ Therefore, the measured quenching efficiency of BAF is attributed to a greater ΔG_{ET} .

2.3.2 Time-Resolved Emission Spectroscopy

A Ti:Sapphire laser system emitting pulses of 30 fs at 800nm and at an 1 kHz repetition rate equipped with an optical parametric generator and frequency mixers was used to excite a PPHT solution in ODCB at $\lambda = 470 \text{ nm}$. The collected ps transient emission of PPHT solution in the forward direction is shown in Figure 2.16.a. The measured decay at $\lambda_{max} = 560 \text{ nm}$ could be fit to a three-exponential function,

with $\tau_1 = 76$ ps ($A_1 = 3962$), $\tau_2 = 407$ ps ($A_2 = 4532$) and $\tau_3 = 756$ ps ($A_3 = 1621$). These values are in agreement with those previously determined by single photon counting (SPC), considering that the 80 ps component is below the temporal resolution of the SPC instrument (Figure 2.16.c).

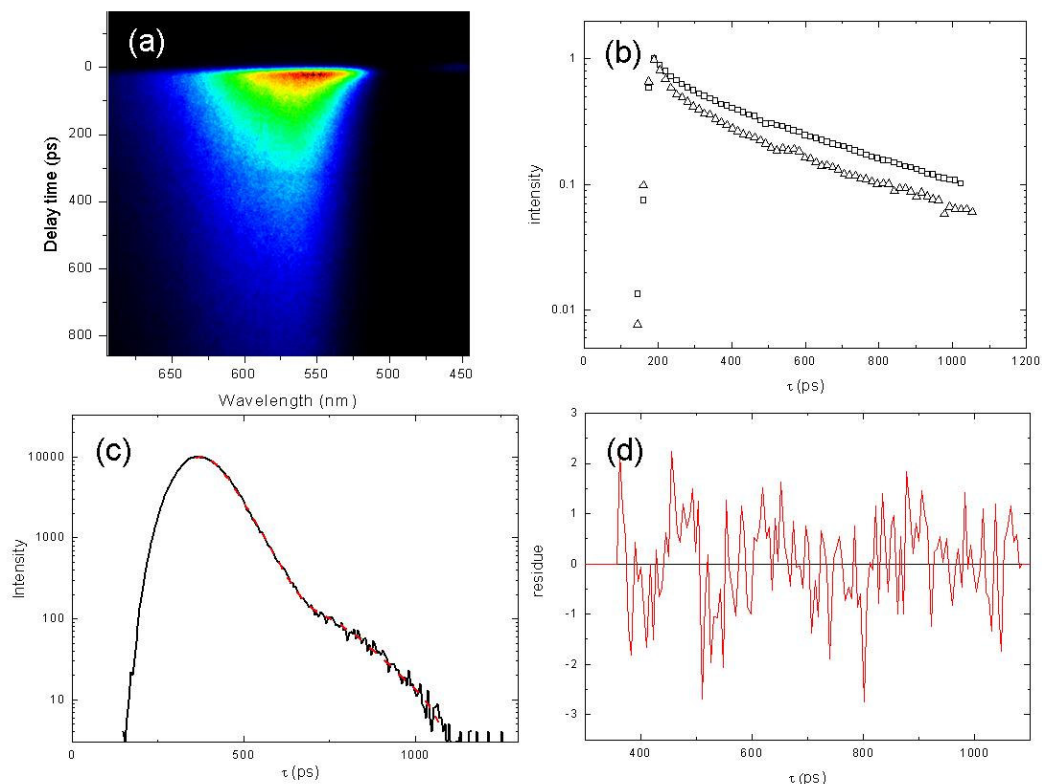


Fig. 2.16. (a) Picocond time-resolved emission spectra of PPHT, (b) normalized temporal evolution of fluorescence intensity at 560 nm of PPHT in the absence (□) and the presence of 2 equivalents (Δ) of BAF, (c) SPC temporal evolution of fluorescence of PPHT, $\tau_1 = 0.52$ ns ($A_1 = 0.13$), $\tau_2 = 0.98$ ns ($A_2 = 6.2 \times 10^{-4}$), $\chi^2 = 0.96$, Durbin-Watson Parameter = 1.6, (d) fitting residues of the measurement in (c).

2.3.3 Time-Resolved Absorption Spectroscopy

The solid state photophysical behaviors of PPHT and PPHT:BAF films coated on glass slides by drop-casting techniques were studied under ambient atmosphere. The films were excited at 470 nm according to the absorption maximum wavelength of

pristine PPHT film. The experiments were carried out using the pump-probe technique (Figure 2.17). The laser setup employed is described in section 2.3.2, but passes through a motor-driven optical delay line and then excites PPHT to its S_1 state. A white light continuum (390 nm – 1000 nm) generated from the laser pulse is used as a probe light. The absorption spectra were collected using a streak camera.

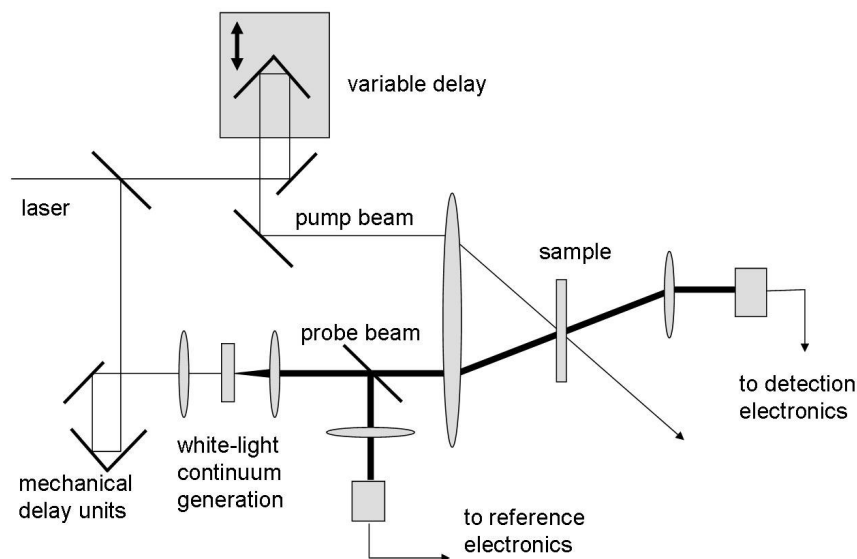


Fig. 2.17. Instrumental setup for pump-probe techniques.

In the case of pristine PPHT films (Figure 2.18.a), a broad absorption peak with $\lambda_{\max} \sim 850$ nm (fwhm = 0.39 eV) was found. This peak is assigned to the $S_n \leftarrow S_1$ transition, and appeared to be somewhat blue-shifted by *ca.* 50 nm from the reported value of $\lambda_{\max} = 900$ nm for P3HT films.¹⁰⁰ The transient absorptions at various delay times showed that the $S_n \leftarrow S_1$ absorption band decays rapidly within 10 ps (Figure 2.18.b). A bi-exponential decay was fitted with decay times of 5 ps and 380 ps (Figure 2.18.c). The two component decay is different from the reported single exponential decay (1.1 ns)¹⁰⁰ and may be due to different structure induced by the H-bonding on terminal melamine groups.

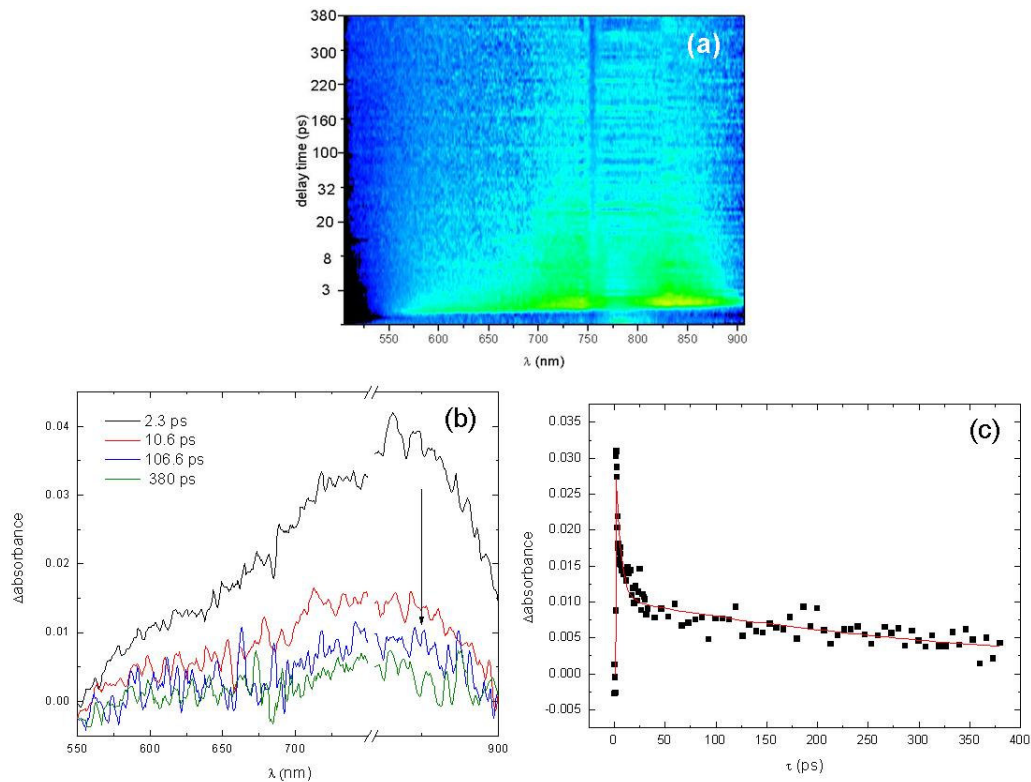


Fig. 2.18. (a) 2-dimensional time-resolved absorption spectra of PPHT film. (b) Transient absorption bands of PPHT film recorded at different delay time. (c) Transient absorption decay of PPHT film at 850 nm.

When BAF is present, the $S_n \leftarrow S_1$ absorption of PPHT was found to be totally suppressed, and a new band at 725 nm was observed (Figure 2.19.a). The transient absorption spectra at different delay times showed that a gradual decay of the broad peak was followed by a very slow decay which exceeded the time frame of measurement (Figure 2.19.c). The broad band at 725 nm was assigned to $PPHT^{*+}$ absorption band based on the previously reported spectra of P3HT.¹⁰¹ From this, it is concluded that the excitation of PPHT:BAF solid samples induces a charge transfer process whose rate exceeds the temporal resolution of the instrumentation (*ca.* 60 fs). As the separated charges drift away, the associated dipole moment is increased which screens the electric field in the illuminated area.¹⁰² The perturbed electric field induces a Stark effect in the absorption onset resulting in a broad peak spanning a

large portion of measuring window.¹⁰³ The absorption decay is fit to a two exponential equation with a short 16 ps and a long >3 ns components (Figure 2.19.c). The fast decay is assigned to geminate recombination, which accounts for approximate 50% of separated the charges based on the initial absorption intensity. The remaining 50% of charges persist on the nanosecond timescale.

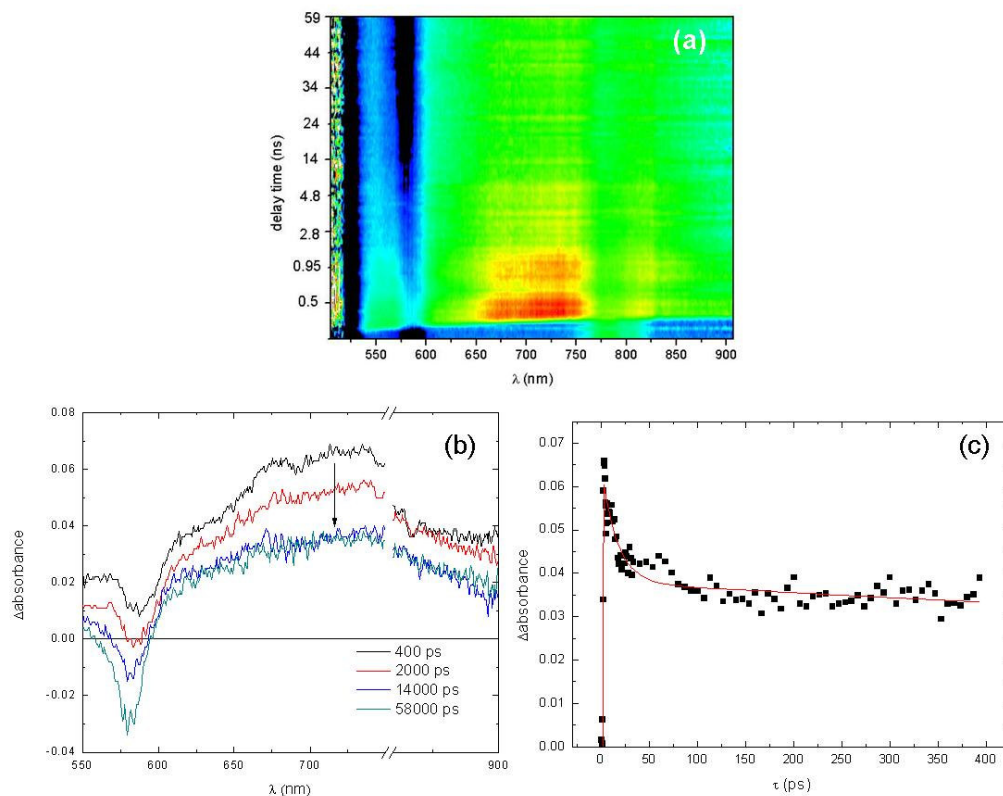


Fig. 2.19. (a) 2-dimensional time-resolved absorption spectra of PPHT:BAF film. (b) Transient absorption bands of PPHT:BAF film recorded at different delay time. (c) Transient absorption decay of PPHT:BAF film at 725 nm.

2.3.4 Supramolecular Photo-polymerization of Fullerene

Due to the unique physical properties of C_{60} , fullerene-based polymers drew much attention in the development of novel materials.¹⁰⁴ Initial research on supramolecular interactions to guide fullerene dimerization in dilute solution was reported to show an enhanced yield of dimerization only with a supramolecular

“template” possessing complementary H-bonds to fullerene derivatives (Figure 2.20).⁹²

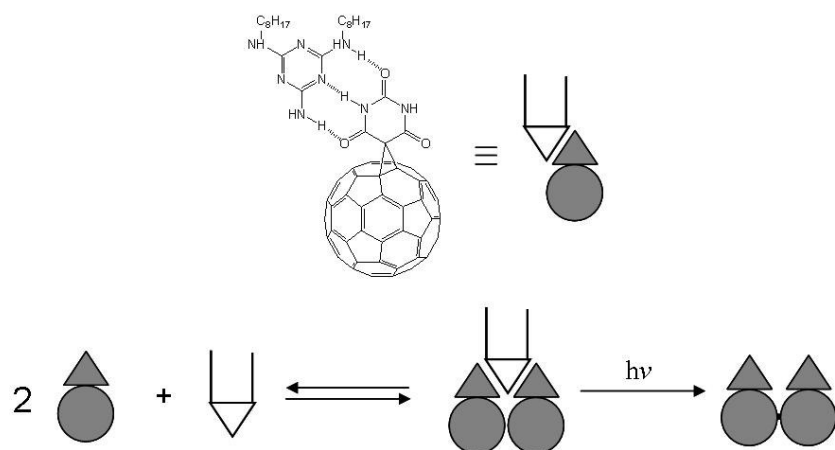
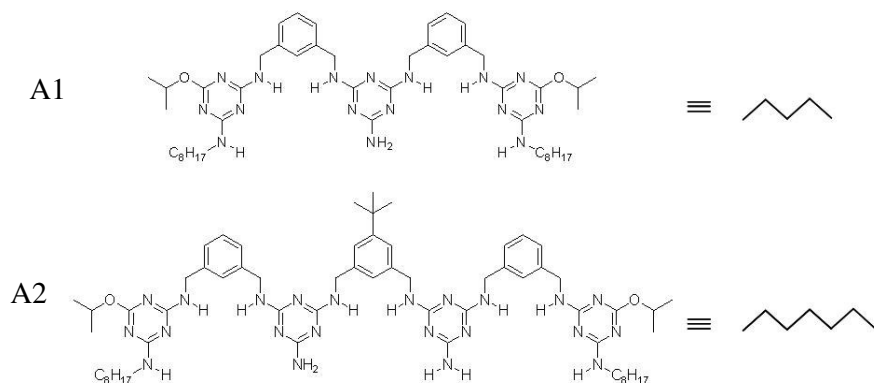


Fig. 2.20. Graphical presentation of dimerization of **2.2** with a supramolecular template possessing complementary H-bonding motifs.

The enhanced solubility of BAF compared to **2.2** may provide the possibility of extending the supramolecular approach to linear fulleropolymer comprising >2 fullerenes. Polymerization experiments of BAF were thus conducted in the presence of two new supramolecular templates (A1 and A2) designed to linearly constrain two or three molecules of BAF (Scheme 2.27).



Scheme 2.27. Fused Hamilton type acceptors

To test the propensity of A1 and A2 to promote the dimerization or trimerization

of BAF, solutions (2×10^{-4} M) in degassed chlorobenzene containing 0.5 and 1/3 equivalent of acceptor A1 and A2, respectively, were prepared. After irradiation ($\lambda > 350$ nm), a small amount of BAF dimer was observed by MALDI-ms spectroscopy in the experiment with catalyst A1 (Figure 2.21). No dimerization took place in BAF-only control experiment or in the presence of A2. In the case of A1, it is postulated that two BAF modules were drawn in proximity by the two complementary recognition sites induced by H-bonding pairs, which facilitated the [2+2] cycloaddition of the two fullerenes. The low yield might be due to the poorly aligned fullerene moieties, which can adopt C_s or C_2 symmetry.

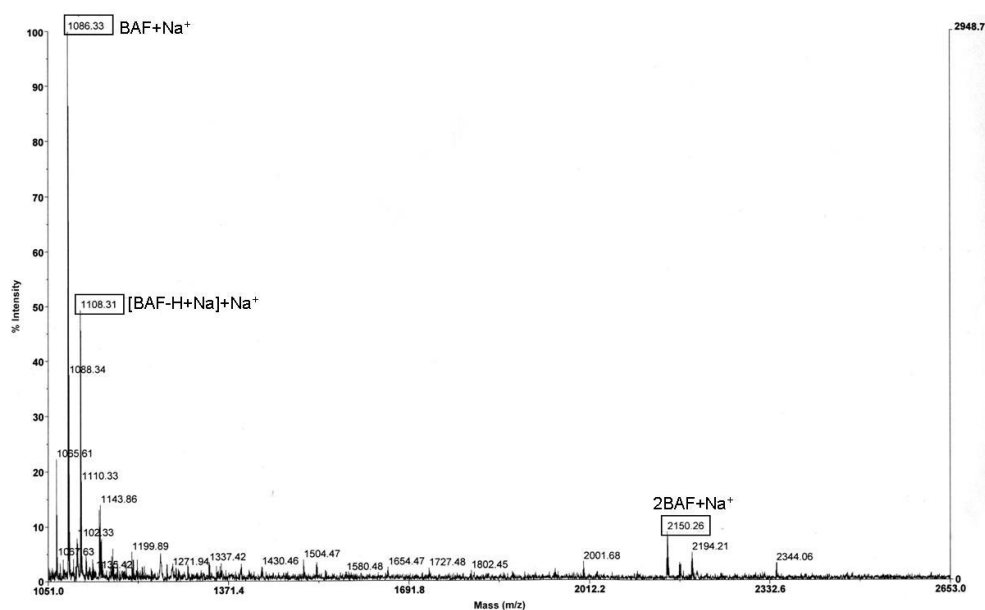
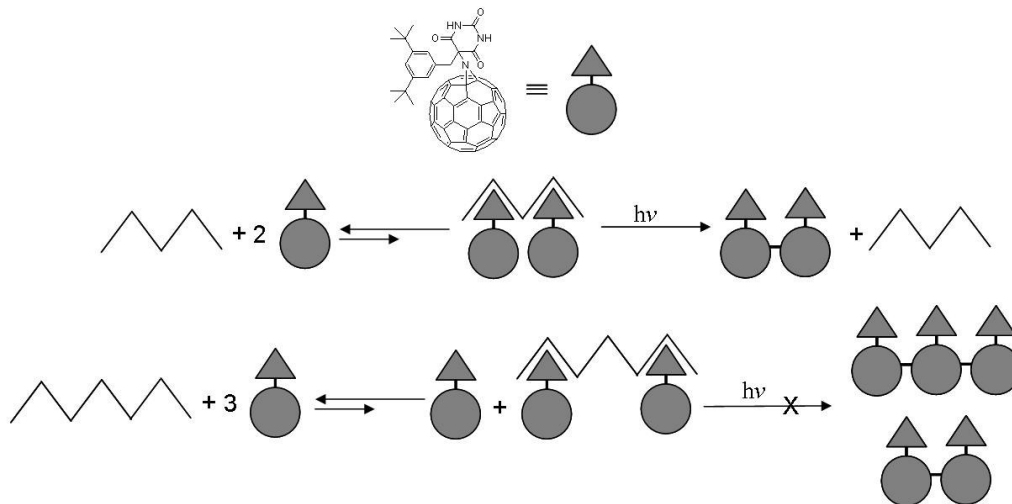


Fig. 2.21. MALDI-ms result of photodimerization of BAF with A1.

On the other hand, neither BAF dimer nor trimer was detected during the irradiation in the presence of A2. This may be due to the bulky di-*tert*-butylbenzyl group on BAF which disfavors binding in the central position. The first two BAF molecules may bind the two terminal sites rather than to the two neighboring sites in order to reduce geometric strain. The fitting of third BAF may then be too

energetically unfavored, and the spacing between BAFs remains too distant to allow photoinduced cycloaddition to occur (Scheme 2.28).



Scheme 2.28. Graphical presentation of the dimerization of BAF in the presence of A1 and A2.

2.3.5 BAF Crystal and Devices

Organic single crystals of conjugated compounds are of unusual interests not only for the fundamental study of charge transport properties,¹⁰⁵ but also for device application on the nanometer scale such as FET transistors owing to the absence of grain boundaries and defects.¹⁰⁶ Single crystals of BAF were obtained (by a slow diffusion of chloroform into a ODCB solution containing BAF and 10% DMSO) and revealed the molecular packing in the solid state. Two BAF molecules and two chloroform molecules are present in the unit cell (space group: P-1 Figure 2.22.a). The barbituric acid moieties are coplanar and inter-linked by two H-bonds which are assigned according to the distance between the oxygen atom of carbonyl group and the hydrogen atom of amide group on two BAF (1.92 Å, Figure 2.22.b).

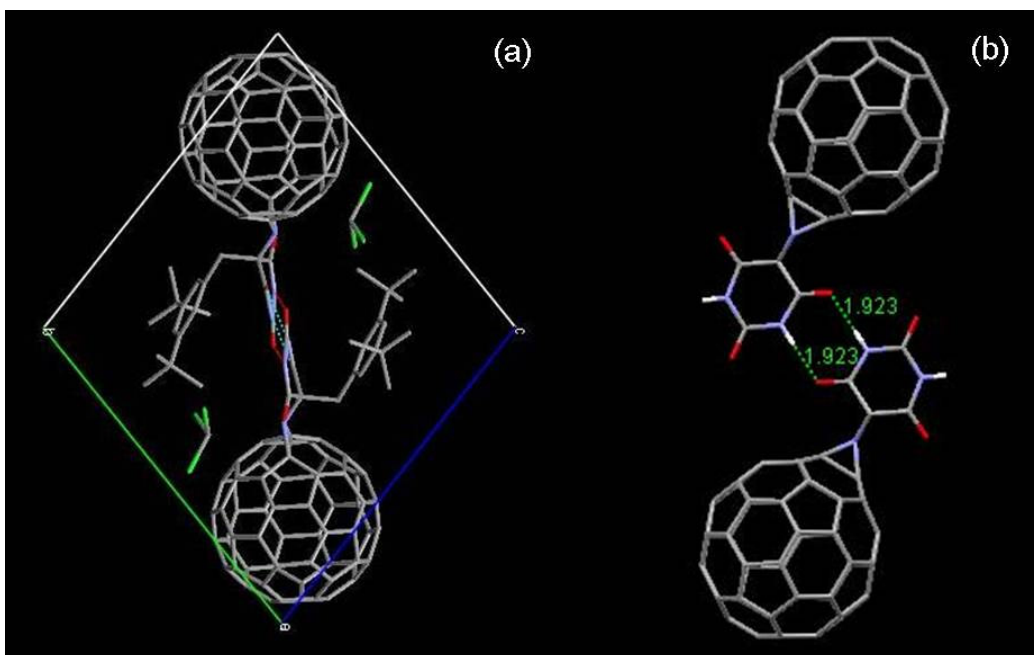


Fig. 2.22. (a) Capped stick representation of an unit cell of BAF viewed from *a* axis. Two chloroform (Cl: green) molecules are present in the unite cell. (b) The H-Bonds between oxygen (red) and hydrogen (white) are presented as green dots between neighboring BAFs, the di-*tert*-butylbenzyl group and chloroform molecules are omitted for clarity.

Along the *a* axis direction of the unit cell, the fullerenes are located on both sides of a barbituric acid H-bonded tape with a spacing of 3.38 Å (Figure 2.23.a). Along the *b* and *c* axes, the fullerenes are arranged in a zig-zag fashion with a spacing of ~ 3.37 Å (Figure 2.23.b). Such close alignment of C₆₀ moieties provides possible channels for electrons to be transported by hopping between neighboring fullerenes.

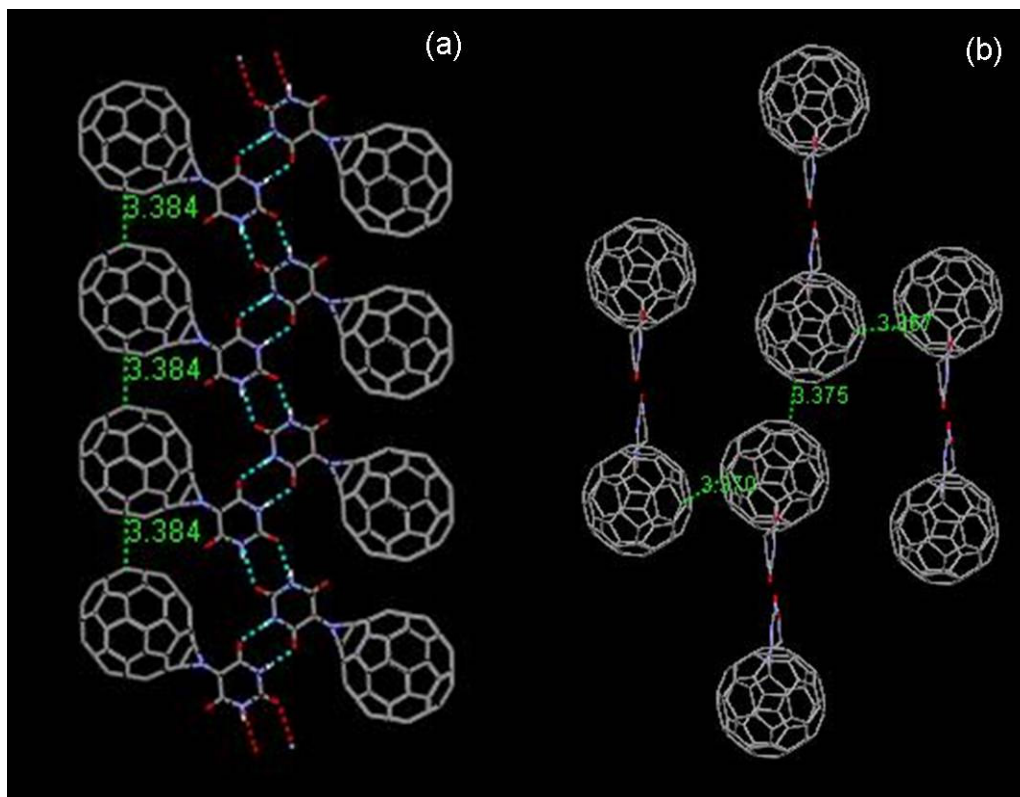


Fig. 2.23. Two possible pathways in BAF single crystal for electron transport on the direction (a) along *a* axis and (b) between *b* and *c* axes. The di-*tert*-butylbenzyl group and chloroform molecules are omitted for clarity.

Devices based on BAF single crystals were prepared in order to measure their conductive properties. Different patterns of Ca electrodes could be prepared by depositing Ca electrodes through a transmission electron microscopy grid placed on top of a BAF single crystal on substrates (Figure 2.24). The current characteristics obtained were close to the detection limit of instrument (10^{-12} A) and might be the consequence of inefficient electron injection due to poor energy level match on the organic-metal interface or misalignment between the applied electric field and the possible path for electron transport on fullerene moieties as shown in Figure 2.23. The optimization of device preparation is undergoing.

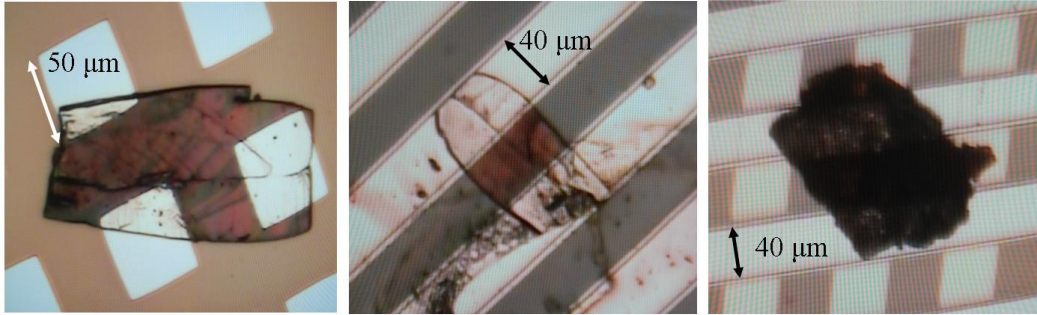


Fig. 2.24. Devices based on BAF single crystals with different Ca electrode (white squares and strips) geometry.

2.4 Conclusion

Small molecule donors, such as pentathiophene and heptathiophene, were synthesized but their low solubility and low overall yield prevent further fabrication of solid state PV cells. A controlled polymerization approach was thus adopted to afford O3HT with DP ~ 10. Further modification of O3HT gave α - ω -melamine-functionalized PPHT *via* Vilsmeier-Haack formylation and Schiff base formation sequentially. A fullerene derivative linked to barbituric acid, BAF, was obtained through synthetically simple reactions. The difficulties associated to the low solubility of the compounds, therefore, were resolved by obtaining PPHT and BAF.

The fluorescence of PPHT was quenched by BAF molecules in dilute solution and no prominent static quenching was observed due to the dilute concentration. In transient spectra, PPHT emission was quenched efficiently in solid state films and the absorption of $S_n \leftarrow S_1$ was replaced by the absorption of the PPHT^{•+} that decayed with two lifetimes, 16 ps and >3 ns.

The polymerization of BAF was tested with two supramolecular templates A1 and A2. Dimerization was observed due to the proximity induced by complementary H-bonding with A1. The lack of dimerization nor trimerization observed in the presence A2 is attributed to the steric strain preventing neighboring sites in A2 to bind BAF molecules.

BAF single crystals were obtained and the solid-state structure was determined by X-ray diffraction crystallography. Two BAFs and two chloroform molecules were found in a unit cell. Two possible transport pathways through neighboring BAFs for electrons were postulated in the crystal. Preliminary devices based on single crystals were prepared and the optimization of the device and measurement set-up is undergoing, with the aim of obtaining a FET on single crystal.

2.5 Reference

- 1 D. J. Cram, R. H. Bauer, *J. Am. Chem. Soc.* **1959**, *81*, 5971.
- 2 C. J. Pedersen, *J. Am. Chem. Soc.* **1967**, *89*, 7017.
- 3 B. Dietrich, J.M. Lehn and J.-P. Sauvage, *Tetrahedron Lett.* **1969**, *10*, 2885.
- 4 J.-M. Lehn, *Supramolecular Chemistry*, 1st ed., VCH, Weinheim, **1995**.
- 5 (a) N. O. Mchedlov-Petrossyan, L. N. Vilkova, N. A. Vodolazkaya, A. G. Yakubovskaya, R. V. Rodik, V. I. Boyko, V. I. Kalchenko, *Sensors* **2006**, *6*, 962. (b) F. Faridbod, M. R. Ganjali, R. Dinarvand, P. Norouzi, S. Riahi, *Sensors* **2008**, *8*, 1645. (c) M. Becuwe, D. Landy, F. Delattre, F. Cazier, S. Fourmentin, *Sensors* **2008**, *8*, 3689.
- 6 Z. Yang, G. Liang, B. Xu, *Acc. Chem. Res.* **2008**, *41*, 315.
- 7 A. R. Pease, J. O. Jeppesen, J. F. Sroddart, Y. Lou, C. P. Collier, J. R. Heath, *Acc. Chem. Res.* **2001**, *34*, 433.
- 8 S. Matile, H. Tanaka, S. Litvinchuk, *Top. Curr. Chem.* **2007**, *277*, 219.
- 9 A. Ben-Shem, F. Frolow, N. Nelson, *Nature* **2003**, *426*, 630.
- 10 B. Loll, J. Kern, W. Saenger, A. Zouni, J. Biesiadka, *Nature* **2005**, *438*, 1040.
- 11 G. Groth, E. Pohl, *J. Biol. Chem.* **2001**, *276*, 1345.
- 12 D. Stroebel, Y. Choquet, J.-L. Popot, D. Picot, *Nature* **2003**, *426*, 413.
- 13 K. Müller-Dethlefs, P. Hobza, *Chem. Rev.* **2000**, *100*, 143.
- 14 J. W. Steed, J. L. Atwood, *Supramolecular Chemistry*, 2nd Ed. Wiley & Sons, Chichester, **2009**.
- 15 C. T. Seto, G. M. Whitesides, *J. Am. Chem. Soc.* **1993**, *115*, 905.
- 16 J. Wouters, *Protein Sci.* **1998**, *7*, 2472.
- 17 J. L. Brédas, D. Beljonne, V. Coropceanu, J. Cornil, *Chem. Rev.* **2004**, *104*, 971.
- 18 G. D. Andreeti, R. Ungaro, A. Pochini, *J. Chem. Soc. Chem. Commun.* **1979**, *24*,

-
- 1005.
- 19 M. Berger, F. P. Schmidtchen, *Angew. Chem. Int. Ed.* **1998**, *37*, 2694.
- 20 V. Balzani, M. Gómez-López, J. F. Stoddart, *Acc. Chem. Res.* **1998**, *31*, 405.
- 21 J. Maier, *Physical chemistry of ionic materials: ions and electrons in solids*, J. Wiley Chichester, **2004**.
- 22 L. Senchez, M. Sierra, N. Martin, A. J. Myles, T. J. Dale, J. Rebek Jr., W. Seitz, D. M. Guldi, *Angew. Chem. Int. Ed.* **2006**, *45*, 4637.
- 23 G. R. Desiraju, *Angew. Chem. Int. Ed.* **1995**, *34*, 2311.
- 24 Z. Li, F. W. Fowler, J. W. Lauher, *J. Am. Chem. Soc.* **2009**, *131*, 634.
- 25 (a) N. C. Gianneschi, M. S. Masar, C. A. Mirkin, *Acc. Chem. Res.* **2005**, *38*, 825.
(b) S. Leininger, B. Olenyuk, P. J. Stang, *Chem. Rev.* **2000**, *100*, 853.
- 26 N. C. Gianneschi, S. T. Nguyen, C. A. Mirkin, *J. Am. Chem. Soc.* **2005**, *127*, 1644.
- 27 K. Schmidt, S. Barlow, A. Leclerc, E. Zojer, S.-H. Jang, S. R. Marder, A. K.-Y. Jen, J. L. Brédas, *J. Mater. Chem.* **2007**, *17*, 2944.
- 28 X. Jiang, X. Yang, C. Zhao, K. Jin, L. Sun, *J. Phys. Chem. C* **2007**, *111*, 9595.
- 29 S. E.-D. H. Etaiw, T. A. Fayed, N. Z. Saleh, *J. Photochem. Photobiol. A* **2006**, *177*, 238.
- 30 T. Edvinsson, C. Li, N. Pschirer, J. Scholneboom, F. Eickemeyer, R. Sens, G. Boschloo, A. Herrmann, K. Müllen, A. Hagfeldt, *J. Phys. Chem. C* **2007**, *111*, 15137.
- 31 S. Yao, U. Beginn, T. Gress, M. Lysetska, F. Würthner, *J. Am. Chem. Soc.* **2004**, *126*, 8836.
- 32 J. Xu, L. Wen, W. Zhou, J. Lu, Y. Guo, M. Zhu, H. Liu, Y. Li, L. Jiang, *J. Phys. Chem. C* **2009**, *113*, 5924.

-
- 33 J. Luo, Z. Xie, J. W. Y. Lam, L. Cheng, H. Chen, C. Qiu, H. S. Kwok, X. Zhan, Y. Liu, D. Zhu, B. Z. Tang, *Chem. Commun.* **2001**, 1740.
- 34 J. C. Ma, D. A. Dougherty, *Chem. Rev.* **1997**, 97, 1303.
- 35 J. P. Gallivan, D. A. Dougherty, *Proc. Natl. Acad. Sci. U.S.A.* **1999**, 96, 9459.
- 36 E. A. Meyer, R. K. Castellano, F. Diederich, *Angew. Chem. Int. Ed.* **2003**, 42, 1210.
- 37 J. S. Lamoureux, J. T. Maynes, J. N. Glover, *J. Mol. Biol.* **2004**, 335, 399.
- 38 C. A. Hunter, J. K. M. Sanders, *J. Am. Chem. Soc.* **1990**, 112, 5525.
- 39 (a) J. L. Brédas, J. P. Calbert, D. A. da Silva Filho, J. Cornil, *Proc. Natl. Acad. Sci. U.S.A.* **2002**, 9, 5804.
- 40 H. Yang, T. J. Shin, L. Yang, K. Cho, C. Y. Ryu, Z. Bao, *Adv. Func. Mater.* **2005**, 15, 671.
- 41 H. Sirringhaus, P. J. Brown, R. H. Friend, M. M. Nielsen, K. Bechgaard, B. M. W. Langeveld-Voss, A. J. H. Spiering, R. A. J. Janssen, E. W. Meijer, P. Herwig, D. M. de Leeuw, *Nature* **1999**, 401, 685.
- 42 H. J. Fell, E. J. Samuelsen, J. Als-Nielsen, G. Grtibel, J. Mårdalen, *Solid State Commun.* **1995**, 94, 843.
- 43 M. Bokvist, F. Lindström, A. Watts, G. Gröbner, *J. Mol. Biol.* **2004**, 335, 1039.
- 44 V. Balzani, A. Credi, F. M. Raymo, J. F. Stoddart, *Angew. Chem. Int. Ed.* **2000**, 39, 3349.
- 45 A. Credi, M. Venturi, *Cent. Eur. J. Chem.* **2008**, 6, 325.
- 46 A. I. Prikhodko, J.-P. Sauvage, *J. Am. Chem. Soc.* **2009**, 131, 6794.
- 47 L.-E. Perret-Aebi, A. von Zelewsky, C. Dietrich-Buchecker, J.-P. Sauvage, *Angew. Chem. Int. Ed.* **2004**, 43, 4482.
- 48 K. S. Chichak, S. J. Cantrill, A. R. Pease, S.-H. Chiu, G. W. V. Cave, J. L.

-
- Atwood, J. F. Stoddart, *Science* **2004**, *304*, 1308.
- 49 (a) M. J. Krische, J.-M. Lehn, In: M. Fujita, Editor, *Structure & Bonding*, Springer-Verlag, Berlin, **2000**, *96*, 3. (b) J. R. Fredericks, A. D. Hamilton, *Comprehensive Supramolecular Chemistry*; J.-M. Lehn Ed. Pergamon, New York, **1996**, Chapter 16.
- 50 (a) Y. Kyogoku, R. C. Lord, A. Rich, *Biochim. Biophys. Acta* **1969**, *179*, 10. (b) Y. Kyogoku, R. C. Lord, A. Rich, *Proc. Natl. Acad. Sci. U.S.A.* **1967**, *57*, 250. (c) T. J. Murray, S. C. Zimmerman, *J. Am. Chem. Soc.* **1992**, *114*, 4010.
- 51 (a) W. L. Jorgenson, J. Pranata, *J. Am. Chem. Soc.* **1990**, *112*, 2008. (b) J. Pranata, S. G. Wierschke, W. L. Jorgenson, *J. Am. Chem. Soc.* **1991**, *113*, 2810.
- 52 (a) V. Berl, M. Schmutz, M. J. Krische, R. G. Khoury, J.-M. Lehn, *Chem. Eur. J.*, **2002**, *8*, 1227. (b) F. J. M. Hoeben, P. Jonkheijm, E. W. Meijer, A. P. H. J. Schenning, *Chem. Rev.* **2005**, *105*, 1491.
- 53 A. P. H. J. Schenning, E. W. Meijer, *Chem. Commun.* **2005**, *26*, 3245.
- 54 J. H. K. K. Hirschberg, F. H. Beijer, H. A. van Aert, P. C. M. M. Magusin, R. P. Sijbesma, E. W. Meijer, *Macromolecules* **1999**, *32*, 2696.
- 55 (a) G. M. Whitesides, E. E. Simanek, J. P. Mathias, C. T. Seto, D. N. Chin, M. Mammen, D. M. Gordon, *Acc. Chem. Res.* **1995**, *28*, 37. (b) K. Ariga, T. Kunitake, *Acc. Chem. Res.* **1998**, *31*, 371. (c) P. Timmerman, L. Prins, *Eur. J. Org. Chem.* **2001**, 3191. (d) D. C. Sherrington, K. A. Taskinen, *Chem. Soc. Rev.* **2001**, *30*, 83.
- 56 (a) J. A. Zerkowski, G. M. Whitesides, *J. Am. Chem. Soc.* **1994**, *116*, 4298. (b) J.-M. Lehn, M. Mascal, J. Fischer, *J. Chem. Soc., Chem. Commun.* **1990**, 479. (c) L. J. Prins, P. Timmerman, D. N. Reinhoudt, *J. Am. Chem. Soc.* **2001**, *123*, 10153. (d) T. Kawasaki, M. Tokuhira, N. Kimizuka, T. Kunitake, *J. Am. Chem. Soc.* **2001**, *123*, 6792.

-
- 57 S. Yagai, T. Nakajima, K. Kishikawa, S. Kohmoto, T. Karatsu, A. Kitamura, *J. Am. Chem. Soc.* **2005**, *127*, 11134.
- 58 I. S. Choi, X. Li, E. E. Simanek, R. Akaba, G. M. Whitesides, *Chem. Mater.* **1999**, *11*, 684.
- 59 L. J. Prins, D. N. Reinhoudt, P. Timmerman, *Angew. Chem. Int. Ed.* **2001**, *40*, 2382.
- 60 (a) J.-F. Eckert, J.-F. Nicoud, J.-F. Nierengarten, S.-G. Liu, L. Echegoyen, F. Barigelletti, N. Armaroli, L. Ouali, V. Krasnikov, G. Hadziioannou, *J. Am. Chem. Soc.* **2000**, *122*, 7467 (b) P. A. van Hal, S. C. J. Meskers, R. A. J. Janssen, *Appl. Phys. A* **2004**, *79*, 41. (c) J. J. Apperloo, C. Martineau, P. A. van Hal, J. Roncali, R. A. J. Janssen, *J. Phys. Chem. A* **2002**, *106*, 21. (d) S. Romain, J.-C. Leprêtre, J. Chauvin, A. Deronzier, M.-N. Collomb, *Inorg. Chem.* **2007**, *46*, 2735. (e) L. C. Sun, L. Hammarstrom, B. Akermark, S. Styring, *Chem. Rev. Soc.* **2001**, *30*.
- 61 D. Gonzalez-Rodriguez, C. G. Claessens, T. Torres, S. Liu, L. Echegoyen, N. Vila, S. Nonell, *Chem. Eur. J.* **2005**, *11*, 3881.
- 62 A. P. H. J. Schenning, J. v. Herrikhuyzen, P. Jonkheijm, Z. Chen, F. Würthner, E. W. Meijer, *J. Am. Chem. Soc.* **2002**, *124*, 10252.
- 63 (a) P. A. Liddell, D. Kuciauskas, J. P. Sumida, B. Nash, D. Nguyen, A. L. Moore, T. A. Moore, D. Gust, *J. Am. Chem. Soc.* **1997**, *119*, 1400. (b) N. Martín, L. Sánchez, M. A. Herranz, D. M. Guldi, *J. Phys. Chem. A* **2000**, *104*, 4648.
- 64 P. A. van Hal, E. H. A. Beckers, S. C. J. Meskers, R. A. J. Janssen, B. Joussetme, P. Blanchard, J. Roncali, *Chem. Eur. J.* **2002**, *8*, 5415.
- 65 (a) E. H. A. Beckers, P. A. van Hal, A. P. H. J. Schenning, A. El-ghayoury, E. Peeters, M. T. Rispens, J. C. Hummelen, E. W. Meijer, R. A. J. Janssen, *J. Mater. Chem.* **2002**, *12*, 2054. (b) M. Segura, L. Sánchez, J. de Mendoza, N. Martín, D.

-
- M. Guldi, *J. Am. Chem. Soc.* **2003**, *125*, 15093.
- 66 N. D. McClenaghan, Z. Grote, K. Darriet, M. Zimine, R. M. Williams, L. De Cola, D. M. Bassani, *Org. Lett.* **2005**, *7*, 807.
- 67 V. Coropceanu, J. Cornil, D. A. De Silva Filho, Y. Olivier, R. Silbey, J.-L. Brédas, *Chem. Rev.* **2007**, *107*, 926.
- 68 (a) B. Servet, G. Horowitz, S. Ries, O. Lagorsse, P. Alnot, A. Yassar, F. Deloffre, P. Srivastava, R. Hajlaoui, P. Lang, F. Gamier, *Chem. Mater.* **1994**, *6*, 1809. (b) G. Horowitz, F. Garnier, A. Yassar, R. Hujhoui, F. Kouki, *Adv. Mater.* **1996**, *8*, 52.
- 69 R. J. Kline, M. D. McGehee, E. N. Kadnikova, J. Liu, J. M. J. Fréchet, *Adv. Mater.* **2003**, *15*, 1519.
- 70 G. Wang, J. Swensen, D. Moses, A. J. Heeger, *J. Appl. Phys.* **2003**, *93*, 6137.
- 71 J.-F. Chang, B. Sun, D. W. Breiby, M. M. Nielsen, T. I. Sølling, M. Giles, I. McCulloch, H. Sirringhaus, *Chem. Mater.* **2004**, *16*, 4772.
- 72 A. Zen, J. Pflaum, S. Hirschmann, W. Zhuang, F. Jaiser, U. Asawapirom, J. P. Rabe, U. Scherf, D. Neher, *Adv. Func. Mater.* **2004**, *14*, 757.
- 73 (a) C.-H. Huang, N. D. McClenaghan, A. Kuhn, J. W. Hofstraat, D. M. Bassani, *Org. Lett.* **2005**, *7*, 3409. (b) C.-H. Huang, N. D. McClenaghan, A. G. Bravicc, D. M. Bassani, *Tetrahedron* **2006**, *62*, 2050.
- 74 C. Ringenbach, A. De Nicola, Ziessel, *J. Org. Chem.* **2003**, *68*, 4708.
- 75 J. Krömer, P. Bäuerle, *Tetrahedron* **2001**, *57*, 3785.
- 76 A. Vilsmeier, A. Haack, *Chem. Ber.* **1927**, *60*, 119.
- 77 (a) J. Roncali, *Chem. Rev.* **1992**, *92*, 711. (b) R. D. McCullough, *Adv. Mater.* **1998**, *10*, 93.
- 78 R. D. McCullough, R. D. Lowe, *J. Chem. Soc. Chem. Commun.* **1992**, *1*, 70.

-
- 79 A. Yokoyama, R. Miyakoshi, T. Yokozawa, *Macromolecules* **2004**, *37*, 1169.
- 80 E. E. Sheina, J. Liu, M. C. Iovu, D. W. Laird, R. D. McCullough, *Macromolecules* **2004**, *37*, 3526.
- 81 J. Liu, R. D. McCullough, *Macromolecules* **2002**, *35*, 9882.
- 82 R. C Hiorns, A. Khoukh, B. Gourdet, C. Dagron-Lartigau, *Polymer Int.* **2006**, *55*, 608.
- 83 R. C. Hiorns, R. de Bettignies, J. Leroy, S. Bailly, M. Firon, C. Sentein, A. Khoukh, H. Preud'homme, C. Dagron-Lartigau, *Adv. Funct. Mater.* **2006**, *16*, 2263.
- 84 A. P. Zoombelt, M. A. M. Leenen, M. Fonrodona, M. M. Wienk, R. A. J. Janssen, *Thin Solid Film*, **2008**, *516*, 7176.
- 85 H. W. Kroto, J. R. Heath, S. C. O'Brien, R. F. Curl, R. E. Smalley, *Nature* **1985**, *318*, 162.
- 86 (a) M. Prato, *J. Mater. Chem.* **1997**, *7*, 1097. (b) Y. Chen, Z.-E. Huang, R.-F. Cai, B.-C. Yu, *Eur. Polym. J.* **1998**, *34*, 137. (c) E. Namura, H. Isobe, *Acc. Chem. Res* **2003**, *36*, 807. (d) F. Giacalone, N. Martín. *Chem. Rev.* **2006**, *106*, 5136.
- 87 Q. Xie, E. Perez-Cordero, L. Echegoyen, *J. Am. Chem. Soc.* **1992**, *114*, 3978.
- 88 N. S. Sariciftci, L. Smilowitz, A. J. Heeger, F. Wudl, *Science* **1992**, *258*, 1474.
- 89 (a) A. Hirsch, *The chemistry of the fullerenes*; Thieme, Stuttgart, **1994**. (b) F. Diederich, C. Thilgen, *Science* **1996**, *271*, 317. (c) S. Samal, S. K. Sahoo, *Bull. Mater. Sci.* **1997**, *20*, 141.
- 90 M. Wolffs, F. J. M. Hoeben, E. H. A. Beckers, A. P. H. J. Schenning, E. W. Meijer, *J. Am. Chem. Soc.* **127**, *39*, 13484.
- 91 F. Wessendorf, J.-F. Gnichwitz, G. H. Sarova, K. Hager, U. Hartnagel, D M. Guldi, A. Hirsch, *J. Am. Chem. Soc.* **2007**, *129*, 16057.

-
- 92 N. D. McClenaghan, C. Absalon, D. M. Bassani, *J. Am. Chem. Soc.* **2003**, *125*, 13004.
- 93 J. Zhuang, W. Zhou, X. Li, Y. Li, N. Wang, X. He, H. Liu, Y. Li, L. Jiang, C. Huang, S. Cui, S. Wang, D. Zhu, *Tetrahedron* **2005**, *61*, 8686.
- 94 N. A. Beare, J. F. Hartwig, *J. Org. Chem.* **2002**, *67*, 541.
- 95 H. Yorimitsu, H. Shinokubo, S. Matsubara, K. Oshima, K. Omoto, H. Fujimoto, *J. Org. Chem.* **2001**, *66*, 7776.
- 96 W. P. Reeves, M. L. Bahr, *Synthesis*, **1976**, 823.
- 97 J. Averdung, J. Mattay, *Tetrahedron* **1996**, *52*, 5407. (b) L. Ulmer, J. Mattay, *Eur. J. Org. Chem.* **2003**, 2933.
- 98 N. J. Turro, *Modern Molecular Photochemistry*, **1991**, California University Science Books, 246.
- 99 L. Echegoyen, L. E. Echegoyen, *Acc. Chem. Res.* **1998**, *31*, 593.
- 100 D. Grebner, M. Helbig, S. Rentsch, *J. Phys. Chem.* **1995**, *99*, 16991.
- 101 J. Piris, T. E. Dykstra, A. A. Bakulin, P. H. M. van Loosdrecht, W. Knulst, M. T. Trinh, J. M. Schins, L. D. A. Siebbeles, *J. Phys. Chem. C* **2009**, *113*, 14500.
- 102 V. Gulbinas, R. Kananavicius, L. Valkunas, H. Bäessler, *Phys. Rev. B* **2002**, *66*, 233203.
- 103 J. Cabanillas-Gonzalez, T. Virgili, A. Gambetta, G. Lanzani, T. D. Anthopoulos, D. M. de Leeuw, *Phys. Rev. Lett.* **2006**, *96*, 106601.
- 104 F. Giacalone, N. Martín, *Chem. Rev.* **2006**, *106*, 5136.
- 105 B. Moulton, M. J. Zaworotko, *Chem. Rev.* **2001**, *101*, 1629.
- 106 (a) C. Reese, Z. Bao, *Mater. Today* **2007**, *10*, 20. (b) I. N. Hulea, S. Fratini, H. Xie, C. L. Mulder, N. N. Iossad, G. Rastelli, S. Ciuchi, A. F. Morpurgo, *Nature Mater.* **2006**, *5*, 982.

3 Supramolecular Interaction Assisted Organic Photovoltaic Solar Cells

Supramolecular Interaction Assisted Organic Photovoltaic Solar Cells

3.1 Introduction

The first generation of organic solar cells was based on an organic layer sandwiched between two different metal electrodes (Figure 3.1).¹ The current was extracted by the potential difference induced by the asymmetric work functions of the two metal electrodes under light irradiation. However, due to the large exciton binding energy in organic semiconductors,² the difference in the work functions of the electrodes is usually not high enough to yield sufficient photoinduced charge generation. In addition, the exciton diffusion distance is short (~10 nm),³ and only excitons generated in the region close to the electrodes can afford separated charges that are collected. Despite these limits, a remarkable efficiency of 0.7% for merocyanine dyes was reported.⁴

In order to improve the efficiency of metal-insulator-metal-structured organic PV cells, the heterojunction bilayer (Figure 3.1) structure, where two separate layers for the electron and hole transporting organic materials are stacked between the electrodes are used, was introduced. At the interface between the electron and the hole transporting materials, electrostatic forces result from the difference in the electron affinity of the electron transporting material and the ionization potential of the hole transporting material. When this local electric field is strong enough to exceed the exciton binding energy, the excitons are dissociated into electrons and holes. However, bilayer heterojunction structured PV cells are also limited by the exciton diffusion length. The first high efficiency bilayer architecture solar cell achieved 1%, as reported by Tang in 1986.⁵

A thickness of *ca.* 100 nm for the active layer is usually required to absorb most

of the incident radiation. Considering that the exciton diffusion length is less than a few tens of nm, only a small fraction of the excitons can reach the interface and dissociate. This problem is alleviated by blending the electron donor and acceptor molecules to form a bulk (dispersed) heterojunction (B-H, Figure 3.1), in which the D and A molecules are intimately mixed in the active layer. The largely increased interfacial area resulting from the thorough dispersion of the material improves the probability that the excitons will dissociate into charges. In this approach, efficient charge separation can be achieved within the exciton lifetime, and geminate recombination is greatly reduced. For an optimal morphology, the electron D and A materials must be interpenetrated with a domain size close to the typical exciton diffusion length in the material.

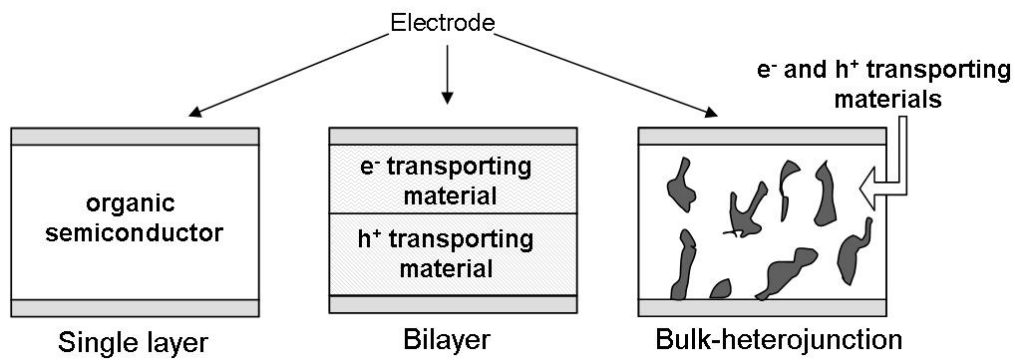


Fig. 3.1. Different structures employed in organic PV cells.

3.1.1 Working Principle

The process of converting light irradiation to electric current can be divided in four steps (Figure 3.2).

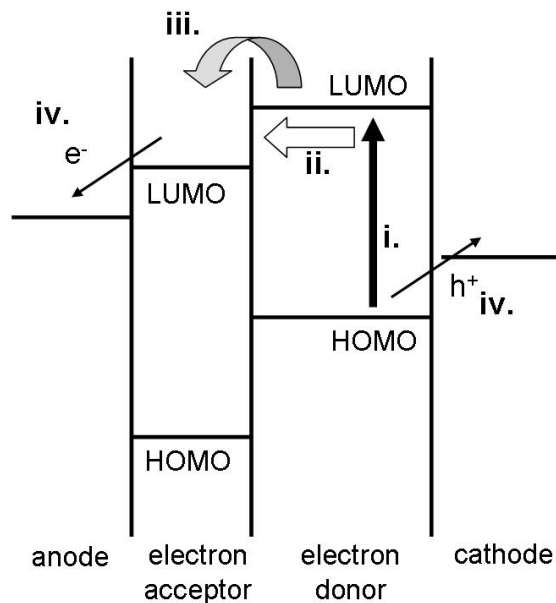


Fig. 3.2. The working principle of an organic solar cell. (i) exciton formation induced by photon absorption, (ii) exciton diffusion to the interface, (iii) charge separation between electron donor molecule and an electron acceptor molecule, (iv) charge transport to the corresponding electrodes.

The first step is exciton formation induced by photon absorption. Due to the high absorption (*ca.* 10^5 Au/cm^{-1} for solid films), π -conjugated polymers employed in organic PV cells absorb efficiently at their absorption maximum wavelength. However, the absorption bands of most conjugated polymers are relatively narrow compared to Si-based PV cells. For example, the optical band gap of P3HT is ~ 1.9 eV which corresponds to the absorption of only 30% of AM 1.5 solar photon flux (Figure 3.3).⁶

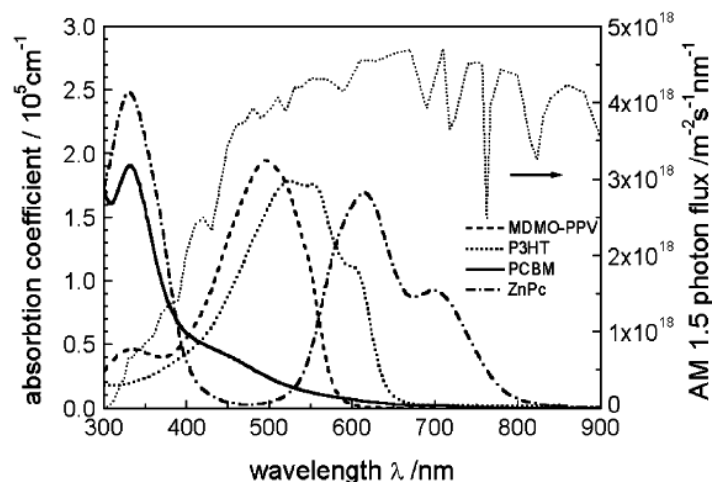
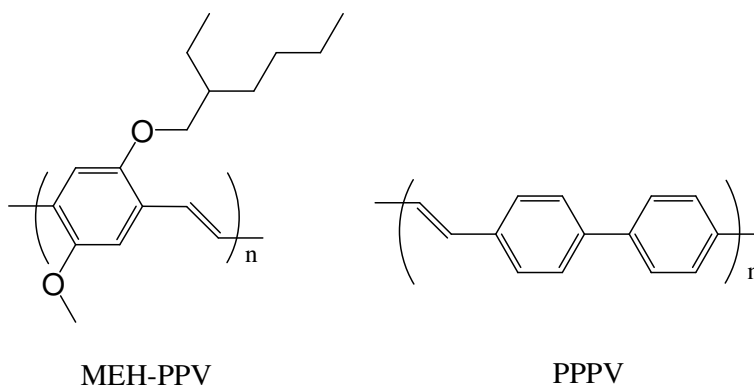


Fig. 3.3. The comparison between solar spectra and the electronic absorptions of MDMO-PPV (poly[2-methoxy-5-(3',7'-dimethyloctyloxy)-1,4-phenylene vinylene]), P3HT, PCBM and ZnPc (Zinc phthalocyanine)⁷.

Excitons are coulombically bound electron-hole pairs with a typical binding energy of several hundreds of meV² in organic materials. Compared to inorganic solar cell whose exciton binding energy is only in the meV range, this prevents spontaneous charge separation due to thermal energy at room temperature. For example, the exciton binding energies in MEH-PPV and poly(*p*-phenylphenylenevinylene) (PPPV) were determined to be 200 ~ 600 mV⁸ and 400 mV⁹ (Scheme 3.1), respectively, resulting in Frenkel type excitons¹⁰ which decreases the charge separation efficiency. It is estimated that only 10% of the photoinduced excitons in conjugated polymers chains dissociate into electrons and holes.¹¹



Scheme 3.1.

Due to the large exciton binding energy, excitons diffuse within the material instead of spontaneously dissociating into charges unless the dissociation is assisted by an applied potential or by the presence of electron acceptors. The exciton diffusion lengths were reported to range from 5 to 15 nm¹² in various polymer-based device experiments.

Due to the low relative dielectric constant (ϵ_R) of organic materials, ranging from 2 to 4, the photoinduced electron-hole pairs are strongly bonded by Coulombic attraction. These electron-hole pairs either dissociate into free electrons and holes, or recombine resulting in energy loss. If the interface between the electron D and A materials is located within the diffusion length of the exciton, the electron-hole pair may be separated owing to the assistance of the energetic difference between the LUMOs of the materials in the interface. Furthermore, theoretical calculations suggest that a dipolar layer is formed at the interface due to partial charge transfer¹³ prior to photon absorption, which reduces the back electron transfer and hence the probability of charge recombination¹⁴. From ultrafast transient absorption experiments, the time scale of charge separation from electron D polymers to an electron A fullerene derivatives is estimated to be ~ 45 ps.¹⁵ In such cases, charge transfer is faster than other competing relaxation processes giving efficient charge separation.

The separated holes and electrons then may be transported through the corresponding materials to the electrodes without being trapped. A driving force is needed to extract charges from the active layer. In the case of bilayer junction solar cells, the gradient of charge concentration can provide a driving force for the charges to diffuse to the electrodes. However, this is not the case in bulk heterojunction solar cells, where the asymmetrical contacts (a high work function metal for the hole collection electrode and a low work function metal for the electron collection electrode), assure directional charge transport by the induction of an internal field.

3.1.2 Characterization of PV Cells

When a PV cell is irradiated with light, the voltage across the electrodes shifts from 0 Volt (open circuit) to the open-circuit voltage (V_{oc}), that is the maximum voltage difference attainable between the electrodes (Figure 3.4). The origin of V_{oc} is still not clear, but it follows an empirical formula which reveals the relationship between the V_{oc} , the HOMO of the donor polymer and LUMO of PCBM based on the statistic of polymer-PCBM PV cells (Equation 3.1).¹⁶ The short-circuit current (I_{sc} , J_{sc} is used when the current is calculated based on unit surface area, A/cm^2) is the maximum current the cell delivered by the cell under short circuit voltage ($V = 0$). Short circuit current gives the information about the charge separation and transport efficiency in the cell and is dependent on the illumination intensity.

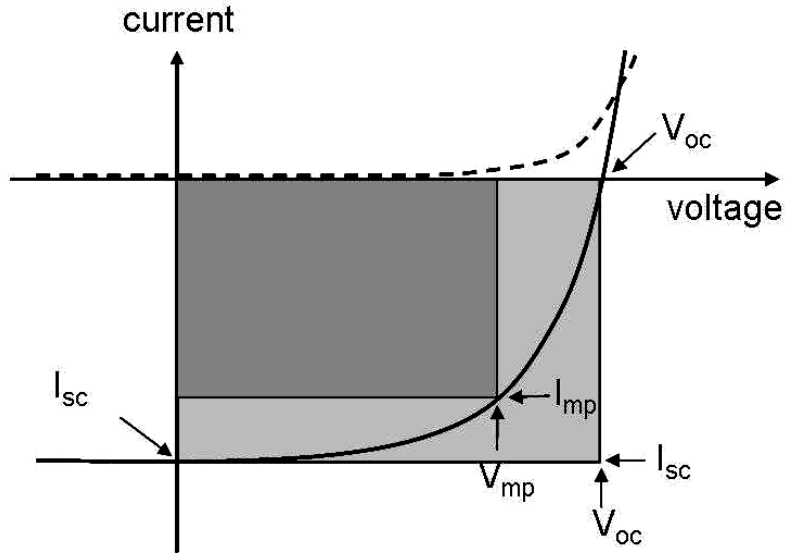


Fig. 3.4. I - V characteristics of a PV cell. The characteristic intersections with the X and the Y axes give the open-circuit voltage (V_{oc}) and short-circuit current (I_{sc}), respectively. The maximum output power is at the point $I_{mp} \times V_{mp}$. The FF is the ratio of the maximum output power delivered by the cell to $I_{sc} \times V_{oc}$ and corresponds to the ratio between light and dark rectangles.

$$V_{oc} = \frac{1}{e} (|E_{DonorHOMO}| - |E_{PCBMLUMO}|) - 0.3V \quad \text{Eq. 3.1}$$

Under illumination, a PV cell generates power which is equal to the product of the current and voltage. At a certain point, this reaches a maximum, hence, $I_{mp} \times V_{mp}$. To determine the efficiency of a PV cell, the power output needs to be compared to the input power (P_{in}) which corresponds to the total radiative energy falling on the device surface. The filling factor (FF) is calculated as $FF = V_{mp} \times I_{mp} / (V_{oc} \times I_{sc})$ to indicate the portion of power that can be extracted from a PV cell. With the value of FF , the power conversion efficiency (η) can be written as

$$\eta_{power} = \frac{P_{out}}{P_{in}} = \frac{I_{mp} V_{mp}}{P_{in}} = \frac{FF \times I_{sc} V_{oc}}{P_{in}} \quad \text{Eq. 3.2}$$

The corresponding equivalent circuit of a PV cell is shown in Figure 3.5. An ideal PV cell can be viewed as a current generator generating photocurrent (I_{PH}) in parallel with a diode. In a real PV cell, the power is lost through the resistance of contacts and through leakage current passing the active layer. The power loss can be expressed in the serial resistance (R_S) in series and shunt resistance (R_{SH}) in parallel to the equivalent circuit of an ideal PV cell, respectively. The serial resistance is induced from the resistance of whole device to current flow while shunt resistance is caused from the leakage of current due to poor insulating between two electrodes. An efficient PV cell requires high R_{SH} in order to block the leakage of current through active layer and low R_S to generate sharp rise of current in forward bias.

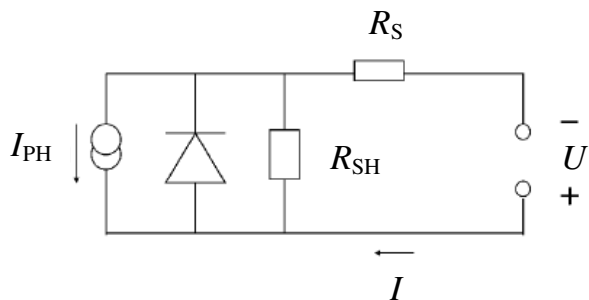


Fig. 3.5. Equivalent circuit of a PV cell. I_{PH} : photocurrent; I : total current; R_S : serial resistance; R_{SH} : shunt resistance; U : bias across electrodes.

3.1.3 Bulk Heterojunction Solar cell

The occurrence of efficient photoinduced electron transfer from a conjugated polymer chain to C_{60} ¹⁷ and conductivity of polymer chains doped with C_{60} ¹⁸ has guided the development of polymer-fullerene B-H solar cells. Extended interface between electron D and A can be achieved by applying the concept of a bulk heterojunction (Figure 3.6). In a B-H PV cell active layer, the electron D and A are mixed prior to deposition, but phase separation takes place to form micro- to nano-sized domains resulting in part from different degrees of crystallinity. The domains of electron D and A materials in the active layer are randomly oriented and no internal field with a preferred direction is produced under illumination to direct the charges to the corresponding electrodes. Therefore, the use of asymmetrical contact is necessary in a B-H PV cell.

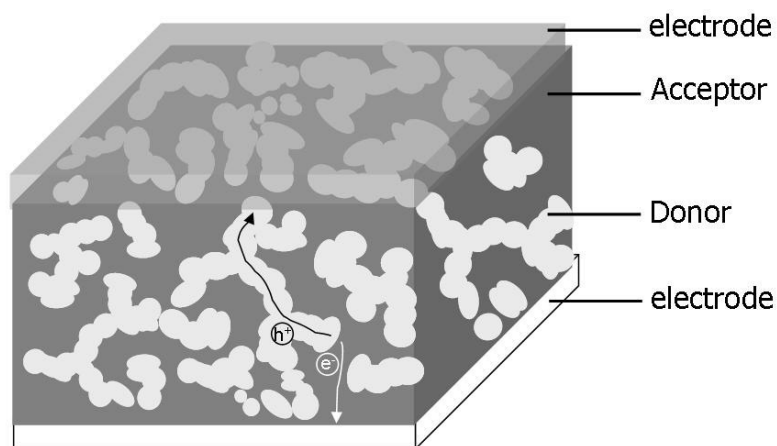


Fig. 3.6. Micro domains formed in B-H PV cell facilitate charge separation and transport.

Many factors affect the extent and size of the micro- and nano- domains, such as choice of solvent,¹⁹ material properties,²⁰ D-A pair ratio²¹ and post deposition treatment.²² When the domain size is similar to the exciton diffusion length, photogenerated excitons in either material possess a higher probability to diffuse to the interface and then dissociate into free charges. If such micro domains form bicontinuous and interpenetrated networks stretching from the interface to the electrodes, the separated charges may travel to the contacts and deliver current to the external circuit. So, in B-H PV cells, the efficiency is extremely sensitive to the morphology of the active layer. In past years, improved conversion efficiency of B-H solar cells was achieved with different materials and fabrication procedures (Figure 3.7).²³

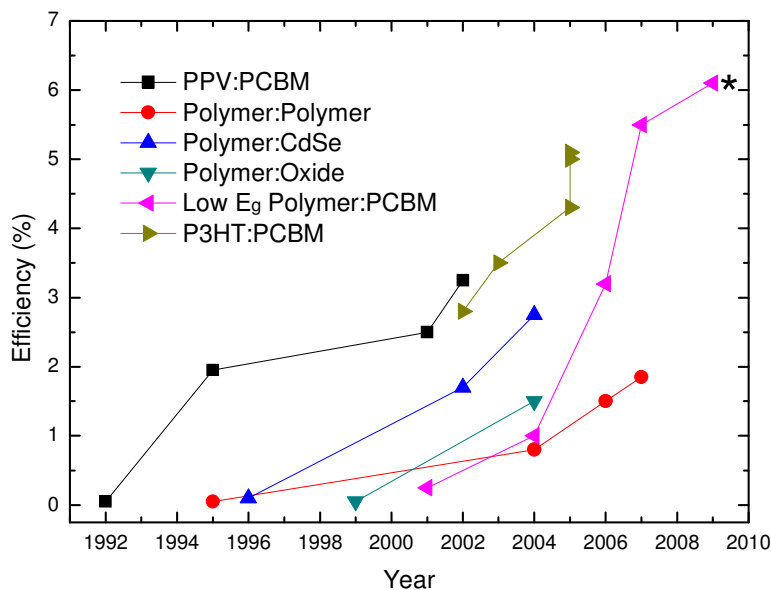


Fig. 3.7. Reported efficiencies of different B-H solar cells over past years.²³ *The value was reported with PC₇₀BM.²⁴

3.1.4 Strategies to Improve B-H PV Cell Efficiency

In a B-H PV cell, both photocurrent generation and charge transport are dependant on the active layer morphology. Blending of the electron D and A molecules on the scale of exciton diffusion length is necessary for efficient charge separation, while continuous micro domains are required to provide channels for charges to reach the electrodes. One of many strategies to master the morphology is by controlling the molecular structure of the electron D and A components using covalent or non-covalent interactions to guide phase separation at the molecular level.²⁵

Diblock copolymers²⁶ are known to form self organized structure depending on the portion of each block.²⁷ The nano-scaled structures corresponding to the block lengths can be tuned by changing the ratio between blocks, and their size are similar to the ideal micro domains in a B-H PV cell active layer. The sequential structure of electron D and A materials in diblock copolymers chains ensure effective

photoinduced charge transfer (Figure 3.8.a). Early applications of block-copolymer-based PV cells show enhanced V_{oc} and J_{sc} compared to a statistical copolymer with the same monomer molar ratio.²⁸ On the other hand, covalently linked D-A blocks may suffer from phase separation and clustering of the fullerene block, which limits efficient charge separation due to diminished interface area. Additionally, the increased phase separation may break up the continuity of the micro domains of the respective blocks, necessary for charges to be transported to the electrodes and, consequently, reduces the charge transport efficiency.²⁹

In addition to block copolymers, the concept of double-cable polymers was also introduced, where electron accepting moieties, such as C_{60} , are covalently functionalized onto the electron donating π -conjugated polymer backbones (Figure 3.8.b).³⁰ Such polymers allow the promotion of bicontinuous phase separated domains and provide large electron D-A interfaces in the solid phase. Electrons generated by photoinduced charge transfer from the electron donating polymer backbone are transported by hopping mechanism between the pendent electron accepting moieties while holes left on the backbone migrate through the π -conjugated systems.

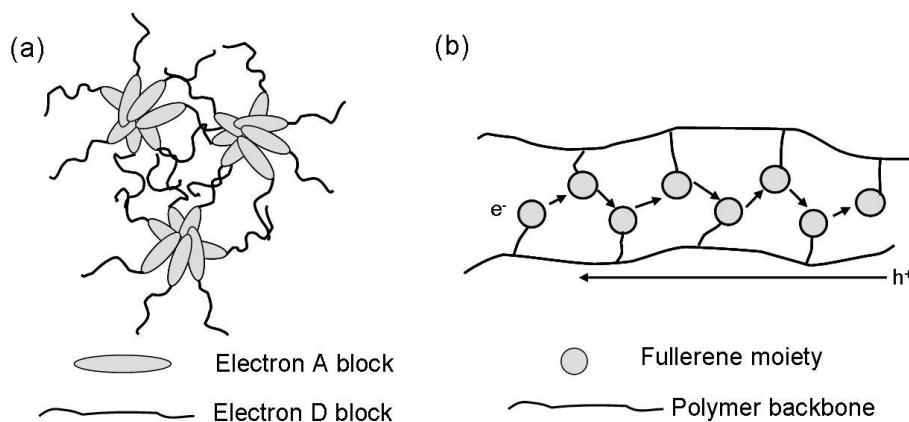
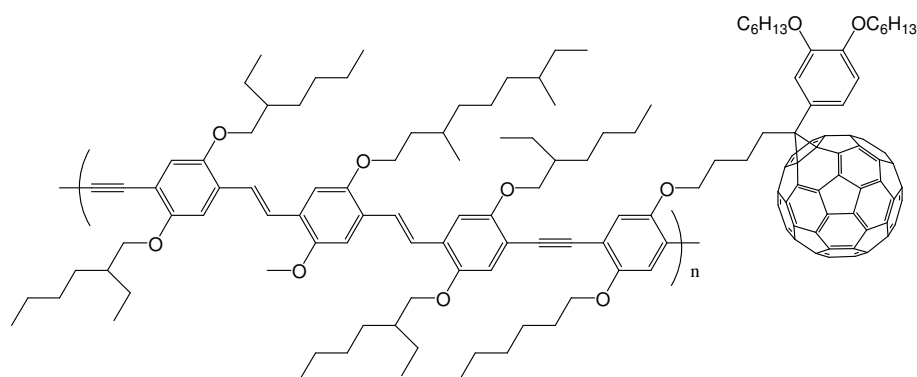


Fig. 3.8. Micro structures formed by different polymers. (a) D-A block copolymer. (b) Double-cable polymer.

Early reports of double-cable polymer-based PV cells using hybrid PPV or poly-(*p*-phenylene ethynylene) backbone with tethered fullerene derivatives (Scheme 3.2) showed promising result under standard light irradiation ($J_{sc} = 0.42 \text{ mA/cm}^2$, $V_{oc} = 0.83 \text{ V}$, IPCE = 6% at 480 nm).³¹ The portion of fullerene to polymer monomer was found to be crucial in order to guarantee electron transport because a sufficient fullerene content is required to reach the percolation threshold for efficient charge transport.²⁹ Different copolymer structures designs were proposed and tested for PV cell applications,³² but due to the packed arrangement of electron D and A in double-cable polymers geminate recombination³³ is enhanced, which increases current loss. Meanwhile, the efficiency of interchain charge transfer also affects the overall electronic characteristics. Therefore, the discreet design of a double cable polymer structure able to lead to a metastable long-lived charge separate state is crucial while increasing charge mobilities on both the electron donating and accepting materials is important to compensate the efficiency loss from recombination.



Scheme 3.2. Example of a double-cable polymer from Janssen's group tested in PV cell.³¹

In addition to employing covalent linkages between electron D and A materials, non-covalent approaches, based on supramolecular interactions, offer an appealing alternative which combine modularity and efficiency of synthesis due to the use of

self-assembly as described in chapter 2. Previously, in solution-phase electrochemical PV cell studies, it was observed that 2.5-fold higher photogenerated current was obtained in devices composed of a pentathiophene donor and a fullerene acceptor functionalized with complementary H-bonding sites (Figure 3.9.a).³⁴ The enhanced current was attributed to the formation of self-assembled structure induced by H-bonding.³⁵ In these supramolecular assemblies, ordered alignment of electron A fullerene (compound 2.2) and electron D material (compound 2.1) would provide charges with improved transport pathways (Figure 3.9.b).

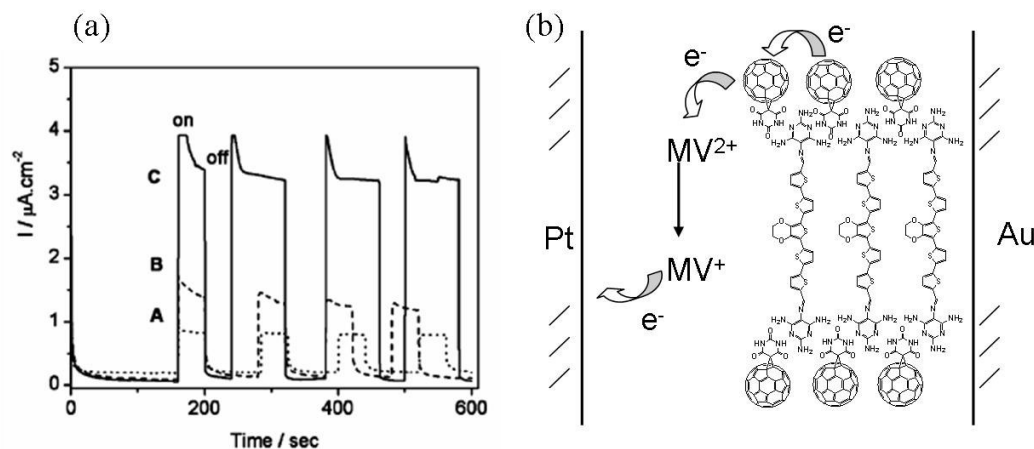


Fig. 3.9. (a) Photocurrent characteristics of three devices consisting of different D-A pairs. A: pentathiophene-only device, B: pentathiophene/pristine $\text{C}_{60} = 1:2$ device, C: pentathiophene/modified $\text{C}_{60} = 1:2$ device. Enhanced current was observed under light illumination in C which is attributed to H-bonding induced supramolecular self-assembly. (b) The graphic presentation of solution phase PV cell possessing enhanced photogenerated current. MV: methyl viologen.

3.2 Supramolecular Solid State Solar Cell

In the active layer of a B-H PV cell, the presence of a bicontinuous channel for charge transport is important for overall PV cell efficiency. Ideally, a direct route for the charges to reach the electrodes results in higher current than a random path (Figure 3.10). The concept of complementary H-bonding is utilized to induce electron D and A molecules to form supramolecular self-assembled architectures which are envisaged to reduce transport distance for electron and hole to the corresponding electrodes.

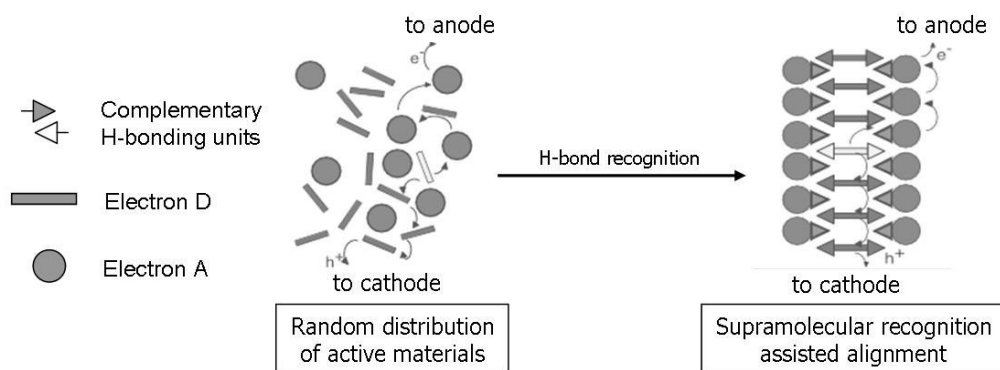


Fig. 3.10. Electron D and A molecules are guided by complementary H-binding to form organized arrangement.

The PV cells tested have the structure as indicated in Figure 3.11. Partially etched ITO glass was spin-coated with a layer of PEDOT-PSS. An active layer of blend was sandwiched between the PEDOT-PSS layer and an upper Al electrode. Details of PV cell fabrication are described in the experimental section.

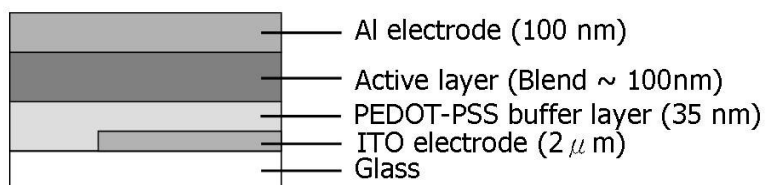


Fig. 3.11. PV cell configuration used in this work.

3.2.1 Different Electron D and A Pairs

3.2.1.1 Blend of PPHT and 2.2

Blends composed of compound **2.1** and **2.2** shows promising results in previous studies conducted in solution-phase electrochemical solar cells.³⁵ The same combination was employed in the fabrication of solid-state devices but gave poor efficiencies due to high leakage currents. The high leakage current and large proportion of short-circuited devices was attributed to the rough surface morphology due to the low solubility of the materials.³⁴

Soluble oligothiophene PPHT was utilized to replace compound **2.1** in order to improve surface morphology. *I-V* characteristics of these devices are shown in Figure 3.12. PPHT:**2.2** molar ratio was 1:1 because ideal 1:2 ratio produced insoluble aggregates which were unsuitable for the fabrication of solid PV cells. Both current in the dark and under illumination under reverse bias (-1.0 Volt) had similar intensity. The high slope of *I-V* curve in 3rd quadrant under illumination indicates a low shunt resistance in the device.

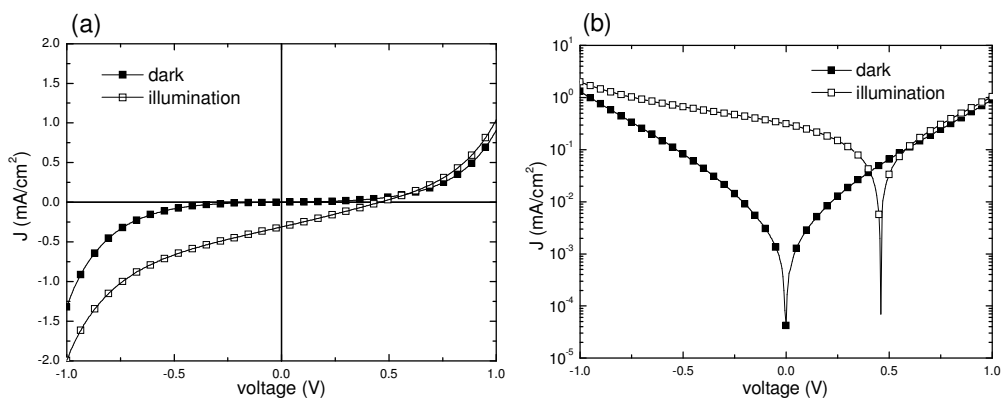


Fig. 3.12. (a) Linear and (b) semi-log plot of *I-V* characteristics from PPHT:**2.2**=1:1 (mole) PV cell, $V_{oc} = 460$ mV, $J_{sc} = 0.31$ mA/cm², $FF = 0.26$, $\eta = 0.037\%$ under AM1.5 solar simulator set at 100 mW/cm².

These results reveal that a high leakage current is still passing through the cell under external bias. The surface morphology was examined by profilometric measurements and scanning electron microscopy (SEM). The results from the profilometer measurement showed that surface height deviation is up to 300 nm (Figure 3.13.a). In the SEM images, aggregates were observed whose size ranged from hundreds of nm to several μm (Figure 3.13.b). Comparing PPHT:PCBM (Figure 3.12.c) or PPHT:C₆₀ (Figure 3.13.d) blends, where no self complementary H-bonds can form, SEM images show smooth surfaces (surface height deviation <10 nm). Therefore, the large aggregates were only induced by the presence of complementary H-bond between PPHT and **2.2**. Pinholes on the surface were observed and provide close contact between the indium tin oxide (ITO) electrode and the upper Al electrode where leakage current can pass.

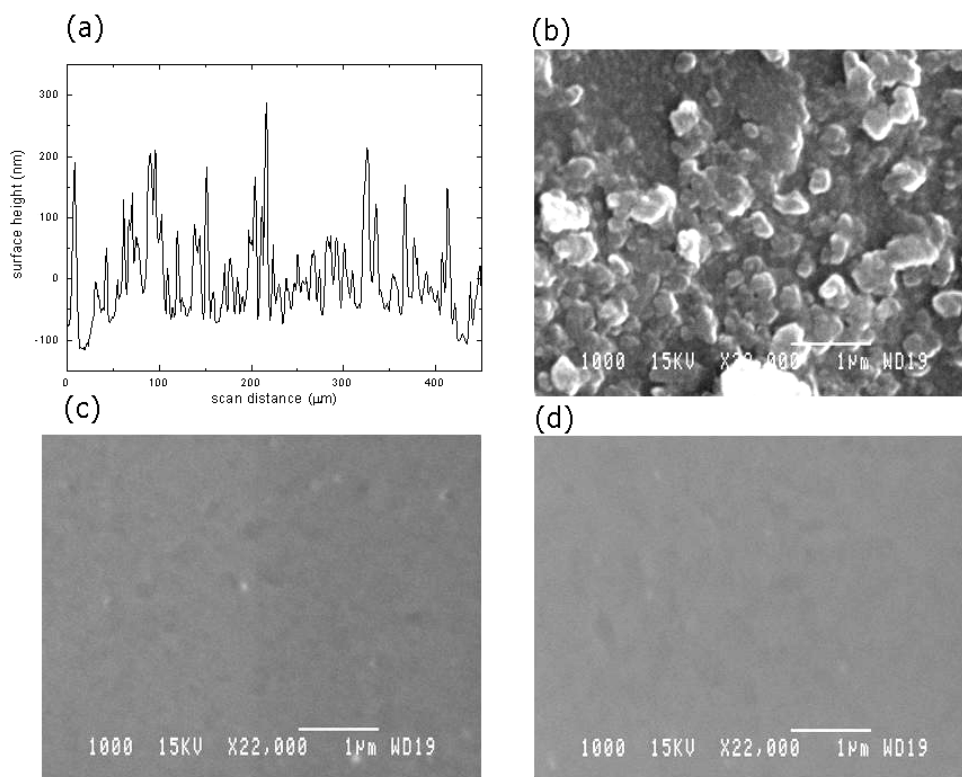


Fig. 3.13. (a) Surface morphology of PPHT:**2.2** PV cell, (b) SEM image of PPHT:**2.2**, (c) PPHT:PCBM, (d) PPHT:C₆₀ PV cells. The scale bar in SEM images is 1 μm

Annealing is a post-deposition treatment that is reported to improve the efficiency of P3HT:PCBM PV cell due to enhanced phase segregation.³⁶ This treatment was applied to the PPHT:**2.2** cells. After 5 min annealing at 170°C, the PPHT:**2.2** cells showed unchanged V_{oc} . On the other hand, lowered current, FF and efficiency were noticed (Table 3.1). The weaker J_{sc} might be attributed to the decomposition of acceptor **2.2** with high temperature treatment since **2.2** was observed to be unstable in solution at room temperature. Furthermore the decomposition product might act as traps in active layer which would further reduce charge transport from the D-A pair interfaces to electrodes.

Table 3.1. PPHT:**2.2** PV cell performances before and after annealing. Annealing condition: 170°C for 5 min.

Annealing	V_{oc} (mV)	J_{sc} ($\mu A/cm^2$)	FF	η (%)
Before	460	313	0.26	0.037
After	460	108	0.17	0.008

Zinc oxide is one of few metal oxides that possess quantum confinement effect in the experimentally accessible size.³⁷ The high electron mobility³⁸ and simple preparation procedure of ZnO nanoparticles makes it useful for application in inorganic-organic hybrid PV cells.³⁹ ZnO nanoparticles were synthesized according to literature procedures and characterized with spectroscopic methods. The nanometer-scale-sized particles used as a buffer layer on the top the active layer. A thin layer of ZnO nanoparticles was envisaged to smooth the rough surface morphology. ZnO nanoparticles were synthesized⁴⁰ by hydrolysis and condensation of zinc acetate dihydrate using potassium hydroxide in methanol following the reported procedure.⁴¹ The nanoparticle size was calculated to be 3.3 nm from Equation 3.3 where $\lambda_{1/2}$ and D represent the wavelength at half maximum absorption (Figure 3.14) in nm and nanoparticle diameter in Å, respectively.^{41b}

$$\frac{1240}{\lambda_{1/2}} = 3.301 + \frac{294}{D^2} - \frac{1.09}{D} \quad \text{Eq. 3.3}$$

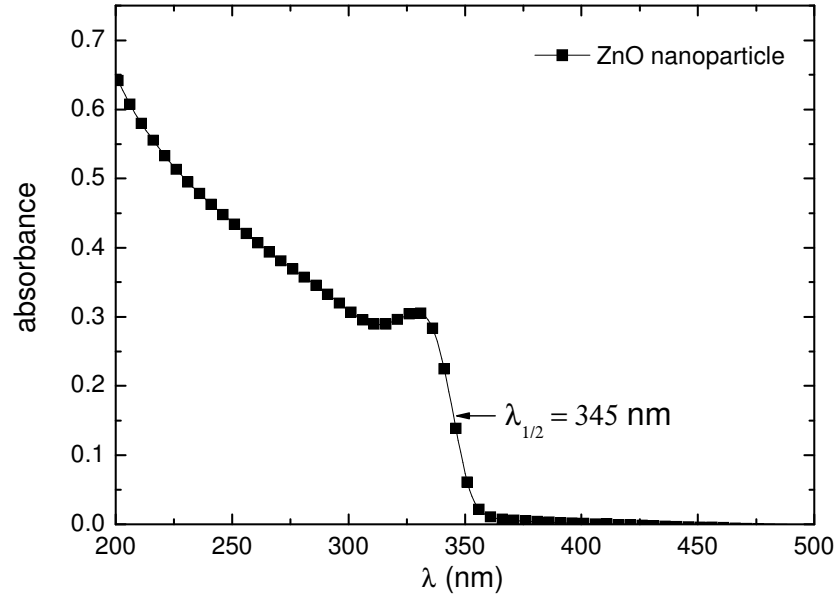


Fig. 3.14. Electronic absorption spectra of ZnO nanoparticles in solvent. $\lambda_{1/2} = 345$ nm.

The current density, J_{sc} , was doubled in the PV cell I, where the active layer was coated with ZnO nanoparticles (Table 3.2). The doubled power efficiency was due to higher current since V_{oc} and FF were less significantly affected.

Table 3.2 Performances of three different PV cells. Tilt evaporation is denoted as *te*.

cell	blend	V_{oc} (mV)	J_{sc} (mA/cm ²)	FF	η (%)
	PPHT: 2.2	460	0.31	0.26	0.04
I	PPHT: 2.2 /ZnO	400	0.67	0.29	0.08
II	PPHT: 2.2 /ZnO ^{<i>te</i>}	570	0.85	0.30	0.14

PV cells with the same configuration were subject to “tilt evaporation”, denoted as *te.*, of the Al electrode (cell II). In this set up, the PV cells were displaced from the position where PV cell surface is normal to the incident Al vapor beam (Figure 3.15.a). The Al vapor beam was oriented at a certain angle ($\theta \sim 30^\circ$) to the normal onto the PV

cell surface to avoid filling any pinholes with Al metal. Higher efficiency was observed, which resulted from improved J_{sc} and V_{oc} in cell II. The diminished current in dark under reverse bias and higher shunt resistance under illumination indicated that the leakage current was partially blocked (Figure 3.15.b). It must be noticed that ZnO also acts as an n-type semiconductor. Thus contribution to the PV effect from oligothiophene:ZnO interface can therefore not be ruled out.

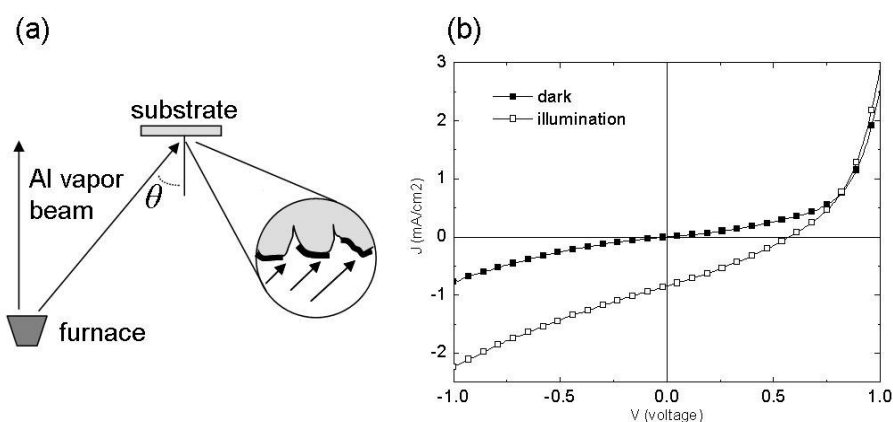


Fig. 3.15. (a) Graphical presentation of tilt evaporation, pinholes were shadowed by surrounding and no direct Al deposition took place, (b) I - V characteristics of cell II, compared to PPHT:2.2 cell, the current in dark under reverse bias was diminished and higher shunt resistance was obtained. $V_{oc} = 570$ mV, $J_{sc} = 0.85$ mA/cm², $FF = 0.30$, $\eta = 0.143\%$.

3.2.1.2 Blend of PPHT and BAF

Compound **2.68** (BAF) was tested in the fabrication of solid-state PV cells, as its improved thermal stability and solubility may overcome the problem in PPHT:2.2 devices. The procedure of preparation of blend solution is crucial in fabricating solid state PV cells. A PPHT solution in ODCB with ~1% DMSO was prepared in advance in order to ensure all PPHT oligomers were dissolved in the solvent. Ten mg/mL was found to be the optimal concentration of the PPHT solution because higher concentration requires more DMSO, which is deleterious to the PEDOT-PSS buffer

layer, while lower concentrations reduce the final thickness of the active layer (average thickness of PPHT:BAF cell ~ 80 nm). The PPHT solution then was added to the BAF solid powder. Aggregates formed immediately and a minimum amount of DMSO was added gradually until *ca.* 2~3% of total volume depending on the dissolution inspected visually. After overnight stirring at 50°C, the blend solution is free from aggregates. Note that adding solvents to a mixture of PPHT and BAF solid will result in insoluble aggregates even with the additional DMSO. The strong association between PPHT and BAF in the blend is due to the presence of multiple H-bonds between the melamine and the barbituric acid complementary recognition sites.

The *I-V* characteristics of PPHT:BAF blend were collected from 6 different cells (Figure 3.16). The dark current density at -1 Volt was 275 times weaker (from 1.32 mA/cm² to 0.0049 mA/cm²) in PPHT:BAF (Figure 3.16.c.) than in PPHT:2.2 (Figure 3.16.a) blend. The diminished leakage current was attributed to improved surface morphology as observed under microscopy. In PPHT:2.2, large aggregates as described in 3.2.1.1 was found (Figure 3.16.b) while a flat surface was obtained from PPHT:BAF (Figure 3.16.d). The di-*tert*-butylbenzyl group on BAF promotes the solubility of fullerene component and thus also facilitates the solvation of PPHT:BAF supramolecular assembly by ODCB molecules. The V_{oc} increased from 460 mV to 540 mV but the J_{sc} decreased from 0.31 mA/cm² to 0.06 mA/cm² (Table 3.3). An unusual low *FF* below 0.25 was measured due to the presence of a counter diode.

Table 3.3. Performances of PPHT:2.2 and PPHT:BAF cells.

Cell	V_{oc} (mV)	J_{sc} (mA/cm ²)	<i>FF</i>	η (%)
PPHT:2.2	460	0.31	0.26	0.037
PPHT:BAF	540	0.06	0.21	0.007

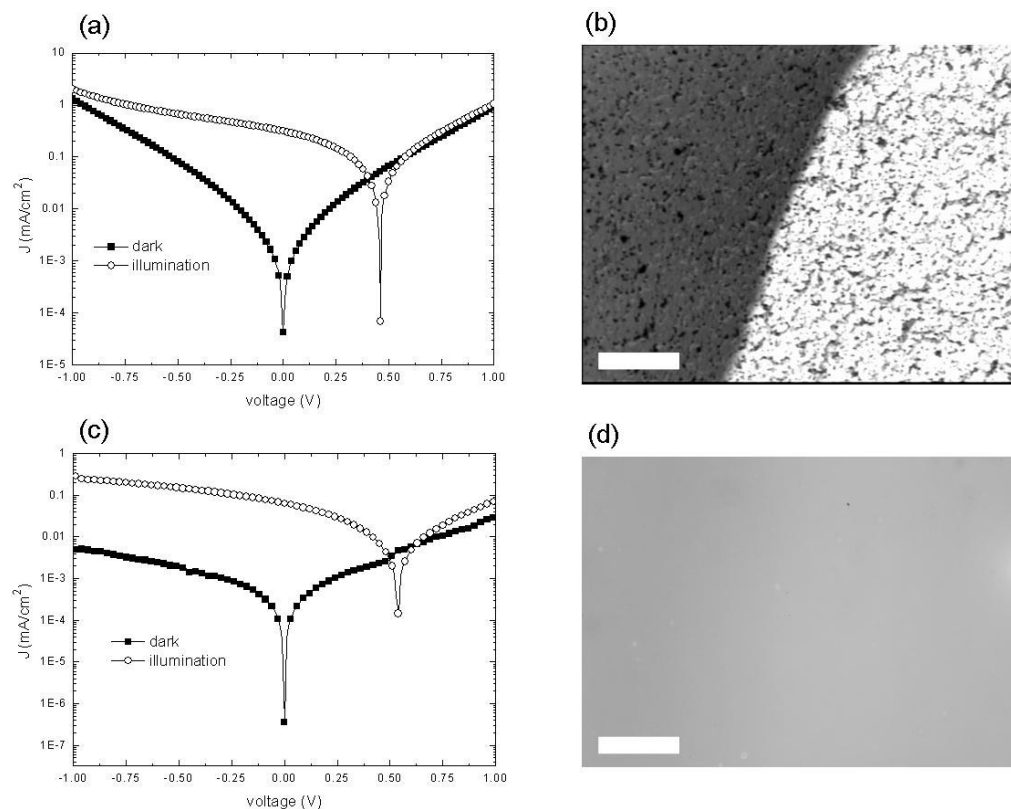


Fig. 3.16. (a) *I-V* characteristics and (b) microscopic surface image of PPHT:2.2 cell. (c) *I-V* characteristics and (d) microscopic surface image of PPHT:BAF cell. The scale bar is 50 μm .

3.2.2 Ratio and annealing

3.2.2.1 Variation of D/A Ratio

Four PV cells of varying ratio of PPHT:BAF = 1:0.2, 1:0.6, 1:1, 1:2 were prepared. For each ratio, the V_{oc} , J_{sc} , FF and efficiency (η) were recorded for at least 6 individual cells. In cell 1:0.2, the point distribution spans ~ 300 mV and was more scattered than in other cells (Figure 3.17.a). The wide distribution and low V_{oc} may indicate poor surface morphology, which induces partial short circuit in the device. The low V_{oc} was also observed in PPHT-only single layer PV cells. Due to the low portion of BAF with complementary recognition sites, different orientations of H-bonding other than “tape” supramolecular assembly can co-exist between terminal melamine groups on individual oligothiophene chains. This allows alternative aggregation modes in addition to parallel packing of PPHT. Random aggregate

formation is expected to result in poor surface morphology (Figure 3.18).

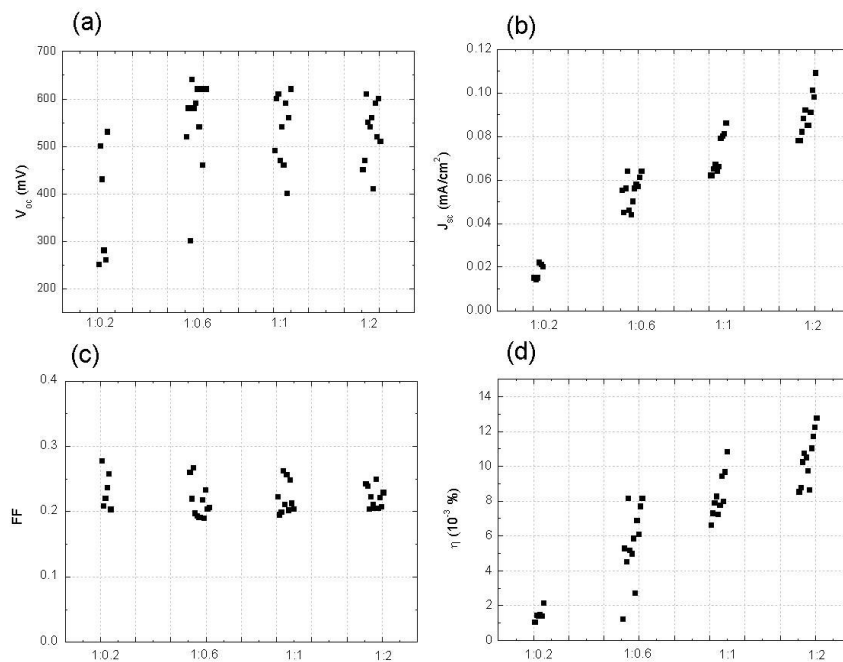


Fig. 3.17. (a) V_{oc} , (b) J_{sc} , (c) FF and (d) efficiency results from cell 1:0.2, 1:0.6, 1:1 and 1:2. With increase of BAF content, higher J_{sc} was obtained, therefore, elevated efficiency was observed. Each point represents a PV cell

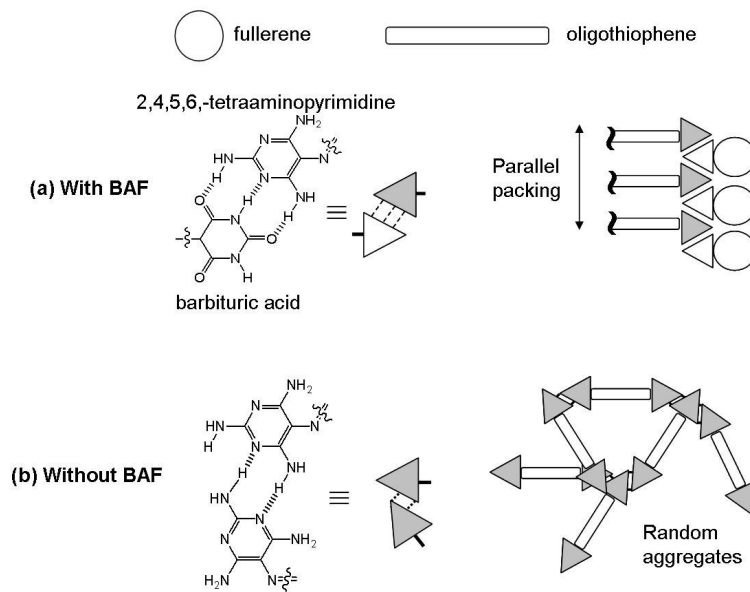


Fig. 3.18. (a) With the presence of BAF, parallel tape packing is induced by complementary H-bonding between melamine of barbituric acid, instead, (b) in the absence of BAF, random aggregates may result from two H-bond D-A pairs

The V_{oc} obtained in cell 1:0.6 ~ 570 mV remains constant even with higher BAF content in cell 1:1 and 1:2 (Figure 3.17.a). The large increment of V_{oc} in cell 1:0.6 implies that at certain ratio between 1:0.2 and 1:0.6, the BAF portion reaches a threshold concentration. Once passed this threshold, random aggregation could be reduced and better charge transport occurs in active layer.

It is observed that with increasing BAF portion, higher J_{sc} are obtained (Figure 3.17.b). When more BAF is present in the blend, the interface between the electron donating and accepting materials is increased, which facilitates charge separation and increases current. The expanded interface facilitates charge separation after excitons are generated on the oligothiophene chains. In addition, with rising portion of BAF, phase separation might take place to a relatively wider extent, offering additional channels for charge transport to the corresponding electrodes.

From atomic force microscopy (AFM), the change in V_{oc} between 1:0.2 and 1:0.6 cells could not be attributed to a morphological change of the active layer (Figure 3.19). Similar surface morphology was found in 1:0.2, 1:0.6 and 1:1 cells. However, a distinct change in 1:2 cell was noticed (Figure 3.19.d): The blend with ratio 1:2 gave finer micro structure than the one with a 1:1 ratio. The cross section of a small area scan revealed that the micro structure was in the 10 nanometer range. When more BAF is presenting in the blend, the supramolecular interactions between melamines and barbituric acid moieties break the aggregates of PPHT. The weight ratio 1:2 between PPHT and BAF allows higher extent of D-A pairing which resulting in smaller structure. Furthermore, with a larger proportion of BAF, better percolation can be obtained, so that increased J_{sc} was observed in 1:2 cells.

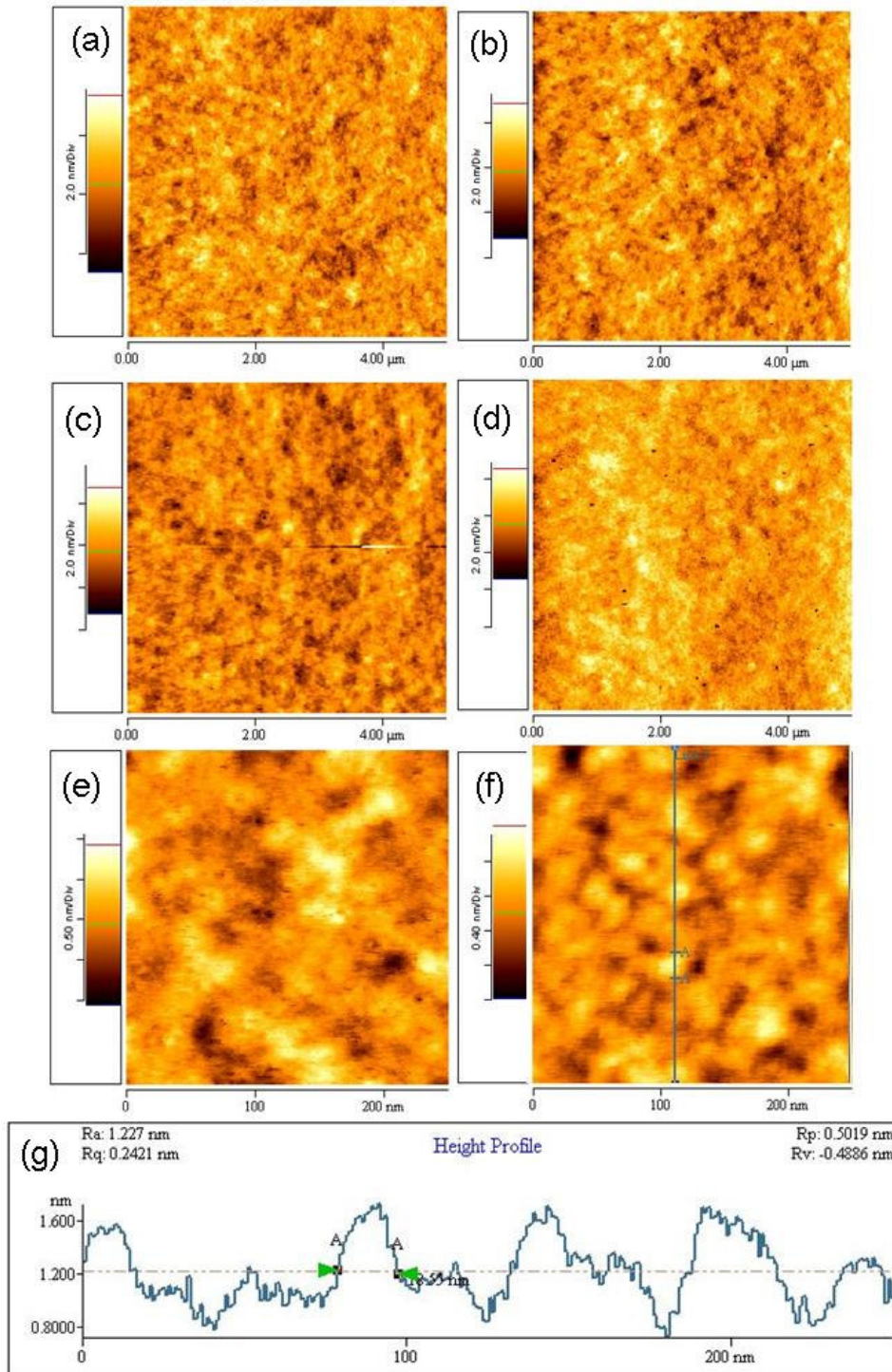


Fig. 3.19. AFM scans of (a) 1:0.2, (b) 1:0.6, (c) 1:1 and (d) 1:2 cells. A distinct morphological change was observed between (c) and (d). Small area scan of (e) 1:1 and (f) 1:2 cells. The cross section analysis in (g) is indicated as the vertical line in (f).

The cell efficiency has the same evolution as J_{sc} , which indicates that the improved efficiency is mainly due to increased J_{sc} . It was noticed that in all cells, low FF values were obtained. For each ratio, the cells were divided into two groups according to their relative values, half with higher and another half with lower V_{oc} . In every case, FF showed a reverse trend to V_{oc} (Figure 3.20.a.). Of the cells tested, 95% cells have relatively low FF when they have relatively high V_{oc} compared within the same ratio. On the other hand, J_{sc} exhibited no clear correlation to FF (Figure 3.20.b.).

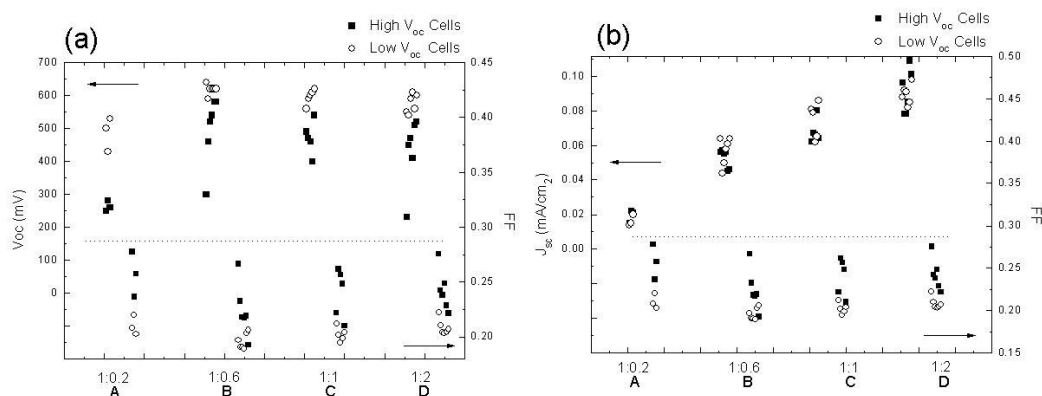


Fig. 3.20. Comparison between (a) V_{oc} and FF , FF has reversed trend to V_{oc} in each ratio, and (b) J_{sc} and FF , there is no clear relation between these two parameters. In each ratio, cells were divided into two groups, one half is with relatively high V_{oc} , the another half is with relatively low V_{oc} .

3.2.2.2 Annealing Treatment

The efficiency of organic PV cells are reported to be improved with thermal post treatment.⁴² Annealing results in increased domain size and more ordered molecular packing due to crystallinity and, therefore, to higher efficiency toward charge separation and collection. The annealing effect was investigated at two temperatures: 80°C (30 min) and 170°C (10 min) (Figure 3.21).

It was observed that V_{oc} slightly increased (~100mV) while J_{sc} decreased with rising annealing temperature in PPHT:BAF cells. The lowered efficiency was correlated to the diminished J_{sc} . The reduced J_{sc} at 170°C might be the result of

decomposition of BAF which shows thermal stability only up to 90°C under nitrogen atmosphere. The decomposed molecules could be additional traps for charges and contribute to reduced charge transport efficiency. The drop of FF at 170°C indicates that a dramatic change takes place which induces the deviation in the series resistance and the shunt resistance.

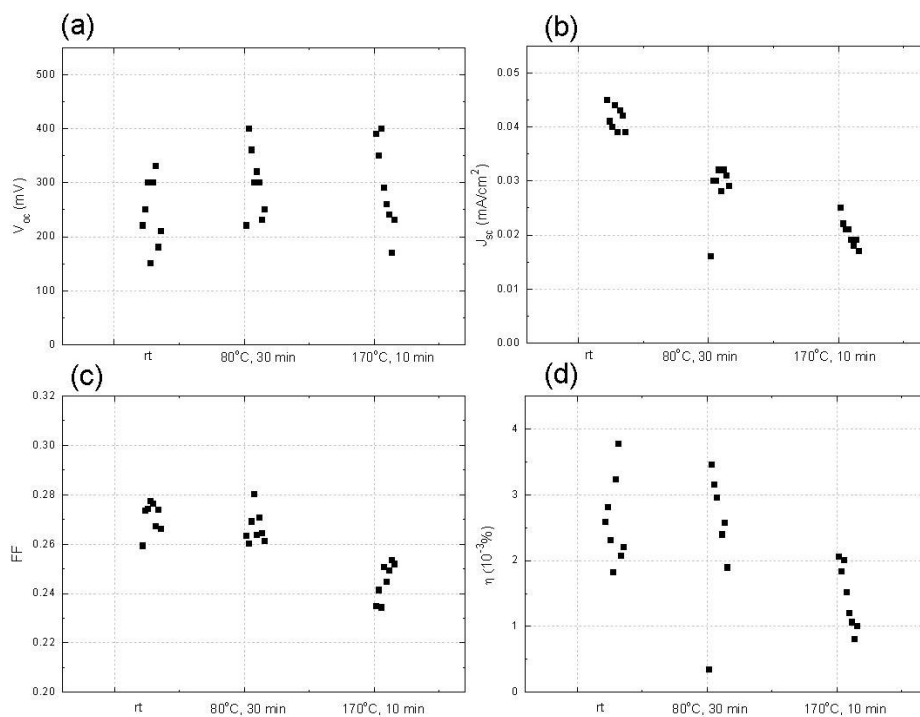


Fig. 3.21. (a) V_{oc} , (b) J_{sc} , (c) FF and (d) efficiency of PPHT:BAF PV cells annealed at different temperature.

Cells fabricated with commercial P3HT and synthesized O3HT blended with PCBM were subjected to annealing, and compared to PPHT:BAF cells (Figure 3.22). In P3HT:PCBM cells, V_{oc} , J_{sc} , FF and efficiency were improved with increased annealing temperature as observed by others. On the other hand, the performance were lowered in O3HT:PCBM cells with annealing temperature and the evolution of the electronic characteristics was similar to PPHT:BAF cells. The observation of reduced values was attributed to the relatively short oligothiophene chains employed

in blends. Low molecular weight O3HT does not possess sufficiently long backbones to form fiber-like strands required to ensure high charge mobility.⁴³ Therefore, the low values J_{sc} obtained in PPHT:BAF cells may be partially the consequence of using a short oligothiophene backbone.

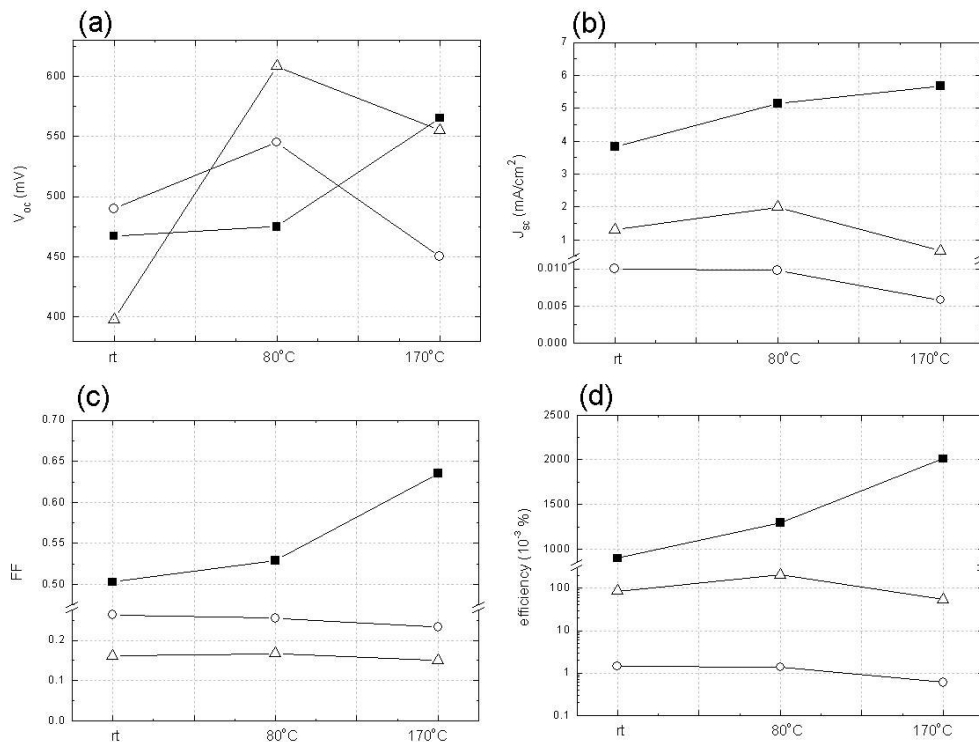


Fig. 3.22. P3HT:PCBM(■), O3HT:PCBM(△) and PPHT:BAF(○) cells were compared in (a) V_{oc} , (b) J_{sc} , (c) FF and (d) efficiency at different annealing temperatures. The reduced characteristics in O3HT:PCBM and PPHT:BAF cells were attributed to the short O3HT backbones which are not sufficiently long to form fiber-like strands

When the dark current is not negligible compared to the net photocurrent, the photogenerated current I_{photo} can be calculated by subtracting the I - V curve in dark (I_{dark}) from I - V curve under illumination (I_{light}) (Equation 3.4).

$$I_{light}(V) = I_{dark}(V) + I_{photo}(V) \quad \text{Eq. 3.4}$$

$$I_{photo}(V) = I_{light}(V) - I_{dark}(V) \quad \text{Eq. 3.5}$$

The $I_{\text{photo}}-V$ characteristics of P3HT:PCBM, O3HT:PCBM and PPHT:BAF were plotted in Figure 3.23. In each blend, similar shunt resistances (R_{SH} , the inverse of the slope in the 3rd quadrant) were observed at different annealing temperature. In O3HT:PCBM cells, an increment of only $\sim 14\%$ in I_{photo} was found, while a 38% increment in I_{photo} was recorded for P3HT:PCBM cell with 170°C annealing treatment. The less pronounced annealing effect in O3HT:PCBM cell indicates a very limit change in micro structure in the active layer where short O3HT chains can not form micro domains due to poor crystallinity. Serial resistances (R_s , the inverse of slope in 1st quadrant) in P3HT:PCBM and O3HT:PCBM cells were found to decrease while PPHT:BAF cell showed doubled R_s after annealing. The different evolution of I_{photo} with annealing temperature may result from the degradation of materials.

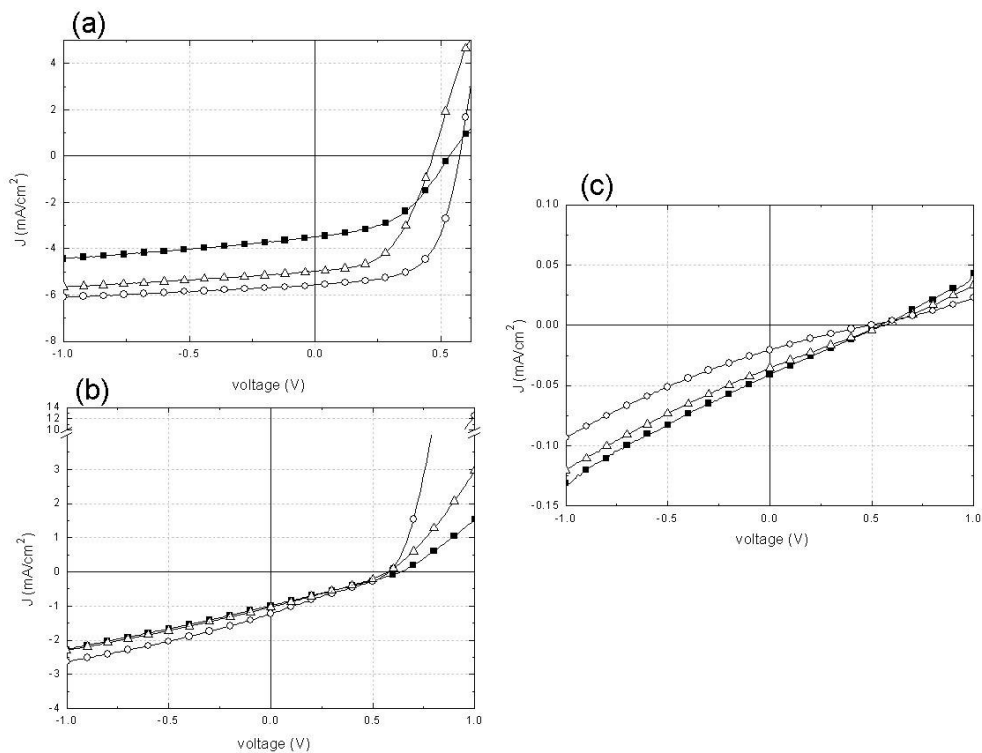


Fig. 3.23. $I_{\text{photo}}-V$ characteristics of (a) P3HT:PCBM, (b) O3HT:PCBM and (c) PPHT:BAF cells. ■: untreated cells, △: annealing at 80°C for 30 min, ○: annealing at 170°C for 10 min.

In a device, the charge transport corresponds to the charge drift length (d) when an external field is applied. The charge drift length is influenced by three factors: mobility (μ), lifetime of the charges carrier (τ) and electric field (E) according to:

$$d = \mu \times \tau \times E \quad \text{Eq. 3.6}$$

If the charge drift length exceeds the active layer thickness (l), the charges can be collected on the electrodes before recombination. On the other hand, if the drift length is shorter than the layer thickness, only a fraction which equals to the ratio d/l can be extracted from the cell. The relationship proposed between I_{photo} and drift length is shown in Equation 3.7.⁴⁴

$$I_{\text{photo}} = \begin{cases} |I_{sc}| & \text{if } d > l \\ |I_{sc}| \times d/l & \text{if } d < l \end{cases} \quad \text{Eq. 3.7}$$

In Figure 3.23.a, an almost constant I_{photo} as a function of the electric field demonstrates that the charge drift length is longer than the thickness of the active layer, so all charges passed through the blend electrode interface and are collected at the electrodes. In the region close to V_{oc} , because the applied external potential offsets the growing potential exerted from D-A pair, the net electric field is diminished. The charge drift length, therefore, is shortened and a line with constant slope corresponding to d/l is obtained. However, in PPHT:BAF cell (Figure 3.23.c), only a line with an almost constant slope is observed across the scanning window. This implies that charges in this blend have a lower drift length than the thickness of the active layer due to a small $\mu \times \tau$. The gradually diminished slope as annealing temperature increased indicates that $\mu \times \tau$ decreases with rising temperature.

3.2.2.3 Addition of DMSO

As mentioned above, a small amount of DMSO (1% ~ 3% in volume) is required to fully dissolve the PPHT:BAF blend (section 3.2.1.2). In addition to the standard drying process used for the preparation of all cells (**Un**: dried in vacuum chamber for 15 min as for standard procedure), three kinds of cells were prepared with different drying processes in order to examine the influence of the drying process: **He** (heated at 50°C for 16h), **Va** (subjected to vacuum for 40h), **VaHe** (subjected to vacuum for 40h followed by heating at 80°C for 2h). The cell performances are compared in Figure 3.24. The same V_{oc} in **Un** and **He** cells was observed. On the other hand, the V_{oc} value was 100 mV and 150 mV smaller than **Un** cells in **Va** and **VaHe** cells (Figure 3.24.a). Increased J_{sc} was found in **He** cells while similar values are recorded in other cells (Figure 3.24.b). The heating temperature (50°C) for **He** cells was sufficiently below 90°C employed in Figure 3.24.c, so the decomposition of BAF was excluded. The slight increment in J_{sc} may thus be a result of annealing over a long period (16h). The efficiency was found to follow the evolution of J_{sc} (Figure 3.24.d). The drop of efficiency in **Va** and **VaHe** cells could be the consequence of aging (40h) which may induce material degradation. Overall, comparing **Un** and other post-treated cells, the cell characteristics remained similar, which indicates that the added DMSO was already removed in the standard drying process. Therefore, the use of DMSO to promote solubility of PPHT:BAF blend is deemed applicable to cell fabrication.

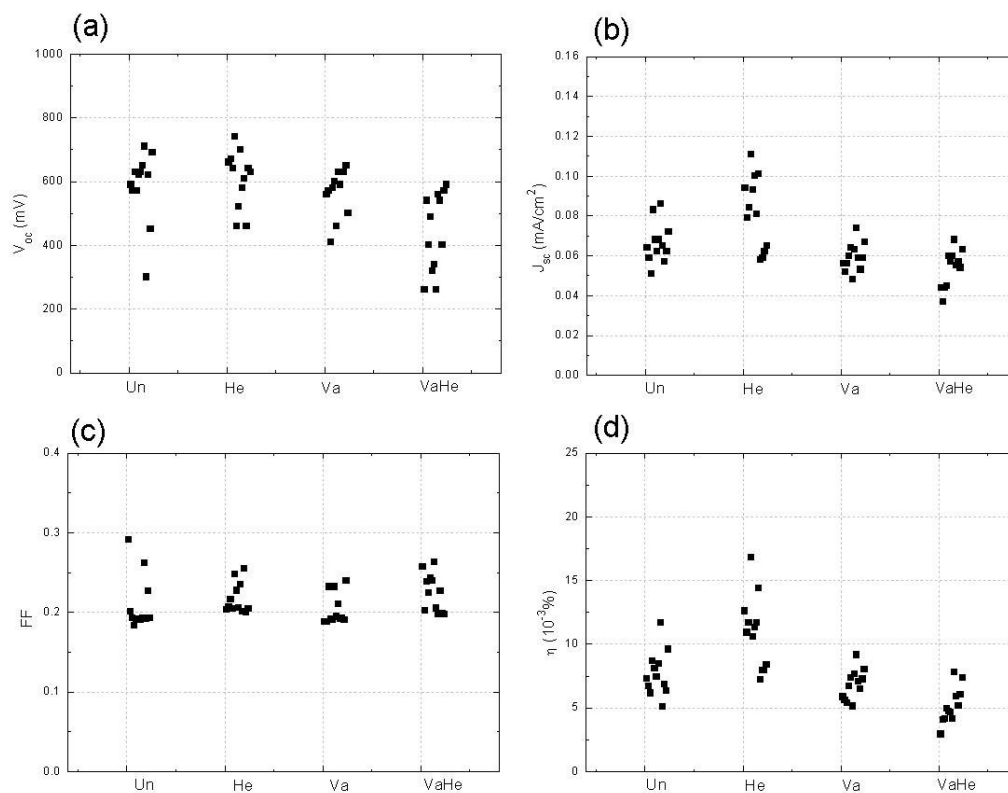


Fig. 3.24. (a) V_{oc} , (b) J_{sc} , (c) FF , (d) efficiencies of cells treated with different drying process: **Un** (untreated cells), **He** (heated at 50°C for 16h), **Va** (subjected to vacuum for 40h), **VaHe** (subjected to Vacuum 40h followed by heating at 80°C for 2h)

3.2.3 Cell Analysis

3.2.3.1 Incident Photon to Current Efficiency (IPCE)

The electronic absorption and IPCE of PPHT:BAF cell is shown in Figure 3.25. The absorption maximum from the oligothiophene backbone is located at 434 nm. The measurement started from 360 nm in order to avoid the absorption from the ITO layer. The highest IPCE was found to be 0.8%, which is consistent with the low efficiencies recorded under AM1.5 illumination. Comparing the IPCE curve to the UV/Vis absorption spectra, the major contribution is attributed from the oligothiophene chains, while a shoulder at ~ 600 nm is attributed to the photoinduced current from BAF. From the IPCE spectrum, the calculated J_{sc} was 0.046 mA/cm^2 which is of the same order of magnitude that obtained from I - V characterization in the

glove box under standard illumination (100 mW/cm^2). The small reduction in J_{sc} may be due to the short exposure of the PV cells to air during measurement of the IPCE.

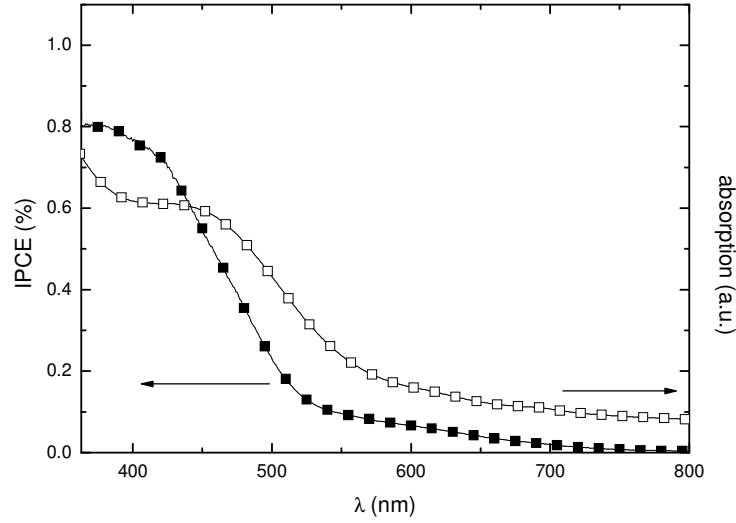


Fig. 3.25. Electronic absorption (□) and IPCE (■) spectrum of PPHT:BAF cell.

3.2.3.2 Recombination Mechanism

Following their generation of charges within the active layer, the charges may recombine before they reach the electrodes. The main recombination mechanisms are non-geminate recombination and geminate recombination. Both forms of recombination result in the loss of photogenerated current.

The relation between photogenerated charge carrier density (n_{photo}) and charge carrier generation rate (G) can be represented by Equation 3.8,⁴⁵ where τ is the carrier lifetime and β is the bimolecular recombination coefficient.

$$\frac{dn_{photo}}{dt} = G(t) - \frac{n_{photo}(t)}{\tau} - \beta n_{photo}^2(t) \quad \text{Eq. 3.8}$$

Under steady state conditions, when the photogenerated charge carrier density

$\frac{dn_{photo}}{dt} = 0$, the charge carrier generation rate is given by:

$$G(t) = \frac{n_{photo}(t)}{\tau} + \beta n_{photo}^2(t) \quad \text{Eq. 3.9}$$

Non-geminate recombination is a direct recombination mechanism where a charge enters the capture cross-section of a counter charge. In the case where only non-geminate recombination dominates the recombination mechanism, $\frac{n_{photo}}{\tau}$ can be neglected in Eq. 3.9, and the following relationship between the charge carrier generation rate and the charge carrier density can be obtained:

$$G(t) = \beta n_{photo}^2(t) \quad \text{Eq. 3.10}$$

On the other hand, in geminate recombination the hole and the electron separated from the same exciton are still electron bonded by coulombic attraction. In this case, βn_{photo}^2 can be neglected and Eq. 3.9 gives:

$$G(t) = \frac{n_{photo}(t)}{\tau} \quad \text{Eq. 3.11}$$

It is known that charge generation rate is proportional to irradiation light intensity (P_{opt})⁴⁶ where ε , E_{ph} and A represent the extinction coefficient, photon energy and irradiation area, respectively:

$$G = \varepsilon \frac{P_{opt}}{E_{ph} A} \quad \text{Eq. 3.12}$$

Considering that J_{sc} is proportional to n_{photo} ,

$$J_{sc} \propto n_{photo} \quad \text{Eq. 3.13}$$

One can combine either Eq. 3.10 or 3.11 with 3.12 and 3.13 to deduce relationship between J_{sc} and P_{opt} .

$$J_{sc} \propto P_{opt}^\alpha \quad \begin{cases} \alpha = 1 \\ \alpha = 0.5 \end{cases} \quad \text{Eq. 3.14}$$

By recording J_{sc} as a function of P_{opt} , the dominant recombination mechanism in the active layer can be determined.

The J_{sc} obtained from four different types of cells: O3HT:PCBM, PPHT:PCBM, O3HT:BAF and PPHT:BAF were recorded at varying irradiation power from 0.02

mW to 4 mW (Figure 3.26). The proportionality between J_{sc} and P_{opt} was kept within the measurement range. Values of α are listed in Table 3.4 and were obtained from the linear fitting of the data points in Figure 3.26.

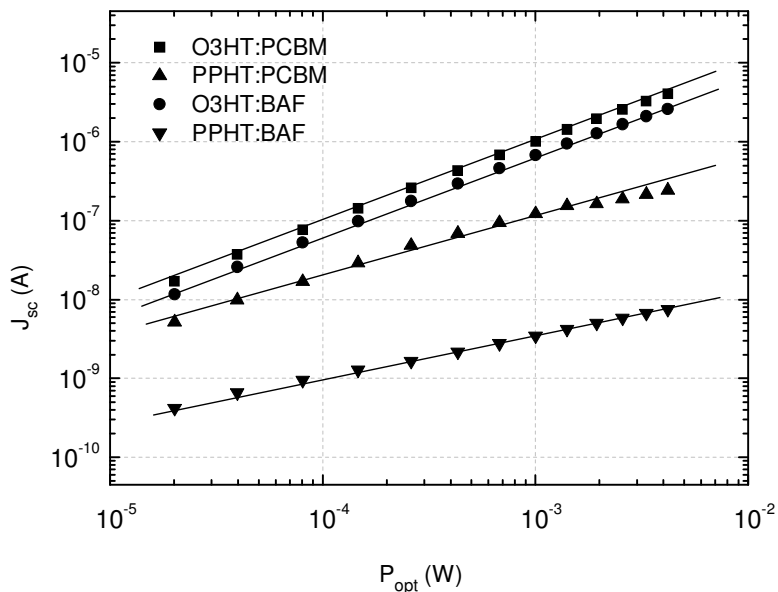


Fig. 3.26. J_{sc} - P_{opt} double-logarithmic plot of O3HT:PCBM (■), PPHT:PCBM (▲), O3HT:BAF(●) and PPHT:BAF (▼) cells.

Table 3.4. values of α from cells with four different blends

Blend	α
O3HT:PCBM	1.02
PPHT:PCBM	1.01
O3HT:BAF	0.72
PPHT:BAF	0.53

A value of $\alpha \sim 1$ was found for O3HT:PCBM and PPHT:PCBM cells, which is similar to reported results from P3HT:PCBM cells.⁴⁷ The value of unity indicates that charge losses in the bulk are dominated by geminate recombination. Charge separation was therefore followed by efficient charge transport through a percolated network: holes within O3HT matrix to PEDOT:PSS layer and electrons *via* PCBM aggregates toward the Al electrode. Apparently, the small chain size in O3HT and terminal recognition groups on PPHT did not affect the portion of non-geminate

recombination.

An intermediate value of $\alpha = 0.72$, between pure geminate ($\alpha = 1$) and non-geminate ($\alpha = 0.5$) recombination, was observed in the O3HT:BAF cell, and both mechanisms may be involved in charge recombination. Increased probability of charge recombination during migration to the electrodes implies less phase separation when PCBM was replaced by BAF. This inference is supported by optical microscopy (Figure 3.27): PCBM micro crystals gradually formed after annealing, but a homogeneous layer was always found in BAF-based cells.

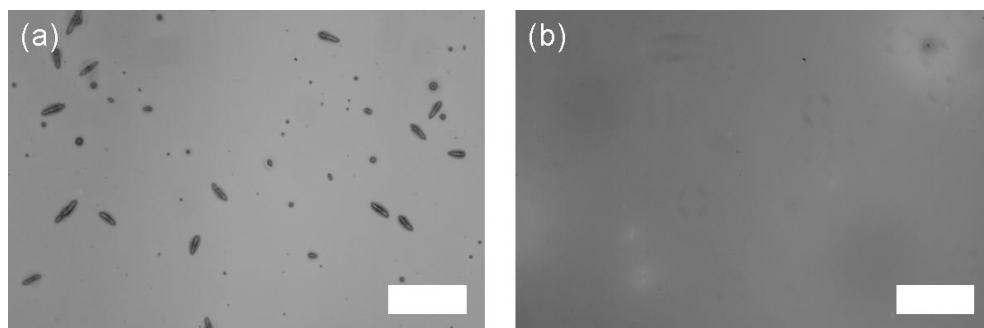


Fig. 3.27. Microscopic photograph of (a) PPHT:PCBM and (b) O3HT:BAF cells after annealing treatment at 170°C for 10 min. Needle-like crystals were found in PCBM-based cells (a). The scale bar 50 μm .

Pure non-geminate recombination, where J_{sc} follows a square-root dependence on P_{opt} , was obtained for the PPHT:BAF cell. In this case, therefore, charge recombination mainly originates from charges from different excitons. The dominating non-geminate recombination may indicate thorough mixing of the donor PPHT and the acceptor BAF materials. Due to the presence of molecular recognition groups, H-bonds between D-A pairs prevent phase separation from occurring during solvent evaporation, and most separated charges fell into the capture cross section of counter charges from neighboring molecules. Even with annealing, α did not change because the active layer micro structure was not altered as noted in section 3.2.2.3.

3.2.3.3 Charge Transport Characteristics of Materials

Metal-insulator-semiconductor field effect transistors (MISFET) devices were employed to determine the charge mobilities of the electron and hole transporting materials (Figure 3.28). In the saturation region of a plot of I_{ds} versus drain-source voltage (V_{ds}), I_{ds} follows equation 3.15:⁴⁸

$$I_{ds} = \frac{WC_i}{2L} \mu (V_g - V_t)^2 \quad \text{Eq. 3.15}$$

where W and L represent the channel width and length between source and drain electrodes, respectively, C_i stands for the capacitance per unit surface of the insulating layer (SiO_2 200 nm, $C_i = 17.24 \text{ nF/cm}^2$) and μ symbolizes charge mobility. A plot of the square root of the drain-source current ($I_{ds}^{0.5}$) versus source-gate voltage (V_g) was recorded. The mobility can be deduced from the slope of linear fitting. The metal contacts employed in the measurement (Au or Ca) were designed as two half semicircles to form a channel length $L = 3 \text{ mm}$ and width $W = 50 \text{ }\mu\text{m}$.

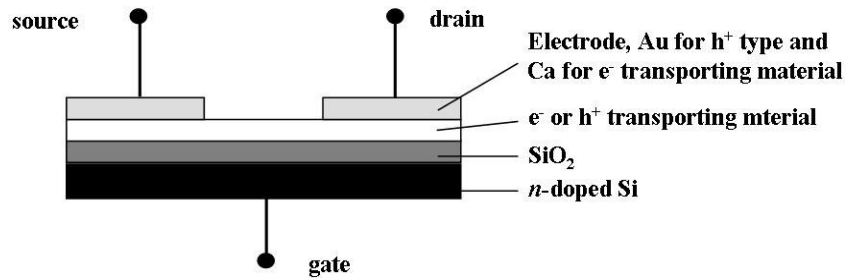


Fig. 3.28. The configuration of MISFET used to determine charge mobilities of electron or hole transporting materials.

3.2.3.3.1 Hole Mobility

Commercial P3HT and O3HT in ODCB were spin coated on heavily n -doped silicon wafer, followed by the evaporation of the Au drain and source contacts through a shadow mask on the semiconductor in a glove box. A variation of two orders of magnitude I_{ds} in output characteristics (V_{ds} scan at constant V_{gs}) between P3HT and O3HT was observed when $V_{gs} = -50$ V and $V_{ds} = -50$ V. On/off ratios of the devices are of the same order of magnitude (76 for P3HT and 34 for O3HT at $V_{ds} = -50$ V and $V_{gs} = -50$ V). In the O3HT device, prominent hysteresis was also detected (Figure 3.29.a) with varying V_{gs} . The charge transport characteristics were extracted from the plot $I_{ds}^{0.5}$ versus V_{gs} where field effect hole mobilities were calculated to be 5.6×10^{-4} cm²/sV and 4.3×10^{-6} cm²/sV for P3HT and O3HT, respectively (Figure 3.29.b). These values are similar to reported data for high and low M_n polythiophenes.⁴⁹ Low hole mobility was attributed to poor organization of O3HT chains. The π - π interactions in short O3HT are not sufficient to drive face to face stacking of the π -conjugation systems, and hole transport *via* a hopping mechanism is blocked by randomly oriented O3HT chains. With annealing at 170°C for 10 min, the same transport characteristics were obtained in O3HT transistor, which is consistent with the observation in section 3.2.2.2.

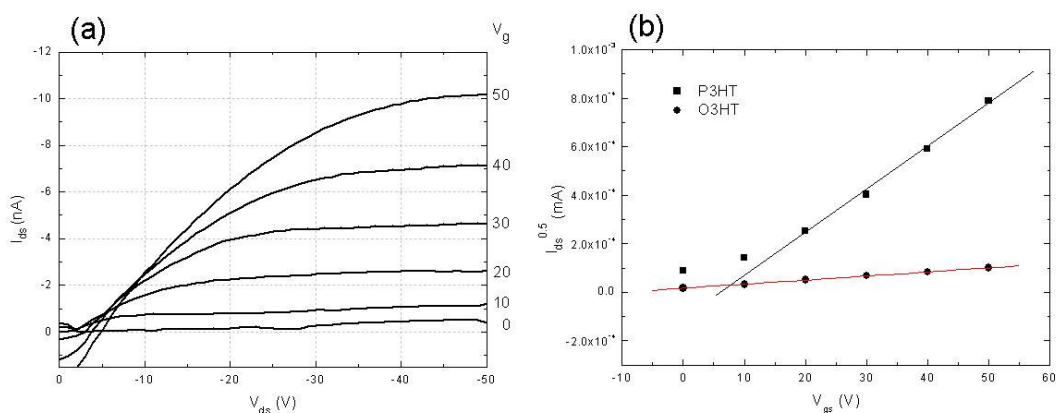


Fig.3.29. (a) Output characteristic of O3HT and (b) transport characteristics of P3HT and O3HT ($V_t = 50$ V)

3.2.3.3.2 Electron Mobility

Electron transporting materials (BAF and C₆₀) were thermally evaporated onto a Si substrate and Ca drain and source contacts were then thermally evaporated through a shadow mask. Different temperatures were applied to the substrate holders in order to provide annealing effect to the deposited film. Reasonable data were obtained from substrates at 44°C for C₆₀ and 57°C for BAF.

The field effect mobility of electrons in C₆₀ was estimated to be $1.2 \times 10^{-2} \text{ cm}^2/\text{sV}$, and which is comparable to reported values ($8 \times 10^{-2} \text{ cm}^2/\text{sV}$).⁵⁰ The mobility of electrons in BAF was calculated to be $1.2 \times 10^{-4} \text{ cm}^2/\text{sV}$ which is one order of magnitude weaker than the value reported for PCBM.⁵¹ A very low threshold voltage (V_t) was found for BAF film (3.1 V) while $V_t = 31 \text{ V}$ was obtained for C₆₀ from the extrapolated intersect in Figure 3.30.b. The low V_t of BAF film might be a result from better match of energy level between the Ca work function (2.87 eV) and BAF electron affinity (2.82 eV) compared to C₆₀ (electron affinity = 2.65 eV) which facilitates the electron injection.

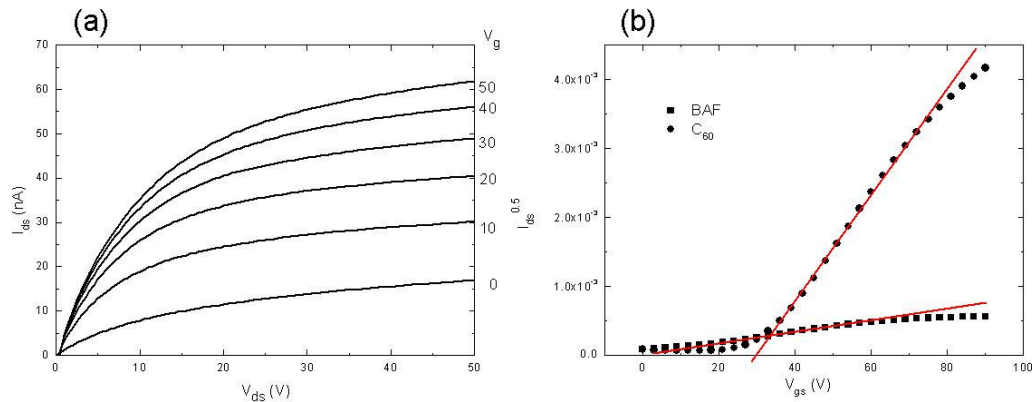


Fig. 3.30. (a) Output characteristics of BAF film and (b) transport characteristics of C₆₀ and BAF films.

The devices were examined by AFM, and it was observed that large grains were scattered on the surface for the BAF transistor (Figure 3.31). The large aggregates may be a consequence of the H-bonds in barbituric acid units on BAF.

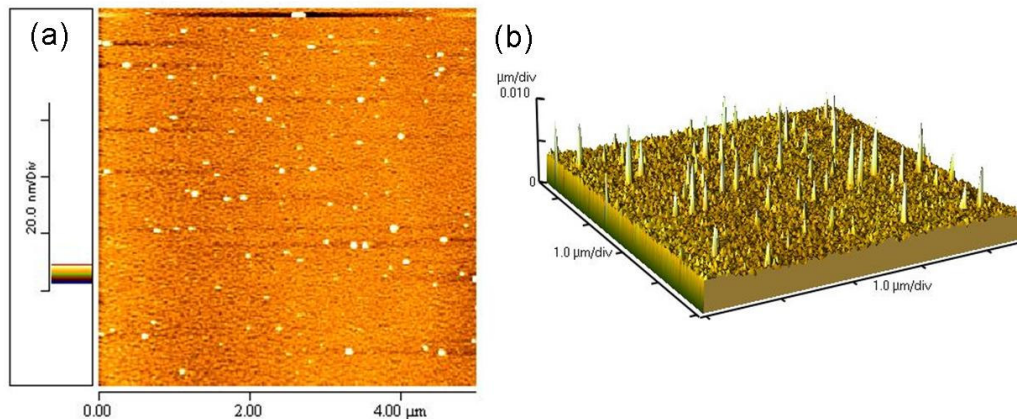


Fig. 3.31. Atomic force microscopy scan of the surface of BAF a transistor presented in 2-D (a) and 3-D (b). White spots are large gains with the size exceeding height gradient.

A scan at higher resolution revealed the structure of the films (Figure 3.32). Homogeneous granular assemblies were observed in both devices, but the grain size in BAF film is half that in the C_{60} film (Figure 3.32.e and f), which induces more inter-grain boundaries in the BAF transistor. This and lower dimensionality of BAF crystals compared to C_{60} may explain the lower efficiency of electron transport in the BAF material. Within each grain, BAF assemblies may adopt the architecture described in section 2.3.5, where the directionality of C_{60} moieties is induced by H-bonding. The conductivity of BAF electron transport is therefore expected to be anisotropic. Smaller assemblies are formed and are randomly distributed in the film, which is contrast to the assembly of C_{60} crystals possessing isotropic electronic properties. The low FET mobility of BAF is consistent to the observed weak J_{sc} and efficiency in a PPHT:BAF PV cell, if indeed electrons are poorly transported through BAF.

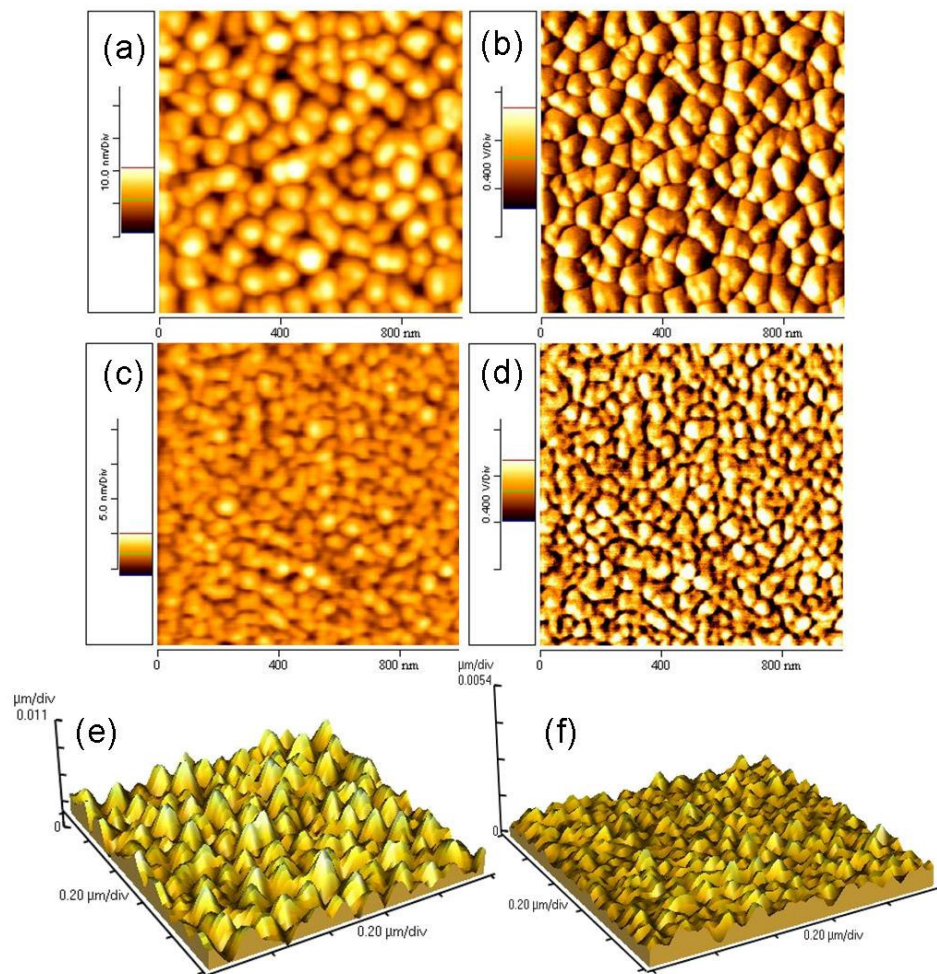


Fig. 3.32. Atomic force microscopy scan of C_{60} (a) in topology mode and (b) in phase mode, and BAF transistors (c) in topology mode and (d) in phase mode. The surface profiles of (e) C_{60} and (f) BAF transistors are presented in 3-D image.

3.3 Conclusion

The processability of oligothiophene electron D molecule was improved by using newly prepared PPHT. Blend solution of PPHT:2.2 were prepared but the solid state devices still suffered from poor surface morphology which induced large leakage currents. By using BAF, consistent device fabrication was achieved and the stability of the electron accepting material was improved. With increasing ratio of BAF to PPHT, improved J_{sc} was obtained which increased PV cell efficiency. With more BAF present in the blend, better percolation can occur, therefore, higher current was obtained. With annealing treatment, PPHT:BAF based PV cells exhibited decreased J_{sc} which is attributed to molecular degradation.

Non-geminate recombination dominates the recombination mechanism, which is in contrast to conventional P3HT:PCBM PV cells. Extensive non-geminate recombination indicates poor phase separation, where PPHT and BAF molecules are throughout mixed. Due to homogeneous distribution of PPHT and BAF, most charges can recombine after excitons dissociation. From OFET mobility experiments, it was calculated that the PPHT chains are too short for sufficient hole mobility, while BAF might form anisotropic aggregates which hamper electron transport.

3.4 Reference

- 1 D. Whrle, D. Meissner, *Adv. Mater.* **1991**, *3*, 129.
- 2 M. Knupfer, *Appl. Phys. A* **2003**, *77*, 623.
- 3 P. Peumans, A. Yakimov, S. R. Forrest *J. Appl. Phys.* **2003**, *93*, 3693.
- 4 D. L. Morel, A. K. Gosh, T. Feng, E. L. Stogryn, P. E. Purwin, R. F. Shaw, C. Fishman, *Appl. Phys. Lett.* **1978**, *32*, 495.
- 5 C. W. Tang, *Appl. Phys. Lett.* **1986**, *48*, 183.
- 6 J. M. C. R. Nunzi, *Physique* **2002**, *3*, 523.
- 7 H. Hoppe, N. S. Sariciftci, *J. Mater. Res.* **2004**, *19*, 1924.
- 8 (a) T. W. Hagler, K. Pakbaz, A. J. Heeger, *Phys. Rev. B* **1994**, *49*, 10968. (b) Y. Yang, Q. Pei, A. J. Heeger, *Synth. Met.* **1996**, *78*, 263. (c) I. H. Campbell, T. W. Hagler, D. L. Smith, J. P. Ferraris, *Phys. Rev. Lett.* **1996**, *76*, 1900.
- 9 R. Kersting, U. Lemmer, M. Deussen, H.J. Bakker, R.F. Marth, H. Kurz, V. I. Arkhipov, H. Bässler, E.O. Göbel, *Phys. Rev. Lett.* **1994**, *73*, 1440.
- 10 R. C. Powell; Z. G. Soos, *J. Lumin.* **1975**, *11*, 1.
- 11 P. B. Miranda, D. Moses, A. J. Heeger, *Phys. Rev. B* **2001**, *64*, 81201.
- 12 (a) M. Theander, A. Yartsev, D. Zigmantas, V. Sundstrom, W. Mammo, M. R. Andersson, O. Inganas, *Phys. Rev. B* **2000**, *61*, 12957. (b) A. Haugeneder, M. Neges, C. Kallinger, W. Spirkl, U. Lemmer, J. Feldmann, U. Scherf, E. Harth, A. Gugel, K. Mullen, *Phys. Rev. B* **1999**, *59*, 15346. (c) T. Stubinger, W. Brutting, *J. Appl. Phys.* **2001**, *90*, 3632.
- 13 V. I. Arkhipov, P. Heremans, H. Bässler, *Appl. Phys. Lett.* **2003**, *82*, 4605.
- 14 J. G. Müller, J. M. Lupton, J. Feldmann, U. Lemmer, M. C. Scharber, N. S. Sariciftci, C. J. Brabec, U. Scherf, *Phys. Rev. B* **2005**, *72*, 195208.
- 15 C. Brabec, G. Zerza, G. Cerullo, S. De Silvestri, S. Luzatti, J. C. Hummelen, N. S.

-
- Sariciftci, *Chem. Phys. Lett.* **2001**, *340*, 232.
- 16 M. C. Scharber, D. Mühlbacher, M. Koppe, P. Denk, C. Waldauf, A. J. Heeger, C. J. Brabec, *Adv. Mater.* **2006**, *18*, 789.
- 17 N. S. Sariciftci, L. Smilowitz, A. J. Heeger, F. Wudl, *Science* **1992**, *258*, 1474.
- 18 (a) C. H. Lee, G. Yu, D. Moses, K. Pakbaz, C. Zhang, N. S. Sariciftci, A. J. Heeger, F. Wudl, *Phys. Rev. B* **1993**, *48*, 15425. (b) S. Morita, A. A. Zakhidov, K. Yoshino, *Solid State Commun.* **1992**, *82*, 249. (c) S. Morita, S. Kiyomatsu, X. H. Yin, A. A. Zakhidov, T. Noguchi, T. Ohnishi, K. Yoshino, *J. Appl. Phys.* **1993**, *74*, 2860.
- 19 (a) J. Liu, Y. Shi, Y. Yang, *Adv. Funct. Mater.* **2001**, *11*, 420. (b) H. Hoppe, M. Niggenmann, C. Winder, J. Kraute, R. Hiesgen, A. Hinsch, D. Meissner, N. S. Sariciftci, *Adv. Funct. Mater.* **2004**, *14*, 1005.
- 20 (a) C. J. Brabec, C. Winder, N. S. Sariciftci, J. C. Hummelen, A. Dhanabalan, P. A. van Hal, R. A. J. Janssen, *Adv. Funct. Mater.* **2002**, *12*, 709. (b) S. H. Park, A. Roy, S. Beaupre, S. Cho, N. Coates, J. S. Moon, D. Moses, M. Leclerc, K. Lee, A. J. Heeger, *Nature Photon.* **2009**, *3*, 297.
- 21 (a) J. K. van Duren, X. Yang, J. Loos, C. W. T. Bulle-Lieuwma, A. B. Sieval, J. C. Hummelen, R. A. J. Janssen, *Adv. Funct. Mater.* **2004**, *14*, 425.
- 22 (a) F. Padinger, R. S. Rittberger, N. S. Sariciftci, *Adv. Funct. Mater.* **2003**, *13*, 1. (b) P. Peumans, S. Uchida, S. R. Forrest, *Nature* **2003**, *425*, 158.
- 23 A. C. Mayer, S. R. Scully, B. E. Hardin, M. W. Rowell, M. D. McGehee, *Mater. Today* **2007**, *10*, 28.
- 24 S. H. Park, A. Roy, S. Beaupré, S. Cho, N. Coates, J. S. Moon, D. Moses, M. Leclerc, K. Lee, A. J. Heeger *Nature Photonics* **2009**, *3*, 297.
- 25 H. Hoppe, N. S. Sariciftci, *J. Mater. Chem.* **2006**, *16*, 45.

-
- 26 U. Scherf, A. Gutacker, N. Koene, *Acc. Chem. Res.* **2008**, *41*, 2086.
- 27 C. Park, J. Yoon, E. L. Thomas, *Polymer* **2003**, *44*, 6725.
- 28 (a) U. Stalmach, B. de Boer, C. Videlot, P.F. van Hutten, G. Hadziioannou, *J. Am. Chem. Soc.* **2000**, *122*, 5464. (b) G. Hadziioannou, *MRS Bull.* **2002**, *27*, 456.
- 29 H. Spanggaard, F. C. Krebs, *Sol. Energy Mater. Sol. Cells* **2004**, *83*, 125.
- 30 A. Cravino, N. S. Sariciftci, *J. Mater. Chem.* **2002**, *12*, 1931.
- 31 A. Marcos Ramos, M. T. Rispens, J. K. J. Van Duren, J. C. Hummelen, R. A. J. Janssen, *J. Am. Chem. Soc.* **2001**, *123*, 6714.
- 32 (a) T. Benincori, E. Brenna, F. Sannicolo, L. Trimarco, G. Zotti, P. Sozzani, *Angew. Chem., Int. Ed.* **1996**, *35*, 648. (b) F. Zhang, M. Svensson, M. R. Andersson, M. Maggini, S. Bucella, E. Menna, O. Inganas, *Adv. Mater.* **2001**, *13*, 1871. (c) J. Roncali, *Chem. Soc. Rev.* **2005**, *34*, 483.
- 33 (a) P. Schilinsky, C. Waldauf, C. J. Brabec, *Appl. Phys. Lett.* **2002**, *81*, 3885. (b) A. F. Nogueira, I. Montanari, J. Nelson, J. R. Durrant, C. Winder, N. S. Sariciftci, C. Brabec, *J. Phys. Chem. B* **2003**, *107*, 1567.
- 34 C.-H. Huang “*Toward supramolecular heterojunctions: Self-assembled hydrogen-bonded architectures for organic photovoltaic devices*” Thesis, Université Bordeaux 1, **2006**.
- 35 C.-H. Huang, N. D. McClenaghan, A. Kuhn, J. W. Hofstraat, D. M. Bassani, *Org. Lett.* **2005**, *7*, 3409.
- 36 F. Padinger, R. S. Rittberger, N. S. Sariciftci, *Adv. Func. Mater.* **2003**, *13*, 1.
- 37 U. Koch, A. Fojtik, H. Weller, A. Henglein, *Chem. Phys. Lett.* **1985**, *122*, 507.
- 38 A. L. Roest, J. J. Kelly, D. Vanmaekelbergh, E. A. Meulenkaamp, *Phys. Rev. Lett.*, **2008**, *89*, 036801.
- 39 W. J. E. Beek, M. M. Wienk, R. A. J. Janssen, *Adv. Mater.* **2004**, *16*, 1009.

-
- 40 The detailed synthesis procedure of ZnO nano particle is described in experimental section.
- 41 (a) E. A. Meulenkaamp, *J. Phys. Chem. B* **1998**, *102*, 5566 (b) W. J. E. Beek, M. M. Wienk, M. Kemerink, X. Yang, R. A. J. Janssen, *J. Phys. Chem. B* **2005**, *109*, 9505.
- 42 (a) F. Paudinger, R. S. Rittberger, N. S. Sariciftci, *Adv. Func. Mater.* **2003**, *13*, 1. (b) P. Peumans, S. Uchida, S. R. Forrest, *Nature* **2003**, *425*, 158.
- 43 R. C. Hirons, R. de Bettignies, J. Leroy, S. Bailly, M. Firon, C. Sentein, A. Khoukh, H. Preud'homme, C. Dagron-Lartigau, *Adv. Funct. Mater.* **2006**, *16*, 2263.
- 44 P. schilinsky, C. Waldauf, J. Hauch, C. J. Brabec, *J. Appl. Phys.* **2004**, *95*, 2816.
- 45 (a) S.M. Sze. *Physics of Semiconductor Devices*. Wiley New York, **1981**. (b) R. Pacios, J. Nelson, J. R. Durrant, D. D. C. Bradley, M. Westerling, R. Österbacke, C. J. Brabec, *Proc. SPIE* **2004**, *264*, 5215.
- 46 B. Van Zeghbroeck, *Principles of Semiconductor Devices and Heterojunctions*, Prentice Hall, **2007**.
- 47 (a) C. Waldauf, M. C. Scharber, P. Schilinsky, J. A. Hauch, C. J. Brabec, *J. Appl. Phys.* **2006**, *99*, 104503. (b) V. D. Mihailetschi, H. Xie, B. de Boer, L. J. A. Koster, P. W. M. Blom, *Adv. Func. Mater.* **2006**, *16*, 699.
- 48 G. Horowitz, *Adv. Mater.* **1998**, *10*, 365.
- 49 (a) A. Zen, J. Pflaum, S. Hirschmann, W. Zhuang, F. Jaiser, U. Asawapirom, J. P. Rabe, U. Scherf, D. Necher *Adv. Func. Mater.* **2004**, *14*, 757. (b) A. M. Ballantyne, L. Chen, J. Dane, T. Hammant, F. M. Braun, M. Heeney, W. Duffy, I. McCulloch, D. D. C. Bradley, J. Nelson, *Adv. Func. Mater.* **2008**, *18*, 2373.
- 50 (a) R. C. Haddon, A. S. Perel, R. C. Morris, T. T. M. Palstra, A. F. Hebard, R. M. Fleming, *Appl. Phys. Lett.* **1995**, *67*, 121. (b) T. Kanbara, K. Shibata, S. Fujiki, Y. Kubozono, S. Kashino, T. Urisu, M. Sakai, A. Fujiwara, R. Kumashiro, K.

Tanigaki, *Chem. Phys. Lett.* **2003**, 379, 223.

51 C. Waldauf, C. Schilinsky, M. Perisutti, J. Hauch, C. J. Brabec, *Adv. Mater.* **2003**, 15, 2084.

4 Summary and Conclusion

Summary and Conclusion

With growing global demand on energy supplies, environmentally friendly and renewable energy sources to replace limited fossil fuels are important for the present and future. Solar energy provides a clean and nearly limitless alternative to solve the looming energy crisis, and organic solar PV cells are envisaged to be economical and widely-applicable forms of collecting solar irradiation and converting it into electricity. In this research, a supramolecular self-assembly approach using complementary H-bonding recognition was used in an attempt to control material morphology in the active layers of these devices.

A small molecule electron donor, pentathiophene functionalized with terminal melamine groups was prepared as an electron donating material. Due to its low solubility after introduction of the melamine groups, this material was not conducive to the preparation of solid-state devices. Short oligo-3-hexylthiophenes with terminal melamine molecular recognition moieties (PPHT) were synthesized, which overcame the solubility problems previously met in device fabrication process. In parallel, a new fullerene derivative with a barbituric acid motif (BAF) possessing superior solubility as an electron accepting material was also prepared to replace compound **2.2** which exhibits limited solubility.

Strong association induced by the complementary H-bonding sites between PPHT and BAF was observed and led to the formation of aggregates in an ODCB solution. This phenomenon was verified by adding DMSO to block the inter-molecular H-bonding between PPHT and BAF, resulting in full dissolution. The supramolecular self-assembly was also observed in the photoinduced dimerization of BAF where close proximity of fullerene moieties was induced by a fused Hamilton receptor. Additionally, in the single crystal of BAF, two pairs of H-bonds were

observed between every two BAF molecules, leading to the formation of infinite 1-D H-bonded tapes.

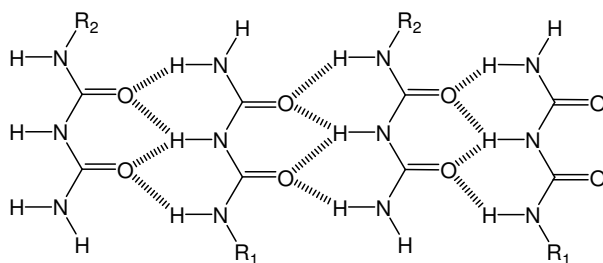
In the solid-state film experiments, the suppression of $S_N \leftarrow S_1$ state absorption and appearance of PPHT^{**+} absorption indicated that a rapid charge transfer from PPHT to BAF occurred upon excitation of PPHT in the presence of BAF. By utilizing a PPHT:BAF blend, smooth surfaces were obtained in PV cells which limited leakage current passing through the active layer. PPHT:BAF PV cells seemed inert to annealing treatment as concluded from similar drift length obtained after different annealing temperature. However, a drop in J_{sc} was noted, suggesting that too high temperatures (over 80°C) are not applicable. With increasing proportion of BAF, higher J_{sc} were observed, attributed to better percolation allowing more efficient charge transport.

Non-geminate recombination dominates in PPHT:BAF PV cells, suggesting that extensive mixing of PPHT and BAF in the active layer. Dissociated excitons, thus easily recombine with a counter charge due to the close mixing of electron D and A molecules. This observation is consistent with the low J_{sc} obtained in PV cells, which also points to the absence of a bicontinuous network for charge transport to the corresponding electrodes.

Low field-effect hole mobility of O3HT, attributed to the poor crystallinity of the short polymer chain employed was observed. IPCE experiments indicate that photon-to-current conversion is low. The field-effect electron mobility of BAF was found to be two orders lower than the pristine C₆₀. This may be explained by the increased boundaries due to smaller grains as observed from AFM measurements, combined with the anisotropic conductivity of BAF.

In conclusion, the balance between inter-polymer π - π interactions and inter-molecular H-bonding is important in controlling the morphology in solid-state

films. Sufficient phase segregation and charge carrier mobility are keys for improving overall device efficiency. Using oligothiophenes with proper molecular weight between 10 kD to 15 kD¹ could provide reasonable crystallinity for inter-polymer self-assembly while still possessing viability for characterization of end group functionalization. On the other hand, the variety of H-bonding motifs² offers the possibility to adjust inter-molecular association stabilities. For example, the biuret motif provides three H-bonding donating and three accepting sites, with possible formation of continuous tape (Scheme 4.1). Improved understanding of how inter-molecular interactions affect the active layer structure can lead to better control of film morphology on the molecular scale.



Scheme 4.1.

References

-
- 1 (a) R. J. Kline, M. D. McGehee, E. N. Kadnikova, J. Liu, J. M. J. Fréchet, M. F. Toney, *Macromolecules* **2005**, *38*, 3312. (b) A. M. Ballantyne, L. Chen, J. Dane, T. Hammant, F. M. Braun, M. Heeney, W. Duffy, I. McCulloch, D. D. C. Bradley, J. Nelson, *Adv. Funct. Mater.* **2008**, *18*, 2373. (c) A. Zen, J. Pflaum, S. Hirschmann, W. Zhuang, F. Jasier, U. Asawapirom, J. P. Rabe, U. Scherf, D. Neher, *Adv. Funct. Mater.* **2004**, *14*, 757.
 - 2 L. J. Prins, D. N. Reinhoudt, P. Timmerman, *Angew. Chem. Int. Ed.* **2001**, *40*, 2382.

5 Experimental Section

Experimental Section

5.1 General

^1H and ^{13}C NMR spectra were recorded at room temperature on a Bruker AC-250 FT or DPX-300 FT spectrometer using the residual solvent peak as internal reference unless otherwise indicated. Chemical shifts are given in ppm (δ) with respect to trimethylsilane. Abbreviations used s = singlet, d = doublet, t = triplet, q = quartet, m = multiplet, b = broad. IR spectra were obtained on a Perkin Elmer Spectrum 100 FT IR Spectrometer with KBr pellet. MALDI-ms spectra were recorded on an Applied Biosystem Voyager. ESI–ma spectra were recorded on an Applied Biosystem QStar. Electronic absorption spectra were obtained using a Varian Cary 5000 or Safas Monaco UVmc2. Fluorescence spectra were recorded on a Hitachi F-4500 fluorescence spectrophotometer. Single photon counting experiments were performed on a Fluorolog 3 fluorimeter equipped with a Hamamatsu R2158 photomultiplier. The thickness of organic films obtained by spin-coating were measured on an Alpha-Step IQ Surface Profilometer. Scanning electron microscopic images were captured by a Jeol JSM-820. Thermal gravimetric analyses were performed on a Netzsch STA 409 under $\text{N}_{2(\text{g})}$ atmosphere. Atomic force microscope scans were obtained on a Thermomicroscope Autoprobe CP Research AFM with Si probe (NCL, tip diameter $r \sim 6$ nm, spring constant = 40 N/m, eigenfrequency = 160 KHz, Nanosensor) in tapping mode.

5.2 Materials

Commercially-available starting materials were obtained from Aldrich, Lancaster, or Avocado unless otherwise mentioned. Anhydrous solvents, such as absolute ethanol, chlorobenzene, 1,2-dichlorobenzene, DMSO and DMF were used as received. Dichloromethane, toluene and acetonitrile were distilled over calcium hydride (CaH_2). Tetrahydrofuran (THF) and diethyl ether were dried over sodium/benzophenone and distilled immediately before use.

5.3 X-ray Diffraction Crystallography

Data were collected on the PROXIMA1 beamline at the SOLEIL synchrotron. The phasing and refinement program were SHELXD and SHELXL,¹ respectively. The data have been processed with XDS² and prepared with XPREP.¹ The detailed data is listed in the Appendix.

5.4 Electrochemistry Measurements

Cyclic voltammetric measurements were carried out on a μ Autolab General Purpose EC system Type II using a three-electrode arrangement, an Ag/Ag^+ counter electrode, Pt wire auxiliary electrode, Pt disk or Ag wire working electrode. The data were collected with Pt disk (1 cm^2) coated with PPHT or a Ag wire in a solution of BAF (1 mM in ODCB:AcCN = 2:1). Tetrabutylammonium hexafluorophosphate (Bu_4NPF_6 , 0.1M in AcCN for PPHT and in ODCB:AcCN = 2:1 for BAF) was used as supporting electrolyte. The reported redox potentials were obtained with a scan rate of 100 mV/S and calibrated from the oxidation potential of Fc/Fc^+ used as internal standard.

5.5 Picosecond Time-resolved Spectroscopy

The time-resolved spectroscopy experiments were performed in Centre de Physique Moléculaire Optique et Hertzienne (CPMOH) in Bordeaux.

5.5.1 Transient Absorption Set-up

A Ti:Sapphire laser system emitting 30 fs pulses of 0.6 mJ at 800nm and 1 kHz pulse repetition rate (Femtopower Compact Pro) equipped with a home built optical parametric generator and frequency mixers were used to excite samples at the chosen wavelength. A white light continuum (390 nm – 1000 nm) generated in a 5 mm methanol cell was used as the probe pulse. Variable delay times between pump and probe pulses were obtained using a mechanical delay line with 0.1 μm resolution. For solid state films, PPHT or PPHT/BAF solutions in ODCB were drop-cast on a glass slide and dried. White light signal and reference spectra were recorded using a two channel fibre spectrometer (Avantes Avaspec-2048-2). Transient spectra were averaged to obtain an error less than 10^{-4} O.D. for all wavelengths. The temporal resolution of the set-up was *ca.* 60 fs. The temporal chirp of the probe pulse was corrected by a computer program with respect to a Lorentzian fit of a Kerr signal generated in a 0.2 mm glass plate used in a place of sample.

5.5.2 Time resolved Fluorescence Set-ups

The fluorescence excitation light pulses were obtained in the same way as in transient absorption experiment outlined above. The highest pulse energies used to excite the sample did not exceed 100 nJ and the average power of excitation beam was 0.1 mW at a pulse repetition rate of 1 kHz focused onto a spot with a diameter of 0.1 mm in a 10 mm path length silica cell. The fluorescence emitted in the forward

direction was collected by reflective optics and focused with a spherical mirror through a polarizer onto the input slit of a spectrograph (Chromex 250) coupled to a streak camera (Hamamatsu 5680 equipped with a fast single sweep unit M5676, temporal resolution 2 ps). For liquid phase fluorescence measurement, the solutions were placed in 1 mm circulating cell made from fused silica. The convolution of a rectangular streak camera slit in the sweep range of 250 ps with the electronic jitter of the streak camera trigger pulse provided a Gaussian (over 4 decades) temporal apparatus function with a FWHM of 20 ps.

5.6 General Procedure to Prepare Solid State Cells

Indium tin oxide (ITO)/glass slides were etched by mixing Zn powder with HCl solution, followed by rinsing with water. Etched ITO / glass were cleaned sequentially in ultrasonic bath of acetone, ethanol, and *iso*-propanol for 15 min each. The rinsed ITO/glasses were transferred to a Jelight Company Inc. UVO Cleaner 42 – 220 for surface cleaning for 5 min. A poly(3,4-ethylenedioxythiophene) doped with polystyrene sulfonic acid (PEDOT:PSS) buffer layer was coated onto cleaned ITO/glass on a Specialty Coating System Spincoat G3-8 by spin-coating (Acceleration time: 2 sec., 4000 r.p.m., 60 sec.). The PEDOT:PSS coated ITO/glass were cured at 110°C under vacuum for 1 h. After curing, the substrates were stored in glove box for the next step.

All blends were prepared in glove box with solvent stored in glove box and were stirred overnight. The blends were coated onto substrates using a Specialty Coating System Spincoater P6700 (Stage 1: acceleration time: 10 sec., 1000 r.p.m., 60 sec. stage 2: acceleration time: 10 sec., 2000 r.p.m., 30 sec.). Blend-coated substrates were dried under vacuum for 15 min. Deposition of the top electrode (Al) was done by

thermal evaporation under vacuum ($1 \times 10^{-6} \sim 5 \times 10^{-6}$ mbar) through a shadow mask (Figure 5.1) to define a device area of 0.1 cm^2 . The evaporation of Al electrode was monitored by an oscillating quartz monitor to obtain a thickness of the Al electrodes of $\sim 100 \text{ nm}$. The I - V characteristics of the cells were measured in the glove box using a Keithley 4200 characterization system.

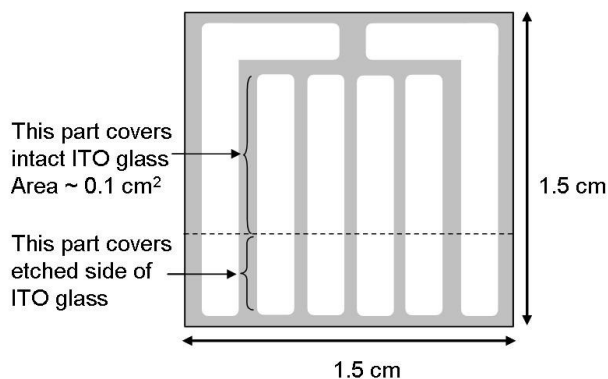


Fig. 5.1. Mask used in the Al electrode deposition. Four electrodes can be fabricated on one substrate.

5.7 General Procedure to Prepare Field Effect Transistors

The SiO_2/Si substrates were cleaned in stirred acetone and *iso*-propanol for 30 min each. The cleaned substrates were transferred to a Jelight Company Inc. UVO Cleaner 42 – 220 for surface cleaning for 5 min.

5.7.1 O3HT Transistors

O3HT solutions (10 mg/mL) in 1,2-dichlorobenzene were prepared in a glove box and were spin-coated onto the cleaned SiO_2/Si substrates using a Specialty Coating System Spincoater P6700 (Stage 1: acceleration time: 10 sec., 1000 r.p.m., 60 sec. stage 2: acceleration time: 10 sec., 2000 r.p.m., 30 sec.). Deposition of the gold electrodes was done by thermal evaporation under vacuum ($1 \times 10^{-6} \sim$

5×10^{-6} mbar) through a shadow mask to define a round device of 3 mm in diameter possessing a central gap of 50 μm in width. The characterization was carried out in glove box using a Keithley 4200 characterization system.

5.7.2 C₆₀ and BAF Transistors

C₆₀ or BAF was thermally evaporated under vacuum ($1 \times 10^{-6} \sim 5 \times 10^{-6}$ mbar) onto the cleaned SiO₂/Si substrates at different temperatures (44°C for C₆₀ and 57°C for BAF) on an Edwards Auto 306 evaporator. The substrate temperatures were monitored by the sample holder resistance. An empirical formula was used to estimate sample hold temperatures (T) from recorded resistances (R):

$$T(K) = -243.75 + 2.32R + 0.0012R^2 - 2.3 \times 10^{-7} R^3 + 273$$

The coated SiO₂/Si substrates were transferred to an evaporator in the glove box and calcium electrodes were deposited by thermal evaporation under vacuum ($1 \times 10^{-6} \sim 5 \times 10^{-6}$ mbar) through a shadow mask to define a round device of 3 mm in diameter possessing a central gap of 50 μm or 25 μm in width. The characterization was carried out in the glove box using a Keithley 4200 characterization system.

5.8 J_{sc} vs. Irradiation Measurements

The PV cells prepared as mentioned above were transferred from the glove box to a dark enclosure and irradiated by a LED lamp (CML, Model-ILL3A0001, 3 W) at 470 nm with power adjusted from 0.02 mW to 4 mW. The current characteristics were recorded using a Keithley 6487 picoammeter/voltage source.

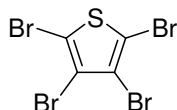
5.9 IPCE Measurements

A Xe lamp (500W) light source equipped with a monochromator (Horiba, Triax 180) was used to excite the samples. The blank measurement of irradiation intensities

were converted to current using an integrating sphere (Sphere Optics, 6", SR-5-S) equipped with a Si diode (Sphere Optics, 10", TO-8). The PV cells prepared as mentioned above were transferred from the glove box to a dark enclosure and irradiated by diffracted light through an optical fiber. The current characteristics were recorded using a Keithley 6487 picoammeter/voltage source.

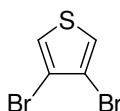
5.10 Synthesis

2,3,4,5-Tetrabromothiophene³ (2.3, C₄Br₄S, MW: 399.72)



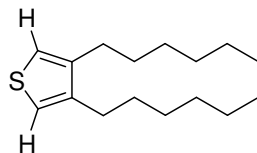
To a CHCl₃ solution (5 mL) containing thiophene (5 mL, 62.5 mmol) was added Br₂ dropwise at rt. The mixture was stirred for 24 h then refluxed for 2 h. After cooling to rt, KOH (6 g) dissolved in EtOH (36 mL) was added dropwise into the mixture then refluxed for 4 h. After cooling, the solution was extracted with CHCl₃ and dried with Na₂SO₄ to afford white powder product (23.9 g, yield = 96%) which was used without further purification. ¹³C NMR (75MHz, CHCl₃) δ 116.9, 110.3 GC-ms m/z (%) 399.7 (M⁺, 100).

3,4-Dibromothiophene³ (2.4, C₄H₂Br₂S, MW: 241.93)



To a solution of AcOH/H₂O (10 mL/20 mL) was added Zn dust (3.37 g) and 2,3,4,5-tetrabromothiophene (4.0 g, 10 mmol) in small portions. The mixture was kept stirred at rt for 1 h, then refluxed for 3.5 h. The cooled solution was filtered through celite and extracted with ether. The extracts were dried to afford a yellow oily product (1.45 g, yield = 60%). ¹H NMR (250 MHz, CHCl₃) δ 7.22 (s, 2H); ¹³C NMR (75MHz, CHCl₃) δ 123.8, 113.9 GC-ms m/z (%) 242 (M⁺, 100).

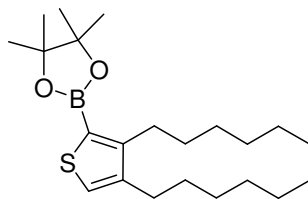
3,4-Dihexylthiophene⁴ (2.5, C₁₆H₂₈S, MW: 252.46)



To a toluene (20 mL) solution containing 3,4-dibromothiophene (550 mg, 2.24 mmol) and [1,3-bis(diphenylphosphino)propane]-nickel(II)chloride (162 mg, 0.3 mmol) was added 2N *n*-hexylmagnesiumbromide in THF (8 mL, 16 mmol) dropwise at 0°C under N₂. The mixture was then refluxed for 16 h before being added dropwise into a dilute HCl solution. The aqueous layer was extracted with ether and the organic extracts were washed with water and brine and dried using Na₂SO₄. The solvent was removed under reduced pressure and the residue was purified by flash column chromatography (silica gel, pentane) to afford a pale yellow oil (491 mg, yield = 87%). ¹H NMR (250 MHz, CHCl₃) δ 6.88 (s, 1H), 2.50 (t, *J* = 7.5 Hz, 4H), 1.59 (m, 4H), 1.33 (m, 12H), 0.89 (t, *J* = Hz, 6H); ¹³C NMR (75MHz, CHCl₃) δ 142.1, 119.8, 31.7, 29.6, 29.2, 28.8, 22.6, 14.0; GC-ms *m/z* 251.9 (M⁺, 100).

2-[2',5'-Bis(3',4'-ehtylenedioxythienyl)]-3,4-dihexylthiophene⁵

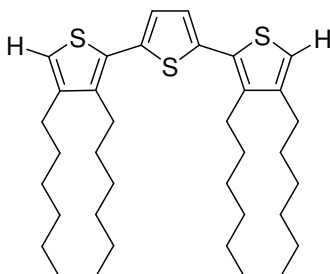
(2.6, C₂₂H₃₉BO₂S, MW: 378.42)



To a THF solution (20 mL) containing 3,4-dihexylthiophene (620 mg, 2.5 mmol)

was added with *n*-BuLi (2 mL, 5 mmol) dropwise at -80°C under N₂. The mixture was warmed to -50°C, stirred for 1 h, and then cooled to -80°C. After cooling to rt, to the solution was added 2-isopropoxy-4,4,5,5-tetramethyl-1,3,2-dioxaborolane (0.55 mL, 2.7 mmol) in THF (2.5 mL) dropwise and stirred overnight. The mixture was poured into NH₄Cl (1 M, 50 mL) and extracted with ether. The organic layer was collected and washed with water, brine and dried with Na₂SO₄. The solvent was removed under reduced pressure to afford a yellow liquid (0.84 g, yield = 89%). ¹H NMR (250 MHz, CHCl₃) δ 7.16 (s, 1H), 2.79 (t, *J* = 7.0 Hz, 2H), 2.52 (t, *J* = 7.3 Hz, 2H), 1.59 (m, 4H), 1.31 (m, 12H), 1.24 (s, 12H), 0.89 (m, 6H).

3,3'',4,4''-Tetrahexyl-2,2':5',2''-terthiophene⁶ (2.7, C₃₆H₅₆S₃, MW: 585.02)

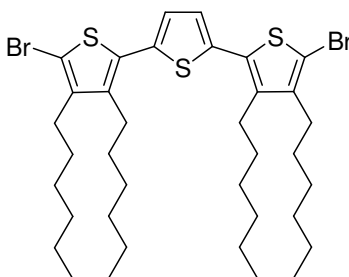


To a THF/toluene/H₂O solution (15 mL/15 mL/1 mL) was added 2-[2',5'-bis(3',4'-ethylenedioxythienyl)]-3,4-dihexylthiophene (4.10 g, 9.7 mmol), 2,5-dibromothiophene (0.66 g, 3.2 mmol), K₂CO₃ (3.54 g, 25.6 mmol) and Pd(PPh₃)₄ (0.37 g, 0.32 mmol). The mixture was bubbled with nitrogen for 20 min, then refluxed overnight. After cooling the solution was filtered through celite and washed with THF. The collected organic solution was dried with Na₂SO₄ and the solvent was removed under reduced pressure. The crude product was purified by column chromatography (silica gel, *n*-hexane) to afford a pale green oil (2.76 g, yield = 50%). ¹H NMR

(300 MHz, CDCl₃) δ 7.05 (s, 2H), 6.87 (s, 2H), 2.27 (t, $J = 7.9$ Hz, 4H), 2.54 (t, $J = 7.9$ Hz, 4H) 1.70-1.32 (m, 32H), 0.91 (m, 12H); ¹³C NMR (75MHz, CDCl₃) δ 143.6, 138.9, 136.6, 130.9, 125.1, 119.0, 31.8, 31.6, 30.5, 29.7, 29.6, 29.3, 29.3, 27.8, 22.7, 14.1, 14.0; MALDI-ms 584.35 m/z (M⁺).

5,5''-Dibromo-3,3'',4,4''-tetrahexyl-2,2':5',2''-terthiophene⁷

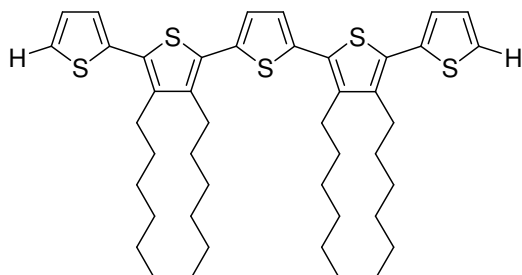
(2.8, C₃₆H₅₄Br₂S₃, MW: 742.82)



To a DMF solution (15 mL) containing 3,3'',4,4''-Tetrahexyl-2,2':5',2''-terthiophene (0.94 g, 1.65 mmol) was added NBS in DMF (5 mL) dropwise at 0°C over 10 min. After stirring for 6 h, the solution was poured into ice (100 mL) and extracted with ether. The organic layer was dried with Na₂SO₄ and the solvent was removed under reduced pressure. The crude product was purified by column chromatography (silica gel, *n*-hexane) to afford a pale green oil (0.62 g, yield = 50%). ¹H NMR (250 MHz, CDCl₃) δ 6.98 (s, 1H), 2.68 (t, $J = 7.5$ Hz, 4H), 2.58 (t, $J = 7.5$ Hz, 4H), 1.53 (m, 8H), 1.33 (m, 24H), 0.89 (m, 12H); ¹³C NMR (75MHz, CDCl₃) δ 142.7, 139.0, 135.7, 130.7, 126.2, 108.7, 31.6, 31.5, 30.7, 29.6, 29.5, 29.4, 28.7, 28.5, 22.6, 14.1.

2,5-Bis(3',4'-dihexyl-5',2''-bithienyl-2'-yl)-thiophene⁶

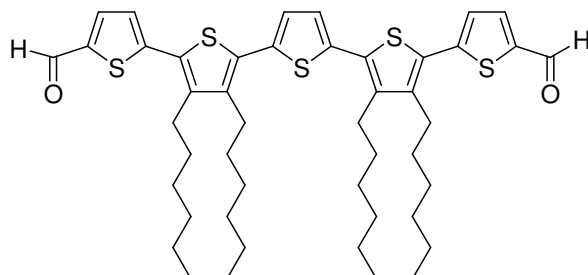
(2.10, C₄₄H₆₀S₅, MW: 749.27)



To a THF / toluene / H₂O solution (15 mL / 15 mL / 1 mL) was added 2-[2',5'-bis(3',4'-ethylenedioxythienyl)]-3,4-dihexylthiophene (0.56 g, 2.4 mmol), 5,5''-dibromo-3,3'',4,4''-tetrahexyl-2,2':5',2''-terthiophene (0.60 g, 0.8 mmol), K₂CO₃ (0.88 g, 6.4 mmol) and Pd(PPh₃)₄ (0.09 g, 0.08 mmol). The mixture was bubbled with nitrogen for 20 min, then refluxed overnight. After cooling, the solution was filtered through celite, and washed with THF. The collected organic solution was dried with Na₂SO₄ and the solvent was removed under reduced pressure. The crude product was purified by column chromatography (silica gel, *n*-hexane) to afford a pale green oil (0.35 g, yield = 58%). ¹H NMR (250 MHz, CDCl₃) δ 7.31 (d, *J* = 4.9 Hz, 2H), 7.14 (d, *J* = 4.9 Hz, 2H), 7.08 (m, 4H), 2.71 (m, 8H), 1.57 (m, 8H), 1.37 (m, 24H), 0.90 (m, 12H); ¹³C NMR (75MHz, CDCl₃) δ 140.3, 140.1, 136.2, 136.0, 129.9, 129.7, 127.3, 125.9, 125.8, 125.3, 31.5, 31.4, 30.7, 29.6, 29.5, 28.3, 28.1, 22.7, 22.6, 14.0; MALDI-ms 748.21 m/z [M]⁺.

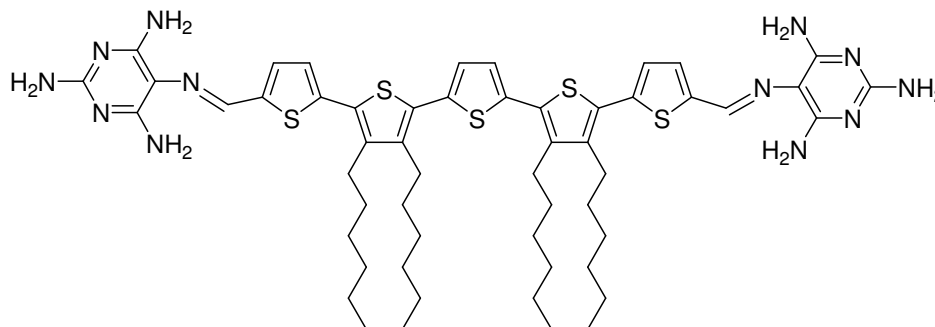
2,5-Bis(5'-formyl-3',4'-dihexyl-5'',2''-bithienyl-2'-yl)-thiophene⁶

(2.12, C₄₆H₆₀O₂S₅, MW: 805.29)



To a dichloroethane solution (20 mL) containing 2,5-bis(3',4'-dihexyl-5'',2''-bithienyl-2'-yl)-thiophene (0.21 g, 0.29 mmol), and DMF (0.66 g, 8.7 mmol) was added POCl₃ dropwise at 0°C over 3 min. The solution was allowed to warm to rt over 3 h and then refluxed overnight. After cooling, a sodium acetate (1.0 M, 5 mL) aqueous solution was added and the mixture was refluxed for 7 h. The solution was extracted with dichloromethane. The crude product was dried and purified by column chromatography (silica gel, EA / hexane = 95 / 5) to afford a red solid (135 mg, yield = 58%). ¹H NMR (250 MHz, CDCl₃) δ 9.89 (s, 1H), 7.71 (d, *J* = 3.8 Hz, 2H), 7.24 (d, *J* = 3.8 Hz, 2H), 7.14 (s, 2H), 2.74 (m, 8H), 1.59 (m, 8H), 1.37 (m, 24H), 0.90 (m, 12H); ¹³C NMR (75MHz, CDCl₃) δ 182.5, 146.3, 142.7, 142.2, 140.9, 136.8, 135.9, 131.9, 129.0, 126.6, 126.1, 31.5, 31.4, 30.7, 30.4, 29.6, 28.4, 28.2, 22.7, 22.6, 14.8, 14.1, 14.0; MALDI-ms 804.31 m/z [M]⁺; UV/Vis (1.6 × 10⁻⁴ M, CHCl₃) λ_{max} = 432 nm, ε = 4.4 × 10⁴ cm⁻¹M⁻¹.

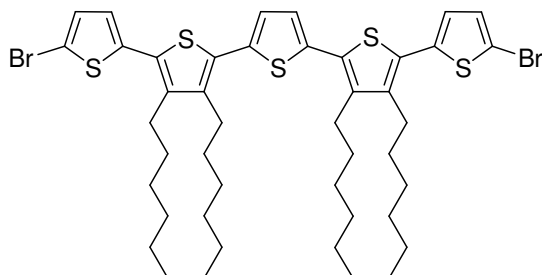
2,5-Bis{[(2''',4''',6'''-triaminopyrimidinyl-5''')-5''-enaminy]-3',4'-dihexyl-5',2''-bithienyl-2'-yl}-thiophene⁶ (2.13, C₅₄H₇₂N₁₂S₅, MW: 1049.55)



To a solution of the 2,5-bis(5''-formyl-3',4'-dihexyl-5',2''-bithienyl-2'-yl)-thiophene (200 mg 0.25 mmol) and 2,4,5,6-tetraaminopyrimidine sulfate (1.91 g, 4.99 mmol) in EtOH / DMSO (50 mL / 2mL) was added K₂CO₃ (1.04 g, 7.54 mmol), and the reaction mixture was refluxed under nitrogen for 5 d. After cooling to rt, the mixture was poured into water (200 mL) and the precipitate collected by centrifugation (3900 rpm, 10 min.). The solvent was removed then distilled water added to wash any remaining pyrimidine. The aqueous layer was again removed by centrifugation. The solid residue was purified through re-precipitation with distilled THF and Et₂O to afford a red powder (197 mg, yield = 75%). ¹H NMR (300MHz, CDCl₃) δ 8.68 (s, 2H), 7.15–7.11 (m, 6H), 4.83 (s, 8H), 4.09 (s, 4H), 2.76 (m, 8H), 1.59 (m, 8H), 1.36 (m, 24 H), 0.90 (m, 12H); MALDI-ms m/z (%) 525.4 (M²⁺, 92.5); 1049.4 (M⁺, 100.0), 1050.5 ([M + H]⁺, 70.5) ; UV/Vis (3.2×10⁻⁴ M, CHCl₃) λ_{max} = 452 nm, ε = 2.4 × 10⁴ cm⁻¹M⁻¹.

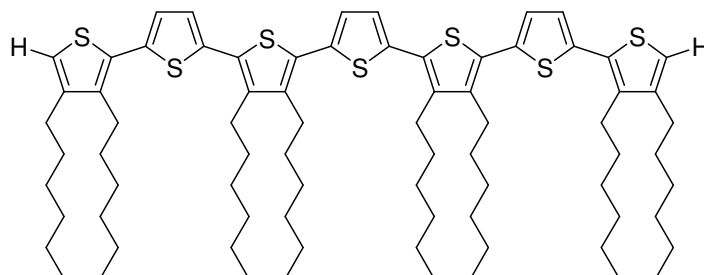
2,5-Bis(5''-bromo-3',4'-dihexyl-5',2''-bithienyl-2'-yl)-thiophene⁷

(2.14, C₄₄H₅₈Br₂S₅, MW: 907.06)



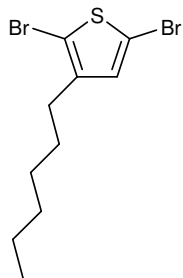
To a DMF solution (10 mL) containing 2,5-bis(3',4'-dihexyl-5',2''-bithienyl-2'-yl)-thiophene (29 mg, 0.038 mmol) was added NBS (15.84 mg, 0.090 mmol) in DMF (1mL) at 0°C in the absence of light. The mixture was allowed to warm to rt and stirred for 9 h. The solution was then poured into ice-water and extracted with Et₂O. The crude product was purified through re-precipitation with hexane and MeOH to afford an orange solid (25.8 mg, yield = 75%). ¹H NMR (300MHz, CDCl₃) δ 7.07 (s, 2H), 7.01 (d, *J* = 3.8 Hz, 2H), 6.87 (d, *J* = 3.8 Hz, 2H), 2.66 (m, 8H), 1.53 (m, 8H), 1.31 (m, 24H), 0.89 (m, 12H); ¹³C NMR (75MHz, CDCl₃) δ 140.8, 140.2, 137.7, 135.9, 130.2, 128.9, 126.1, 111.8, 31.5, 31.4, 30.8, 30.7, 29.6, 29.5, 28.2, 28.1, 22.6, 22.5, 14.1; MALDI-ms 906.14 m/z [M]⁺.

2,5-Bis[5'-(3''',4''-dihexyl-2''',5''-bithienyl-2''-yl)-,3',4'-dihexylthienyl-2'-yl]-thiophene⁶ (2.15, C₇₆H₁₁₂S₇, MW: 1250.16)



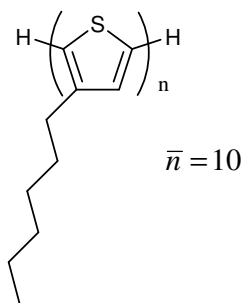
To a THF/toluene/H₂O solution (10 mL/10 mL/1 mL) was added 2-[2',5'-bis(3',4'-ethylenedioxythienyl)]-3,4-dihexylthiophene (70 mg, 0.137 mmol), 2,5-bis-(5''-bromo-3',4'-dihexyl-5',2''-bithienyl-2'-yl)-thiophene (31 mg, 0.034 mmol), K₂CO₃ (37.6 g, 0.27 mmol) and Pd(PPh₃)₄ (3.93 g, 0.0034 mmol). The mixture was bubbled with nitrogen for 20 min, then refluxed for 3h. After cooling, the solution was filtered through celite, and washed with THF. The collected organic solution was dried with Na₂SO₄ and the solvent was removed under reduced pressure. The crude product was purified by column chromatography (silica gel, *n*-hexane) to afford an orange solid (6.8 mg, yield = 40%). ¹H NMR (300 MHz, CDCl₃) δ 7.09 (m, 6H), 6.88 (s, 2H), 2.80 (m, 16H), 1.62 (m, 16H), 1.32 (m, 48H), 0.91 (m, 24H).

2,5-Dibromo-3-hexylthiophene⁸ (2.16, C₁₀H₁₄Br₂S, MW: 326.09)



To a solution of 3-hexylthiophene (3.51 g, 20.8 mmole) in a mixture of chloroform and acetic acid (25 mL / 25 mL) was added NBS (7.77 g, 43.7 mmole) in portions during 10 minutes at 30°C. The mixture was refluxed for 2 h. After being diluted with water, the mixture was extracted with chloroform. The extracts were washed with KOH aqueous solution and dried. The residue was purified using column chromatography (silica gel, n-pentane) to afford a colorless oil (5.77 g, yield = 85%). ¹H NMR (250 MHz, CDCl₃) 6.78 (s, 1H), 2.50 (t, *J* = 7.6 Hz, 2H), 1.53 (m, 2H), 1.29 (m, 6H), 0.89 (t, *J* = 4.2 Hz, 3H); ¹³C NMR (75MHz, CDCl₃) δ 142.9, 130.9, 110.3, 107.9, 21.6, 29.5, 29.4, 28.8, 22.6, 14.1; GC-ms *m/z* 326 (M⁺, 100).

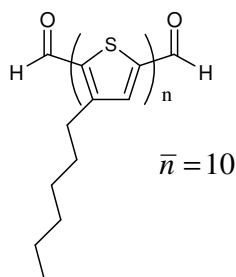
Poly-3-hexylthiophene⁹ (2.24, P3HT)



To dry THF was added 2,5-dibromothiophene (1 g, 3.06 mmole) and *iso*-propyl magnesiumbromide (1.53 mL, 3.06 mmole) the solution was heated to 30°C and stirred for 3 hours under N₂. A dried THF suspension of Ni(dppp)Cl₂ (dppp = 1,3-bis(diphenylphosphino)propane, 168 mg, 0.31 mmole, 0.1 equivalent to

2,5-dibromothiophene) was added in one portion and the mixture was stirred for 2 h. LiAlH_4 was then added in small portions and the mixture was stirred overnight. The mixture was passed through celite to remove the precipitate. The solvent of the residue was reduced to small amount under vacuum and the slurry residue poured into EtOH. The precipitate was collected by centrifugation and the collected solid was washed with EtOH three times and again collected by centrifugation. The collected solid was dried in a heated vacuum oven overnight to afford a deep red solid (203 mg, 40%). PDI = 1.12 from MALDI-ms.

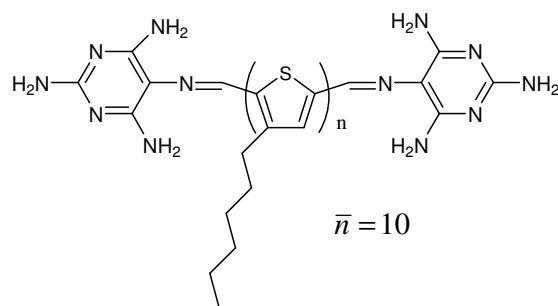
α,ω -Diformylpoly-3-hexylthiophene¹⁰ (2.25)



To anhydrous toluene (100 mL) containing P3HT (1.00 g) was added *N*-methylformanilide (31.76 g) and POCl_3 (36.15 g) under nitrogen. The reaction was carried out at 75°C for 24 h. The solution was cooled to rt and saturated $\text{KOH}_{(\text{aq})}$ was added dropwise until no more bubbles formed. The mixture was stirred for 2 h, and the organic layer was collected. The solvent was reduced to small amount and the slurry residue was poured into EtOH. The precipitate was washed with EtOH three times and collected by centrifugation. The polymer was dried under vacuum in a heated oven overnight to afford a red solid (622 mg, 62%). PDI = 1.07. The NMR spectra and MALDI-ms result are shown in section 2.2.1.2.

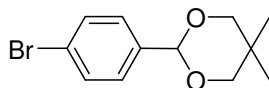
α,ω -Bis[(2',4',6'-triaminopyrimidinyl-5'-yl)-5-enaminy]poly-3-hexylthiophene⁶

(2.26, PPHT)



To a solution of EtOH and chlorobenzene (50 mL/50 mL) was suspended α,ω -diformylpoly-3-hexylthiophene (328 mg). The mixture was sonicated for 30 min. and 2,4,5,6-tetraaminopyrimidine sulfate (1.839 g), K_2CO_3 (1.598 g) and DMSO (1 mL) were added, followed by refluxing under N_2 for 3 days. After cooling to rt, the mixture was poured into water and stirred vigorously for 5 min. The organic layer was collected and washed with water till no color appeared in the aqueous layer. The organic layer was then passed through a glass filter to remove the emulsion and the solvent was removed under reduced pressure. The resulting solid was dried in heated vacuum oven overnight. The dried crude product was dissolved in chlorobenzene and filtered through a microfilter (0.45 μ m). The solvent was removed under reduced pressure to yield dark red product (262 mg, yield = 80%). The NMR spectrum is shown in section 2.2.1.2.

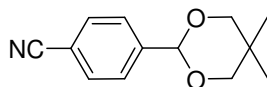
2-(4-Bromophenyl)-5,5-dimethyl-1,3-dioxane¹¹ (2.35, $C_{12}H_{15}BrO_2$, MW: 271.15)



4-Bromobenzaldehyde (5.01 g, 27.2 mmol) and 2,2-dimethyl-1,3-propanediol

(28.33 g, 272 mmol) were dissolved in toluene (150 mL) in a round-bottom flask. Trifluoroacetic acid (TFA, 0.75 mL, 9×10^{-3} mmol) was then added, and the mixture was heated at 90 °C overnight. The next day, the reaction mixture was cooled and washed with a saturated solution of K_2CO_3 , and then with water. The organic layer was concentrated, and the product was recrystallized from water to give white solid product. (7.05 g, yield = 96%). 1H NMR (250 MHz, $CDCl_3$) δ 7.50 (d, J = 8.5 Hz, 2H), 7.38 (d, J = 8.5 Hz, 2H), 5.35 (s, 1H), 3.76 (d, J = 11.0 Hz, 2H), 3.64 (d, J = 11.0 Hz, 2H), 1.57 (s, 3H), 0.80 (s, 3H); ^{13}C NMR (75MHz, $CDCl_3$) δ 137.5, 131.4, 127.9, 122.8, 100.9, 77.6, 30.2, 23.0, 21.9; ESI-TOF-ms m/z (%) 271.036($[M + H]^+$, 52.30); 293.0152 ($[M + Na]^+$, 24.74).

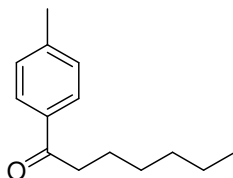
2-(4-Cyanophenyl)-5,5-dimethyl-1,3-dioxane¹² (2.37, $C_{13}H_{15}NO_2$, MW: 217.26)



4-Formylbenzonitrile (5.0 g, 38.1 mmol) and 2,2-dimethyl-1,3-propanediol (19.80 g, 190.5 mmol) were dissolved in toluene (50 mL) in a round-bottom flask. TFA (0.75 mL, 9×10^{-3} mmol) and molecular sieve (3A) were then added, and the mixture was heated at 90°C 17 h. In next step, the reaction mixture was washed with a saturated solution of K_2CO_3 and then with water. The organic layer was concentrated, and a 15% $Na_2S_2O_4$ solution was added and stirred for 90 min. The organic layer was separated, washed with water, and worked up to afford the desired product as a white solid (7.03 g, yield = 85%). 1H NMR (300 MHz, $CDCl_3$) δ 7.67 (d, J = 7.9 Hz, 2H), 7.62 (d, J = 7.9 Hz, 2H), 5.42 (s, 1H), 3.78 (d, J = 10.9 Hz, 2H), 3.66 (d, J = 10.9 Hz, 2H), 1.27 (s, 3H), 0.81 (s, 3H); ^{13}C NMR (75MHz, $CDCl_3$); δ ESI-TOF-ms m/z (%)

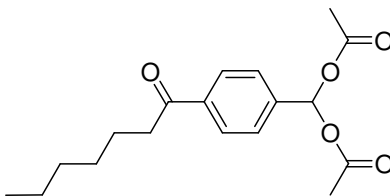
240.0938 ($[M+Na]^+$, 100.00); 218.1157 ($[M+H]^+$, 28.65).

1-*p*-Tolylheptan-1-one¹³ (2.39, C₁₄H₂₀O, MW: 204.31)



To a toluene solution (200 mL) containing AlCl₃ (5.38 g, 40.3 mmol) was added heptanoyl chloride (6.0 g, 40.3 mmol) at 0°C dropwise. The mixture was heated to 100°C for 1 h. After cooling, the crude product was poured into ice-water (200 mL) and extracted with ether. The organic layer was washed with NaOH solution and water then dried to afford a white powder (4.52 g, yield = 55%). ¹H NMR (300 MHz, CDCl₃) δ 7.86 (d, *J* = 8.3 Hz, 2H), 7.25 (d, *J* = 8.3 Hz, 2H), 2.93 (t, *J* = 7.5 Hz, 2H), 2.41 (s, 3H), 1.70 (m, 2H), 1.37 (m, 6H), 0.89 (t, *J* = 6.4 Hz, 3H); ¹³C NMR (75 MHz, CDCl₃) δ 200.2, 143.5, 134.6, 129.2, 128.1, 38.5, 31.6, 29.0, 24.4, 22.5, 21.6, 14.0; ESI-TOF-ms *m/z* (%) 205.1590 ($[M+H]^+$, 100.00); 277.1392 ($[M+Na]^+$, 30.21).

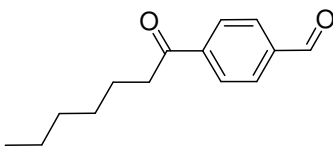
(4-Heptanoylphenyl)methylene diacetate¹⁴ (2.40, C₁₈H₂₄O₅, MW: 320.38)



To a solution of AcOH/AcOAc (1/1 = *v/v*, 9.6 mL) containing 1-*p*-tolylheptan-1-one (6.0 g, 29.36 mmol) was added concentrated H₂SO₄ (4.8 mL) dropwise at 0-5°C. To this solution was then added CrO₃ (14.98 g, 146.8 mmol) in

AcOAc (20 mL) at 0-5°C. During the addition, to the mixture was added silica gel (50 g) when green CrSO₄ formed. The mixture was stirred at 0-5°C for 3 h, the color changing from deep brown to deep green which indicated the consumption of CrO₃. The mixture was filtered and washed with Et₂O. To the filtrate was added silica gel to adsorb any remaining chromium salt, then filtered again until no apparent green color. The organic solution was washed with NaOH, water then dried. The crude product was recrystallized from ethyl acetate/pentane to afford a white solid (1.88 g, yield = 20%). ¹H NMR (250 MHz, CDCl₃) δ 8.02 (d, *J* = 8.5 Hz, 2H), 7.70 (s, 1H), 7.60 (d, *J* = 8.5 Hz, 2H), 2.96 (t, *J* = 7.3 Hz, 2H), 1.72 (m, 2H), 1.32 (m, 6H), 0.88 (t, *J* = 6.4 Hz, 3H); ¹³C NMR (75MHz, CDCl₃) δ 199.9, 168.7, 139.8, 138.1, 128.3, 126.9, 89.0, 38.8, 31.6, 29.0, 24.2, 22.5, 20.8, 14.0; ESI-TOF-ms *m/z* (%) 343.1528 ([M+Na]⁺, 100.00); 321.1702 ([M+H]⁺, 16.16).

4-Heptanoylbenzaldehyde (2.41, C₁₄H₁₈O₂, MW: 218.29)

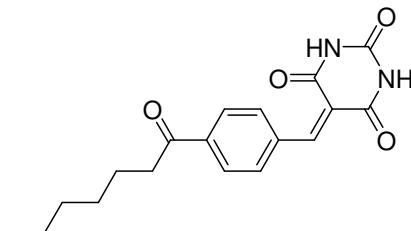


To a mixture of water/EtOH (3 mL/3 mL) containing (4-Heptanoyl-phenyl)methylene diacetate (1.11 g, 3.43 mmol) was added TFA, then the mixture was refluxed overnight. After cooling, the solution was extracted with ether. The organic layer was washed with water, then dried to afford a white solid (598 mg, yield = 80%). ¹H NMR (300 MHz, CDCl₃) δ 10.10 (s, 1H), 8.10 (d, *J* = 7.9 Hz, 2H), 7.97 (s, 1H), 7.60 (d, *J* = 7.9 Hz, 2H), 3.00 (t, *J* = 7.2 Hz, 2H), 1.75 (m, 2H), 1.35 (m, 6H), 0.89 (t, *J* = 6.4 Hz, 3H); ¹³C NMR(75MHz, CDCl₃) δ 199.9, 191.6, 141.3, 138.9, 39.1, 31.6,

30.9, 28.9, 24.1, 22.5, 14.0.

5-(4-Heptanoylbenzylidene)pyrimidine-2,4,6(1H,3H,5H)-trione⁶

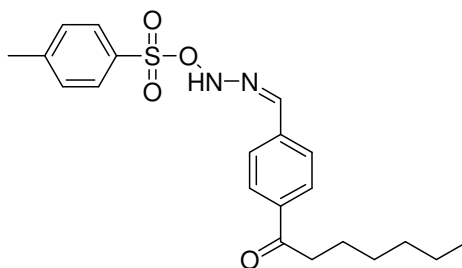
(2.42, C₁₈H₂₀N₂O₄, MW: 328.36)



To a solution of water and EtOH (2 mL/10 mL) containing 4-heptanoylbenzaldehyde was added barbituric acid. The solution was heated to reflux for 10 min then stirred at room temperature overnight. The crude product was poured into water and collected by centrifugation. The solid was collected and washed with pentane to afford the product as a white solid (89.05 mg, yield = 59%). ¹H NMR (300 MHz, DMSO) δ 11.45 (s, 1H), 11.28 (s, 1H), 8.30 (s, 1H), 8.03 (d, *J* = 8.7 Hz, 2H), 7.98 (d, *J* = 7.9 Hz, 2H), 3.05 (t, *J* = 7.1 Hz, 2H), 1.61 (m, 2H), 1.29 (m, 6H), 0.86 (t, *J* = 6.4 Hz, 3H); ¹³C NMR (75MHz, CDCl₃); δ ESI-ms *m/z* (%) 351.1351 ([M+Na]⁺, 40.87); 329.1460 ([M+H]⁺, 11.74).

(Z)-1-(4-((2-(Tosyloxy)hydrazono)methyl)phenyl)heptan-1-one¹⁵

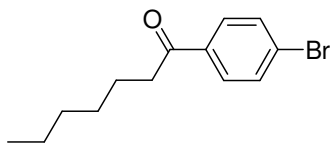
(2.44, C₂₁H₂₆N₂O₄S, MW: 402.51)



To a MeOH solution (5 mL) containing 4-heptanoylbenzaldehyde (1.0 g,

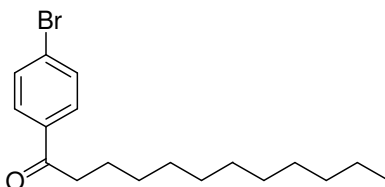
3.12 mmol) was added *p*-toluenesulfonyl hydrazide (813 mg, 4.37 mmol) and refluxed overnight. The mixture was filtered and the collected solid was washed with cold MeOH. The solid was dried under reduced pressure to afford a yellow product that was used without further purification. ¹H NMR (300 MHz, DMSO) δ 9.93 (d, *J* = 8.3 Hz, 2H), 9.88 (d, *J* = 8.3 Hz, 2H), 7.76 (s, 1H), 7.64 (d, *J* = 8.3 Hz, 2H), 7.33 (d, *J* = 8.3 Hz, 2H), 2.94 (t, *J* = 7.5 Hz, 2H), 2.41 (s, 3H), 1.72 (m, 2H), 1.33 (m, 6H), 0.89 (t, *J* = 6.4 Hz, 3H); ¹³C NMR (75MHz, CDCl₃); δ ESI-ms *m/z* (%) 387.1743 ([M+H]⁺, 55.51).

1-(4-Bromophenyl)heptan-1-one¹⁶ (2.46-1, C₁₃H₁₇BrO, MW: 269.18)



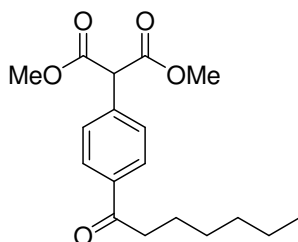
To a CS₂ solution (10 mL) containing AlCl₃ (5.1 g, 38.2 mmol) and heptanoyl chloride (5.68 g, 38.2 mmol) was added bromobenzene (6.0 g, 38.2 mmol) dropwise under gentle reflux. The mixture was refluxed for 1 hr. After cooling, CS₂ was removed under reduced pressure. The reaction was quenched by pouring it into ice/water (100 g/100 mL) and extracted with ether. The organic layer was collected and the solvent was removed under reduce pressure. The crude product was recrystallized from ether to afford a white powder (5.66 g, yield = 55%). ¹H NMR (300 MHz, CDCl₃) δ 7.82 (d, *J* = 8.7 Hz, 2H), 7.60 (d, *J* = 8.7 Hz, 2H), 2.92 (t, *J* = 7.5 Hz, 2H), 1.72 (m, 2H), 1.36 (m, 6H), 0.89 (t, *J* = 6.8 Hz, 3H); ¹³C NMR (75MHz, CDCl₃) δ 199.5, 135.8, 131.8, 129.6, 127.9, 38.6, 31.6, 29.0, 24.2, 22.5, 14.0; ESI-ms *m/z* (%) 269.0537 ([M + H]⁺, 100.00).

1-(4-Bromophenyl)dodecan-1-one (2.46-2, C₁₈H₂₇BrO, MW: 339.31)



To a CS₂ solution (10 mL) containing AlCl₃ (4.66 g, 34.9 mmol) and dodecanoyl chloride (5.49 g, 34.9 mmol) was added bromobenzene (7.0 g, 34.9 mmol) dropwise at under gentle reflux. The mixture was refluxed for 1 hr. After cooling, CS₂ was removed under reduced pressure. The reaction was quenched by pouring the mixture into ice/water (100 g/150 mL) and extracted with ether. The organic layer was collected and the solvent was removed under reduce pressure. The crude product was recrystallized from ether to afford a white powder (5.9 g, yield = 50%). ¹H NMR (300 MHz, DMSO) δ 7.82 (d, *J* = 8.6 Hz, 2H), 7.60 (d, *J* = 8.6 Hz, 2H), 2.92 (t, *J* = 7.2 Hz, 2H), 1.72 (m, 2H), 1.25 (m, 16H), 0.88 (t, *J* = 6.0 Hz, 3H); ¹³C NMR (75MHz, CDCl₃) δ 199.5, 135.7, 131.8, 129.6, 127.9, 38.6, 36.0, 33.8, 31.9, 29.6, 29.4, 29.3, 24.2, 22.7, 16.2, 14.1; ESI-ms *m/z* (%) 339.1318 ([M + H]⁺, 28).

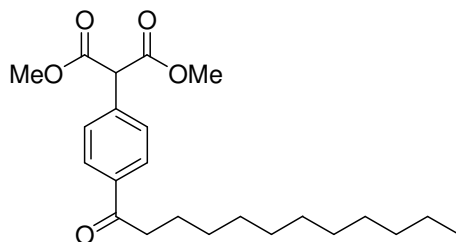
Dimethyl-2-(4-heptanoylphenyl) malonate¹⁷ (2.47-1, C₁₈H₂₄O₅, MW: 320.38)



To a Schlenk tube containing 1-(4-bromophenyl)heptan-1-one (2.77 g, 10.3 mmol) and dimethyl malonate (1.49 g, 11.3 mmol) was added K₃PO₄ (6.56 g,

30.9 mmol), Pd(dba)₂ catalyst (119 mg, 0.206 mmol), and tri-*tert*-butylphosphine (83.25 g, 0.412 mmol) followed by toluene (100 mL) in a glove box. The mixture in the sealed Schlenk tube was heated at 70°C overnight. After cooling, the mixture was filtered through a plug of celite and the solvent was removed under reduced pressure. The crude product was recrystallized from ethylacetate and pentane (1/10 = v/v) to afford a white powder (2.63 g, yield = 80%). ¹H NMR (300 MHz, CDCl₃) δ 7.96 (d, *J* = 8.2 Hz, 2H), 7.50 (d, *J* = 8.2 Hz, 2H), 4.71 (s, 1H), 2.95 (t, *J* = 7.3 Hz, 2H), 1.72 (m, 2H), 1.33 (m, 6H), 0.88 (t, *J* = 6.0 Hz, 3H); ¹³C NMR (75MHz, CDCl₃) δ 200.0, 168.0, 137.2, 130.0, 128.4, 57.4, 53.1, 38.7, 31.629.0, 24.3, 22.5, 14.0; ESI-ms m/z (%) 343.1527 ([M + Na]⁺, 100), 663.3145 ([2M + Na]⁺, 51).

Dimethyl-2-(4-dodecanoylphenyl)malonate¹⁷ (2.47-2, C₂₃H₃₄O₅, MW: 390.51)

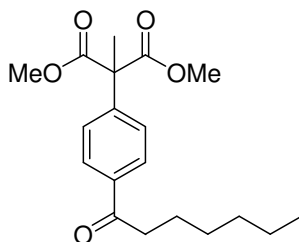


To a Schlenk tube containing 1-(4-bromophenyl)dodecan-1-one (2.16 g, 6.4 mmol) and dimethyl malonate (926 mg, 7.0 mmol) was added K₃PO₄ (3.76 g, 17.7 mmol), bis(dibenzylideneacetone)palladium (Pd(dba)₂, 73 mg, 0.127 mmol), and tri-*tert*-butylphosphine (51.4 g, 0.254 mmol) followed by toluene (100 mL) in a glove box. The mixture in the sealed Schlenk tube was heated at 70°C overnight. After cooling, the mixture was filtered through a plug of celite and concentrated under reduced pressure. The crude product was recrystallized from pentane to afford a white powder (2.15 g, yield = 86%). ¹H NMR (250 MHz, CDCl₃) δ 7.96 (d, *J* = 8.3 Hz, 2H),

7.50 (d, $J = 8.3$ Hz, 2H), 4.71 (s, 1H), 2.95 (t, $J = 7.2$ Hz, 2H), 1.72 (m, 2H), 1.25 (m, 16H), 0.88 (t, $J = 6.0$ Hz, 3H). ^{13}C NMR (75MHz, CDCl_3) δ 200.0, 168.0, 137.2, 136.9, 129.5, 128.4, 57.4, 53.1, 38.7, 31.9, 30.9, 29.6, 29.5, 29.4, 29.3, 29.3, 24.3, 14.1 ESI-ms m/z (%) 413.2298 ($\text{M} + \text{Na}^+$, 41).

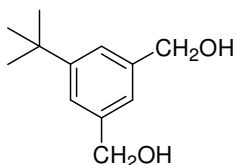
Dimethyl-2-(4-heptanoylphenyl)-2-methyl malonate¹⁸

(2.48, $\text{C}_{19}\text{H}_{26}\text{O}_5$, MW: 334.41)



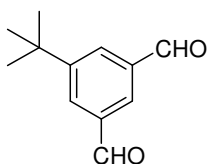
To a suspension of NaH (143.8 mg, 6.0 mmol) in THF (20 mL), dimethyl-2-(4-heptanoylphenyl) malonate (1.0 g, 3.12 mmol) in THF (20 mL) was added at 0°C, and the solution was stirred for 30 min at rt, then iodomethane (596 mg, 4.3 mmol) was added. After the mixture was refluxed overnight, cold water (5 mL) was added. The mixture was extracted with ether, and the organic extracts were washed with saturated Na_2SO_3 , water and brine. The solvent was removed under reduced pressure to afford crude product (990 mg, yield = 95%) as a white solid. ^1H NMR (250 MHz, CDCl_3) δ 7.93 (d, $J = 8.3$ Hz, 2H), 7.44 (d, $J = 8.3$ Hz, 2H), 3.77 (s, 1H), 2.94 (t, $J = 7.1$ Hz, 2H), 1.89 (s, 3H), 1.72 (m, 2H), 1.32 (m, 6H), 0.88 (m, 3H); ^{13}C NMR (75MHz, CDCl_3) δ 199.9, 171.4, 142.9, 136.3, 58.9, 53.0, 38.6, 31.6, 29.0, 24.2, 22.5, 22.3, 14.0; ESI-ms m/z (%) 691.33 ($[2\text{M} + \text{Na}]^+$, 91), 357.17 ($[\text{M} + \text{Na}]^+$, 100), 335.18 ($[\text{M} + \text{H}]^+$, 25).

(5-*tert*-Butyl-1,3-phenylene)dimethanol¹⁹ (2.53, C₁₂H₁₈O₂, MW: 194.27)



To a vigorously stirred solution of 5-*tert*-butyl-1,3-benzenedicarboxylic acid (3.0 g, 13.5 mmol) in dried THF (30 mL) was added a solution of borane-SMe₂ complex in THF (41 mL, 2M) via an addition funnel over 20 min at rt. The mixture was stirred at 70°C for 2 h. Water (100 mL) was added slowly to quench the reaction. The mixture was extracted with CH₂Cl₂. The organic phase was dried under reduced pressure. The crude product was used without further purification in next step. (2.10 g, yield = 80%) ¹H NMR (250 MHz, CDCl₃) δ 7.31 (2s, 2H), 7.19 (s, 1H), 4.67 (s, 4H), 1.95 (s, 2H), 1.32 (m, 9H); ¹³C NMR (75MHz, CDCl₃) δ 151.8, 140.6, 123.3, 122.9, 65.3, 34.7, 31.3; ESI-ms m/z (%) 217.1197 ([M + Na]⁺, 100.00).

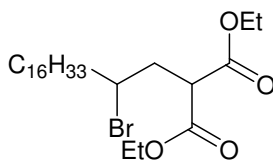
5-*tert*-Butylisophthalaldehyde¹⁹ (2.54, C₁₂H₁₄O₂, MW: 190.24)



(5-*tert*-Butyl-1,3-phenylene)dimethanol (265 mg, 1.36 mmol) was added to a vigorously stirring mixture of pyridinium chlorochromate (882 mg, 4.09 mmol) and celite (1.2 g) in CH₂Cl₂ (10 mL). The mixture was stirred for 36 hr and filtered over a short pad of celite, then rinsed with CH₂Cl₂. The solvent was removed under reduced

pressure to give the desired product as a white powder (233 mg, yield = 90%). ^1H NMR (250 MHz, CDCl_3) δ 10.11 (s, 2H), 8.18 (s, 3H), 1.41 (s, 9H); ^{13}C NMR (75MHz, CDCl_3) δ 191.4, 153.6, 136.8, 131.5, 128.9, 35.0, 31.0.

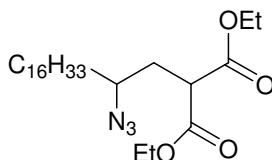
Diethyl-2-(2-bromooctadecyl) malonate²⁰ (2.57, $\text{C}_{25}\text{H}_{47}\text{BrO}_4$, MW: 491.54)



To distilled water (20 mL) containing octadecene (504 mg, 2 mmol) and bromomalonate (478 mg, 3 mmol) was added triethylborane (1 M in hexane, 1 mL, 1 mmol) in one portion at rt under N_2 while stirring vigorously. Air (10 mL) was immediately introduced into the reaction flask (not by bubbling). CAUTION: Triethylborane may ignite spontaneously when exposed to air. The reaction mixture was treated with additional air (10 mL) every 30 min. After one hour, more triethylborane (1 M in hexane, 1 mL, 1 mmol) was added to the reaction. After stirring for 1.5 h, hexane (10 mL) was added to quench the reaction. The mixture was extracted with ethyl acetate. The organic portion was dried under reduced pressure. The crude product was purified by silica gel flash column chromatography (first pentane to wash out starting material, then pentane/ethyl acetate = 10/1) to afford a colorless oil (687 mg, yield = 70%). ^1H NMR (250 MHz, CDCl_3) δ 4.22 (m, 4H), 3.99 (m, 1H), 3.80 (dd, J = 10.2, 4.2 Hz, 1H), 2.45 (m, 1H), 2.25 (m, 1H), 1.83 (m, 2H), 1.21 (m, 28H), 0.88 (t, J = 6.3 Hz, 3H); ^{13}C NMR (75MHz, CDCl_3) δ 169.1, 168.8, 61.6, 61.3, 55.0, 49.2, 37.9, 31.9, 29.6, 29.5, 29.4, 29.3, 29.2, 28.9, 28.7, 27.4, 22.3, 14.0; ESI-ms m/z (%) 1005.52 ($[\text{2M} + \text{Na}]^+$, 85), 515.25 ($[\text{M} + \text{Na}]^+$, 56), 491.27 (M^+ ,

66), 411.35 (M^+ - Br, 26).

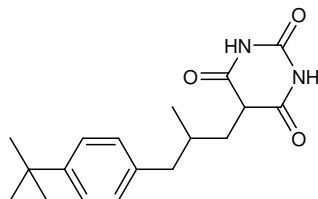
Diethyl-2-(2-azidooctadecyl) malonate²¹ (2.58, C₂₅H₄₇N₃O₄, MW: 453.66)



Diethyl-2-(2-bromooctadecyl)malonate (0.68 g, 1.39 mmol) was added to a stirred 25% aqueous solution of sodium azide (180 mg, 2.77 mmol). Aliquat[®] 336 (trioctylmethyl ammonium chloride, 25.34 mg, 0.07 mmol) was added and the mixture was stirred vigorously at 100°C overnight. After cooling, the mixture was extracted with ethyl acetate. The collected organic layer was dried with MgSO₄ and the solvent was removed under reduced pressure to give a crude oily product (378 mg, yield = 60%). The product was used without purification in next step. IR (KBr) 2104 cm⁻¹; ESI-ms *m/z* (%) 396.45 (M^+ - C₂H₅N₂, 100), 424.49 (M^+ - HN₂, 76), 452.52 (M^+ - H, 4).

5-(3-(4-*tert*-Butylphenyl)-2-methylpropyl)pyrimidine-2,4,6(1H,3H,5H)-trione⁶

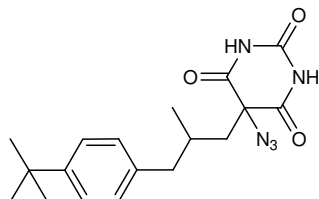
(2.60, C₁₈H₂₄N₂O₃, MW: 316.39)



To an acetic acid solution (60 mL) containing lilyal (5.0 g, 24.5 mmol) and barbituric acid (15.6 g, 122 mmol) was added Pt-C (0.5 g, 5 %). The mixture was stirred for 3 days under H₂ atmosphere, then filtered through celite. The solvent was

removed under reduced pressure, then the remaining solid was dissolved in THF. Water was added to the solution and the precipitate was collected by filtration. The collected solid was dried under vacuum to give a white powder (3.87 g, yield = 51 %). ^1H NMR (300 MHz, CDCl_3) δ 11.16 (s, 1H), 11.15 (s, 1H), 7.28 (d, 2H, $J = 8.3$ Hz), 7.05 (d, 2H, $J = 8.3$ Hz), 3.57 (t, 1H, $J = 6.0$ Hz), 2.59 (m, 1H), 2.27 (m, 1H), 1.90 (m, 1H), 1.75 (m, 1H), 1.25 (s, 9H), 0.75 (d, 3H, $J = 6.0$ Hz); ^{13}C NMR (75MHz, CDCl_3) δ 170.3, 150.5, 147.4, 136.8, 128.2, 124.3, 45.8, 41.4, 34.4, 33.6, 31.8, 30.7, 18.2; ESI-ms m/z 339.17(%) ($[\text{M} + \text{Na}]^+$, 100).

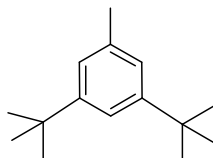
**5-Azido-5-(3-(4-*tert*-butylphenyl)-2-methylpropyl)-
pyrimidine-2,4,6(1H,3H,5H)-trione (2.61, $\text{C}_{18}\text{H}_{23}\text{N}_5\text{O}_3$, MW: 357.41)**



A DMF solution (20 mL) containing 5-[3-(4-*tert*-butylphenyl)-2-methylpropyl]-pyrimidine-2,4,6(1H,3H,5H)-trione (1.07 g, 3.38 mmol) was added *N*-bromosuccinimide (NBS, 662 mg, 3.73 mmol) in portions and stirred at rt overnight. Sodium azide (439 mg, 3.72 mmol) in DMF (4 mL) was added and stirred at 50°C for 2 h. Water was added and the precipitate was collected by centrifugation. The collected solid was washed with MeOH, and dried under vacuum to afford a white solid (652 mg, yield = 54 %). ^1H NMR (300 MHz, CD_2Cl_2) δ 8.2 (broad, 2H), 7.31 (d, 2H, $J = 8.3$ Hz), 7.04 (d, 2H, $J = 8.3$ Hz), 2.59 (m, 1H), 2.45 (m, 1H), 2.29 (m, 1H), 2.14 (m, 1H), 1.30 (s, 9H), 0.94 (d, 3H, $J = 6.4$ Hz); ^{13}C NMR (75MHz, acetone-*d*6) δ

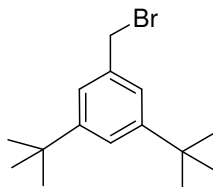
168.9, 168.8, 149.9, 149.3, 137.7, 129.5, 125.8, 68.4, 44.1, 43.5, 34.7, 31.8, 31.6, 20.1;
IR (KBr) 2120 cm⁻¹; ESI-ms m/z (%) 380.17 ([M + Na]⁺, 100).

1,3-Di-*tert*-butyl-5-methylbenzene²² (2. 63, C₁₅H₂₄, MW: 204.35)



To a rapidly stirred solution of 2-chloro-2-methylpropane (20.09 g, 23.61 mL, 0.22 mol) in toluene (10 g, 11.54 mL, 0.11 mol) was added AlCl₃ (969 mg, 7.3 mmol) solid in portions over 8 h at rt. After stirring for 24 h, the solution was poured into water. The mixture was extracted with ether, and the solvent in the organic layer was removed under reduced pressure. The residual liquid was purified by Vigreux distillation. The second portion was collected (First portion: 54°C - 56°C/4 mmHg, second portion: 85°C - 88°C/4 mmHg) and stored at 5°C for 24 h. A solid formed, which was collected by filtration to afford a white crystalline solid (17.8 g, yield = 40 %). ¹H NMR (300 MHz, CDCl₃) δ 7.24 (s, 1H), 7.04 (s, 2H), 2.35 (s, 3H), 1.32 (s, 18H).

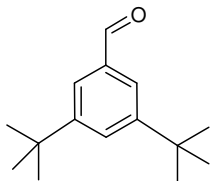
1-(Bromomethyl)-3,5-di-*tert*-butylbenzene²² (2.64, C₁₅H₂₃Br, MW: 283.25)



A mixture of 1,3-di-*tert*-butyl-5-methylbenzene (25.77 g, 0.126 mol), NBS (33.67 g, 0.189 mol) and benzoyl peroxide (435 mg, 1.26 mmol) in benzene was

refluxed under visible light for 5 h. After cooling, the solid was filtered off and dried under reduced pressure to afford a white product (34.5 g, NMR yield = 60 %). ^1H NMR (300 MHz, CDCl_3) δ 7.39 (s, 2H), 7.23 (s, 1H), 4.52 (s, 2H), 1.33 (s, 18H).

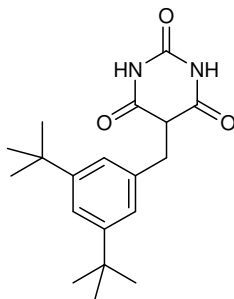
3,5-Di-*tert*-butylbenzaldehyde²³ (2.65, $\text{C}_{15}\text{H}_{22}\text{O}$, MW: 218.33)



A mixture of 3,5-di-*tert*-butylbromomethyltoluene (35.69 g, 126 mmol) and hexamethylenetetraamine (74.16 g, 529 mmol) in MeOH/water (60 mL/40 mL) solution was refluxed for 4 h. Concentrated HCl (30 mL) was added dropwise and the solution was refluxed for a further 30 min. After cooling, the mixture was extracted with dichloromethane and washed with water. The organic phase was dried under reduced pressure. The solid obtained was recrystallized from EtOH/water to afford a white solid (24.7 g, yield = 90 %). ^1H NMR (300 MHz, CDCl_3) δ 10.01 (s, 1H), 7.72 (s, 3H), 1.37 (s, 18H); ^{13}C NMR (75MHz, CDCl_3) δ 193.1, 151.8, 136.2, 128.8, 124.1, 34.9, 31.2.

5-(3,5-Di-*tert*-butylbenzyl)pyrimidine-2,4,6(1H,3H,5H)-trione⁶

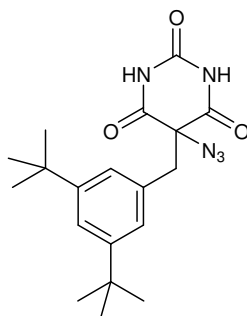
(2.66, C₁₉H₂₆N₂O₃, MW: 330.42)



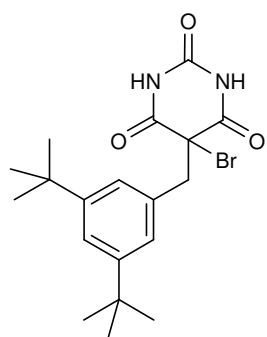
To a solution of toluene/acetic acid (100/300 in mL) containing 3,5-di-*tert*-butylbenzaldehyde (11.8 g, 54.0 mmol) and barbituric acid (20.8 g, 162 mmol) was added Pt-C (0.5 g, 5 %). The mixture was stirred for 5 days under H₂ atmosphere then filtered through celite. The solvent was removed under reduced pressure to a minimum amount, then to the remained slurry was added THF. The mixture was added to 500 mL of rapidly stirred water and the precipitate obtained collected by filtration. The collected solid was dried under vacuum to give a white powder (15.1 g, yield = 85 %). ¹H NMR (300 MHz, CDCl₃) δ 8.25 (s, 2H), 7.27 (s, 1H), 6.95 (s, 2H), 3.69 (t, *J* = 5.5 Hz, 1H), 3.49 (d, *J* = 5.5 Hz, 2H), 1.26 (s, 18H); ¹³C NMR (75MHz, acetone-d₆); δ ESI-ms *m/z* (%) 353.18 ([M + Na]⁺, 40).

5-Azido-5-(3,5-di-*tert*-butylbenzyl)pyrimidine-2,4,6(1H,3H,5H)-trione

(2.67, C₁₉H₂₅N₅O₃, MW: 371.43)

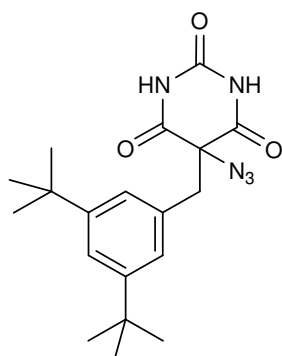


To a DMF solution (20 mL) containing 5-(3,5-di-*tert*-butylbenzyl)pyrimidine-2,4,6(1H,3H,5H)-trione (2.0 g, 6.1 mmol) was added NBS (1.19 g, 6.6 mmol) dropwise and stirred at rt for 4 h. Sodium azide (786 mg, 12.1 mmol) in DMF (4 mL) was then added and stirring continued at 60°C overnight. Water was added and the mixture was extracted with ethyl acetate. The organic layer was washed with water and dried. The solvent was removed under reduced pressure to afford a pale brown oil. (2.08 g, yield = 92 %).



Intermediate :

¹H NMR (300 MHz, acetone-d₆) δ 10.59 (s, 1H), 7.35 (d, *J* = 1.5 Hz, 1H), 7.05 (d, *J* = 1.5 Hz, 1H), 3.79 (s, 2H), 1.25 (s, 18H); ¹³C NMR (75MHz, acetone-d₆) 167.6, 151.8, 148.4, 133.8, 125.5, 122.2, 51.0, 43.6, 35.3, 31.6 ESI-ms *m/z* 431.09 ([M + Na]⁺).

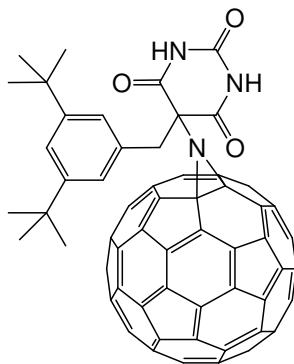


Product:

¹H NMR (300 MHz, CDCl₃) δ 7.30 (d, *J* = 1.5 Hz, 1H), 6.94 (d, *J* = 1.5 Hz, 1H), 3.57 (s, 2H), 1.25 (s, 18H); ¹³C NMR (75MHz, CDCl₃) 167.5, 151.6, 147.5, 129.4, 124.0, 122.1, 67.1, 43.7, 34.7, 31.2; IR (KBr) 2216 cm⁻¹; ESI-ms *m/z* (%)

394.18 ($[M + Na]^+$, 100), 765.37 ($[2M + Na]^+$, 27).

**N-[5''-(3''',5'''-di-tert-butylbenzyl)-2'',4'',6''-trioxo-hexahydropyrimidin-5''-yl]
aziridino[2',3':1,2][60]fullerene²⁴ (2.68, BAF, C₇₉H₂₅N₃O₃, MW: 1064.06)**



A chlorobenzene solution (200 mL) containing C₆₀ (1.223 g, 1.62 mmol) was degassed by three cycles of freeze-pump-thaw. The solution was brought to reflux and azido di-*tert*-butylbenzyl barbiturate (276 mg, 0.81 mmol) in chlorobenzene (this solution was degassed by three cycles of freeze-pump-thaw) was added dropwise. After refluxing for 2 days, the solvent was removed under reduced pressure. The crude product was dry-loaded onto a column and washed with toluene to remove C₆₀ prior to eluting with mixture of ethyl acetate in toluene (5%) to afford the desired product. The solvent was dried under vacuum to afford brown powder product. (315 mg, yield = 37%) MALDI-ms m/z (%) 1063.95 ($[M + H]^+$, 83), 1085.98 ($[M + Na]^+$, 100), 1101.93 ($[M + K]^+$, 30), 1314.08 ($[M + DCTB]^+$, 44), 1337.10 ($[M + DCTB + Na]^+$, 20).

Synthesis of ZnO nanoparticles²⁵

Zinc acetate dihydrate (2.95 g, 13.4 mmol) was dissolved in methanol (125 mL) at 60°C, a solution of KOH (87%, 1.48 g, 23 mmol) in methanol (65 mL) was then added over 10 min to the zinc acetate dihydrate solution while vigorously stirring. Zinc hydroxide precipitated, but dissolved again. After 2 h and 15 min, the heater and stirrer were removed and the nanoparticles were allowed to precipitate overnight. Precipitate and mother liquor were separated, and the precipitate was washed twice with methanol (50 mL) and precipitated for 2 h. A minimum amount of MeOH was allowed to remain in the mixture in order to keep the nanoparticles wet. The solution was diluted to 192.5 mg/mL with MeOH before spin coating onto the active layer. The method to determine the size of synthesized nanoparticles was described in section **3.2.1.1**.

5.11 Reference

- 1 G. M. Sheldrick, *Acta Cryst.* **2008**, A64, 112.
- 2 W. J. Kabsch, *Appl. Cryst.* **1993**, 26, 795.
- 3 K. Araki, H. Endo, G. Masuda, T. Ogawa, *Chem. Eur. J.* **2004**, 10, 3331.
- 4 C. Ringenbach, A. Di Nicola, R. Ziessel, *J. Org. Chem.* **2003**, 68, 4708.
- 5 F.-C. Fang, C.-C. Chu, C.-H. Huang, G. Raffy, A. Del Guerzo, K.-T. Wong, D. M. Bassani, *Chem. Commun.* **2008**, 47, 6369.
- 6 C.-H. Huang, N. D. McClenaghan, A. Kuhn, J. W. Hofstraat, D. M. Bassani, *Org. Lett.* **2005**, 7, 3409.
- 7 J. Krömer, P. Bäuerle, *Tetrahedron* **2001**, 57, 3785.
- 8 H. Higuchi, T. Nakayama; H. Koyama, J. Ojima; T. Wada; H. Sasabe, *Bull. Chem. Soc. Jpn.* **1995**, 68, 2363.
- 9 R. C. Hiorns, A. Khoukh, B. Gourdet, C. Dagron-Lartigau, *Polymer Int.* **2006**, 55, 608.
- 10 J. Liu, R. D. McCullough, *Macromolecules* **2002**, 35, 9882.
- 11 C. Querner, P. Reiss, J. Bleuse, A. Pron, *J. Am. Chem. Soc.* **2004**, 126, 11574.
- 12 J. S. Lindsey, I. C. Schrieman, H. C. Hsu, P. C. Kearny, A. M. Marguerettaz, *J. Org. Chem.* **1987**, 52, 827.
- 13 A. I. Vogel, *Practical Organic Chemistry*, 3rd ed. pp. 729, Longman, London, **1974**.
- 14 (a) A. Orahovatz, M.I. Levinson, P.J. Carroll, M.V. Lakshminathan, M.P. Cava, *J. Org. Chem.* **1985**, 50, 2437. (b) S. M. Tsang, E. H. Wood, J. R. Johnson, *Org. Synth. Coll.* **1955**, 3, 641.
- 15 J. C. Hummelen, B. W. Knight, F. LePeq, F. Wudl, *J. Org. Chem.* **1995**, 60, 532.

-
- 16 A. I. Vogel, *Practical Organic Chemistry*, 3rd ed. pp. 732, Longman, London, **1974**.
- 17 N. A. Beare, J. F. Hartwig, *J. Org. Chem.* **2002**, *67*, 541.
- 18 J. Kim, S. Matsuyama, T. Suzuki, *J. Label. Compd. Radiopharm.* **2004**, *47*, 921.
- 19 (a) Y. L. Bennani, K. S. Marron, D. E. Mais, K. Flatten, A. M. Nadzan, M. F. Boehm, *J. Org. Chem.* **1998**, *63*, 543. (b) D.-M. Du, T. Fang, J. Xu, S.-W. Zhang, *Org. Lett.* **2006**, *8*, 1327.
- 20 H. Yorimitsu, H. Shinokubo, S. Matsubara, K. Oshima, K. Omoto, H. Fujimoto, *J. Org. Chem.* **2001**, *66*, 7776.
- 21 W. Reeves, L. Bahr, *Synthesis* **1976**, 823.
- 22 S. A. Davis, T. Ritthiwigrom, S. G. Pyne, *Tetrahedron* **2008**, *58*, 2405.
- 23 M. J. Plater, S. Aiken, G. Bourhill, *Tetrahedron* **2002**, *58*, 2405.
- 24 C. K.-F. Shen, H.-H. Yu, C.-G. Juo, K.-M. Chien, G.-R. Her, T.-Y. Luh, *Chem. Eur. J.* **1997**, *3*, 744.
- 25 (a) E. A. Meulenkamp *J. Phys. Chem. B*, **1998**, *102*, 5566. (b) W. J. E. Beek, M. M. Wienk, M. Kemerink, X. Yang, R. A. J. Janssen, *J. Phys. Chem. B* **2005**, *109*, 9505.

Appendix

X-ray diffraction crystallography data of BAF (2.68)

Empirical formula: $C_{80}H_{26}Cl_3N_3O_3$

Formula weight: 1183.39

Temperature: 100(2) K

Wavelength: 0.85500 Å

Crystal system, space group: triclinic, P-1

Unit cell dimensions:

a = 9.952(2) Å, α = 77.41(3) deg.

b = 15.876(3) Å, β = 83.69(3) deg.

c = 15.877(3) Å, γ = 88.42(3) deg.

Volume: 2433.4(8) Å³

Z, Calculated density: 2, 1.615 Mg/m³

Absorption coefficient: 0.257 mm⁻¹

F(000), 1204

Crystal size: 0.01 × 0.01 × 0.01 mm

Theta range for data collection: 1.59 to 26.74 deg.

Limiting indices: $-10 \leq h \leq 10$, $-16 \leq k \leq 16$, $-16 \leq l \leq 16$

Reflections collected / unique: 21128 / 5465 [R(int) = 0.0416]

Completeness to theta = 26.74, 91.8 %

Refinement method: Full-matrix least-squares on F²

Data / restraints / parameters: 5465 / 3 / 803

Goodness-of-fit on F²: 1.657

Final R indices [$I > 2\sigma(I)$]: R1 = 0.1122, wR2 = 0.3345

R indices (all data): R1 = 0.1250, wR2 = 0.3490

Extinction coefficient: 0.044(9)

Largest diff.: peak and hole 0.944 and -1.271 e.Å⁻³

Table 2. Atomic coordinates ($\times 10^4$) and equivalent isotropic displacement parameters ($\text{Å}^2 \times 10^3$). U(eq) is defined as one third of the trace of the orthogonalized U_{ij} tensor.

	x	y	z	U(eq)
Cl(2)	3559(2)	5309(1)	1731(2)	65(1)
Cl(3)	2170(4)	4503(2)	633(2)	114(2)
O(1)	5334(5)	4045(3)	4595(3)	32(1)
N(1)	4172(5)	3321(3)	3466(3)	26(1)

N(3)	3330(5)	4632(3)	4970(3)	22(1)
CI(1)	701(3)	5220(2)	2004(4)	175(3)
O(2)	1403(5)	3376(3)	3558(3)	42(1)
C(008)	4153(7)	2641(4)	2998(4)	27(2)
O(3)	1338(4)	5161(3)	5437(3)	35(1)
N(2)	1339(5)	4272(3)	4488(3)	28(1)
C(011)	2868(6)	2911(4)	6486(4)	24(2)
C(012)	2106(6)	3015(4)	7236(4)	23(2)
C(013)	8506(7)	-35(4)	802(4)	27(2)
C(014)	1956(7)	3675(4)	4053(4)	29(2)
C(015)	3171(6)	2544(4)	5004(4)	24(2)
C(016)	3374(6)	3383(4)	4279(4)	25(2)
C(017)	9776(7)	-29(5)	2026(4)	36(2)
C(018)	9621(6)	231(4)	1110(4)	28(2)
C(019)	3890(6)	1716(4)	3302(4)	26(2)
C(020)	1955(7)	4704(4)	4998(4)	26(2)
C(021)	2318(6)	2655(3)	5823(4)	20(1)
C(022)	4108(7)	4047(4)	4618(4)	22(2)
C(023)	5764(8)	1468(5)	4200(4)	41(2)
C(024)	7667(8)	-814(4)	2269(5)	38(2)
C(025)	2793(7)	3315(4)	7948(4)	28(2)
C(026)	926(7)	2500(3)	5908(4)	26(2)
C(027)	6544(8)	3426(4)	2707(5)	42(2)
C(028)	95(6)	2588(3)	6653(4)	23(2)
C(029)	10073(7)	1113(4)	791(4)	35(2)
C(030)	4894(9)	273(5)	3794(5)	53(3)
C(031)	4615(7)	1185(5)	3886(4)	40(2)
C(032)	723(6)	2847(4)	7306(4)	24(2)
C(033)	6192(6)	2276(4)	3932(4)	27(2)
C(034)	7500(7)	-567(4)	1384(5)	35(2)
C(035)	6178(7)	-317(4)	1132(5)	36(2)
C(036)	9393(8)	1651(5)	180(5)	44(2)
C(037)	-1421(6)	2443(4)	6734(4)	27(2)
C(038)	3722(8)	570(6)	2486(7)	56(2)
C(039)	4175(7)	2855(4)	2055(4)	35(2)
C(040)	3484(7)	1392(5)	2586(6)	43(2)
C(041)	7821(8)	554(5)	171(4)	40(2)
C(042)	6344(9)	3641(4)	1829(5)	44(2)
C(043)	5200(8)	3373(4)	1508(4)	42(2)
C(044)	5113(8)	-343(4)	1780(5)	45(2)
C(045)	4184(7)	2896(4)	8059(4)	36(2)
C(046)	7000(10)	3311(5)	430(5)	58(3)
C(047)	7270(12)	2100(7)	-227(5)	65(3)
C(048)	9705(9)	1759(6)	3218(7)	61(3)
C(049)	7700(9)	2451(5)	3695(5)	50(2)
C(050)	3663(7)	2110(6)	1789(5)	53(3)
C(051)	6211(10)	45(5)	4077(5)	57(3)
C(052)	5439(9)	1022(7)	269(5)	60(3)
C(053)	8406(8)	-345(4)	3430(4)	40(2)
C(054)	7801(12)	2793(6)	2(5)	74(3)
C(055)	-2014(8)	2173(5)	7658(4)	47(2)
C(056)	8811(8)	-539(4)	2592(4)	38(2)
C(057)	10365(8)	696(7)	2297(6)	56(3)
C(058)	8911(8)	3168(5)	2297(6)	50(2)
C(059)	6507(10)	-811(4)	2901(6)	55(3)
C(060)	7525(12)	3632(5)	1193(7)	71(3)
C(061)	1948(8)	3099(5)	8828(4)	44(2)
C(062)	9963(9)	882(7)	3098(6)	66(3)

C(063)	8601(8)	1803(6)	3800(5)	57(3)
C(064)	9113(10)	2552(6)	272(7)	75(4)
C(065)	10539(7)	1436(6)	1486(7)	65(3)
C(066)	-1751(8)	1685(5)	6301(5)	49(2)
C(067)	9033(9)	363(6)	3655(5)	57(3)
C(068)	6758(9)	742(5)	4306(4)	45(2)
C(069)	7866(7)	3141(4)	2957(5)	40(2)
C(070)	8274(10)	1383(6)	-118(5)	58(3)
C(071)	5606(10)	3179(5)	670(5)	53(2)
C(072)	6987(9)	-487(4)	3658(5)	49(2)
C(073)	10307(10)	2255(7)	1579(9)	79(4)
C(074)	5026(10)	2474(6)	430(5)	62(3)
C(075)	4397(9)	9(5)	3125(7)	57(3)
C(076)	6323(9)	377(5)	386(5)	46(2)
C(077)	4321(9)	1038(5)	890(6)	57(3)
C(078)	5952(12)	1913(6)	-65(5)	61(3)
C(079)	4069(10)	1930(7)	988(6)	67(3)
C(080)	4100(8)	391(7)	1660(7)	64(3)
C(081)	9623(11)	2830(6)	959(8)	75(4)
C(082)	5287(10)	-583(5)	2669(6)	56(2)
C(083)	8077(11)	922(5)	4145(5)	54(3)
C(084)	2982(8)	4294(4)	7661(5)	42(2)
C(085)	8741(11)	3393(5)	1416(8)	70(3)
C(086)	-2091(8)	3261(5)	6269(6)	59(2)
C(087)	9924(8)	2434(7)	2418(8)	76(4)
C(088)	2150(8)	4708(5)	1665(6)	62(3)
C(1)	5495(7)	2969(4)	3372(4)	30(2)

Symmetry transformations used to generate equivalent atoms

Table 3. Bond lengths [Å] and angles [°].

Cl(2)-C(088)	1.743(9)
Cl(3)-C(088)	1.737(9)
O(1)-C(022)	1.217(7)
N(1)-C(1)	1.422(8)
N(1)-C(008)	1.440(8)
N(1)-C(016)	1.460(7)
N(3)-C(022)	1.366(7)
N(3)-C(020)	1.367(8)
Cl(1)-C(088)	1.728(8)
O(2)-C(014)	1.191(8)
C(008)-C(039)	1.458(9)
C(008)-C(019)	1.463(9)
C(008)-C(1)	1.660(10)
O(3)-C(020)	1.220(7)
N(2)-C(020)	1.370(8)
N(2)-C(014)	1.383(8)
C(011)-C(021)	1.376(9)
C(011)-C(012)	1.379(8)
C(012)-C(032)	1.397(9)
C(012)-C(025)	1.547(9)
C(013)-C(018)	1.374(10)
C(013)-C(041)	1.431(10)
C(013)-C(034)	1.439(10)
C(014)-C(016)	1.529(9)

C(015)-C(021)	1.514(8)
C(015)-C(016)	1.560(8)
C(016)-C(022)	1.521(9)
C(017)-C(056)	1.387(11)
C(017)-C(018)	1.446(9)
C(017)-C(057)	1.471(12)
C(018)-C(029)	1.447(10)
C(019)-C(031)	1.365(10)
C(019)-C(040)	1.445(10)
C(021)-C(026)	1.400(9)
C(023)-C(033)	1.327(10)
C(023)-C(031)	1.417(11)
C(023)-C(068)	1.491(10)
C(024)-C(034)	1.401(10)
C(024)-C(056)	1.415(11)
C(024)-C(059)	1.445(10)
C(025)-C(061)	1.526(9)
C(025)-C(045)	1.531(9)
C(025)-C(084)	1.532(9)
C(026)-C(028)	1.397(8)
C(027)-C(042)	1.395(12)
C(027)-C(069)	1.448(11)
C(027)-C(1)	1.483(10)
C(028)-C(032)	1.407(9)
C(028)-C(037)	1.519(9)
C(029)-C(036)	1.370(11)
C(029)-C(065)	1.439(12)
C(030)-C(075)	1.368(14)
C(030)-C(051)	1.444(13)
C(030)-C(031)	1.501(11)
C(033)-C(1)	1.466(9)
C(033)-C(049)	1.524(11)
C(034)-C(035)	1.438(10)
C(035)-C(044)	1.388(10)
C(035)-C(076)	1.427(11)
C(036)-C(070)	1.369(13)
C(036)-C(064)	1.485(13)
C(037)-C(055)	1.495(9)
C(037)-C(086)	1.523(10)
C(037)-C(066)	1.569(10)
C(038)-C(040)	1.360(11)
C(038)-C(080)	1.412(12)
C(038)-C(075)	1.413(14)
C(039)-C(043)	1.418(11)
C(039)-C(050)	1.461(12)
C(040)-C(050)	1.504(12)
C(041)-C(070)	1.367(12)
C(041)-C(076)	1.512(12)
C(042)-C(043)	1.410(12)
C(042)-C(060)	1.465(12)
C(043)-C(071)	1.443(10)
C(044)-C(082)	1.408(13)
C(044)-C(080)	1.514(12)
C(046)-C(054)	1.365(11)
C(046)-C(071)	1.406(13)
C(046)-C(060)	1.557(15)
C(047)-C(078)	1.338(14)
C(047)-C(054)	1.366(15)

C(047)-C(070)	1.487(12)
C(048)-C(063)	1.366(13)
C(048)-C(062)	1.458(13)
C(048)-C(087)	1.472(15)
C(049)-C(063)	1.341(11)
C(049)-C(069)	1.417(11)
C(050)-C(079)	1.379(11)
C(051)-C(072)	1.360(10)
C(051)-C(068)	1.380(13)
C(052)-C(076)	1.328(11)
C(052)-C(077)	1.407(13)
C(052)-C(078)	1.482(14)
C(053)-C(067)	1.429(12)
C(053)-C(072)	1.431(12)
C(053)-C(056)	1.442(10)
C(054)-C(064)	1.436(16)
C(057)-C(062)	1.382(12)
C(057)-C(065)	1.539(14)
C(058)-C(069)	1.387(10)
C(058)-C(085)	1.395(14)
C(058)-C(087)	1.513(14)
C(059)-C(082)	1.326(13)
C(059)-C(072)	1.533(13)
C(060)-C(085)	1.320(15)
C(062)-C(067)	1.365(14)
C(063)-C(083)	1.474(13)
C(064)-C(081)	1.409(17)
C(065)-C(073)	1.352(13)
C(067)-C(083)	1.546(12)
C(068)-C(083)	1.336(12)
C(071)-C(074)	1.416(13)
C(073)-C(081)	1.410(17)
C(073)-C(087)	1.431(15)
C(074)-C(079)	1.402(15)
C(074)-C(078)	1.535(13)
C(075)-C(082)	1.517(11)
C(077)-C(080)	1.415(14)
C(077)-C(079)	1.470(13)
C(081)-C(085)	1.481(13)
C(1)-N(1)-C(008)	70.9(4)
C(1)-N(1)-C(016)	126.5(5)
C(008)-N(1)-C(016)	127.6(5)
C(022)-N(3)-C(020)	125.6(5)
N(1)-C(008)-C(039)	119.7(5)
N(1)-C(008)-C(019)	131.1(5)
C(039)-C(008)-C(019)	108.4(5)
N(1)-C(008)-C(1)	54.0(4)
C(039)-C(008)-C(1)	114.7(5)
C(019)-C(008)-C(1)	113.4(5)
C(020)-N(2)-C(014)	125.5(5)
C(021)-C(011)-C(012)	122.8(6)
C(011)-C(012)-C(032)	117.1(6)
C(011)-C(012)-C(025)	119.8(6)
C(032)-C(012)-C(025)	123.1(5)
C(018)-C(013)-C(041)	120.0(6)
C(018)-C(013)-C(034)	120.3(6)
C(041)-C(013)-C(034)	107.8(6)

O(2)-C(014)-N(2)	122.5(6)
O(2)-C(014)-C(016)	121.5(5)
N(2)-C(014)-C(016)	116.0(6)
C(021)-C(015)-C(016)	114.9(4)
N(1)-C(016)-C(022)	104.7(5)
N(1)-C(016)-C(014)	106.7(5)
C(022)-C(016)-C(014)	112.9(5)
N(1)-C(016)-C(015)	117.9(4)
C(022)-C(016)-C(015)	109.1(5)
C(014)-C(016)-C(015)	105.7(5)
C(056)-C(017)-C(018)	120.7(7)
C(056)-C(017)-C(057)	119.0(7)
C(018)-C(017)-C(057)	108.3(7)
C(013)-C(018)-C(017)	119.4(6)
C(013)-C(018)-C(029)	118.7(6)
C(017)-C(018)-C(029)	109.3(6)
C(031)-C(019)-C(040)	118.4(6)
C(031)-C(019)-C(008)	123.4(7)
C(040)-C(019)-C(008)	107.9(6)
O(3)-C(020)-N(3)	120.3(6)
O(3)-C(020)-N(2)	123.0(6)
N(3)-C(020)-N(2)	116.7(5)
C(011)-C(021)-C(026)	118.9(5)
C(011)-C(021)-C(015)	122.0(5)
C(026)-C(021)-C(015)	119.1(5)
O(1)-C(022)-N(3)	121.4(6)
O(1)-C(022)-C(016)	121.4(5)
N(3)-C(022)-C(016)	117.2(5)
C(033)-C(023)-C(031)	120.9(6)
C(033)-C(023)-C(068)	120.0(7)
C(031)-C(023)-C(068)	107.6(7)
C(034)-C(024)-C(056)	120.4(6)
C(034)-C(024)-C(059)	119.1(8)
C(056)-C(024)-C(059)	108.7(7)
C(061)-C(025)-C(045)	107.6(5)
C(061)-C(025)-C(084)	109.6(5)
C(045)-C(025)-C(084)	108.3(6)
C(061)-C(025)-C(012)	112.1(6)
C(045)-C(025)-C(012)	111.7(5)
C(084)-C(025)-C(012)	107.5(5)
C(028)-C(026)-C(021)	121.4(6)
C(042)-C(027)-C(069)	119.6(6)
C(042)-C(027)-C(1)	121.5(7)
C(069)-C(027)-C(1)	109.0(7)
C(026)-C(028)-C(032)	116.7(6)
C(026)-C(028)-C(037)	121.4(5)
C(032)-C(028)-C(037)	121.8(5)
C(036)-C(029)-C(065)	119.8(7)
C(036)-C(029)-C(018)	119.2(7)
C(065)-C(029)-C(018)	109.6(7)
C(075)-C(030)-C(051)	124.5(7)
C(075)-C(030)-C(031)	118.0(8)
C(051)-C(030)-C(031)	106.9(8)
C(019)-C(031)-C(023)	122.7(7)
C(019)-C(031)-C(030)	119.3(8)
C(023)-C(031)-C(030)	107.0(7)
C(012)-C(032)-C(028)	123.1(5)
C(023)-C(033)-C(1)	125.2(6)

C(023)-C(033)-C(049)	119.4(6)
C(1)-C(033)-C(049)	106.2(6)
C(024)-C(034)-C(035)	119.0(6)
C(024)-C(034)-C(013)	119.6(7)
C(035)-C(034)-C(013)	109.6(6)
C(044)-C(035)-C(076)	121.6(7)
C(044)-C(035)-C(034)	118.3(7)
C(076)-C(035)-C(034)	108.4(6)
C(070)-C(036)-C(029)	121.8(7)
C(070)-C(036)-C(064)	106.3(8)
C(029)-C(036)-C(064)	118.7(9)
C(055)-C(037)-C(028)	112.4(5)
C(055)-C(037)-C(086)	111.5(6)
C(028)-C(037)-C(086)	108.9(5)
C(055)-C(037)-C(066)	104.9(6)
C(028)-C(037)-C(066)	110.8(5)
C(086)-C(037)-C(066)	108.3(6)
C(040)-C(038)-C(080)	121.2(10)
C(040)-C(038)-C(075)	117.5(9)
C(080)-C(038)-C(075)	110.6(7)
C(043)-C(039)-C(008)	122.5(7)
C(043)-C(039)-C(050)	119.5(6)
C(008)-C(039)-C(050)	107.8(6)
C(038)-C(040)-C(019)	123.5(8)
C(038)-C(040)-C(050)	118.0(7)
C(019)-C(040)-C(050)	107.6(6)
C(070)-C(041)-C(013)	119.9(8)
C(070)-C(041)-C(076)	120.2(7)
C(013)-C(041)-C(076)	107.4(6)
C(027)-C(042)-C(043)	122.6(6)
C(027)-C(042)-C(060)	117.7(9)
C(043)-C(042)-C(060)	109.0(8)
C(042)-C(043)-C(039)	122.2(6)
C(042)-C(043)-C(071)	108.8(7)
C(039)-C(043)-C(071)	117.6(8)
C(035)-C(044)-C(082)	122.6(8)
C(035)-C(044)-C(080)	117.3(7)
C(082)-C(044)-C(080)	107.9(7)
C(054)-C(046)-C(071)	123.8(10)
C(054)-C(046)-C(060)	119.7(10)
C(071)-C(046)-C(060)	105.0(7)
C(078)-C(047)-C(054)	122.0(8)
C(078)-C(047)-C(070)	119.1(10)
C(054)-C(047)-C(070)	108.5(10)
C(063)-C(048)-C(062)	112.0(10)
C(063)-C(048)-C(087)	119.7(7)
C(062)-C(048)-C(087)	114.7(9)
C(063)-C(049)-C(069)	120.3(8)
C(063)-C(049)-C(033)	120.8(8)
C(069)-C(049)-C(033)	108.3(6)
C(079)-C(050)-C(039)	122.0(9)
C(079)-C(050)-C(040)	120.3(8)
C(039)-C(050)-C(040)	107.0(6)
C(072)-C(051)-C(068)	121.5(9)
C(072)-C(051)-C(030)	117.0(9)
C(068)-C(051)-C(030)	109.6(7)
C(076)-C(052)-C(077)	120.0(9)
C(076)-C(052)-C(078)	118.7(9)

C(077)-C(052)-C(078)	108.9(7)
C(067)-C(053)-C(072)	119.6(6)
C(067)-C(053)-C(056)	118.7(7)
C(072)-C(053)-C(056)	110.1(7)
C(046)-C(054)-C(047)	120.7(11)
C(046)-C(054)-C(064)	118.9(11)
C(047)-C(054)-C(064)	108.1(8)
C(017)-C(056)-C(024)	119.6(6)
C(017)-C(056)-C(053)	119.3(7)
C(024)-C(056)-C(053)	109.1(7)
C(062)-C(057)-C(017)	121.3(9)
C(062)-C(057)-C(065)	119.6(8)
C(017)-C(057)-C(065)	106.3(6)
C(069)-C(058)-C(085)	123.9(9)
C(069)-C(058)-C(087)	116.6(8)
C(085)-C(058)-C(087)	107.4(8)
C(082)-C(059)-C(024)	122.0(9)
C(082)-C(059)-C(072)	118.6(7)
C(024)-C(059)-C(072)	107.2(8)
C(085)-C(060)-C(042)	122.9(10)
C(085)-C(060)-C(046)	119.1(8)
C(042)-C(060)-C(046)	105.7(9)
C(067)-C(062)-C(057)	119.0(10)
C(067)-C(062)-C(048)	107.0(8)
C(057)-C(062)-C(048)	122.8(10)
C(049)-C(063)-C(048)	123.3(9)
C(049)-C(063)-C(083)	117.5(8)
C(048)-C(063)-C(083)	108.3(7)
C(081)-C(064)-C(054)	123.0(9)
C(081)-C(064)-C(036)	118.4(9)
C(054)-C(064)-C(036)	108.1(11)
C(073)-C(065)-C(029)	122.5(11)
C(073)-C(065)-C(057)	118.8(9)
C(029)-C(065)-C(057)	106.5(7)
C(062)-C(067)-C(053)	122.7(8)
C(062)-C(067)-C(083)	109.2(8)
C(053)-C(067)-C(083)	115.3(8)
C(083)-C(068)-C(051)	122.1(7)
C(083)-C(068)-C(023)	119.0(8)
C(051)-C(068)-C(023)	108.8(8)
C(058)-C(069)-C(049)	122.8(7)
C(058)-C(069)-C(027)	117.3(8)
C(049)-C(069)-C(027)	108.6(6)
C(041)-C(070)-C(036)	120.5(7)
C(041)-C(070)-C(047)	118.9(9)
C(036)-C(070)-C(047)	108.9(9)
C(046)-C(071)-C(074)	116.7(7)
C(046)-C(071)-C(043)	111.4(8)
C(074)-C(071)-C(043)	120.2(8)
C(051)-C(072)-C(053)	121.4(8)
C(051)-C(072)-C(059)	121.7(8)
C(053)-C(072)-C(059)	104.9(6)
C(065)-C(073)-C(081)	119.3(11)
C(065)-C(073)-C(087)	120.6(12)
C(081)-C(073)-C(087)	109.2(9)
C(079)-C(074)-C(071)	122.3(9)
C(079)-C(074)-C(078)	107.7(8)
C(071)-C(074)-C(078)	118.2(9)

C(030)-C(075)-C(038)	123.0(7)
C(030)-C(075)-C(082)	117.1(9)
C(038)-C(075)-C(082)	107.3(8)
C(052)-C(076)-C(035)	121.9(8)
C(052)-C(076)-C(041)	120.2(8)
C(035)-C(076)-C(041)	106.8(6)
C(052)-C(077)-C(080)	122.5(7)
C(052)-C(077)-C(079)	109.3(9)
C(080)-C(077)-C(079)	115.8(8)
C(047)-C(078)-C(052)	122.9(8)
C(047)-C(078)-C(074)	118.6(9)
C(052)-C(078)-C(074)	104.9(9)
C(050)-C(079)-C(074)	118.1(10)
C(050)-C(079)-C(077)	121.1(10)
C(074)-C(079)-C(077)	109.1(8)
C(038)-C(080)-C(077)	123.5(8)
C(038)-C(080)-C(044)	107.0(9)
C(077)-C(080)-C(044)	116.8(7)
C(064)-C(081)-C(073)	121.1(8)
C(064)-C(081)-C(085)	117.4(12)
C(073)-C(081)-C(085)	108.2(10)
C(059)-C(082)-C(044)	119.1(8)
C(059)-C(082)-C(075)	120.9(9)
C(044)-C(082)-C(075)	107.2(8)
C(068)-C(083)-C(063)	123.0(7)
C(068)-C(083)-C(067)	119.9(8)
C(063)-C(083)-C(067)	103.4(8)
C(060)-C(085)-C(058)	118.3(9)
C(060)-C(085)-C(081)	121.9(11)
C(058)-C(085)-C(081)	108.5(11)
C(073)-C(087)-C(048)	123.5(9)
C(073)-C(087)-C(058)	106.8(11)
C(048)-C(087)-C(058)	117.2(7)
Cl(1)-C(088)-Cl(3)	114.1(5)
Cl(1)-C(088)-Cl(2)	109.4(5)
Cl(3)-C(088)-Cl(2)	110.6(5)
N(1)-C(1)-C(033)	131.9(5)
N(1)-C(1)-C(027)	120.6(5)
C(033)-C(1)-C(027)	106.4(6)
N(1)-C(1)-C(008)	55.1(4)
C(033)-C(1)-C(008)	113.9(5)
C(027)-C(1)-C(008)	115.9(6)

Symmetry transformations used to generate equivalent atoms:

Table 4. Anisotropic displacement parameters ($\text{Å}^2 \times 10^3$).

The anisotropic displacement factor exponent takes the form:

$$-2 \pi^2 [h^2 a^{*2} U_{11} + \dots + 2 h k a^* b^* U_{12}]$$

	U11	U22	U33	U23	U13	U12
Cl(2)	64(2)	43(1)	92(2)	-17(1)	-24(1)	10(1)
Cl(3)	179(3)	59(2)	99(2)	30(2)	-84(2)	-47(2)
O(1)	29(3)	26(2)	46(3)	-22(2)	3(2)	6(2)
N(1)	38(3)	17(3)	24(3)	-10(2)	4(2)	5(2)

N(3)	27(3)	17(3)	27(3)	-15(2)	2(2)	6(2)
CI(1)	55(2)	39(2)	428(8)	-55(3)	-2(3)	14(1)
O(2)	40(3)	44(3)	51(3)	-31(3)	-11(2)	16(2)
C(008)	39(4)	21(3)	20(3)	-8(3)	1(3)	6(3)
O(3)	35(3)	29(3)	44(3)	-16(2)	1(2)	14(2)
N(2)	33(3)	25(3)	31(3)	-17(2)	-2(2)	14(2)
C(011)	28(4)	17(3)	26(4)	-4(3)	3(3)	3(3)
C(012)	37(4)	15(3)	16(3)	-5(2)	1(3)	7(3)
C(013)	31(4)	25(3)	27(4)	-19(3)	11(3)	5(3)
C(014)	34(4)	21(3)	34(4)	-15(3)	-3(3)	7(3)
C(015)	28(4)	16(3)	27(3)	-8(3)	5(3)	8(3)
C(016)	31(4)	22(3)	24(3)	-14(3)	7(3)	12(3)
C(017)	34(4)	43(4)	38(4)	-25(3)	-4(3)	29(3)
C(018)	25(4)	31(4)	29(4)	-19(3)	10(3)	16(3)
C(019)	20(3)	25(3)	35(4)	-17(3)	8(3)	4(3)
C(020)	39(4)	8(3)	29(4)	-6(3)	2(3)	10(3)
C(021)	21(4)	14(3)	26(4)	-8(3)	5(3)	3(2)
C(022)	33(4)	13(3)	19(3)	-6(2)	7(3)	3(3)
C(023)	61(6)	40(4)	21(4)	-12(3)	7(3)	7(4)
C(024)	57(5)	20(3)	34(4)	-11(3)	15(4)	16(3)
C(025)	36(4)	25(3)	22(3)	-8(3)	2(3)	-2(3)
C(026)	50(5)	12(3)	16(3)	-6(2)	-1(3)	3(3)
C(027)	53(5)	8(3)	65(6)	-21(3)	22(4)	-4(3)
C(028)	31(4)	12(3)	23(3)	-3(2)	4(3)	6(3)
C(029)	31(4)	37(4)	38(4)	-21(4)	20(3)	-3(3)
C(030)	61(6)	32(4)	42(5)	19(4)	39(4)	13(4)
C(031)	40(5)	47(4)	27(4)	-6(3)	16(3)	11(4)
C(032)	34(4)	19(3)	18(3)	-5(3)	6(3)	6(3)
C(033)	30(4)	37(4)	23(3)	-25(3)	-9(3)	18(3)
C(034)	39(4)	27(4)	46(5)	-33(3)	3(3)	9(3)
C(035)	33(4)	33(4)	50(5)	-37(4)	8(3)	-6(3)
C(036)	41(5)	43(5)	44(5)	-15(4)	26(4)	-1(4)
C(037)	32(4)	27(3)	20(3)	-2(3)	1(3)	2(3)
C(038)	32(5)	55(5)	92(7)	-45(5)	11(4)	-5(4)
C(039)	48(5)	34(4)	26(4)	-14(3)	-8(3)	29(3)
C(040)	15(4)	42(4)	87(6)	-48(4)	5(3)	-1(3)
C(041)	54(5)	50(5)	23(4)	-24(3)	-3(3)	27(4)
C(042)	67(6)	10(3)	44(5)	2(3)	27(4)	11(3)
C(043)	62(5)	27(4)	26(4)	7(3)	8(4)	28(4)
C(044)	43(5)	31(4)	69(6)	-37(4)	15(4)	-10(3)
C(045)	40(4)	36(4)	33(4)	-8(3)	-9(3)	1(3)
C(046)	101(8)	26(4)	31(4)	11(3)	31(4)	22(4)
C(047)	98(8)	69(7)	16(4)	6(4)	11(4)	34(6)
C(048)	43(5)	49(5)	111(8)	-45(6)	-44(5)	7(4)
C(049)	69(6)	60(5)	35(4)	-42(4)	-9(4)	2(5)
C(050)	27(4)	98(7)	48(5)	-47(5)	-22(3)	45(4)
C(051)	98(7)	32(4)	28(4)	2(3)	21(4)	36(5)
C(052)	58(6)	98(8)	44(5)	-58(5)	-14(4)	27(5)
C(053)	64(6)	26(4)	26(4)	-3(3)	-5(3)	30(4)
C(054)	132(10)	34(5)	34(5)	12(4)	41(5)	27(6)
C(055)	36(4)	72(5)	31(4)	-10(4)	1(3)	-6(4)
C(056)	52(5)	29(4)	30(4)	-6(3)	3(4)	28(4)
C(057)	22(4)	96(7)	72(6)	-61(6)	-19(4)	33(4)
C(058)	47(5)	39(4)	68(6)	-38(4)	27(4)	-23(4)
C(059)	70(6)	12(3)	71(6)	-2(4)	31(5)	5(4)
C(060)	102(9)	12(4)	83(7)	3(4)	38(6)	-4(4)
C(061)	52(5)	52(5)	28(4)	-13(3)	1(3)	-6(4)
C(062)	43(5)	109(8)	65(6)	-58(6)	-22(5)	37(6)

C(063)	43(5)	92(7)	55(5)	-57(5)	-15(4)	25(5)
C(064)	70(7)	44(5)	76(7)	30(5)	59(6)	14(5)
C(065)	8(4)	77(6)	127(9)	-75(7)	18(4)	-8(4)
C(066)	47(5)	55(5)	50(5)	-24(4)	0(4)	-3(4)
C(067)	48(5)	79(6)	43(5)	-1(4)	-28(4)	28(5)
C(068)	67(6)	52(5)	13(4)	-5(3)	-3(3)	32(4)
C(069)	39(5)	30(4)	60(5)	-37(4)	16(4)	-10(3)
C(070)	87(7)	58(6)	23(4)	-12(4)	19(4)	25(5)
C(071)	88(7)	36(4)	25(4)	5(3)	1(4)	38(5)
C(072)	85(7)	20(4)	29(4)	6(3)	19(4)	25(4)
C(073)	48(6)	54(6)	139(10)	-55(7)	46(6)	-21(5)
C(074)	70(6)	68(6)	39(5)	14(5)	-25(5)	23(5)
C(075)	56(6)	39(5)	78(7)	-40(5)	48(5)	-31(4)
C(076)	63(6)	57(5)	32(4)	-36(4)	-15(4)	9(4)
C(077)	64(6)	52(5)	74(7)	-39(5)	-49(5)	20(5)
C(078)	118(9)	53(5)	20(4)	-18(4)	-33(5)	41(6)
C(079)	65(6)	104(8)	47(5)	-41(5)	-32(5)	45(6)
C(080)	19(4)	108(8)	93(7)	-89(7)	3(4)	-10(5)
C(081)	78(7)	43(6)	108(9)	-57(6)	73(7)	-45(5)
C(082)	75(7)	24(4)	72(7)	-23(4)	16(5)	-21(4)
C(083)	94(8)	46(5)	33(4)	-23(4)	-38(5)	34(5)
C(084)	63(5)	22(4)	43(4)	-10(3)	-13(4)	2(3)
C(085)	75(8)	33(5)	93(8)	-11(5)	28(6)	-25(5)
C(086)	42(5)	46(5)	76(6)	9(4)	0(4)	5(4)
C(087)	14(4)	113(9)	135(10)	-106(9)	10(5)	-19(5)
C(088)	60(6)	36(4)	86(7)	1(4)	-15(5)	8(4)
C(1)	33(4)	17(3)	37(4)	-10(3)	14(3)	4(3)

Table 5. Hydrogen coordinates ($\times 10^4$) and isotropic displacement parameters ($\text{Å}^2 \times 10^3$).

	x	y	z	U(eq)
H(3)	3741	4986	5194	27
H(2)	497	4381	4434	34
H(011)	3791	3017	6425	29
H(01A)	2752	2113	4771	29
H(01B)	4052	2325	5156	29
H(026)	547	2336	5459	31
H(032)	192	2910	7809	29
H(04A)	4573	3088	8512	54
H(04B)	4762	3057	7525	54
H(04C)	4089	2279	8211	54
H(05A)	-2966	2075	7678	70
H(05B)	-1874	2619	7961	70
H(05C)	-1585	1650	7929	70
H(06A)	2410	3292	9252	66
H(06B)	1816	2486	9001	66
H(06C)	1086	3384	8787	66
H(06D)	-1382	1811	5703	74
H(06E)	-2713	1620	6337	74
H(06F)	-1360	1159	6598	74
H(08A)	3399	4501	8095	63
H(08B)	2118	4568	7590	63
H(08C)	3549	4426	7120	63
H(08D)	-1690	3416	5679	88

H(08E)	-1966	3721	6557	88
H(08F)	-3040	3161	6279	88
H(088)	2210	4151	2073	75

Table 6. Torsion angles [°].

C(1)-N(1)-C(008)-C(039)	-100.4(6)
C(016)-N(1)-C(008)-C(039)	137.6(6)
C(1)-N(1)-C(008)-C(019)	91.1(8)
C(016)-N(1)-C(008)-C(019)	-30.8(10)
C(016)-N(1)-C(008)-C(1)	-121.9(6)
C(021)-C(011)-C(012)-C(032)	0.2(8)
C(021)-C(011)-C(012)-C(025)	-179.3(5)
C(020)-N(2)-C(014)-O(2)	-173.2(6)
C(020)-N(2)-C(014)-C(016)	9.9(9)
C(1)-N(1)-C(016)-C(022)	68.7(7)
C(008)-N(1)-C(016)-C(022)	162.0(5)
C(1)-N(1)-C(016)-C(014)	-171.3(6)
C(008)-N(1)-C(016)-C(014)	-78.1(7)
C(1)-N(1)-C(016)-C(015)	-52.7(8)
C(008)-N(1)-C(016)-C(015)	40.6(8)
O(2)-C(014)-C(016)-N(1)	43.2(8)
N(2)-C(014)-C(016)-N(1)	-139.9(5)
O(2)-C(014)-C(016)-C(022)	157.6(6)
N(2)-C(014)-C(016)-C(022)	-25.4(7)
O(2)-C(014)-C(016)-C(015)	-83.2(7)
N(2)-C(014)-C(016)-C(015)	93.8(6)
C(021)-C(015)-C(016)-N(1)	-179.2(5)
C(021)-C(015)-C(016)-C(022)	61.7(7)
C(021)-C(015)-C(016)-C(014)	-60.0(7)
C(041)-C(013)-C(018)-C(017)	138.3(6)
C(034)-C(013)-C(018)-C(017)	0.0(8)
C(041)-C(013)-C(018)-C(029)	0.5(8)
C(034)-C(013)-C(018)-C(029)	-137.8(6)
C(056)-C(017)-C(018)-C(013)	-0.2(8)
C(057)-C(017)-C(018)-C(013)	-142.4(6)
C(056)-C(017)-C(018)-C(029)	141.1(6)
C(057)-C(017)-C(018)-C(029)	-1.1(7)
N(1)-C(008)-C(019)-C(031)	-57.5(10)
C(039)-C(008)-C(019)-C(031)	133.1(6)
C(1)-C(008)-C(019)-C(031)	4.4(8)
N(1)-C(008)-C(019)-C(040)	158.2(6)
C(039)-C(008)-C(019)-C(040)	-11.3(7)
C(1)-C(008)-C(019)-C(040)	-139.9(5)
C(022)-N(3)-C(020)-O(3)	169.3(5)
C(022)-N(3)-C(020)-N(2)	-13.4(8)
C(014)-N(2)-C(020)-O(3)	-172.6(6)
C(014)-N(2)-C(020)-N(3)	10.1(8)
C(012)-C(011)-C(021)-C(026)	0.5(8)
C(012)-C(011)-C(021)-C(015)	180.0(5)
C(016)-C(015)-C(021)-C(011)	-86.6(7)
C(016)-C(015)-C(021)-C(026)	92.9(7)
C(020)-N(3)-C(022)-O(1)	177.6(5)
C(020)-N(3)-C(022)-C(016)	-4.1(8)
N(1)-C(016)-C(022)-O(1)	-43.0(7)
C(014)-C(016)-C(022)-O(1)	-158.7(5)
C(015)-C(016)-C(022)-O(1)	84.0(6)

N(1)-C(016)-C(022)-N(3)	138.6(5)
C(014)-C(016)-C(022)-N(3)	23.0(7)
C(015)-C(016)-C(022)-N(3)	-94.3(6)
C(011)-C(012)-C(025)-C(061)	-160.1(6)
C(032)-C(012)-C(025)-C(061)	20.4(8)
C(011)-C(012)-C(025)-C(045)	-39.3(7)
C(032)-C(012)-C(025)-C(045)	141.2(6)
C(011)-C(012)-C(025)-C(084)	79.3(7)
C(032)-C(012)-C(025)-C(084)	-100.1(7)
C(011)-C(021)-C(026)-C(028)	-1.0(8)
C(015)-C(021)-C(026)-C(028)	179.6(5)
C(021)-C(026)-C(028)-C(032)	0.7(8)
C(021)-C(026)-C(028)-C(037)	178.3(5)
C(013)-C(018)-C(029)-C(036)	-1.2(8)
C(017)-C(018)-C(029)-C(036)	-142.8(6)
C(013)-C(018)-C(029)-C(065)	142.3(6)
C(017)-C(018)-C(029)-C(065)	0.6(7)
C(040)-C(019)-C(031)-C(023)	135.8(7)
C(008)-C(019)-C(031)-C(023)	-5.1(10)
C(040)-C(019)-C(031)-C(030)	-3.6(10)
C(008)-C(019)-C(031)-C(030)	-144.5(6)
C(033)-C(023)-C(031)-C(019)	-0.2(10)
C(068)-C(023)-C(031)-C(019)	-143.6(6)
C(033)-C(023)-C(031)-C(030)	143.3(6)
C(068)-C(023)-C(031)-C(030)	0.0(7)
C(075)-C(030)-C(031)-C(019)	-0.4(10)
C(051)-C(030)-C(031)-C(019)	146.0(7)
C(075)-C(030)-C(031)-C(023)	-145.4(7)
C(051)-C(030)-C(031)-C(023)	1.0(7)
C(011)-C(012)-C(032)-C(028)	-0.4(8)
C(025)-C(012)-C(032)-C(028)	179.0(5)
C(026)-C(028)-C(032)-C(012)	0.0(8)
C(037)-C(028)-C(032)-C(012)	-177.6(5)
C(031)-C(023)-C(033)-C(1)	6.1(10)
C(068)-C(023)-C(033)-C(1)	145.0(6)
C(031)-C(023)-C(033)-C(049)	-136.2(6)
C(068)-C(023)-C(033)-C(049)	2.7(9)
C(056)-C(024)-C(034)-C(035)	-138.7(6)
C(059)-C(024)-C(034)-C(035)	0.0(10)
C(056)-C(024)-C(034)-C(013)	0.4(9)
C(059)-C(024)-C(034)-C(013)	139.1(7)
C(018)-C(013)-C(034)-C(024)	-0.1(8)
C(041)-C(013)-C(034)-C(024)	-142.9(6)
C(018)-C(013)-C(034)-C(035)	142.4(6)
C(041)-C(013)-C(034)-C(035)	-0.3(7)
C(024)-C(034)-C(035)-C(044)	-0.8(9)
C(013)-C(034)-C(035)-C(044)	-143.6(6)
C(024)-C(034)-C(035)-C(076)	142.8(6)
C(013)-C(034)-C(035)-C(076)	0.0(7)
C(065)-C(029)-C(036)-C(070)	-137.9(7)
C(018)-C(029)-C(036)-C(070)	1.9(10)
C(065)-C(029)-C(036)-C(064)	-2.1(10)
C(018)-C(029)-C(036)-C(064)	137.7(7)
C(026)-C(028)-C(037)-C(055)	154.0(6)
C(032)-C(028)-C(037)-C(055)	-28.5(8)
C(026)-C(028)-C(037)-C(086)	-82.0(7)
C(032)-C(028)-C(037)-C(086)	95.5(7)
C(026)-C(028)-C(037)-C(066)	37.0(7)

C(032)-C(028)-C(037)-C(066)	-145.5(6)
N(1)-C(008)-C(039)-C(043)	55.5(8)
C(019)-C(008)-C(039)-C(043)	-133.6(6)
C(1)-C(008)-C(039)-C(043)	-5.7(8)
N(1)-C(008)-C(039)-C(050)	-159.7(6)
C(019)-C(008)-C(039)-C(050)	11.2(7)
C(1)-C(008)-C(039)-C(050)	139.1(5)
C(080)-C(038)-C(040)-C(019)	-141.0(8)
C(075)-C(038)-C(040)-C(019)	0.3(11)
C(080)-C(038)-C(040)-C(050)	-1.2(11)
C(075)-C(038)-C(040)-C(050)	140.1(7)
C(031)-C(019)-C(040)-C(038)	3.7(11)
C(008)-C(019)-C(040)-C(038)	150.2(7)
C(031)-C(019)-C(040)-C(050)	-139.5(6)
C(008)-C(019)-C(040)-C(050)	6.9(7)
C(018)-C(013)-C(041)-C(070)	-0.5(9)
C(034)-C(013)-C(041)-C(070)	142.4(6)
C(018)-C(013)-C(041)-C(076)	-142.4(6)
C(034)-C(013)-C(041)-C(076)	0.5(7)
C(069)-C(027)-C(042)-C(043)	136.0(7)
C(1)-C(027)-C(042)-C(043)	-6.0(9)
C(069)-C(027)-C(042)-C(060)	-4.7(9)
C(1)-C(027)-C(042)-C(060)	-146.7(7)
C(027)-C(042)-C(043)-C(039)	-0.7(10)
C(060)-C(042)-C(043)-C(039)	142.9(6)
C(027)-C(042)-C(043)-C(071)	-143.2(6)
C(060)-C(042)-C(043)-C(071)	0.4(7)
C(008)-C(039)-C(043)-C(042)	6.8(9)
C(050)-C(039)-C(043)-C(042)	-134.0(7)
C(008)-C(039)-C(043)-C(071)	146.2(6)
C(050)-C(039)-C(043)-C(071)	5.4(9)
C(076)-C(035)-C(044)-C(082)	-137.1(7)
C(034)-C(035)-C(044)-C(082)	1.6(10)
C(076)-C(035)-C(044)-C(080)	0.7(11)
C(034)-C(035)-C(044)-C(080)	139.4(7)
C(023)-C(033)-C(049)-C(063)	-3.6(9)
C(1)-C(033)-C(049)-C(063)	-152.2(6)
C(023)-C(033)-C(049)-C(069)	141.1(6)
C(1)-C(033)-C(049)-C(069)	-7.5(7)
C(043)-C(039)-C(050)-C(079)	-5.2(10)
C(008)-C(039)-C(050)-C(079)	-151.1(7)
C(043)-C(039)-C(050)-C(040)	139.2(6)
C(008)-C(039)-C(050)-C(040)	-6.8(7)
C(038)-C(040)-C(050)-C(079)	-0.6(11)
C(019)-C(040)-C(050)-C(079)	145.0(7)
C(038)-C(040)-C(050)-C(039)	-145.7(7)
C(019)-C(040)-C(050)-C(039)	-0.1(7)
C(075)-C(030)-C(051)-C(072)	-1.7(11)
C(031)-C(030)-C(051)-C(072)	-145.3(7)
C(075)-C(030)-C(051)-C(068)	141.9(8)
C(031)-C(030)-C(051)-C(068)	-1.6(8)
C(071)-C(046)-C(054)-C(047)	0.4(13)
C(060)-C(046)-C(054)-C(047)	138.1(9)
C(071)-C(046)-C(054)-C(064)	-137.3(9)
C(060)-C(046)-C(054)-C(064)	0.4(11)
C(078)-C(047)-C(054)-C(046)	1.8(13)
C(070)-C(047)-C(054)-C(046)	-142.7(8)
C(078)-C(047)-C(054)-C(064)	143.5(8)

C(070)-C(047)-C(054)-C(064)	-0.9(9)
C(018)-C(017)-C(056)-C(024)	0.5(9)
C(057)-C(017)-C(056)-C(024)	138.9(6)
C(018)-C(017)-C(056)-C(053)	-138.2(6)
C(057)-C(017)-C(056)-C(053)	0.2(9)
C(034)-C(024)-C(056)-C(017)	-0.7(9)
C(059)-C(024)-C(056)-C(017)	-143.1(6)
C(034)-C(024)-C(056)-C(053)	141.8(6)
C(059)-C(024)-C(056)-C(053)	-0.7(7)
C(067)-C(053)-C(056)-C(017)	-1.0(9)
C(072)-C(053)-C(056)-C(017)	142.2(6)
C(067)-C(053)-C(056)-C(024)	-143.6(6)
C(072)-C(053)-C(056)-C(024)	-0.4(7)
C(056)-C(017)-C(057)-C(062)	-0.8(10)
C(018)-C(017)-C(057)-C(062)	142.3(7)
C(056)-C(017)-C(057)-C(065)	-141.9(6)
C(018)-C(017)-C(057)-C(065)	1.1(7)
C(034)-C(024)-C(059)-C(082)	0.1(11)
C(056)-C(024)-C(059)-C(082)	143.1(8)
C(034)-C(024)-C(059)-C(072)	-141.6(7)
C(056)-C(024)-C(059)-C(072)	1.4(7)
C(027)-C(042)-C(060)-C(085)	3.1(12)
C(043)-C(042)-C(060)-C(085)	-142.5(9)
C(027)-C(042)-C(060)-C(046)	144.8(7)
C(043)-C(042)-C(060)-C(046)	-0.8(7)
C(054)-C(046)-C(060)-C(085)	-0.3(11)
C(071)-C(046)-C(060)-C(085)	144.3(8)
C(054)-C(046)-C(060)-C(042)	-143.7(7)
C(071)-C(046)-C(060)-C(042)	0.9(7)
C(017)-C(057)-C(062)-C(067)	2.1(11)
C(065)-C(057)-C(062)-C(067)	138.3(8)
C(017)-C(057)-C(062)-C(048)	-136.9(9)
C(065)-C(057)-C(062)-C(048)	-0.7(12)
C(063)-C(048)-C(062)-C(067)	-3.1(10)
C(087)-C(048)-C(062)-C(067)	-143.9(8)
C(063)-C(048)-C(062)-C(057)	140.0(9)
C(087)-C(048)-C(062)-C(057)	-0.7(12)
C(069)-C(049)-C(063)-C(048)	-0.4(12)
C(033)-C(049)-C(063)-C(048)	140.2(8)
C(069)-C(049)-C(063)-C(083)	-140.3(8)
C(033)-C(049)-C(063)-C(083)	0.3(10)
C(062)-C(048)-C(063)-C(049)	-140.3(8)
C(087)-C(048)-C(063)-C(049)	-1.8(13)
C(062)-C(048)-C(063)-C(083)	2.7(10)
C(087)-C(048)-C(063)-C(083)	141.2(7)
C(046)-C(054)-C(064)-C(081)	-0.4(12)
C(047)-C(054)-C(064)-C(081)	-143.0(8)
C(046)-C(054)-C(064)-C(036)	143.7(8)
C(047)-C(054)-C(064)-C(036)	1.2(9)
C(070)-C(036)-C(064)-C(081)	145.1(7)
C(029)-C(036)-C(064)-C(081)	3.3(11)
C(070)-C(036)-C(064)-C(054)	-0.9(8)
C(029)-C(036)-C(064)-C(054)	-142.8(8)
C(036)-C(029)-C(065)-C(073)	1.6(11)
C(018)-C(029)-C(065)-C(073)	-141.6(8)
C(036)-C(029)-C(065)-C(057)	143.3(6)
C(018)-C(029)-C(065)-C(057)	0.1(7)
C(062)-C(057)-C(065)-C(073)	0.7(12)

C(017)-C(057)-C(065)-C(073)	142.6(8)
C(062)-C(057)-C(065)-C(029)	-142.7(7)
C(017)-C(057)-C(065)-C(029)	-0.8(7)
C(057)-C(062)-C(067)-C(053)	-3.0(12)
C(048)-C(062)-C(067)-C(053)	141.8(7)
C(057)-C(062)-C(067)-C(083)	-142.6(7)
C(048)-C(062)-C(067)-C(083)	2.2(9)
C(072)-C(053)-C(067)-C(062)	-137.2(8)
C(056)-C(053)-C(067)-C(062)	2.4(10)
C(072)-C(053)-C(067)-C(083)	0.2(9)
C(056)-C(053)-C(067)-C(083)	139.9(7)
C(072)-C(051)-C(068)-C(083)	-1.5(11)
C(030)-C(051)-C(068)-C(083)	-143.2(7)
C(072)-C(051)-C(068)-C(023)	143.4(7)
C(030)-C(051)-C(068)-C(023)	1.7(8)
C(033)-C(023)-C(068)-C(083)	1.5(10)
C(031)-C(023)-C(068)-C(083)	145.2(7)
C(033)-C(023)-C(068)-C(051)	-144.7(7)
C(031)-C(023)-C(068)-C(051)	-1.0(8)
C(085)-C(058)-C(069)-C(049)	134.9(9)
C(087)-C(058)-C(069)-C(049)	-2.6(11)
C(085)-C(058)-C(069)-C(027)	-4.6(10)
C(087)-C(058)-C(069)-C(027)	-142.2(7)
C(063)-C(049)-C(069)-C(058)	2.8(12)
C(033)-C(049)-C(069)-C(058)	-142.1(7)
C(063)-C(049)-C(069)-C(027)	145.3(7)
C(033)-C(049)-C(069)-C(027)	0.4(7)
C(042)-C(027)-C(069)-C(058)	5.4(9)
C(1)-C(027)-C(069)-C(058)	151.7(6)
C(042)-C(027)-C(069)-C(049)	-139.5(6)
C(1)-C(027)-C(069)-C(049)	6.8(7)
C(013)-C(041)-C(070)-C(036)	1.1(10)
C(076)-C(041)-C(070)-C(036)	138.2(7)
C(013)-C(041)-C(070)-C(047)	-137.9(7)
C(076)-C(041)-C(070)-C(047)	-0.8(10)
C(029)-C(036)-C(070)-C(041)	-1.8(10)
C(064)-C(036)-C(070)-C(041)	-142.3(7)
C(029)-C(036)-C(070)-C(047)	140.8(7)
C(064)-C(036)-C(070)-C(047)	0.3(8)
C(078)-C(047)-C(070)-C(041)	-2.0(12)
C(054)-C(047)-C(070)-C(041)	143.7(8)
C(078)-C(047)-C(070)-C(036)	-145.3(8)
C(054)-C(047)-C(070)-C(036)	0.4(9)
C(054)-C(046)-C(071)-C(074)	-1.3(11)
C(060)-C(046)-C(071)-C(074)	-144.1(6)
C(054)-C(046)-C(071)-C(043)	142.0(8)
C(060)-C(046)-C(071)-C(043)	-0.7(7)
C(042)-C(043)-C(071)-C(046)	0.2(8)
C(039)-C(043)-C(071)-C(046)	-144.2(7)
C(042)-C(043)-C(071)-C(074)	142.1(7)
C(039)-C(043)-C(071)-C(074)	-2.4(10)
C(068)-C(051)-C(072)-C(053)	-0.4(11)
C(030)-C(051)-C(072)-C(053)	138.8(8)
C(068)-C(051)-C(072)-C(059)	-137.4(8)
C(030)-C(051)-C(072)-C(059)	1.7(10)
C(067)-C(053)-C(072)-C(051)	0.9(10)
C(056)-C(053)-C(072)-C(051)	-141.9(7)
C(067)-C(053)-C(072)-C(059)	144.0(6)

C(056)-C(053)-C(072)-C(059)	1.3(7)
C(082)-C(059)-C(072)-C(051)	-1.9(11)
C(024)-C(059)-C(072)-C(051)	141.3(7)
C(082)-C(059)-C(072)-C(053)	-144.9(7)
C(024)-C(059)-C(072)-C(053)	-1.6(7)
C(029)-C(065)-C(073)-C(081)	-2.2(12)
C(057)-C(065)-C(073)-C(081)	-139.5(9)
C(029)-C(065)-C(073)-C(087)	138.2(10)
C(057)-C(065)-C(073)-C(087)	0.8(14)
C(046)-C(071)-C(074)-C(079)	138.7(8)
C(043)-C(071)-C(074)-C(079)	-1.3(11)
C(046)-C(071)-C(074)-C(078)	0.2(9)
C(043)-C(071)-C(074)-C(078)	-139.7(7)
C(051)-C(030)-C(075)-C(038)	-135.3(8)
C(031)-C(030)-C(075)-C(038)	4.6(11)
C(051)-C(030)-C(075)-C(082)	1.6(11)
C(031)-C(030)-C(075)-C(082)	141.6(7)
C(040)-C(038)-C(075)-C(030)	-4.6(12)
C(080)-C(038)-C(075)-C(030)	140.5(8)
C(040)-C(038)-C(075)-C(082)	-145.1(7)
C(080)-C(038)-C(075)-C(082)	0.0(9)
C(077)-C(052)-C(076)-C(035)	0.3(12)
C(078)-C(052)-C(076)-C(035)	138.3(8)
C(077)-C(052)-C(076)-C(041)	-138.8(8)
C(078)-C(052)-C(076)-C(041)	-0.7(10)
C(044)-C(035)-C(076)-C(052)	-1.2(11)
C(034)-C(035)-C(076)-C(052)	-143.4(7)
C(044)-C(035)-C(076)-C(041)	142.5(7)
C(034)-C(035)-C(076)-C(041)	0.3(7)
C(070)-C(041)-C(076)-C(052)	2.1(10)
C(013)-C(041)-C(076)-C(052)	143.9(6)
C(070)-C(041)-C(076)-C(035)	-142.3(7)
C(013)-C(041)-C(076)-C(035)	-0.5(7)
C(076)-C(052)-C(077)-C(080)	1.1(13)
C(078)-C(052)-C(077)-C(080)	-140.6(8)
C(076)-C(052)-C(077)-C(079)	141.4(8)
C(078)-C(052)-C(077)-C(079)	-0.3(9)
C(054)-C(047)-C(078)-C(052)	-137.4(8)
C(070)-C(047)-C(078)-C(052)	3.5(12)
C(054)-C(047)-C(078)-C(074)	-2.8(11)
C(070)-C(047)-C(078)-C(074)	138.1(8)
C(076)-C(052)-C(078)-C(047)	-2.2(11)
C(077)-C(052)-C(078)-C(047)	140.1(8)
C(076)-C(052)-C(078)-C(074)	-141.8(7)
C(077)-C(052)-C(078)-C(074)	0.5(9)
C(079)-C(074)-C(078)-C(047)	-142.2(8)
C(071)-C(074)-C(078)-C(047)	1.7(10)
C(079)-C(074)-C(078)-C(052)	-0.4(9)
C(071)-C(074)-C(078)-C(052)	143.5(7)
C(039)-C(050)-C(079)-C(074)	1.5(11)
C(040)-C(050)-C(079)-C(074)	-138.3(8)
C(039)-C(050)-C(079)-C(077)	140.5(9)
C(040)-C(050)-C(079)-C(077)	0.7(12)
C(071)-C(074)-C(079)-C(050)	1.7(11)
C(078)-C(074)-C(079)-C(050)	143.8(7)
C(071)-C(074)-C(079)-C(077)	-141.9(7)
C(078)-C(074)-C(079)-C(077)	0.3(9)
C(052)-C(077)-C(079)-C(050)	-142.2(9)

C(080)-C(077)-C(079)-C(050)	0.9(12)
C(052)-C(077)-C(079)-C(074)	0.0(9)
C(080)-C(077)-C(079)-C(074)	143.2(8)
C(040)-C(038)-C(080)-C(077)	3.0(13)
C(075)-C(038)-C(080)-C(077)	-140.6(9)
C(040)-C(038)-C(080)-C(044)	143.1(8)
C(075)-C(038)-C(080)-C(044)	-0.5(9)
C(052)-C(077)-C(080)-C(038)	135.1(9)
C(079)-C(077)-C(080)-C(038)	-2.8(12)
C(052)-C(077)-C(080)-C(044)	-1.5(11)
C(079)-C(077)-C(080)-C(044)	-139.4(8)
C(035)-C(044)-C(080)-C(038)	-142.6(8)
C(082)-C(044)-C(080)-C(038)	0.9(9)
C(035)-C(044)-C(080)-C(077)	0.6(10)
C(082)-C(044)-C(080)-C(077)	144.1(7)
C(054)-C(064)-C(081)-C(073)	136.7(9)
C(036)-C(064)-C(081)-C(073)	-4.0(12)
C(054)-C(064)-C(081)-C(085)	0.3(13)
C(036)-C(064)-C(081)-C(085)	-140.4(8)
C(065)-C(073)-C(081)-C(064)	3.5(13)
C(087)-C(073)-C(081)-C(064)	-141.0(8)
C(065)-C(073)-C(081)-C(085)	143.3(8)
C(087)-C(073)-C(081)-C(085)	-1.1(10)
C(024)-C(059)-C(082)-C(044)	0.6(11)
C(072)-C(059)-C(082)-C(044)	138.2(7)
C(024)-C(059)-C(082)-C(075)	-135.9(8)
C(072)-C(059)-C(082)-C(075)	1.7(11)
C(035)-C(044)-C(082)-C(059)	-1.5(11)
C(080)-C(044)-C(082)-C(059)	-142.6(7)
C(035)-C(044)-C(082)-C(075)	140.3(7)
C(080)-C(044)-C(082)-C(075)	-0.8(8)
C(030)-C(075)-C(082)-C(059)	-1.7(11)
C(038)-C(075)-C(082)-C(059)	141.5(8)
C(030)-C(075)-C(082)-C(044)	-142.6(8)
C(038)-C(075)-C(082)-C(044)	0.5(9)
C(051)-C(068)-C(083)-C(063)	136.4(7)
C(023)-C(068)-C(083)-C(063)	-5.1(10)
C(051)-C(068)-C(083)-C(067)	2.6(10)
C(023)-C(068)-C(083)-C(067)	-138.9(7)
C(049)-C(063)-C(083)-C(068)	4.2(11)
C(048)-C(063)-C(083)-C(068)	-141.3(8)
C(049)-C(063)-C(083)-C(067)	144.2(7)
C(048)-C(063)-C(083)-C(067)	-1.3(8)
C(062)-C(067)-C(083)-C(068)	140.9(8)
C(053)-C(067)-C(083)-C(068)	-1.9(10)
C(062)-C(067)-C(083)-C(063)	-0.6(8)
C(053)-C(067)-C(083)-C(063)	-143.5(7)
C(042)-C(060)-C(085)-C(058)	-2.2(13)
C(046)-C(060)-C(085)-C(058)	-139.1(8)
C(042)-C(060)-C(085)-C(081)	137.1(9)
C(046)-C(060)-C(085)-C(081)	0.2(12)
C(069)-C(058)-C(085)-C(060)	3.1(12)
C(087)-C(058)-C(085)-C(060)	143.9(8)
C(069)-C(058)-C(085)-C(081)	-141.2(7)
C(087)-C(058)-C(085)-C(081)	-0.4(9)
C(064)-C(081)-C(085)-C(060)	-0.2(13)
C(073)-C(081)-C(085)-C(060)	-141.8(10)
C(064)-C(081)-C(085)-C(058)	142.5(9)

C(073)-C(081)-C(085)-C(058)	0.9(10)
C(065)-C(073)-C(087)-C(048)	-2.5(15)
C(081)-C(073)-C(087)-C(048)	141.4(9)
C(065)-C(073)-C(087)-C(058)	-143.1(10)
C(081)-C(073)-C(087)-C(058)	0.9(9)
C(063)-C(048)-C(087)-C(073)	-135.1(10)
C(062)-C(048)-C(087)-C(073)	2.4(12)
C(063)-C(048)-C(087)-C(058)	1.7(11)
C(062)-C(048)-C(087)-C(058)	139.2(8)
C(069)-C(058)-C(087)-C(073)	143.8(8)
C(085)-C(058)-C(087)-C(073)	-0.3(9)
C(069)-C(058)-C(087)-C(048)	0.4(10)
C(085)-C(058)-C(087)-C(048)	-143.7(8)
C(008)-N(1)-C(1)-C(033)	-92.2(8)
C(016)-N(1)-C(1)-C(033)	31.0(10)
C(008)-N(1)-C(1)-C(027)	101.9(7)
C(016)-N(1)-C(1)-C(027)	-134.9(6)
C(016)-N(1)-C(1)-C(008)	123.2(6)
C(023)-C(033)-C(1)-N(1)	57.6(10)
C(049)-C(033)-C(1)-N(1)	-156.1(7)
C(023)-C(033)-C(1)-C(027)	-135.0(7)
C(049)-C(033)-C(1)-C(027)	11.3(7)
C(023)-C(033)-C(1)-C(008)	-6.0(8)
C(049)-C(033)-C(1)-C(008)	140.3(5)
C(042)-C(027)-C(1)-N(1)	-56.8(9)
C(069)-C(027)-C(1)-N(1)	157.7(6)
C(042)-C(027)-C(1)-C(033)	134.1(6)
C(069)-C(027)-C(1)-C(033)	-11.5(7)
C(042)-C(027)-C(1)-C(008)	6.3(8)
C(069)-C(027)-C(1)-C(008)	-139.2(5)
C(039)-C(008)-C(1)-N(1)	109.9(5)
C(019)-C(008)-C(1)-N(1)	-124.8(6)
N(1)-C(008)-C(1)-C(033)	125.5(6)
C(039)-C(008)-C(1)-C(033)	-124.6(6)
C(019)-C(008)-C(1)-C(033)	0.8(7)
N(1)-C(008)-C(1)-C(027)	-110.5(6)
C(039)-C(008)-C(1)-C(027)	-0.6(7)
C(019)-C(008)-C(1)-C(027)	124.7(6)

Symmetry transformations used to generate equivalent atoms:

Table 7. Hydrogen bonds [\AA and $^\circ$].

D-H...A	d(D-H)	d(H...A)	d(D...A)	$\angle(\text{DHA})$
---------	--------	----------	----------	----------------------

Abbreviation

Chemical Reagents

DMSO	dimethylsulfoxide
P3AT	poly-3-alkylthiophene
P3HT	poly-3-hexylthiophene
O3HT	oligo-3-hexylthiophene
ODCB	<i>o</i> -dichlorobenzene
PCBM	[6,6]-phenyl C61 butyric acid methyl ester
ITO	indium tin oxide
OPV	oligophenylenevinylene
Fc	Ferrocene

Physical and Chemical Characteristics

PDI	polydispersity index
DP	degree of polymerization
r.p.m.	round per minute
I_{sc}	short circuit current
V_{oc}	open circuit voltage
FF	fill factor
η	efficiency
k_{ET}	electron transfer rate constant
K_{SV}	Stern-Volmer constant
P	power
V	bias
λ	wavelength
τ	lifetime
ε	dielectric constant
δ	chemical shift
μ	mobility
LUMO	lowest unoccupied molecular orbital
HOMO	highest occupied molecular orbital
SEM	scanning electron microscopy
SPC	single photon counting
MALDI-ms	matrix-assisted laser desorption/ionization mass spectroscopy
TGA	thermal gravimetric analysis
CV	cyclic voltammetry

AFM	atomic force microscopy
NMR	nuclear magnetic resonance
IPCE	incident photon to current efficiency

Units

W	watt
J	joule
V	volt
eV	electron volt
A	ampere
Å	angstrom
m	meter
L	liter
g	gram
s	second
min	minute
h	hour
d	day
mol	mole
M	molar

Compound List

